Neutrophil migration in primary immunodeficiency

Julien Arnaud Record

Institute of Child Health

University College London

Gower Street, London, WC1E 6BT

A thesis submitted for the degree of Doctor of Philosophy

August 2017

I, Julien Record confirm that the work presented in this thesis is my own. Where information has been derived from other sources, I confirm that this has been indicated in the thesis.

Acknowledgments

First, I would like to thank Professor Alison Condliffe and Doctor Maryse Bailly for having accepted to be my examiners and have reviewed my work. Their input was really appreciated as they have undoubtedly strengthened my manuscript.

I would like to express my deepest gratitude to Adrian for your scientific expertise, patience, enthusiasm, support and guidance without which I could not have completed this work. I am also grateful to Guillaume for your guidance, support and endless knowledge of the actin cytoskeleton that never failed me. I am also very thankful to Dale for your warm welcome, supervision and scientific discussions.

To all those at Molecular and Cellular Immunology Section, formerly known as Molecular and Immunology Unit, thanks for your scientific and technical support in the lab and for your warm welcome to London. I will not forget the companionship and the discussions, especially the ones on the Friday evenings.

To the ones I left across the channel. You have my deepest thanks as despite the distance and the years you are always here to support me and make me laugh. A special thought to my parents for their support and love during all these years. There are no words to say how much I am thankful.

I wish to also dedicate my thesis to my true London family that I met on one unsurprisingly cold and humid winter evening in Queen's gate mews. You filled these years with joy and made everything possible. You will always be in my heart wherever you are.

To the one that is surprisingly still standing by me after all this time. Ln, you are everyday an inspiration for me to be a greater man and a greater scientist. Your love and support during these years made me, writing these lines, possible.

Abstract

Neutrophils are the first cells to reach infection sites and are able to kill pathogens. Therefore, their ability to quickly migrate to infection loci is essential and rely on actin structures called the lamellipodium at the front of the cell and the uropod at the rear. Actin cytoskeleton dynamics are crucial for the formation of these structures, and mutations in actin cytoskeleton regulators in immune cells can result in severe primary immunodeficiencies. These defects are good models to understand the role of actin regulators in neutrophil migration. To allow accurate monitoring of neutrophil migration, a new protocol, based on the Dunn chamber system, was developed. In particular, the stabilization of the chemoattractant gradient over long durations was achieved by embedding it in agarose, which allowed to reliably monitor neutrophil migration and was used throughout the different projects. It was first employed to assess the effect of constitutively activated Wiskott-Aldrich syndrome protein (CA-WASp) which is responsible for an excess of polymerized actin throughout the cytoplasm. Neutrophils expressing CA-WASp displayed a reduced migration speed together with an increased contractile activity. The development of this system further allowed us to identify a neutrophil migratory defect and correlate it to a mutation in Megakaryoblastic Leukemia 1 (MKL1). MKL1 is a transcription cofactor which regulates the expression of numerous actin genes. Study of MKL1 knockdown in neutrophils showed that MKL1 deficient neutrophils displayed severely impaired migration and dramatically reduced levels of globular and polymerised actin. MKL1 deficiency also altered the expression of numerous other actin cytoskeleton regulators indicating that the migratory defect was the consequence of the alteration of several actin cytoskeleton components. Finally, the potential for the modified Dunn chamber protocol to be used as a routine assay to monitor the migration of neutrophils from patients with unknown causes of immunodeficiency was assessed.

Table of Contents

List of Figures and Tables

Acronyms and Abbreviations

ADF	Actin-depolymerisation factor
ADF-H	Actin-depolymerisation factor homology domain
ADP	Adenosine diphosphate
AIP1	Actin interacting protein 1
Arp2/3	Actin related protein 2/3 complex
ARPC2	Actin-related protein 2/3 complex subunit 2
ATP	Adenosine triphosphate
B LCL	B-lymphoblastoid cell line
BSA	Bovine serum albumin
CA-WASp	Constitutively activate WASp
CDC42	Cell division control protein 42 homolog
CENP-A	Centromere protein A
CV	Coefficient of variation
DMEM	Dulbecco's Modified Eagle's Medium
DAAMs	Dishevelled-associated activators of morphogenesis
DAPI	4',6-diamidino-2-phenylindole
DCs	Dendritic cells
dHL-60 MKL1	Neutrophil-like differentiated HL-60MKL1
DIA	Diaphanous
DMSO	Dimethyl sulfoxide
DOCK8	Dedicator of cytokinesis 8
EDTA	Ethylenediaminetetraacetic acid
EVH1	Ena-VASP homology domain
FACS	Fluorescence-Activated Cell Sorting
FCS	Fetal calf serum
FH1	Formin homology domain

FHODs	Formin homology domain-containing proteins
fMLP	N-formyl-methionyl-leucyl-phenylalanine
FMNs	Formins
FRLs	Formin-related proteins in leukocytes
GBD	GTPase binding domain
GDP	Guanosine diphosphate
GEF	Guanine exchange factor
GFP	Green fluorescent protein
H1-SCR	scramble control sequence
HBSS	Hank's balanced salt solution
HeLa ActGFP	HeLa expressing Actin-GFP
HPV	Human papilloma virus
I294T	Substitution of the isoleucine by a threonine at the position 294 in WASp CBD domain
ICAM1	Intracellular adhesion molecule 1
IFN-c	Interferon-c
IL	Interleukine
IL-1b	Interleukine-1b
INFs	Inverted formins
iNKT	Invariant natural killer T cells
IS	Immune synapse
JMY	Junction-mediating regulatory protein
kMT	Kinetochore microtubules
LB	Luria-Bertani broth
LCL	Lymphoblastoid cell line
LFA1	Lymphocyte function-associated antigen 1
LSP1	Leukocyte specific protein 1
LTB4	Leukotriene B4

MKL1	Megakaryoblastic leukemia 1
MMP	Matrix metalloproteinases
MOI	Multiplicity of infection
MPO	Myeloperoxidase
MRTF	Myocardin-related transcription factor
N-WASp	Neuronal Wiskott-Aldrich Syndrome protein
NAD 47/89	Neutrophil actin dysfunction syndrome
NETs	Neutrophil extracellular traps
NM II	Non-muscle myosins II
NPF	Nucleation promoting factor
PAMPs	Pathogens associated molecular patterns
PBMC	Peripheral blood mononuclear cells
PBS	Phosphate buffered saline
PEI	Polyethylenimine
Pen/Strep	Penicillin/Streptromycin
PFA	Paraformaldehyde
Pi	Inorganic phosphate
PIDs	Primary immunodeficiencies
PIP2	Phosphatidylinositol 4,5-bisphosphate
Rac2	Ras-related C3 botulinum toxin substrate 2 protein
rhGM-CSF	Granulocyte-macrophage colony stimulating factor
rhIL-4	Recombinant human interleukin-4
RPMI	Roswell Park Memorial Institute medium
RT	Room temperature
shMKL1	shRNA specific for MKL1
SRF	Serum response factor
TAE	Tris-Acetate EDTA

TBS-T	Tris buffered saline–Tween
TCR	T cell receptor
Th1	T-helper 1
TNF-α	Tumor necrosis factor-α
VCA	Verprolin homology-central-acidic regions
WAHD1	N-terminal WASH homology domain 1
WASH	WASp and SCAR homologue factors
WASp	Wiskott-Aldrich protein
WAVE	WASp-family verprolin homologue
WDR1	WD repeat 1 protein
WHAMM	WASp homologue associated with actin, membranes and microtubules
WIP	Wiskott Interacting protein
XLN	X-linked neutropenia
XLT	X-linked thrombocytopenia

Chapter 1 Introduction

1.1 Neutrophils in immunity

Neutrophils are usually the first leukocytes to reach the site of infection and are capable of clearing pathogens by several means. It has been shown that neutrophils are essential to clear the infection and that reduction of neutrophil numbers in the blood stream results in severe immunodeficiency in humans.

1.1.1 Maturation in bone marrow and egression into blood circulation

Neutrophils are produced in the bone marrow and their population can be subdivided into three groups: the stem cell group, the mitotic group and the post-mitotic group, according their differentiation stage. The stem cells group is made of undifferentiated hematopoietic stem cells while the mitotic group consists of granulocyte progenitor cells going through cell proliferation and differentiation. Finally, the post mitotic group is composed of neutrophils in the last stages of maturation that no longer divide. Once fully mature, neutrophils are held into the bone marrow as reservoir of cells available for mobilisation into the blood stream. Hematopoietic stem cells are located in the bone marrow and held in niches that are provided essentially by perivascular cells expressing both the membrane bound form of stem cell factor and the chemokine CXCL12 (SDF-1) (Ding et al., 2012; Ding and Morrison, 2013) which bind to CD117 (c-Kit) and CXCR4 receptors, respectively. Immature neutrophils are held into the bone marrow by two signals: CXCR4 transduces the retention signal expressed by the perivascular cells in the hematopoietic stem cell niche while CXCR2 transduces the release signal. During neutrophil maturation, CXCR4 expression progressively decreases until finally disappearing. However, expression of CXCR2 - which binds to CXCL1 (neutrophil-activating protein 3), CXCL2 (macrophage inflammatory protein 2-alpha), CXCL3 (macrophage inflammatory protein-2-beta), CXCL5 (epithelial-derived neutrophil-activating peptide 78), CXCL6 (granulocyte chemotactic protein 2) and CXCL8 (Interleukin 8) - increases over time and delivers a release signal leading to the egress of mature neutrophils from the bone marrow into the blood circulation (Furze and Rankin, 2008; Bachelerie et al., 2014).

1.1.2 Neutrophil recruitment cascade

When recruited, leukocytes must first exit the blood flow and migrate through the blood vessel endothelium to reach the tissue. This process is well characterised and, in most tissues, includes the following steps: tethering (capture), rolling, adhesion, crawling, and finally, transmigration (Figure 1-1).

1.1.3 Tethering

The tethering of free circulating neutrophils is achieved through changes on the surface of the endothelium triggered by inflammatory molecules such as histamines, leukotrienes and cytokines secreted by resident sentinel leukocytes when they encounter pathogens in the tissues (reviewed in Phillipson and Kubes, 2011; Sadik et al., 2011). Endothelial cells can also detect pathogens directly through pattern recognition receptors (PRRs) which stimulate the upregulation of prestored P-selectin within minutes. Activation of endothelial cells also stimulates the synthesis of E-selectin that will be upregulated within 90 minutes (Ley et al., 2007; Petri et al., 2008). The combination of E- and P-selectin at the endothelial cell surface amplifies neutrophil recruitment by binding to glycosylated ligands, such as P-selectin glycoprotein ligand 1 (PSGL1), expressed on neutrophil surface allowing the tethering of free circulating neutrophils to the endothelial surface of blood vessel. Similarly, L-selectins on neutrophil surface bind to PSGL1 expressed by endothelial cells and contribute to neutrophil tethering (Bargatze et al., 1994).

1.1.4 Rolling

Once tethered, neutrophils roll along the blood vessel in the direction of the blood flow and are subjected to a shear stress of 1 to 10 dynes/cm^2 (Sundd et al., 2012, 2011). To maintain a smooth rolling in such conditions, a rapid formation and successive breaking of adhesive bonds is necessary (Ramachandran et al., 2004) and the dissociation of the cell rear from the endothelium needs to be stabilised with the creation of a new at attachment at the leading edge (Sundd, 2010). At first, the front bond does not endure any load and it is only when the bond is transferred to the back of the rolling cell that it is forced to support the shear stresses exerted on the cell. The rolling of neutrophils also involves the formation of long tethers at the rear of the cell that “sling” to the front of the cell

(Sundd et al., 2012). The sling is attached to endothelial cells through selectins, and during cell rolling, the sling-selectin bonds are peeled of the sling. Moreover, lymphocyte function-associated antigen 1 (LFA1), that binds to intracellular adhesion molecule 1 (ICAM1) and ICAM2 expressed on the endothelium, is expressed at the surface of tethers and slings and allows the rolling of neutrophils to the endothelium. This interaction could possibly slow down neutrophils further and lead to their arrest (Zarbock et al., 2011; Zarbock and Ley, 2008).

1.1.5 Adhesion

Chemokines are attached to endothelial cells by binding heparin sulphates which act as anchors to avoid the detachment of these molecules by the shear forces of circulating blood (Massena et al., 2010). During the rolling step, neutrophils enter in contact with the chemokines presented at the endothelium surface and this induces their activation. Full activation could be described as a two steps process consisting of, first, a priming step, characterised by an enhanced responsiveness to subsequent stimuli, followed by the full activation. The priming is essential for maximal NADPH oxidase pathway activity and neutrophil degranulation (Condliffe et al., 1998; Guthrie, 1984) and is initiated by pro-inflammatory cytokines, such as tumour necrosis factor-a (TNF-α) and interleukine-1β (IL-1β), or through contact with activated endothelial cells followed by an exposure to pathogens associated molecular patterns (PAMPs), growth factors or chemoattractants (Condliffe et al., 1998). Another molecule involved in neutrophil activation is CXCL8 (IL-8) which signals via the CXCR2 receptor and triggers neutrophil adhesion to the endothelium. Activation of the G-protein-coupled chemokine receptor (GPCR) CXCR2 promotes the change of conformation of integrins expressed at the cell surface which then display a higher affinity to their ligands such as ICAM1 and ICAM2. Neutrophils express high levels of CD11a (also known as LFA1, α1β2 integrins) and CD11b integrins (also known as MAC1, αMβ2 integrins) which, after changing their conformation, bind molecules expressed at the endothelial cell surface, for instance ICAM1 and ICAM2 (Phillipson et al., 2006). It is important to note that there are exceptions to the classical tethering-rolling-adhesion paradigm. In sinusoidal capillaries of the liver, neutrophils do not roll but adhere directly to the hepatic endothelial cells (Wong et al., 1997). Another example is the neutrophils circulating in the lung

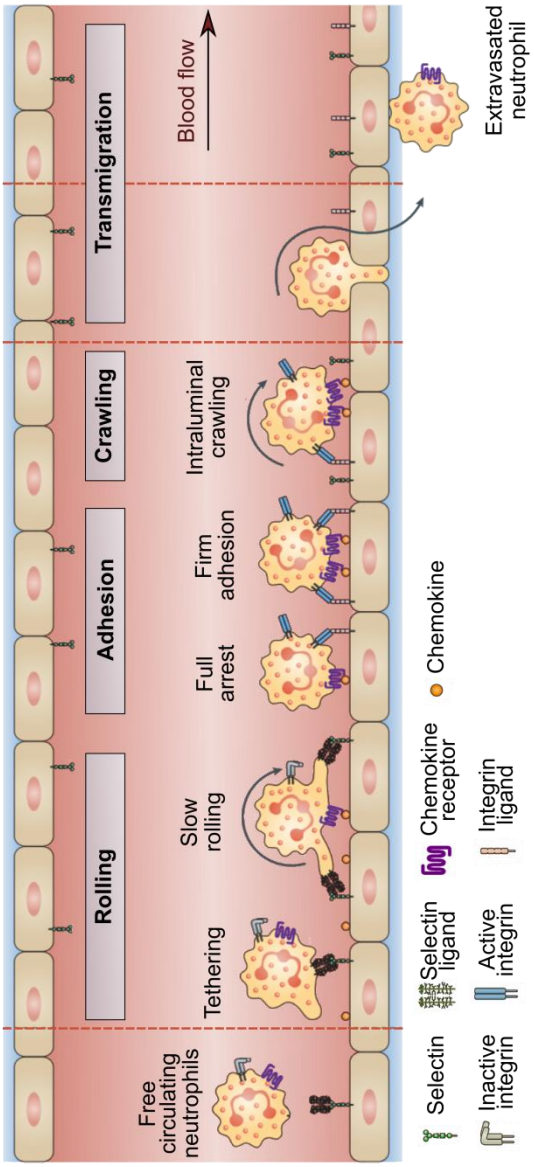

Figure 1-1: Neutrophil adhesion cascade

Leucocyte migration through the blood vessel is necessary to reach the infection site and, in most tissue, occurs through a succession of specific events: tethering (capture), rolling, adhesion, crawling, and transmigration. The tethering of free circulating neutrophils is achieved through changes on the surface of the endothelium in response to a pathogen that trigger the neutrophil binding. Once tethered, neutrophils roll along the blood vessel in the direction of the blood flow through a series of rapid formation and breaking of these adhesive bonds. During this step, contact of neutrophils with the chemokines at the endothelium surface induces their activation. Neutrophils then crawl to reach a transmigration site, typically at the endothelial cell-cell junction, where they can finally cross the endothelium and the basement membrane. (figure modified from Kolaczkowska and Kubes, 2013).

microvasculature. The thin diameter of lung microvasculature suggests that neutrophils need to dramatically change shape to be able to circulate through these thin capillaries (Looney et al., 2011) and highlight the hypothesis that sequestration of neutrophils into the lungs is only due to the mechanical properties of the microvasculature and is independent of integrins and selectins.

1.1.6 Transmigration

Once the neutrophils are adherent on the vascular endothelium, they are ready to transmigrate. However, the transmigration does not necessarily occur at the location where the neutrophils stopped. Some neutrophils display a probing behaviour and send out pseudopods to probe their vicinity while being firmly attached at a specific point of the endothelium (McDonald et al., 2013). Neutrophils typically transmigrate at an endothelial cell-cell junction to which they migrate to. The shear forces due to the blood flow are responsible for the elongated shape of the endothelial cells in the direction of the blood flow (Malek and Izumo, 1996). Under these conditions, neutrophils tend to migrate perpendicularly to the endothelial cell long axis since it is the shortest distance from the neutrophil adhesion position to a cell-cell junction. This migration is dependent of the interaction between ICAM1 on the endothelium surface and CD11b on the neutrophil surface (Phillipson et al., 2006). Neutrophil migration under shear stress is still poorly understood but has been shown to be dependent of a succession of changes in cell shape that allow the cells to be continuously attached to the endothelium while both creating new bonds at their front and detaching their rear at the same time. Such phenomenon involves remodelling of the actin cytoskeleton through the VAV1 and CDC42 pathway which strengthen the high affinity of β2 integrins to their ligands and in return results in an enhanced interaction between integrins and actin cytoskeleton (Hepper et al., 2012). Migration on the endothelium does not require a chemokine gradient as it has been shown that under shear stress and in the absence of chemoattractant gradient neutrophils migrate in straight line in perpendicular direction to the shear forces and return to random migration behaviour as soon as the shear flow is stopped (Phillipson et al., 2009). Nevertheless, various chemokines are present on the vascular endothelial cell surface and may also contribute to define a gradient (Massena et al., 2010; Phillipson et al., 2009) that

guide neutrophil migration through haptotaxis (directional migration through a gradient of cellular adhesion or substrate-bound molecules) towards specific transmigration sites (McDonald et al., 2010).

Once the neutrophils reach a transmigration site, they can leave the vasculature by first crossing the endothelium and then the basement membrane (Ley et al., 2007). Passage through the endothelial cell layer takes place either paracellularly, *i.e.*between cells, or intracellularly, *i.e.* through a cell. It has been shown that, *in vitro*, paracellular transmigration usually happens at tricellular junctions of the endothelium where fewer junctional proteins are present and the endothelium is less well organised (Burns et al., 2000; Woodfin et al., 2011). Neutrophils preferentially use the paracellular migration (Petri et al., 2008; Woodfin et al., 2011) but also use the transcellular migration even though being less efficient and slower (Phillipson et al., 2008). The transcellular migration is a process where endothelial cells use microvilli projections to create a transmigration cup or dome that covers and seals the neutrophil away from the blood flow. This process depends on the leukocyte specific protein 1 (LSP1) which, upon endothelial cell activation, reorganises actin filaments into bundles (Petri et al., 2011). Neutrophil transmigration is also dependent of L-selectin, as the loss of its expression results in impaired neutrophil transmigration (Hickey et al., 2000) probably due to defective cell polarisation (Rzeniewicz et al., 2015). The transmigration ends when the neutrophils migrate through the extracellular matrix proteins of the basement membrane probably using proteases such as MMPs (Kolaczkowska and Kubes, 2013). It has been shown that neutrophils transmigrate preferentially through basement membrane regions that are characterised by low levels of ECM (Wang et al., 2006). These regions also show a gap between the pericytes that wrap around the endothelial cells creating an interface between the vasculature and the interstitial space, suggesting that neutrophils seek regions with the least resistance to emigrate (Proebstl et al., 2012).

1.1.7 Emigration.

Once neutrophils have emigrated, they must be able to move away from the gradient of chemokines that triggered the transmigration and move in the direction of the infection site. The chemoattractants that are secreted in the surroundings of the infected tissues, such as N-formyl-methionyl-leucyl-phenylalanine (fMLP) and the complement C5a, override the chemotactic signals (IL-8 and LTB4)

produced by intermediary sites, such as the endothelium. Hence, chemoattractants can be classified into two groups: intermediary and end-target, the latter over-riding the former. Unlike transendothelial migration which is β2 integrin dependent, migration in tissues is not (Lammermann et al., 2008). When the first wave of neutrophils reaches the infection site, they secrete leukotriene B4 (LTB4) which drives a second wave of neutrophils from more than 200 µm away from the infection site. The LTB4 is once again an intermediary signal that is then superseded by local signals such as fMLP (Lämmermann et al., 2013).

1.1.8 Destruction of pathogens.

Neutrophils are able to kill both intra- and extra-cellular pathogens by several mechanisms. The most well-known mechanism is phagocytosis which consists of the engulfment of the pathogen by the neutrophil into an intracellular vesicle called phagosome. Once the pathogens are encapsulated in the phagosomes, the cells kill them using reactive oxygen species produced by the NADPH oxidase machinery or through the fusion of the phagosome with azurophil granules that deliver antibacterial proteins such as cathepsins, defensins, lactoferrin and lysozyme (reviewed in Borregaard, 2010) to the phagosome. The antibacterial proteins can be released directly into the phagosomes containing the pathogens or into the extracellular environment destroying both intra- or extra-cellular pathogens. The destruction of extracellular pathogens may be accompanied by the destruction of the surrounding tissues by the granules content secreted by the neutrophils.

Neutrophils possess another mean to eliminate extracellular microorganisms by the use of neutrophil extracellular traps (NETs). NETs are fibrous networks constituted by a DNA core to which are bound histones, proteins (lactoferrin, cathepsins,…) and enzymes (MPO, elastase,…). NETs restrain the pathogens preventing them from spreading through the organism and also facilitate the subsequent phagocytosis of the imprisoned pathogens. It has been shown that NETs could directly kill bacteria through its antibacterial activity due to the proteases and histones bound to the DNA core (Papayannopoulos and Zychlinsky, 2009). This suggests that NETs may also be used by neutrophils to directly kill pathogens *in vivo* and would be consistent with the observation that patients with an inherited deficiency in the formation of NETs suffer from repeated infections (Bianchi et al., 2009).

1.1.9 Neutrophils and the adaptative immunity

Recently, accumulating evidences has indicated that neutrophils also modulate adaptative immunity through several distinct mechanisms. It has been shown that they can enter lymphoid organs where they seem to inhibit CD4+ T cell and B cell response to immunisation (Yang et al., 2010). It has also been reported that myeloperoxidase (MPO) - one of the main proteins of neutrophil azurophils granules inhibits the proliferation and activation of dendritic cells (DCs), reducing their numbers in draining lymph nodes. During infection by *M. Tuberculosis* (M. Tb), neutrophils are the first cells to phagocyte and accumulate M. Tb and secrete cytokines that attract DCs. These DCs then ingest the M. Tb-loaded neutrophils preventing the downregulation of CCR7 receptor, which then results in an accelerated DCs migration to the draining lymph nodes to activate CD4+ T cells (Blomgran and Ernst, 2011). Another example is that neutrophils may acquire antigens from dermis, bypassing the draining lymph nodes and transporting it directly to the bone marrow where resident macrophages phagocytose the antigen loaded neutrophils and present the antigen to CD8+ T cells to generate memory T cells (Duffy et al., 2012). Finally, neutrophils also regulate natural killer (NK) cell maturation. Altered granulopoiesis or congenital neutropenia result in diminished NK cell activity and altered NK cell repertoire (Jaeger et al., 2012).

1.1.10 Reverse neutrophil migration

It was believed that during inflammation, neutrophils would die in the infected tissues before being phagocyted by macrophages. This hypothesis is now challenged as it has been shown in zebrafish embryos that, under sterile inflammatory conditions, neutrophils mobilised to a wound in the embryo tail could reverse migrate and mount an effective response to a subconsequent *S. Aureus* aggression (Elks et al., 2011; Ellett et al., 2015). In mouse, emigrated neutrophils were observed to reverse

transmigrate and re-enter the vasculature, contributing to the dissemination of systemic inflammation (Elks et al., 2011; Ellett et al., 2015; Mathias et al., 2006; Woodfin et al., 2011).

This process may happen due to the downregulation of a junctional adhesion protein, which usually prevents reverse transmigration (Woodfin et al., 2011). It has further been reported that as small subpopulation (1-2%) of neutrophils in patients with rheumatoid arthritis were capable of reverse transmigrate and these neutrophils were also more resistant to apoptosis (Buckley et al., 2006). The consequences of the reverse transmigration are so far unknown as it may be a way to preserve neutrophils when there is no more need to fight the infection or it could also spread inflammation into other organs with possible deleterious consequences.

The actin cytoskeleton regulates the changes of cell shape and therefore is an essential component that controls neutrophil functions, from migration to phagocytosis.

1.2 Actin cytoskeleton

1.2.1 Actin polymerisation

Actin is a globular protein of 42 kDa found in nearly all eukaryote cells where it is the subunit of microfilaments. In cells, it can be found either as free monomers (G-actin) or as part of microfilaments (F-actin). Actin monomers constituting the filament are organised in a double helix which allows a monomer newly added to one extremity to interact with two subunits of the microfilament. In order to start the assembly of actin filament, a nucleus composed of a trimer of actin monomer is necessary. The spontaneous nucleation of actin is an unfacilitated process due to the instability of the intermediate actin dimers needed in the formation of the actin trimer; thus the formation of actin dimers is then considered as the limiting step in actin polymerisation (Pollard and Borisy, 2003). The instability of the actin dimer together with the interaction of actin with specific actin-binding proteins that can sequester actin monomers in the cell cytoplasm prevent unregulated nucleation of actin in the cell. Once the nucleation of an actin trimer is completed, the elongation of the actin filament is a favourable and fast process. The two ends of the actin filament are characterised

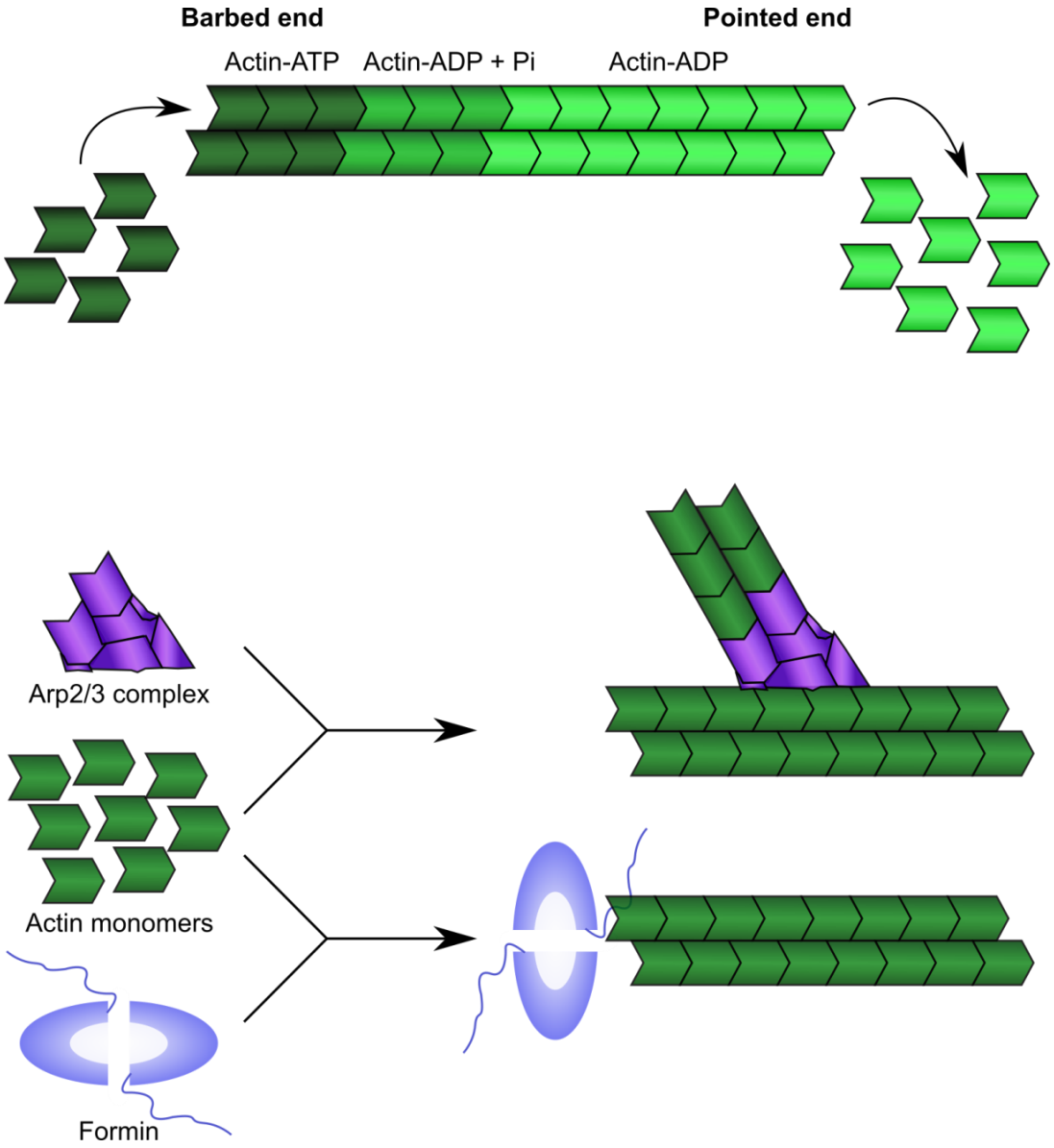

Figure 1-2: Actin polymerisation by the Arp2/3 complex and formins

The actin cytoskeleton is a highly dynamic structure that undergoes continuous cycles of polymerisation and depolymerisation. Actin monomers incorporated in F-actin are initially bound to ATP. Once present in F-actin, ATP is converted in (ADP+Pi), and then in ADP. These differences in hydrolysis states of ATP bound to F-actin create differences in polymerisation kinetics between the two ends of the actin filament (the barbed end and the pointed end). F-actin assembly in various specific structures to respond to the cell needs requires the participation of actin nucleators such as Arp2/3 complex and formins. Remarkably, Arp2/3 complex nucleates new filaments with a 70° Y-branch angle after binding to an existing filament, allowing the arrangement of F-actin in complex branched structures, while formins trigger the nucleation of unbranched actin filaments.

by different polymerisation dynamics, with the barbed end showing faster dynamics than the pointed end resulting in a favourable extension of the actin filament at the barbed-end. In cells, the continuous cycles of actin polymerisation and depolymerisation create a highly dynamic actin cytoskeleton which can rapidly respond to stimuli allowing the cells to quickly change shape. Monomers of actin that are incorporated in F-actin are bound to ATP but once included in the filament, the ATP spontaneously hydrolyses into ADP + inorganic phosphate (ADP + Pi) and subsequently into ADP. The different states of hydrolysis of the ATP bound to actin in the filament can influence the binding of proteins to F-actin that regulate actin dynamics. Depending on the cell's needs, F-actin can be assembled into specific structures such as bundles or branched networks. Actin polymerisation and assembly into structures is highly dynamic and is dependent on numerous proteins such as actin nucleators (the Arp2/3 complex, formins), nucleation promoting factors (WASp, WAVE), and regulating proteins (coronins, cofilin, LSP1). The importance of these actin-polymerisation regulators in the immune response has been largely demonstrated by the description of immunodeficiencies associated with mutations in these proteins. While in the section below, a brief description of the key actin cytoskeleton regulators is provided, the section 1.3 focuses in more details on describing the immune function impairment due to the reported mutations in the actin cytoskeleton regulators and associated proteins (*i.e.* WASp WIP, DOCK8, Rac2, RhoH, β-actin, and LSP1).

1.2.2 The Arp2/3 complex

The actin related protein complex 2/3 (Arp2/3) was the first actin nucleator to be identified (Machesky et al., 1994). Arp2/3 is a protein complex constituted of seven subunits, is highly conserved in nearly all organisms and has a molecular weight of 220 kDa. The seven subunits include ARP2 and ARP3 that are associated with five additional subunits ARPC1, ARPC2, ARPC3, ARPC4 and ARPC5. The Arp2/3 complex is unique as it possesses the aptitude to nucleate actin filaments and arrange then into branched networks. By itself, Arp2/3 has little biochemical activity and needs to interact with nucleation promoting factor (NPF) proteins to be activated, leading to the binding of Arp2/3 to an existing actin filament and the nucleation of a new actin filament from Arp2/3 with an Y-branch angle of 70^{o} between the existing and new filaments (Amann and Pollard, 2001; Mullins et

al., 1998). Structural studies suggest that ARPC2 and ARPC4 establish an essential contact with the mother filament whereas the barbed-end of ARP2 and ARP3 associate together with the pointed end of the growing filament acting as a template (Beltzner and Pollard, 2004; Rouiller et al., 2008). The interaction between the mother filament and the whole Arp2/3 complex require conformational changes from the filament and the complex (Rouiller et al., 2008) that possibly orient ARP2 and ARP3 to act as the first two monomers of the daughter filament. Arp2/3 activity is increased by three mechanisms: the binding with the actin filament, phosphorylation of Threonine and Tyrosine residues in ARP2 (LeClaire et al., 2008) and the activation of the complex by nucleation promoting factors (NPFs). Arp2/3 is usually activated by NPFs through the VCA domain which is organised in three regions constituted of one or more verprolin homology domains (also known as WASp homology 2 domain) that bind actin monomers, a central amphipathic region (also known as cofilin homology domain), and an acidic region that, together with the central region, binds Arp2/3. In cells, the Arp2/3 complex regulates the dynamics of the actin cytoskeleton at the cell cortex, in migratory actin structures such as the lamellipodia and podosomes, and in numerous other actin structures.

1.2.3 WASp and N-WASp

The Wiskott-Aldrich Syndrome protein (WASp) is a 502 amino acid protein whose expression is restricted to hematopoietic cell linages (Thrasher and Burns, 2010). WASp is constituted of five different domains: N-terminal Ena-VASP homology domain (EVH1), a basic domain, the GTPase binding domain (GBD), the polyproline domain, and the C-terminal VCA domain comprising the verprolin homology, a central and an acidic region (Figure 1-3). The neuronal Wiskott-Aldrich Syndrome protein (N-WASp) is the ubiquitously expressed homologue of WASp and both proteins show 46% identity and 72% homology at the amino acid level and 80% identity in the functional domains. In the cytoplasm, WASp is found in an auto-inhibitory conformation where the VCA domain, the active domain of WASp, is bound to the GBD domain. Once activated, WASp releases its VCA domain from autoinhibition and the VCA domain is then free to activate the Arp2/3 complex to trigger the nucleation of a new branched

actin filament. WASp can be activated by the cell division control protein 42 homolog (CDC42), phosphatidylinositol 4,5-bisphosphate (PIP2), phosphorylation on tyrosine 291 and numerous kinases adapters and actin-binding proteins (Campellone and Welch, 2010; Thrasher and Burns, 2010). The high number of WASp activators indicates that WASp integrates a broad range of signals and highlights the complex regulation of its activity. WASp activity is also regulated by WIP which stabilises WASp (Chou et al., 2006; de la Fuente et al., 2007) and by the phosphorylation of tyrosine 291 which controls the proteolysis of the protein. Proteosomal and/or calpain-mediated degradation of WASp is important for podosome disassembly and regulation of WASp activity in the immune synapse in T cells and seems to be regulated by the phosphorylation of tyrosine 291 (Blundell et al., 2009; Reicher et al., 2012) but this mechanism is not fully understood yet. Thus the phosphorylation of tyrosine may regulate both WASp activation and degradation and therefore control the spatio-temporal activity of WASp.

1.2.4 WASp family

Arp2/3 can be stimulated by several NPFs classified in five groups: WASP and N-WASp; the WASp-family verprolin homologue (WAVE) isoforms; the WASp and SCAR homologue factors (WASH); the WASp homologue associated with actin, membranes and microtubules (WHAMM) and the junction-mediating regulatory protein (JMY). All these NPFs activate Arp2/3 through VCA domains but their regulation and functions differ from each other as they comprised varied domains.

1.2.4.1 WAVE

The WAVE group is composed of three isoforms that are expressed in numerous tissues. WAVEs are not autoinhibited and thus are fully active when produced and purified as recombinant proteins. One of the main differences with WASp is that WAVE NPFs do not possess a GBD domain and they also possess distinctive regulatory domains from N-WASp. WAVEs are involved in the formation of membrane protrusions and cell migration where they activate Arp2/3 at the leading edge membrane. WAVE2 deficient cells show severe impairment in membrane ruffling, formation of lamellipodia and cell migration (Innocenti et al., 2004; Steffen et al., 2006; Yamazaki et al., 2003). In the absence of

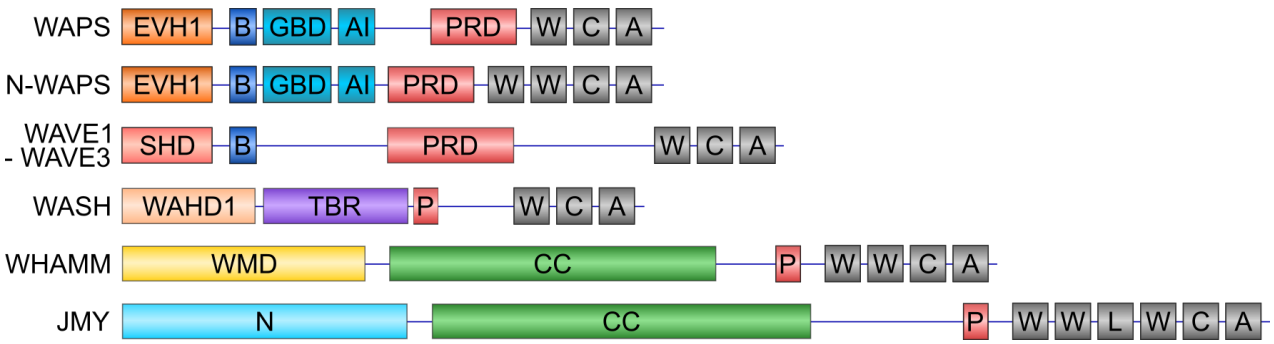

Figure 1-3: WASp family

WASp is a 502 amino acid protein, restrictively present in hematopoietic cell linages and constituted of five different domains: the N-terminal Ena-VASP homology domain (EVH1), a basic domain, the GTPase binding domain (GBD), the polyproline domain, and the C-terminal VCA domain (WCA): verprolin homology/WASp homology 2 domain (W), central amphipathic region/cofilin homology domain (C), and the acidic region (A). With 80% identity in the functional domains, N-WASp is the ubiquitously expressed homologue of WASp. All WASp family members such as WAVE isoforms, WASH, WHAMM and JMY, also possess the VCA domain required for Arp2/3 activation, but the function and regulation of the domain are specific to each of these proteins. B: basic region; CC: coiled-coiled region; N: N-terminal domain; P: polyproline; PRD: Pro-rich domain; SHD: SCAR homology domain; TBR: tubulin-binding region; WAHD1: WASH homology domain; WMD: WHAMM membrane interaction domain 1. (Figure modified from Campellone and Welch, 2010).

WAVE1, cells exhibit defective migration through the extracellular matrix. WAVE1 and WAVE2 expression is the most extensive through the different tissues but is at its highest in the brain.

1.2.4.2 WASH

As for all members of the WASp family, WASH possesses a VCA domain that activates the Arp2/3 complex. WASH is also constituted of the N-terminal WASH homology domain 1 (WAHD1) and the tubulin-binding region (also known as WAHD2). It has been shown that, in mammalians, WASH activity regulates the shape of early and recycling endosomes and also affects trafficking towards late endosomes, the endosomal recycling to the plasma membrane and the retrograde trafficking of endosomes to the trans-Golgi network (Derivery et al., 2009; Duleh and Welch, 2010; Gomez and Billadeau, 2009).

1.2.4.3 WHAMM

Similarly to other NPFs of the WASp family, WHAMM is composed of a C-terminal VCA domain flanked by a polyproline region. It also possesses central regions, that are predicted to form coiled coils, and an N-terminal WHAMM membrane interaction domain (WMD). The WHAMM VCA domain is similar to N-WASp as it has two verprolin homology domains but results showed that WHAMM has a weaker NPF activity that N-WASp. It has been shown that, *in vitro*, WHAMM is constitutively active and does not have an autoinhibited conformation (Campellone et al., 2008). In cells, WHAMM interacts with actin and microtubules and regulates membrane transport and dynamics at the *cis*-Golgi and at the endoplasmic reticulum (Campellone et al., 2008).

1.2.4.4 JMY

Despite 35% of identity with WHAMM, JMY differs at its C-terminal region by the presence of three verprolin homology domains allowing it, with the addition of an actin monomer-binding linker, to nucleate actin filament in the absence of Arp2/3 (Zuchero et al., 2009). JMY is involved in cell motility by translocating to the lamellipodium but also translocates to the nucleus in response to DNA damage (Coutts et al., 2009; Zuchero et al., 2009). Further studies are still needed to understand the activity and spatio-temporal regulation of JMY.

1.2.5 Formins

Formins are actin nucleators that generate unbranched actin filaments and are characterised by their formin homology domains FH1 and FH2. By itself, the FH2 domains are enough to start the nucleation of filaments from purified actin monomers and they are active only as homodimers (Harris et al., 2006; Li and Higgs, 2005; Moseley et al., 2004). Any mutation that disrupts the dimerisation of the FH2 domains results in the loss of the ability to polymerise actin (Copeland et al., 2004; Moseley et al., 2004; Xu et al., 2004). The actin nucleation mechanism used by formins relies on the FH2 domain binding the barbed end of an actin filament where it behaves as a processive cap, avoiding the inhibition of filament elongation by other capping proteins (Harris et al., 2006; Moseley et al., 2004). The formin nucleation mechanism is therefore different than the mechanism Arp2/3 uses, which only caps the pointed end of the filaments. The two FH2 monomers are connected by a flexible tether forming a ring and each FH2 binds two actin monomers. The FH2 dimer is dynamic and changes conformation over time by firstly binding the barbed end of the filament that does not allow the incorporation of actin while the FH1 domain recruits profilin-actin heterodimers. Then, one after the other, the FH1 domains incorporate the actin monomers at the end of the filament. It is still debated if the incorporation of actin at the filament precedes or follows the stepping forward of the FH2 dimer but once the actin is incorporated and the FH2 has stepped forward, the FH2 domains are in closed conformation preventing the capping of the actin filament by other proteins. It is only when the FH1 domain recruits actin monomers that the FH2 dimer changes conformation to allow the incorporation of new actin subunits in the filament (Otomo et al., 2005; Paul and Pollard, 2008). The classification of formins has been established on the differences in the sequence of the FH2 domain. There are seven groups of formins: Diaphanous (DIA), Dishevelled-associated activators of morphogenesis (DAAMs), formin homology, formin-related proteins in leukocytes (FRLs), domain proteins (FHODs), formins (FMNs), delphilin and inverted formins (INFs) (Higgs, 2005).

1.2.6 Coronins

Coronins are actin regulatory proteins conserved in all eukaryotes characterised by the presence of a WD40-repeat containing β-propeller (Appleton et al., 2006). The β-propeller gives coronins the ability to bind F-actin through interaction between the surface of the β-propeller and the actin filament (Cai et al., 2007). The affinity of coronins for F-actin is dependent on the hydrolysis of actin monomers in the filament. Coronin1B has an affinity 50 fold higher for actin filaments containing ATP/ADP+Pi actin, which are present close to the barbed ends of F-actin, compared to ADP actin filaments present closer to the pointed end of F-actin. Coronins also interact with Arp2/3 through their C-terminus acidic domain that is similar to WASp VCA domain but missing the verprolin homology domain used to bind G-actin. The ability to bind F-actin and Arp2/3 without activating it, allows coronins to regulate the nucleation of branched actin filament by either inhibiting the attachment of the Arp2/3 complex (Cai et al., 2008) or directly facilitating debranching (Weaver et al., 2001).

1.2.7 Cofilin/WDR1

Cofilins are part of the actin-depolymerisation factor (ADF)/cofilin family that is expressed in all eukaryotes. These small (15-20 kDa) actin binding proteins are formed by a unique folded domain called ADF-homology domain (ADF-H) (Van Troys et al., 2008). In mammals, three extremely similar paralogs are expressed: cofilin-1, cofilin-2 and ADF (Ono et al., 1994). Cofilins can promote actin filament assembly or disassembly depending on the relative concentration of cofilin to actin and other actin-binding proteins (Van Troys et al., 2008). It has been shown that *in vitro*, low concentrations of cofilin per actin filament result in severing of the actin filament (Bobkov et al., 2006). At high concentrations of cofilin, severing is not observed anymore and the actin dissociation rate at the pointed end is similar to actin dissociation without cofilin. When cofilin is present at very high concentration, it promotes actin assembly (Andrianantoandro and Pollard, 2006). The different functions that cofilins can perform allow them to regulate the actin turn-over and therefore impact the dynamics of F-actin.

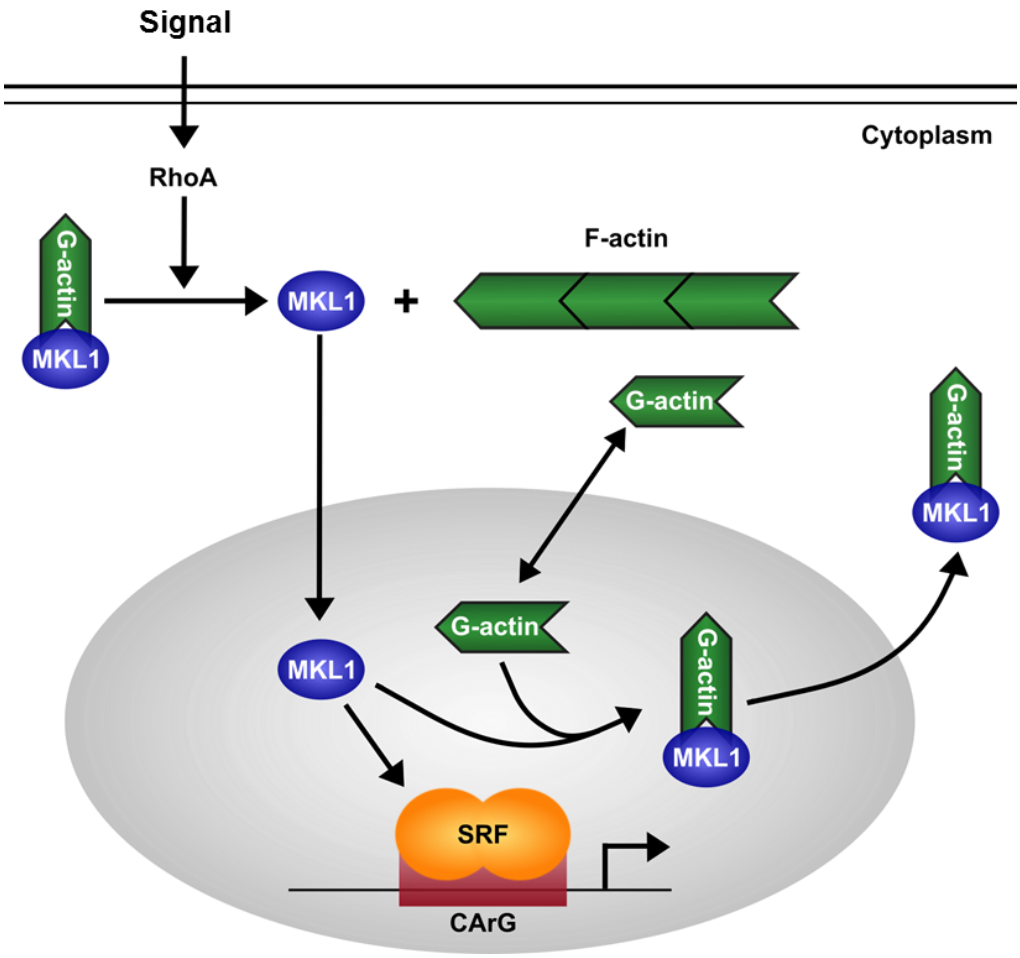

Figure 1-4: MKL1 regulates actin cytoskeleton gene expression

MKL1 continuously shuttles between the nucleus and the cytoplasm. MKL1 interaction with G-actin promotes its nuclear export resulting in a mainly cytoplasmic localisation in resting cells. When stimuli lead to actin polymerisation, G-actin monomers are integrated in actin filament resulting in the decrease of G-actin concentration throughout the cells. The drop of G-actin concentration reduces the interaction between G-actin and MKL1 which leads to MKL1 accumulation in the nucleus where it associates with SFR to activate gene transcription (Esnault et al., 2014; Miralles et al., 2003; Vartiainen et al., 2007).

It has been shown that cofilins are involved in many processes such as T-cell activation, phagocytosis, endocytosis, receptor recycling and cell migration (Van Troys et al., 2008).

WD Repeat Domain 1 (WDR1), also known as actin interacting protein 1 (AIP1) is ubiquitously expressed in eukaryotes and helps actin filament disassembly by cofilin. The mechanism by which WDR1 helps F-actin disassembly is not fully understood and so far two models have been proposed: WDR1 may cap actin filaments preventing their elongation but also cap freshly severed actin filaments to prevent their reannealing. WDR1 may also directly sever actin filaments on which cofilins are bound. It has been shown that WDR1 is involved in cell migration, cytokinesis and in inflammatory diseases (Kato et al., 2008; Kile et al., 2007).

1.2.8 MKL1

The megakaryoblastic leukemia 1 (MKL1) protein belongs to the myocardin-related transcription factor (MRTF) protein family (Olson and Nordheim, 2010). MKL1 has the ability to bind monomeric actin via its RPEL domains and to constantly translocate in and out of the nucleus. MKL1 interaction with G-actin encourages its export from the nucleus resulting in a mainly cytoplasmic localisation in unstimulated cells. Extracellular stimuli that bind to receptors, activate different Rho GTPases which in turn stimulate actin polymerisation. The incorporation of G-actin into new actin filaments results in a drop of concentration of G-actin in the cell disrupting MKL1 interaction with G-actin and promoting MKL1 accumulation in the nucleus (Miralles et al., 2003; Vartiainen et al., 2007). Once in the nucleus, MKL1 binds the serum response factor (SRF) and activates the transcription of genes (Figure 1-4). It has been shown that SRF regulates numerous actin cytoskeleton related genes including genes that are MKL1 dependent (Esnault et al., 2014). Notably, among the genes, the MKL1-SRF pathway regulates beta actin, integrin beta1, myosin light and heavy chain 9, vinculin, and cofilin1 (Olson and Nordheim, 2010). It is then not a surprise that it has been shown that MKL1 is involved in cell adhesion, spreading and migration of metastatic cells (Medjkane et al., 2009), the formation of platelets (Gilles et al., 2009), the maintenance of actin levels within cells (Salvany et al., 2014), and the formation of actin structures such as filopodia, lamellipodia and stress fibres (Esnault et al., 2014; Gilles et al., 2009).

1.2.9 Non-muscle myosin II

Myosins are a superfamily of motor proteins that can generate tension on, walk along, or drive the sliding of actin filaments and they are essential in numerous cellular activities requiring force and translocation (Krendel and Mooseker, 2005). Myosin activity relies on the hydrolysis of ATP, which is performed by catalytic ATPase sites usually located in the head, the N-terminal region, of the myosins. The tail, C-terminal region, possesses specific activities that depend on the type of myosin. For example, it can bind to cargo or self-associate into filaments allowing the head to bind actin and apply tension (Krendel and Mooseker, 2005; Vicente-Manzanares et al., 2007). Non-muscle myosin II (NM II) belong to the class II which contains most of myosins. NM II are smiliar in structure and function to muscle myosins and are composed of three pairs of subunits, or chains: two heavy chains (230 kDa), two regulatory light chains (20 kDa) regulating NM II activity and two essential light chains (17 kDa) that stabilise the heavy chain structure. NM II is essential in cellular processes that rely on cell shape changes and movement such as cell migration, cell adhesion and cell division (Vicente-Manzanares et al., 2007).

1.2.10 Actin cytoskeleton in migration

Cells can sense extracellular signalling molecules called chemokines and migrate in the direction of increased concentrations of chemokine, a process called chemotaxis (Keller et al., 1977). Chemotaxis can be defined as the sum of three events: a directional sensing that allows the cell to respond to a chemokine gradient, the formation of pseudopods and the cell polarisation which increases the sensitivity of the cell leading edge compared to the trailing edge.

Directional sensing

When cells are migrating in a chemokine gradient, new pseudopod are usually formed at the side of the cell facing the source of chemoattractant indicating that the cells sense the direction of the chemoattractant source.

Formation of pseudopod

When not stimulated with chemoattractants, neutrophils are not polarised and do not generated protrusions. Upon stimulation, nucleation of new actin filaments is promoted and a dynamic protrusion called pseudopod is extended from the cell body.

Cell polarisation

Once stimulated, neutrophils become polarised with the formation of pseudopod at the leading edge and of a uropod at the trailing edge (Figure 1-5). When using a pointed source of chemoattracant, modification of the localisation of the chemokine source results in the formation of an additional pseudopod at the leading edge. The cell then uses this new protrusion to make a U-turn towards the new localisation of the chemoattractant source. Cells do not need to be in a gradient of chemokine to become polarised since they also polarise when uniformly stimulated and then show a persistent migration in random directions, a process called chemokinesis (Keller et al., 1977).

Formation of pseudopod, cell polarisation and directional sensing all require signal transduction from the chemokine in the extracellular environment together with a regulation of the actin cytoskeleton in order to form actin based structures that alllow the cell movement.

1.2.10.1 Actin in the pseudopod and in the uropod

To migrate, cells break symmetry and extend sheet-like projections called pseudopods at the leading edge and a uropod, a specific protrusion at the rear. The pseudopod is constituted of actin filaments oriented with their barbed-end towards the cell membrane and the pointed end in the direction of the cell interior (Fritz-Laylin et al., 2017; Pollard and Borisy, 2003). Actin polymerisation at the barbed-end pushes the cell membrane to adapt to the actin filament growth and results in the extension of the cell leading edge. F-actin polymerisation is initiated at the cell membrane by WASp or WAVE proteins that activate the Arp2/3 complex and trigger the nucleation of branched actin filaments (Machesky and Insall, 1998; Rogers et al., 2003; Weiner et al., 2006). The actin cytoskeleton in the pseudopod is composed of short branched filaments nucleated by Arp2/3 but also of unbranched filaments polymerised by formins (Shi et al., 2009b). Recent data suggest that pseudopods are

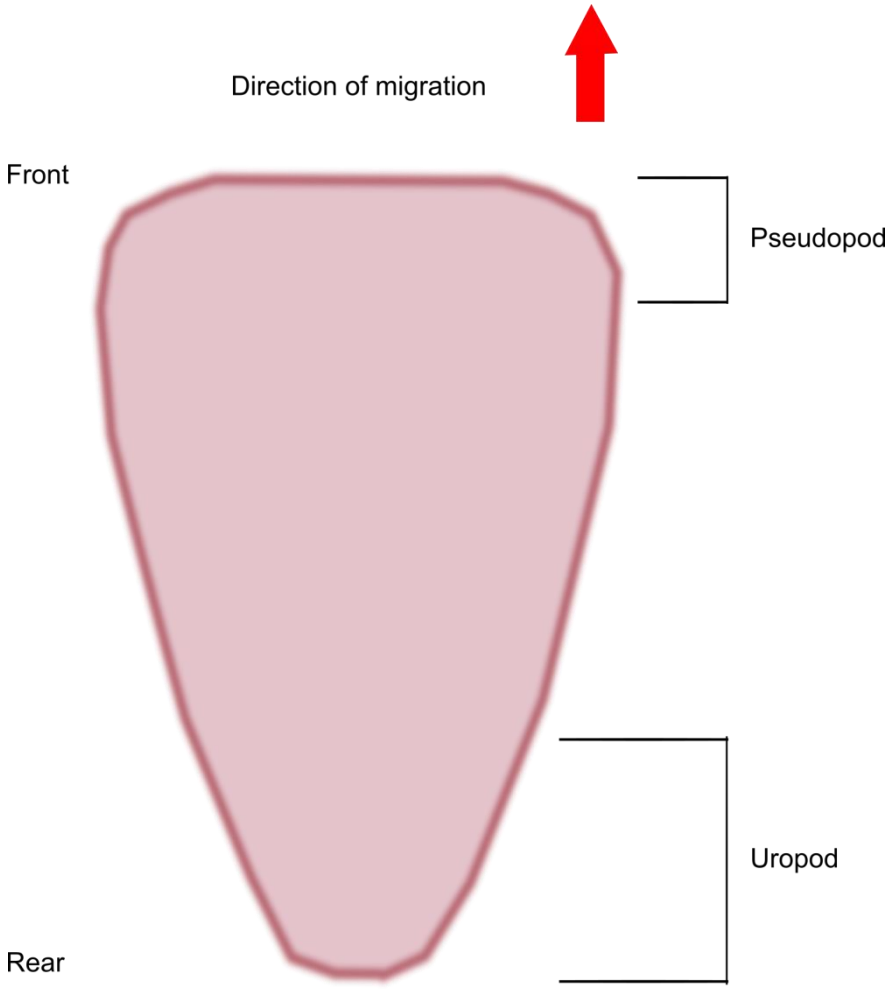

Figure 1-5: Polarisation of a neutrophil

When stimulated with a chemokine, neutrophils become polarised. A pseudopod is formed at the leading edge, the side of the cell in the direction of migration, while a uropod is formed at the trailing edge of the cell.

composed of multiple lamella and are needed to probe the environment for migration cues (Fritz-Laylin et al., 2017). The uropod is the membrane protrusion that is formed at the trailing edge of the leukocytes in response to stimulation with a chemoattractant. The uropod is enriched with specific organelles, cytoskeleton proteins, and with adhesion and signalling receptors and has a role in cell migration, vesicle recycling and intercellular communication (Sánchez-Madrid and Serrador, 2009). The actin filaments localised in the uropod are oriented in parallel to the axis of migration and interact with actin binding proteins such as the ezrin–radixin–moesin (ERM) proteins (Alonso-Lebrero et al., 2000) and myosin motor proteins such as the non-muscle myosin IIA (Eddy et al., 2000). The myosin activity is regulated by the phosphorylation of the myosin light chain by the myosin light chain kinase or by the RhoA-ROCK pathway but also by the integrin CD11b. When neutrophils polarise, CD11b is redistributed at the uropod in a CDC42 dependent manner where it modulates myosin light chain phosphorylation and activity, preventing the formation of lateral protrusions (Szczur et al., 2009). Although the role of the uropod in cell migration is still not completely understood, the cell trailing edge retraction that is mediated through RhoA is important for cell locomotion (Eddy et al., 2000). To allow the cell to migrate, the uropod needs to detach from the substratum before the cell body can retract. Neutrophils reduce uropod adhesion by reducing β1 and β2 integrin expression at the cell rear *via* the junctional adhesion molecule A (JAM-A) (Cera et al., 2009). Together, the decreased integrin expression and the force generated by the non-muscle myosin IIA allow the detachment of the rear of the cell from the substratum. The myosin II also generates forces that squeeze the uropod and cause a flow of intracellular material towards the leading edge of the cell. These waves of contractility also set the direction of migration indicating that, in neutrophils, the uropod has an active role in chemotaxis (Smith et al., 2007).

The regulation of cell polarisation and actin polymerisation during chemotaxis is a complex process that involves numerous actors. These processes are detailed below.

1.2.10.2 Signalling in cell migration

Neutrophil polarisation and chemotaxis in response to fMLP or IL-8 are regulated by receptors from the seven transmembrane domain receptor coupled to G-proteins (GPCR). The formyl peptide

receptor 1 (FPR1) responds to very low fMLP concentrations (Le et al., 2002) and transduces fMLP signal to the actin cytoskeleton regulators through a cytoplasmic heterotrimeric G protein complex constituted of Gα, Gβ and Gγ proteins. Upon FPR1 activation by fMLP, the G protein complex dissociates into Gα and Gβγ complexes which activate numerous proteins involved in neutrophil polarisation and chemotaxis such as Rho family small GTPases, the phospholipase Cβ2 (PLCβ2), phosphoinositide-3-kinase (PI3K), MAP kinases and Tyrosine kinases. For clarity, only the main Rho GTPases and PI3K pathway will be developed here.

1.2.10.3 Phosphoinositide-3-kinase

Four classes I PI3K are expressed in neutrophils and are further divided in two classes: the class IA contains PI3Kα, β and δ while PI3Kγ belongs to the class IB. It has been shown that PI3Kγ and δ have regulatory functions in neutrophil chemotaxis (Hannigan et al., 2002; Hirsch et al., 2000; Puri et al., 2004; Sadhu et al., 2003; Sasaki et al., 2000). PI3Kγ is activated by the G protein complex Gβγ and uses phosphatidylinositol 4,5-bisphosphate (PIP_2) to generate the second messenger phosphatidylinositol 3,4,5-triphosphate (PIP_3) that accumulates at the leading edge of the cell and activates GTPases from the Rho family (Figure 1-6-A). Spatio-temporal accumulation of PIP_3 is also regulated by PIP_3 phosphatases such as the phosphatase and tensin homologue (PTEN) and SH2-containing inositol-5'-phosphatase 1 (SHIP1). It has been shown in human and murine neutrophils that PTEN localisation at the rear of the cells is dependent of RhoA and Rho-associated protein kinase (ROCK) and that PTEN is required for the migration towards bacterial products in an environment with multiple chemotactic cues (Heit et al., 2008). Nevertheless, PTEN deficient murine neutrophils displays an increased extravasation and recruitment to the inflammation site (Sarraj et al., 2009; Subramanian et al., 2007). The discrepancy between these studies suggests that PTEN role might be not identical in human and mouse and that it is important to consider the infection model and type of chemoattractant used when analysing the results (Heit et al., 2008). It has also been shown that SHIP1 regulates neutrophil adhesion, spreading and chemotaxis *in vitro*. These results were supported by *in vivo* results showing an increased recruitment of neutrophils in inflamed lungs

(Mondal et al., 2012; Nishio et al., 2007; Strassheim et al., 2005). However, in human neutrophils, only the reduction of migration speed has been shown when SHIP1 is inhibited (Sapey et al., 2014). The results obtained from murine studies allowed to understand the role of PTEN and SHIP1 in murine models but the differences between murine and human neutrophils suggest that the exact roles of PTEN and SHIP1 in human neutrophils are not fully understood and need further investigation. Many of the PI3K and G proteins effectors are small GTPases that regulate the actin cytoskeleton and the cell polarisation.

1.2.10.4 Small GTPases

Small GTPases are proteins that relay the signal from a GPCR to numerous effectors. GTPases (Figure 1-6-B) cycle between an active state when they are bound to GTP and an inactive state when bound to GDP. The spatio-temporal activation of GTPases is tightly regulated resulting in only a small fraction of the GTPases that are activated at any given time. The cycling between the GTP bound and GDP bound states is regulated by Guanine nucleotide exchange factors (GEFs) and by GTPase-activating proteins (GAPs). GEFs catalyse the replacement of GDP with GTP allowing the activation of the GTPases whereas the GAPs increases the hydrolyse activity of the GTPases resulting in hydrolysis of GTP into GDP and the inactivation of the GTPase.

Rho subfamily

The Rac (Ras-related C3 botulinum toxin) subfamily of the Rho GTPases is composed of Rac1, Rac2 and Rac3. Rac1 and 3 are ubiquitous whereas Rac2 is hematopoietic specific but the three Rac proteins are highly homologous with more than 90% of amino acid identity. In neutrophils, both Rac1 and Rac2 are present, with Rac2 constituting more than 96% of the Rac expressed, and they regulate the polymerisation of branched actin filaments via the Arp2/3 complex (Sun et al., 2007). When activated, Rac mainly localises at the leading edge of neutrophils and regulates cell polarisation and chemotaxis. While Rac2 is the main Rac isoform activated for chemotaxis when neutrophils are stimulated with high concentration of fMLP, Rac1 seems to be the dominant isoform when cells are stimulated with low concentration of fMLP. This suggests a differential role of Rac1 and Rac2 in relation with the distance between the neutrophils and the infection site (H. Zhang et al., 2009). In

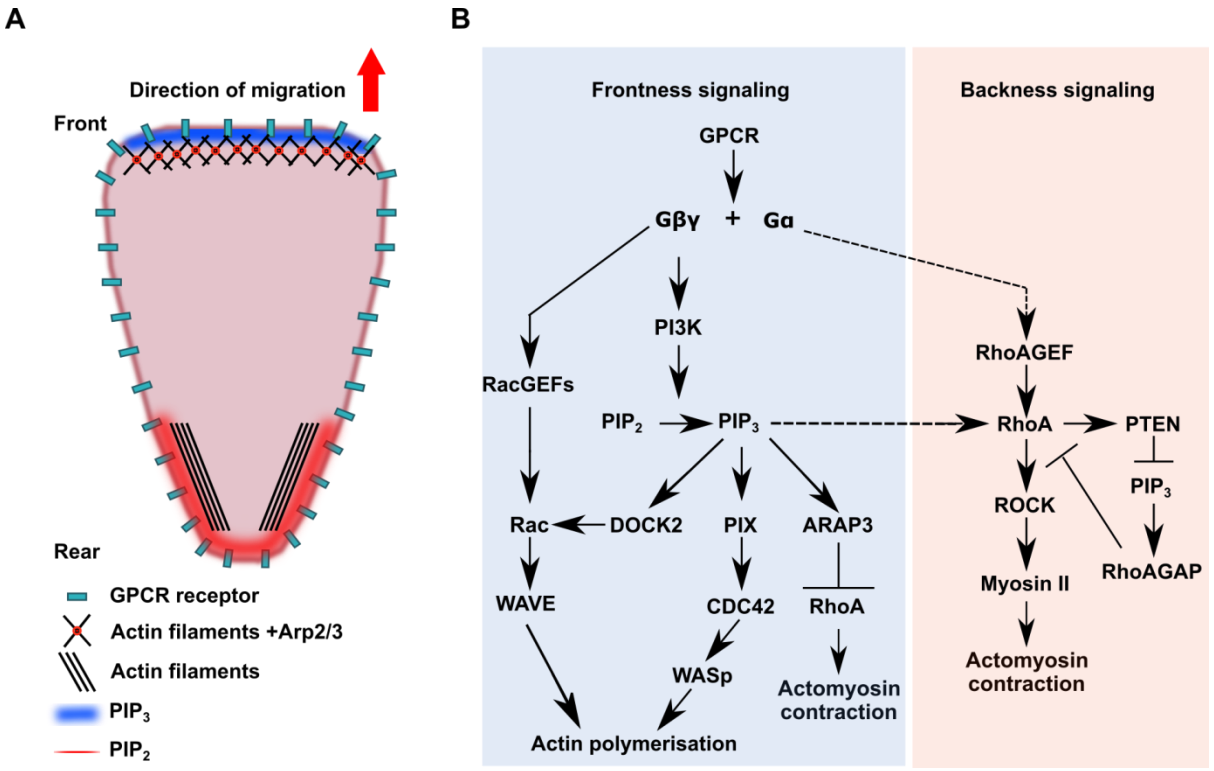

Figure 1-6: Signalling in cell migration

A) Localisation of the intracellular phosphoinositides gradients. PI3K generates PIP_3 from PIP_2 at the leading edge of the cell while PIP_2 is restricted at the back of the cell. B) Signal transduction from the GPCR to the actin polymerisation. When a ligand binds the GPCR, it triggers the release of Gβγ and Gα subunits. Gβγ activates RacGEFs leading to Rac activation and actin polymerisation via the WAVE complex. Gβγ also activates PI3K which generates PIP_3 resulting in the activation of WASp via CDC42 and PIX. The generation of PIP_3 also results in the inhibition of RhoA and cell contractility at the front edge of the cell. Long distance signalling (dashed lines) by Gα causes the activation of RhoA at the trailing end of the cells that regulates cell contractility via ROCK and myosin II. ARAP3: ArfGAP With RhoGAP Domain, Ankyrin Repeat And PH Domain 3; DOCK2: Dedicator of cytokinesis 2; GPCR: G-protein couple receptor; Gα and Gβγ: G protein complex α and βγsubunits; GEF: Guanine nucleotide exchange factors; PI3K: phosphoinositide-3-kinase; PIP_2: Phosphatidylinositol 4,5-bisphosphate ; PIP_3: Phosphatidylinositol 3,4,5-triphosphate; PIX: Pak interacting exchange factor; PTEN: phosphatase and tensin homologue; Rac: Ras-related C3 botulinum toxin; RhoA: Ras Homolog Family Member A; ROCK: Rho-associated protein kinase; WASp: Wiskott-Aldrich Syndrome protein; WAVE: WASp-family verprolin homologue.

mouse, Rac1 deficient neutrophils displays impaired polarisation and directionality while $Rac2^{-/-}$ neutrophils showed defective actin polymerisation and chemotaxis (Glogauer et al., 2003, p. 1; Roberts et al., 1999; Sun et al., 2004). These results confirm the role of Rac1 in neutrophils but are to be taken with precaution as Rac1 expression in mouse is much higher than in human (Glogauer et al., 2003), suggesting a more important role of Rac1 in mouse than in human. It has also been shown that Rac is involved in a positive feedback loop with PI3K that results in the accumulation of PIP3 at the cell leading edge which is important for the establishment of cell polarity during chemotaxis (Srinivasan et al., 2003; Weiner et al., 2002; Yoo et al., 2010). In addition to its role at the front of the cell, Rac is also implicated in RhoA regulation and cell contractility at the rear of the cell. This ensures the stable polarisation of the cell and the correct retraction of the uropod (Gardiner et al., 2002; Pestonjamasp et al., 2006). Rac can be activated by several GEFs such as P-Rex, Vav1, DOCK2 (Dedicator of cytokinesis 2) and ArhGAP15 that lie downstream of PI3K and Gβγ subunits. It has been shown in mice that P-Rex can be activated by both PIP3 and Gβγ and is an important regulator of neutrophil function but its activity seems to be not essential for *in vitro* neutrophil chemotaxis (Welch et al., 2005). Murine Vav1 has also been shown to be required *in vivo* for neutrophil intraluminal crawling and recruitment to the periphery whereas Vav1 has a lesser role in *in vitro* neutrophil chemotaxis (Gakidis et al., 2004; Lawson et al., 2011). In mouse, DOCK2 is recruited to the plasma membrane in a PI3Kγ-dependent manner and regulates the localisation of actin polymerisation together with neutrophil polarisation, directionality and distance migrated in *in vitro* chemotaxis experiments (Kunisaki et al., 2006). Finally, ArhGAP15 also has been shown in mouse to be recruited at the plasma membrane but ArhGAP15 knock-out neutrophils displayed, *in vitro*, increased chemotaxis, polarisation and improved directionality when stimulated with a single chemoattractant. These cells displayed a reduced ability to change direction when stimulated successively with two chemoattractants suggesting that the greater polarisation increased chemotactic speed but reduced the cell ability to effectively migrate in an environment with several chemotactic cues (Costa et al., 2011).

Cdc42

It has been shown that the inactive form of Cdc42 localises at the leading edge of migrating neutrophils where it is activated by the complex PAK1/PIXα, previously recruited by the Gβγ subunit upon fMLP stimulation. The localisation of Cdc42-GTP is dependent on PIP_3 generated by PI3Kγ; and PIXα seems to be involved in the exclusion of PTEN from the leading edge, reinforcing the PIP_3 gradient (Li et al., 2003). Migration of dHL-60 neutrophil-like cells expressing a dominant-negative form of Cdc42 displays multiple and unstable leading edges and poor directionality (Srinivasan et al., 2003). These results were then confirmed in $Cdc42^{-/-}$ primary murine neutrophils (Szczur et al., 2009). It has also been shown that local Cdc42 signal directs cell turning during chemotaxis and *de novo* cell polarisation, reinforcing the role of Cdc42 as compass in neutrophil migration (Yang et al., 2016). Cdc42 controls cell polarity via a cross-talk between the leading edge and the rear of the cell with Cdc42-GTP at the front regulating CD11b/CD18 integrin at the back of the cell. It has been shown that the clustering of CD11b/CD18 integrins at the rear is mediated via WASp (Kumar et al., 2012).

RhoA

In mouse and HL-60 neutrophil like cells, active RhoA is excluded from the leading edge of the cell and confined to the side and rear (Li et al., 2005; Wong et al., 2006). RhoA-GTP co-localises with microtubules, phosphorylated myosin light chain (pMLC) and PTEN at the neutrophil uropod where it regulates cell polarisation. Perturbation of RhoA activity results in alteration of cell morphology, localisation of PIP3 and polymerised actin in migrating neutrophil-like cells (Xu et al., 2003). It has been shown that RhoA regulates cell migration through two of its effectors, the Rho Kinase (ROCK) and the formin mDia. ROCK regulates the phosphorylation of myosin light chain which controls cell contractility needed for the translocation of the cell body during migration. In human cells, inhibtion of RhoA or ROCK results in altered migration characterised by a uropod-retraction defect (Alblas et al., 2001; Worthylake et al., 2001). mDia regulates, at the cell front, the polymerisation of unbranched actin filaments. The knock-out of mDia severely impairs murine neutrophil migration and affects the RhoA-ROCK signalling. $mDia^{-/-}$ neutrophils are also characterised by disturbed localisations of F-actin, pMLC, Rho-GTP and the RhoA GEF LARG. Both mDia and LARG are localised at the leading

edge of murine cell where they interact in a positive feedback loop (Kitzing et al., 2007; Shi et al., 2009a). RhoA can be activated by different GEFs such as Lsc and PDZRhoGEF that are both coupled to the Gα subunit. Lsc localises at both the uropod and leading edge of neutrophils and regulates the adhesion, polarisation and chemotaxis. In mice, cells lacking Lsc displayed a faster migration associated with poor directionality and generation of concurrent simultaneous pseudopods. Despite this, the knock-out of Lsc does not alter the recruitment of neutrophils to inflammatory sites (Francis et al. 2006). PDZRhoGEF is also needed for the correct polarisation of the cells as neutrophils lacking the protein produce multiple pseudopods, migrate slower and show a reduced polarisation together with an altered pMLC distribution (Wong et al., 2006). RhoA GAP can also play an important role in regulating neutrophil chemotaxis. Knock-out of Rhoa GAP ARAP3 leads to an alteration of β2-integrin signalling resulting in the impairment of murine neutrophil migration associated with a defective directionality (Gambardella et al., 2013, 2011). On the other hand, *in vitro* chemotaxis and *in vivo* recruitment of p190RhoGAP$^{-/-}$ neutrophils are not affected (Németh et al., 2010). Mutations in the adapter protein Hax-1 lead to a congenital neutropenic syndrome known as Kostmann disease. It has been shown in human neutrophil like cell line that Hax-1 regulates RhoA at the uropod and Rac at the leading edge, and that the knockdown of the protein results in Rhoa/ROCK/integrin-dependent uropod retraction impairment (Cavnar et al., 2011).

Despite the fact that RhoA-GTP has repeatedly been shown to be confined at the side and rear of neutrophils, several of its regulators and effectors have been reported to be localised at the front of the cells suggesting a possible RhoA activity at the front of neutrophils.

1.3 Actin defects and immunodeficiency

Performance of immunological task by immune cells relies on cell shape changes driven by reorganisation of the actin cytoskeleton making any alteration of the actin filament dynamics and/or structure a possible threat to the correct protection of the organism. It is not surprising that mutations in actin cytoskeleton regulators are responsible for defects in specific immune functions causing primary immunodeficiencies (PIDs). Defects in immune functions caused by actin cytoskeletal impairment impact almost every step of the immune response: hematopoietic cell proliferation in the

bone marrow, migration and endothelial transmigration to the infection foci, cellular interactions needed for the development of mature and effective immune cells, fast changes in cell shape required for the phagocytosis of pathogens, presentation of antigens and direct cell-to-cell interactions essential for signalling and for killing infected cells. As shown in Figure 1-7 (see page 52), mutations in several actin cytoskeleton regulators that lead to immunodeficiencies have been reported. They mainly affect the Arp2/3 dependent actin polymerisation with mutations in WASp, WIP and DOCK8 (WASp pathway) and in RAC2 and RhoH (WAVE pathway). It has further been shown that a mutation in coronin 1A that regulates of the nucleation of branched actin filament by competing with Arp2/3 or by unbranching already formed filament could also lead to immunodeficiency. Mutations in LSP1 and β-actin itself also have been reported and affect actin filament rearrangement and interaction between actin and actin regulators, respectively. This section describes these immunodeficiencies in more details.

1.3.1 Immunodeficiencies due to mutations in the WASp pathway

Mutations affecting actin polymerisation regulated by the WASp pathway have been described in WASp, WIP and DOCK8. Immunodeficiencies due to mutations in WASp can be divided into two categories: the Wiskottt-Aldrich Syndrome (WAS) that results in a loss of function and the X-linked neutropenia (XLN) which leads to a gain of function. Both conditions result in severe immune function impairment and are described below.

1.3.1.1 **Wiskottt-Aldrich Syndrome (WAS)**

More than 300 unique mutations responsible for PID have been described in the WAS gene and novel mutations causing the WAS are frequently identified (Safaei et al., 2012) and added to the database WASPbase (Schwarz et al., 1996). The mutations in WASp are accountable for three distinct pathologies (Jin et al., 2004; Massaad et al., 2013): classical WAS, X-linked thrombocytopenia (XLT), and X-linked neutropenia (XLN). Mutations in the *WAS* gene are essentially located in the EVH1 domain (Jin et al., 2004) preventing its interaction with the chaperone protein Wiskott

Interacting protein (WIP), which protects WASp from proteolysis, and results in a reduced expression or absence of WASp (Chou et al., 2006; de la Fuente et al., 2007; Konno et al., 2007; Stewart et al., 1999). The classical WAS is generally caused by either the expression of truncated WASp or the nearly complete absence of the protein. Mutations in WAS that allow the partial but significantly decreased expression of the protein results in the development of XLT, a milder form of WAS. Other mutations allow the expression of functionally defective WASp, that for example could not correctly bind to the Arp2/3 complex at similar level as the wild-type protein (Austen Worth, personal communication) The X-linked neutropenia is the only Wiskott Aldrich syndrome that is not caused by a loss of function but results from mutations in the GBD domain that disturb the auto-inhibited conformation of the protein engendering a constitutively active form of WASp. So far four different mutations have been described to generate the constitutive form of WAS and causing XLN: L270P, S272P, I294T, and I276S (Ancliff et al., 2006; Beel et al., 2009; Devriendt et al., 2001; Thrasher and Burns, 2010). Classical WAS is characterised by microthrombocytopenia, which is defined by low platelet number together with a reduced platelet size, with persistent eczema and recurrent infections, which depending of the patient varies in severity and frequency and may often be worsened by autoimmunity and occasionally with occurence of lymphoid malignancy. The symptoms of the mildest form of the disease, XLT, are usually restricted to microthrombocytopenia or, in the matter of the severe form of XLT, associated with mild transient eczema and intermittent mild infections.

WAS is the result of defects that strike almost every immune cell types and impact, at different magnitudes, most of the stages of the immune response. The combination of all these defects creates a multi-lineage disease constituted of immunodeficiency, autoimmunity and susceptibility for malignancy.

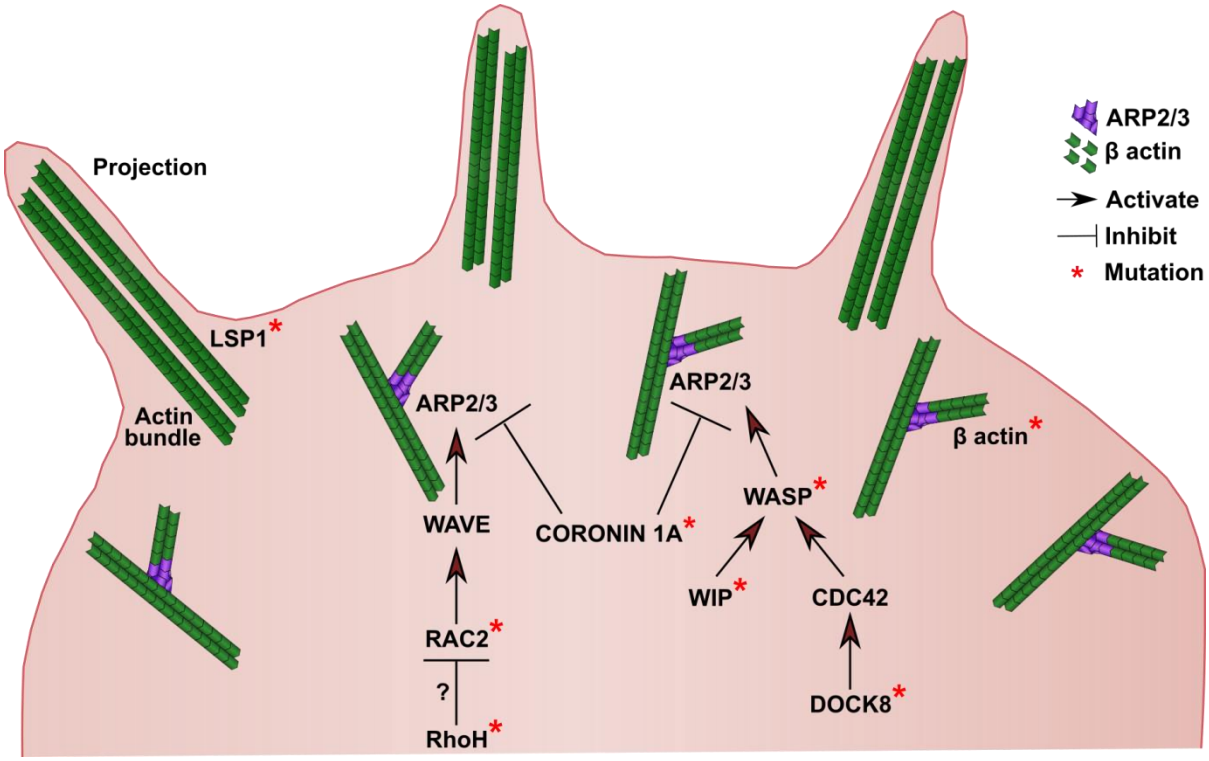

Figure 1-7: Actin defects and immunodeficiency

Immunodeficiencies can be caused by mutations in the β-actin gene or in genes encoding actin cytoskeleton regulators. Mutations in both the WASp pathway (WASP, WIP, DOCK8) and the WAVE pathway (RAC2, RhoH) affect Arp2/3-dependent actin polymerisation and have dramatic consequences on the function of immune cells. A mutation in Coronin 1A which limits nucleation of branched actin filaments by competing with Arp2/3 or by helping in filament unbranching has also been reported. Mutations in LSP1, a protein regulating actin filament bundling also result in actin defect impairing immune functions.

Microthrombocytopenia is a regular symptom in WAS and XLT and results in a predisposition for bleeding that can lead to morbidity and mortality (Mahlaoui et al., 2013). WAS patients show an extremely low expression of WASp in platelets probably due to the limited *de novo* protein synthesis in these cells (Shcherbina et al., 1999). *In vitro* studies indicate that WAS megakaryocytes generate normal size and numbers of pro-platelets and platelets (Haddad et al., 1999) whereas *in vivo*, WASp null megakaryocytes prematurely release pro-platelets (Sabri et al., 2006). Thrombocytopenia in WAS patients seem to be caused by the more rapid clearance of platelets by macrophages in the spleen, bone marrow and liver (Marathe et al., 2009; Prislovsky et al., 2013, 2008).

Investigation of WAS impact on patient derived cells and mouse myeloid cells showed that these cells failed to reorganise their actin cytoskeleton. WASp null macrophages, dendritic cells and neutrophils display impaired chemotaxis towards inflammatory chemokines and chemoattractants such as c5a, MCP-1, CSF-1, and fMLP respectively (Badolato et al., 1998; Ochs and Slichter, 1980; Snapper et al., 2005; Zicha et al., 1998). When studied *in vitro* under shear flow, these defects are more substantial. These results are supported by migration studies in WAS knockout mice and WAS knockdown zebrafish embryos (Cvejic et al., 2008; Snapper et al., 2005; Zhang et al., 2006). The decreased levels or complete absence of WASp are responsible for reduced oxidative burst and degranulation in neutrophils and inhibit the formation of podosomes that are necessary for cell adhesion to the surrounding tissues (Burns et al., 2004; Linder et al., 1999; Tsuboi, 2007; Tsuboi and Meerloo, 2007; Zhang et al., 2006). During migration, WAS cells fail to maintain directional protrusions and are unable to direct and cluster CD11b integrins at the uropod which result in an incorrect polarisation of the leading protrusion and the uropod (Ishihara et al., 2012; Kumar et al., 2012). These migratory defects do not totally abrogate the capacity of WAS cells to reach infection sites but WASp deficient cells also display impaired phagocytosis of pathogens and apoptotic cells, due to an altered actin-driven formation of the phagocytic cup (Leverrier et al., 2001; Lorenzi et al., 2000; Tsuboi, 2007).

WASp deficiency also affects natural killer (NK) cells which are lymphoid innate cells that migrate towards sites of infection and inflammation, where they detect and kill, through the release of cytotoxic proteins, virally infected cells, parasites, and malignant cells (Shi and Pamer, 2011).

Activation of NK cells is dependent on the formation of an immune synapse which relies on actin polymerisation driven by WASp. Consequently, activation of NK cells is defective in WAS patients (Orange et al., 2002). The absence of normal expression of WASp also impacts the number of invariant natural killer T cells (iNKT), which are NK cells expressing receptors that are typical of both NK and T cells. Taken together, the defective NK cells and low number of iNKT cells may participate to the disease.

Antigen presentation is also greatly affected by WASp deficiency. WAS dendritic cells (DCs) show a defect in migration due to the combination of the failure of polarisation and the impaired formation of podosomes needed to migrate over the endothelium (Bouma et al., 2007; Burns et al., 2004, 2001; de Noronha et al., 2005). This impaired migration may prevent the correct localisation of WAS DCs in the secondary lymphoid tissues and may also allow DCs to maturate before reaching the lymph node leading to ectopic release of cytokines and chemokines that could recruit other immune cells and participate to inflammatory processes such as eczema (Bouma et al., 2007; de Noronha et al., 2005).

The development of thymic T lymphocytes is generally intact in WAS patients with few abnormalities detected (Cotta-de-Almeida et al., 2007). Mature WASp deficient T cells are morphologically different from controls with fewer microvilli, although the impact of these changes is not well established (Majstoravich et al., 2004). WAS T cells also exhibit defective migration and an absence of response to CC19 and CCL21 chemokine stimulation (Snapper et al., 2005). One of the most important defects in WAS T lymphocytes is that, when activated following T cell receptor (TCR) ligation or when forming an immune synapse (IS), fail to proliferate (Ochs and Slichter, 1980; Zhang et al., 1999). The IS is the interface between a lymphocyte and an antigen-presenting cell or a target cell, which is characterised by three concentric rings of receptors called supramolecular activation cluster (SMAC): the central SMAC (cSMAC) concentrates the TCR and CD28 is surrounded by the peripheral SMAC (pSMAC) composed of integrins encircled by large glycoproteins, such as CD43 and CD45, which constitute the distal SMAC (Dustin and Depoil, 2011). The IS abnormal formation is a consequence of a defect in actin polymerisation together with an inability to mobilise lipid rafts and defective recruitment of protein involved in signalling that depend on WASp to localise correctly

to the TCR (Badour et al., 2003; Dupré et al., 2002). The immune synapse is a dynamic structure that cycles through a WASp dependent stable symmetrical form, described as three concentric SMAC having a radial symmetry (similarly as rings), and a WASp independent asymmetrical form where pSMAC opens and forms a crescent (Sims et al., 2007). Thus, in WAS T cells, the formation of the IS may initially be normal but its inability to sustain symmetry result in an unstable structure. The signalling downstream of TCR ligation requires the EVH1 domain of WASp, but is independent of the actin polymerisation activity of WASp, to translocate the transcription factor nuclear factor of activated T cells to the nucleus. Therefore, this signalling pathway is also altered in WAS cells (Trifari et al., 2006). These defects in the TCR signalling pathway impact cytokine production, with WAS T cells exhibiting reduced amount of T-helper 1 (Th1) cytokines (IFN-γ and tumor necrosis factor-α (TNF-α)), although Th2 cytokine (IL-4, IL-5, and IL-10) production remains near normal (Trifari et al., 2006).

B cell function in WAS patients has been less studied than other cell types despite a broad range of humoral immune defects such as low immunoglobulin M (IgM) levels, elevated IgA and IgE, levels and increased incidence of B-cell malignancy (Sullivan et al., 1994). Deeper investigation of defects in WAS B cells showed that these cells exhibit defective aggregation, spreading, polarisation, and migration towards CXCL13 *in vitro*, while low number of microvilli and delayed humoral immune response were observed in mice (Westerberg et al., 2005, 2001). These finding were supported by results showing that human pre-B cells display reduced adhesion together with abnormal actin cytoskeletal architecture, impaired IS formation, and increased apoptosis (Sato et al., 2012). Developing B-cells can partially compensate WASp absence through N-WASp (Westerberg et al., 2012) thus defects in B cells are mostly visible in mature cells where WASp is usually at its highest expression level (Meyer-Bahlburg et al., 2008). A common feature in WAS is the production of auto-antibodies but the mechanism driving this process is yet poorly understood (Imai et al., 2004).

1.3.1.2 **X-linked neutropenia**

Patients with XLN display recurrent bacterial infections due to severe neutropenia and monocytopenia, altered CD4+/CD8+ T-cell ratio and significant decrease in NK cells (Devriendt et

al., 2001). Mutations in the GBD domain of WAS are causing the disease, so far four mutations have been described: L270P, S272P, I276S, and I294T (Ancliff et al., 2006; Beel et al., 2009; Devriendt et al., 2001). These mutations disrupt the auto-inhibited conformation of WASp making the protein constitutively active (CA-WASp) resulting in unregulated polymerisation of actin throughout the cell and increasing the cellular F-actin content. CA-WASp alters the cell cytoskeletal dynamics ensuing abnormal phagocytosis, cell migration and podosome dynamics (Devriendt et al., 2001). Neutrophils expressing the mutant WASp display a reduced oxidative burst in response to bacterial peptide (fMLP) or *E. Coli* stimulation but no alteration of the oxidative burst in response to PMA suggesting that cells fail to correctly assemble receptors at the cell membrane (Devriendt et al., 2001). B cells are also impacted by CA-WASp and display an abnormal shape, impaired rolling ability on L-selectin and reduced spreading (Burns et al., 2010; Westerberg et al., 2010). T cells also display reduced spreading and proliferation when stimulated with CD3. Expression of CA-WASp increases Fas-mediated apoptosis of lymphocytes and spontaneous apoptosis of bone marrow-derived progenitor cells. *In vitro* studies using lentiviruses to express WASp I294T have shown that the excess of F-actin in the cell cytoplasm obstructs mitosis and cytokinesis, triggering apoptosis and genomic instability resulting in reduced cell proliferation and cytopenia (Moulding et al., 2007). The unregulated activity of CA-WASp throughout the cytoplasm triggers the nucleation of new branched actin filaments not only at the cell cortex, where it usually happens, but also throughout the cell.

1.3.1.3 **WIP**

A female patient with the classical symptoms of WASp was found to display normal *WAS* gene sequence and mRNA levels but complete absence of WASp expression (Lanzi et al., 2012). Since WASp is stabilised through its interaction with WIP, WIP expression was measured and found absent in the patient whereas the parents showed approximately 50% of residual expression of WIP. Sequencing of the *WIPF1* gene exposed a homozygous nonsense mutation in the patient. The truncated WIP of 435 amino acids lacked the WASp binding domain which is located between the amino acids 451 and 485 (Ramesh et al., 1997). The results from this patient highlight that WASp

deficiency is not always the result of a mutation in WASp and therefore proteins interacting with WASp should be investigated in patients with WAS syndrome but unaltered WASp.

1.3.1.4 **DOCK8**

Dedicator of cytokinesis 8 (DOCK8) is a guanine exchange factor (GEF). GEFs regulate Rho GTPases by assisting the change from the inactive GDP-bound state to the active GTP-bound state. The Rho GTPases then integrate extracellular signalling and transduce it to effector proteins to generate cytoskeletal responses; for example the GTP-bound form of Cdc42 activates WASp (Miyamoto and Yamauchi, 2010). It has been shown that DOCK8 interacts with Cdc42 and binds RhoJ, RhoQ and Rac1 (Ruusala and Aspenström, 2004). The expression of *DOCK8* mRNA is ubiquitous and strong expression of the protein has been observed in hematopoietic cells and peripheral blood mononuclear cells (PBMCs). Mutations in the *DOCK8* gene have been described as the source of severe immunodeficiency in both human and mice (Engelhardt et al., 2009; Randall et al., 2009; Q. Zhang et al., 2009). DOCK8 deficiency is characterised by severe allergies, otitis media, pneumonia or bronchitis, eczema, eosinophilia, IgE dysregulation, and severe cutaneous viral infections mostly caused by human papilloma virus (HPV), molluscum contagiosum virus, herpes simplex virus and varicella-zoster virus (Engelhardt et al., 2009; Randall et al., 2009; Q. Zhang et al., 2009). DOCK8 is an important regulator of actin cytoskeleton and, as such, localises at the leading edge of cells during lamellipodium formation (Ruusala and Aspenström, 2004). Deficiencies in WASp and DOCK8 share numerous clinical similarities which could be explained by the fact that WASp is an effector of Cdc42 and thus is likely to be downstream DOCK8 suggesting the overlapping of DOCK8 and WASP signalling pathways. This implies that WASp activity could be diminished in DOCK8 deficiency but cannot explain the complete features of DOCK8 deficiency, indicating that other effectors might be involved in the disease.

1.3.2 Immunodeficiencies due to mutations in the WAVE pathway

Alterations in the activity of regulators of WAVE-dependent actin polymerisation also result in immunodeficiencies. As mentioned above, Rac2 is an important regulator of the WAVE pathway and

mutations in the protein severely impair immune functions. More recently, loss-of-function of RhoH, that is thought to interact with Rac, has also been described.

1.3.2.1 **Rac2**

The Ras-Related C3 Botulinum Toxin Substrate 2 (Rac2) is a Rho GTPase whose expression is restricted to hematopoietic cell lineages and is highly expressed in neutrophils where it constitutes 96% of the total Rac content (Ambruso et al., 2000). Mutation in the *RAC2* gene is responsible for neutrophil immunodeficiency syndrome in humans (Ambruso et al., 2000; Williams et al., 2000). To date, only three cases have been described and all patients shared the same D57N mutation located in the DX2G motif leading to the expression of a dominant negative Rac2 protein. In response to fMLP stimulation, patient neutrophils display poor chemotaxis, lack of actin polarisation, no oxidative burst and decreased granule release. Nevertheless, oxidative burst could be achieved by directly activating PKC in the cells (Accetta et al., 2011; Ambruso et al., 2000; Williams et al., 2000). The oxidative burst is the quick release of reactive oxygen species (ROS) by immune cells when they are activated by their interaction with pathogens and it allows for example the degradation of internalised bacteria. Immune cells generate ROS via the gp91phox system composed of the catalytic gp91phox and the regulatory subunits p22phox, p40phox, p47phox, p67phox and Rac1/2. The assembly of the gp91phox with the regulatory subunits into an active complex regulates the generation of ROS by the gp91phox system. Three different signals are involved in the activation of the gp91phox system resulting in the assembly of the membrane associated subunits gp91phox and gp22phox together with cytoplasmic regulatory subunits p40phox, p47phox and p67phox. The three triggers of the p91phox system assembly are: 1) the phosphorylation of the autoinhibitory region of p47phox by protein kinases such as protein kinase C and AKT allowing p47phox to interact with p22phox and with lipids via its SRC-homology 3 (SH3) domain and its Phox homology (PX) domain, respectively; 2) the binding of p47phox and p40phox PX domain to PIP3 and phosphatidic acid produced by PI3K and phospholipase D, respectively; 3) the activation of Rac1/2 that promotes the addition of a membrane anchor to Rac1/2 via geranylgeranylation resulting in the association of Rac1/2 to the membrane where it binds to p67phox, helping in the assembly of the complex.

The extreme rarity of the Rac2 disorder limits the study of the disease in humans and the only other cellular defect detected is the impairement of thymic T-cell production, possibly related to defective T-cell integrin function (Accetta et al., 2011). Studies using Rac2 KO mice confirmed the neutrophil defects observed in patients but also the importance of Rac2 in the capture of L-selectin and cell rolling, generation of F-actin and activation via chemoattractant signalling of p38 and p42/44 MAPKs (Roberts et al., 1999). Mouse models expressing the D57N dominant negative Rac2 or Rac2 KO also revealed the extensive impact of Rac2 deficiency on almost all immune functions (Mulloy et al., 2010). Hematopoietic stem cells show a rise of apoptosis, associated with an impaired retention in the bone marrow (Gu et al., 2003, 2001; Yang et al., 2001). T lymphocytes display a decreased activation following TCR activation together with an absence of Th1 signalling and production of IFN-γ (B. Li et al., 2000; Yu et al., 2001) whereas B-cell show defective development, activation via the BCR, and migration toward chemokines (Arana et al., 2008; Walmsley et al., 2003). Both T and B cells also show defective cytoskeletal reorganisation. Similarly to neutrophils, macrophages display phagocytotic and oxidative burst impairment (Yamauchi et al., 2004), while CD8+ dendritic cells also lack oxidative burst capacity (Savina et al., 2009), and eosinophils have defective migration and actin polymerization (Fulkerson et al., 2005).

1.3.2.2 **RhoH**

RhoH is an atypical Rho family GTPase whose expression is restricted to hematopoietic cells. It does not possess any GTPase activity but inhibits other GTPases. A loss of function mutation in RhoH was recently identified in two patients who had recurrent infectious diseases and chronic epidermodysplasia verruciformis related human papillomavirus (EV-HPV) infections. T cells populations were skewed towards effector memory cells and showed restricted TCR usage together with a poor T cell receptor signaling. The lack of β7 integrin expression impaired T-cell homing, which may explain the persistent EV-HPV infections (Crequer et al., 2012).

1.3.3 Immunodeficiencies due to mutations in Coronin 1A

Coronin 1A is an actin regulatory protein specifically expressed in hematopoietic cells that regulates actin filament branching. By inhibiting the attachment of Arp2/3 or directly helping debranching,

Coronin 1A limits the nucleation of branched actin filaments at the leading edge of cells (Chan et al., 2011). Mutations in *CORO1A*, the Coronin 1A encoding gene, have been described causing severe combined immunodeficiency in patients. Coronin 1A deficiency is characterised by severe peripheral T-cell deficiency, especially in naïve T cells, near complete absence of invariant NKT cells, and susceptibility to EBV-induced lymphoproliferation (Moshous et al., n.d.; Shiow et al., 2009, 2008). Studies in mice showed that Coronin 1A regulates actin dynamics in T cells and controls T cell homeostasis and trafficking. It has also been shown that Coronin 1A is essential for calcium signalling downstream of TCR and B-cell receptor activation and that the absence of the protein results in a reduction of cell proliferation and IL-2 production (Föger et al., 2006; Mueller et al., 2008).

1.3.4 Immunodeficiencies due to mutations affecting actin and F-actin rearrangement

Most of the mutations in actin regulators that have been described affect Arp2/3-dependent actin polymerisation. Below are described mutations in the β-actin gene and in the leukocyte specific protein 1, affecting actin interaction with regulators and actin filaments rearrangement, respectively.

1.3.4.1 **β-actin**

Actin is one of the most conserved proteins with as little as 20% of difference in the amino acid sequences between algae and humans. Consequently, it seems unlikely to identify non-lethal mutations in the β-actin gene. A patient presented with recurrent infection thrombocytopenia, intellectual impairment and short stature had a heterozygous mutation in the *ACTB* gene. The mutation resulted in an E346K substitution which is in a region of the protein that has been reported to interact with numerous cytoskeletal regulators (Nunoi et al., 1999). The patient immunodeficiency was the result of poor neutrophil chemotaxis and oxidative burst concomitant with impaired polarisation of the cytoskeleton in response to fMLP.

1.3.4.2 **Leukocyte specific protein 1**

Leukocyte specific protein 1 (LSP1) is a phosphoprotein that binds actin and is essentially expressed in neutrophils, macrophages, lymphocytes and endothelial cells (Jongstra-Bilen, Immunol Res 2006). It has been shown that LSP1 localises to the F-actin in lamellipodia and membranes ruffles where it

reorganises actin filaments into bundles (Jongstra-Bilen et al., 1992; Zhang et al., 2000). LSP1 was first identified as a 47 kDa protein overexpressed in patients suffering neutrophil actin dysfunction syndrome (NAD 47/89). Patient neutrophils displayed numerous projections, which are enriched with actin, and a higher expression of CD11b integrin. This phenotype was associated with recurrent bacterial infections and impaired neutrophil migration (Coates et al., 1991; Howard et al., 1994). These data suggested that LSP1 negatively regulated immune cell migration which was supported by experiments in LSP1 knock out mice, where neutrophils and macrophages display an increased migration towards the infection site and enhanced chemotaxis in response to fMLP (Jongstra-Bilen et al., 2000). The overexpression of LSP1 in the pro-monocytic U937 cell line to a similar level to patient neutrophils resulted in migration defect while cell expressing significantly less LSP1 displayed an improved migration compared to controls, indicating that the expression level of LSP1 regulates its function and the positive or negative influence on cell migration (Y. Li et al., 2000, p. 1). It has been shown that LSP1 negatively regulates the integrin CD11b/CD18 adhesion resulting in a more robust polarisation of F-actin at the leading edge and extended uropod in $LSP1^{-/-}$ neutrophils let to adhere on fibrinogen or ICAM-1 only (Wang et al., 2002). However, the mechanism by which LSP1 regulates CD11b/CD18 activity via F-actin rearrangement is still not understood.

1.4 Summary and aims

Neutrophils are the first line of defence of the organism against pathogens. The destruction of pathogens relies on the ability of neutrophils to quickly migrate to the site of infection and phagocytose microorganisms. Cell shape changes, such as those involved in migration, phagocytosis and cell division, are dependent on actin cytoskeletal dynamics. The actin cytoskeleton is composed of filaments formed by polymerisation of actin monomers and is regulated by numerous proteins that can, for example, promote the polymerisation of actin monomers, regulate the formation of branched networks or sever actin filaments. The control of actin dynamics is complex and allows the quick reshaping of the actin cytoskeleton in response to stimuli. Mutations in genes that are involved in the regulation of actin dynamics in immune cells can lead to immunodeficiencies. While WAS is the most

well-known immunodeficiency caused by mutations in WASp, new mutations in this protein resulted in a constitutively active form of WASp that is associated with a severe neutropenia. The list of candidate proteins causing actin related immunodeficiencies keeps increasing with new mutations in actin regulatory genes being regularly described. The study of these new mutations increase our understanding of the role of actin regulators in immune response. Nevertheless open questions remain, such as, which actin dependent process(es) from cell division to cell migration is/are affected by mutations in actin regulators.

The overall hypothesis of this work was that neutrophil migratory defects may be an important factor in immunodeficiencies in XLN patients and in patients with previously undescribed mutations in actin cytoskeleton regulators.

To test this hypothesis, I first aimed at setting up a neutrophil migration assay that allows monitoring of neutrophil chemotaxis using primary neutrophils or a neutrophil-like cell line. My second aim was to investigate *in vitro* a potential neutrophil migratory impairment in immunodeficient patients with known or suspected actin cytoskeleton defect. As patient samples are scarce, my third aim was to genetically modify a neutrophil-like cell line to mimic mutations in actin regulators observed in patients and confirm their impact on neutrophil migration. Finally, my last aim was to assess the consequences of the studied mutations in actin cytoskeleton regulators on actin polymerisation and dynamics.

Chapter 2 Materials and Methods

2.1 Reagents

Sigma: Dimethyl sulfoxide (DMSO) (D2650), low melting temperature agarose gel (A9045), bovine serum albumin (A9418), recombinant Human Serum Albumin (A9731), fMLP (F3506), fibrinogen (F3879), rabbit anti human MKL1 antibody (HPA030782), Vinculin (V9131), Triton-X (X100), Igepal/NP-40 (I8896), LB broth (L3522), LB agar (L2897), Dextran from *Leuconostoc mesenteroides* (D1662).

Thermo Fisher: 16% Formaldehyde solution, methanol-free (28906), ECL Western Blotting Substrate (32106).

Hawksley: Dunn chambers (DCC100, Hawksley, UK).

PeproTech EC Ltd: Recombinant human MIP-1α (300-08), GM-CSF (300-03) and IL-4 (200-04).

Life Technologies: HBSS (14025050), Cell Trace CFSE Cell Proliferation Kit (C34554), Opti-MEM (31985062), RPMI (61870-044), DMEM (31966-047), skimmed milk powder (LP0031B), Prolong Gold antifade mountant (P10144).

BD Bioscience: Fibronectin (354008). Antibodies: CD11b-PECy5 (555389), CD18-PE (555924), CD29-PE (555443), CD49d-PE (555503), PE-Cy5 Mouse IgG1, κ isotype (555750), PE Mouse IgG1, κ isotype (555749).

Myltenyi Biotec: FPR1-APC antibody (130-100-812), REA-Isotype (130-104-614).

Cell Signalling: protease/phosphatase inhibitor cocktail (5872), PMSF (8553), antiphospho-myosin light chain antibody (3671).

GE Healthcare Life Sciences: Ficoll-Paque PLUS (17-1440-02).

2.2 General Buffers and Solutions

Table 2-1: Buffers and solutions

Name	Composition	Storage
Phosphate buffered saline (PBS)	11.9 mM phosphates, 137 mM NaCl2, 2.7 mM KCl	10X stock from Fisher Bioreagents; for cell culture 1X PBS from Gibco was used; stored at RT
Tris buffered saline–Tween (TBS-T)	150 mM NaCl, 25 mM Tris-HCl pH 7.6 + 0.1% Tween	10X stock solution stored at RT; Tween added to 1X TBS prior to use
BSA blocking buffer	5% BSA in TBS-T	Prepared prior to use
Milk blocking buffer	5% skimmed milk in TBS-T	Prepared prior to use
Tris-Acetate EDTA (TAE)	40 mM Tris-acetate and 5 mM EDTA	10X stock solution stored at RT
6x DNA loading buffer	10 mM Tris pH 7.5, 50 mM EDTA, 15% Ficol 400 and 0.05% bromophenol blue	Stored at RT
Luria-Bertani (LB) broth	Sigma mix (10 g/L tryptone, 5 g/L yeast extract, 5 g/L NaCl)	autoclaved and stored at 4°C
LB-agar	Sigma mix (LB + 15 g/L agar)	autoclaved, poured into Petri dishes (with antibiotic) and stored at 4°C
Cell fixing buffer (adherent cells)	4% PFA in PBS	Made fresh from 16% methanol free PFA vials

Cell fixing buffer (suspension cells)	2% PFA in PBS	Made fresh from 16% methanolfree PFA vials
Cell permeabilisation solution	0.1% Triton X-100 in PBS	Diluted from 10% Triton X-100 stock prior to use
Cell lysis buffer	0.5% IGPAL or NP-40, 150 mM NaCl, 50 mM Tris-HCl pH 8, Protease/Phosphatase Inhibitor Coktails 2x (Cell Signaling), PMSF 1 mM	Stock at 4°C; inhibitors added prior to use
Laemmli buffer 2x	10% β-mercaptoethanol, 4 % sodium dodecyl sulfate, 125 mM Tris pH 6.8, 0.2% Bromophenol Blue, 20% Glycerol	
5% Dextran	5% (weight/volume) Dextran from *Leuconostoc mesenteroides* (average molecular weight 35-45 kDa) in saline solution	Autoclaved
Saline 1x	0.9% (weight/volume) NaCl in distilled water	Sterile (filtered using a 0.22 µm filter)
Saline 2x	1.8% (weight/volume) NaCl in distilled water	Sterile (filtered using a 0.22 µm filter)

2.3 Molecular Cloning

2.3.1 Reagents

The QIAprep Spin Miniprep and Maxiprep kits used for plasmid DNA isolation as well as the QIAquick PCR Purification and Gel Extraction kits were from Qiagen. The recombinant endonucleases enzymes, the Shrimp Alkaline Phosphatase, *Pfu* DNA polymerase, deoxynucleotides (dNTPs) and T4 DNA ligase were from Promega, New England Biolabs or Fermentas. The agarose and 1 kb+ DNA ladder were from Invitrogen. All nucleotides were synthesized by Invitrogen. dNTPs were from Promega and sequencing was performed by Source BioScience.

2.3.2 shRNA

Oligonucleotide MAL short hairpins were synthesized (Eurogentec) and inserted into a pBlue Script vector containing the human H1 promoter. H1-shRNA specific for MKL1 (shMKL1), or H1-SCR (scramble control sequence) cassettes were inserted into a lentiviral vector (pRRLsin-PGK-eGFPWPRE, Genethon).

shMKL1: 5’AGTAGCAGACAGCTCTTCCttcaagagaGGAAGAGCTGTCTGCTACT 3’

shSCR: 5'CGGCAGCTAGCGACGCCAT 3'

2.3.3 mCherry-WASp lentiviruses

As the expression of constitutively activated WASp protein is known to lead to an increase of apoptosis, the establishment of a cell line stably expressing CA-WASp was not possible. Therefore, CA-WASp was expressed by gene transfer before each experiment. Gene transfer was performed by lentivirus transduction, taking advantage of the availability of the lentiviral backbones containing the wild-type or the constitutively activated WASp tagged with green fluorescent protein (GFP). As most of the other proteins of interest owned in the laboratory were tagged with GFP, eGFP was replaced by the fluorescent protein mCherry to allow live imaging of WASp concomitantly with another protein. mCherry protein is excited at 575 nm and emits at 610 nm whereas GFP is excited at 488 nm and emits at 509 nm allowing the expression and detection in live imaging of two different proteins at the same time. eGFP was replaced with mCherry by cutting out the eGFP insert and cloning the mCherry

insert into two different lentiviral backbones, one under the CMV promoter and the other one under the SFFV promoter. SFFV promoter was used because it is less silenced than the CMV promoter in hematopoietic cell lineages resulting in a more stable expression.

To visualise WASp transgene in cells already expressing proteins tagged with GFP, the GFP tag was replaced with mCherry in the lentiviral vectors used to express GFP-WASp or the active WASp mutant GFP-I294T. The two lentivirus plasmids pHR'SINcppt\CEWW and pHR'SINcppt\SEWW, containing the transgenes eGFP-WASp and eGFP-I294T respectively, contained few unique restriction sites suitable for restriction enzyme digesting. The eGFP sequence in the pHR'SINcppt\CEWW vector had two suitable restriction sites: one for BamHI at the 5' end of the transgene (position 8339) and BsrGI at the 3' end of the eGFP sequence (position 9078). Unfortunately, in the pHR'SINcppt\SEWW, BsrGI has two restriction sites one at the positions 425 and 8992 respectively, whereas BamHI's unique restriction site was at the position 8253. Extraction of eGFP only from pHR'SINcppt\SEWW was achieved through partial digestion as follows: the plasmid was first fully digested with BamHI for 1 hour before the product of this digestion was partially digested with BsrGI for 30 minutes. The product of the partial digestion was then run on an agarose gel and visualized using a UVIdoc before the band corresponding to the pHR'SINcppt\SEWW plasmid without eGFP was excised from the gel and purified using a gel extraction kit. The mCherry insert was produced by PCR using the mCherry tag of the LNTcmv\mCherry\alpha tubulin lentivirus plasmid as template. The two primers used for the PCR were: 5' ATGGATCCAT GGTGAGCAAG GGCGAGG 3' for the 5' primer and 5' GATGGAGATG CACTCACGCAC 3' for the 3' primer. The 5' primer included the BamHI restriction site (GGATCC) that was added at the 5' end of mCherry. The PCR product was purified using the PCR purification kit before being digested using BamHI and BsrGI. The mCherry insert was then ligated into the pHR'SINcppt\SEWW lentivirus backbone.

2.3.4

2.3.5 PCR

PCR were performed using 0.2 µg of DNA template together with the two primers (0.5 µM each), the dNTPs (at 200 µM each) and the *Pfu* DNA polymerase (2 µL) in *Pfu* DNA Polymerase 1X buffer with MgSO4. The PCR were carried out on the Eppendorf Mastercycler ep Gradient S using the following program: 96°C for 4 minutes, then 30 cycles of: denaturation at 96°C for 30 seconds; annealing at 62°C for 30 seconds; elongation at 75°C for 1 minute. Then a final step at 75°C for 7 minutes was performed.

2.3.6 Plasmid DNA production

The *Escherichia coli* strain Stbl3 (Invitrogen) was used for all plasmid production and the bacteria were grown at 37°C on solid LB-agar Petri dishes for clone isolation or in liquid LB medium in an orbital shaker at 225 rpm for DNA production. Both the LB-agar and LB medium were supplemented with 100 $\mu g.mL^{-1}$ of ampicillin to select the plasmid-transformed bacteria. Plasmid-transformed bacterial culture storage was done at -80°C in 20% glycerol in LB medium.

Plasmid DNA was isolated using a Miniprep kit, for small-scale plasmid DNA isolation, or using the Maxiprep kit for large-scale plasmid DNA, both according to the manufacturer's instructions. Minipreps were performed using 1.5 mL from a 5 mL overnight bacterial culture whereas Maxipreps were done using 250 mL overnight cultures.

The concentration of DNA samples was determined by the measure of the absorbance at 260 nm on a NanoDrop ND-1000 spectrophotometer. DNA samples were stored at -20°C.

2.3.7 Restriction digests

The digestion of 1-2 µg of plasmid DNA by one or several restriction endonucleases was performed in 1X supplied compatible buffer in a final volume of 10 or 50 µL for 1 hour at 37°C. The volume of enzyme was 5 to 10% of the total reaction volume. Sequential digests were performed using a PCR Purification kit according to the manufacturer's instructions to remove the buffer salt between

successive digests or by isolating the digested DNA by agarose gel electrophoresis prior to subsequent digests.

The 5' DNA terminus of the backbone for a ligation reaction was dephosphorylated after digestion and before gel electrophoresis isolation with Shrimp Alkaline Phosphatase (1 unit/µg of DNA). The ligation reaction was performed for 15 minutes at 37^{o}C using the provided buffer in a total reaction volume of 50 µL. The Shrimp Alkaline Phosphatase was inactivated by heating the reaction mix at 65^{o}C for 15 minutes.

2.3.8 Agarose gel electrophoresis and isolation of DNA fragments

The DNA fragments were resolved in 1% agarose gel electrophoresis in TAE buffer at 100 V. Loading buffer was added to the samples before they were loaded in the agarose gel. The agarose gel was supplemented with Ethidium bromide at a concentration of 0.5 µg.mL^{-1} for subsequent DNA visualisation and a 1 Kb+ DNA Ladder was run alongside the samples. DNA visualisation was performed on a UVIdoc gel documentation system (UVItec). The DNA fragments of interest were excised from the agarose gel and purified using a Gel Extraction kit following the manufacturer's instructions.

2.3.9 Ligation and checking of ligated plasmids

The ligation of the insert in the lentivirus plasmid was performed as follows: 100 ng of backbone was used for ligation with insert DNA in a 1:3 backbone to insert molar ratio using 0.5 µL T4 DNA Ligase in 1X T4 DNA Ligase buffer in a final volume of 10 µL. The ligation was carried out at 4°C overnight before the ligation products were transformed into competent bacteria. The transformed bacteria were then plated onto LB-agar plates and incubated overnight at 37^{o}C. Colonies were picked up individually and transferred to LB medium in order to start small scale cultures overnight at 37^{o}C. Plasmid DNA was then extracted and digested using the endonuclease PstI, which was selected because eGFP did not harbor a PstI restriction site whereas mCherry did. This allowed validation of the presence of the mCherry insert in the plasmid by visualisation of the pattern of the restriction fragments after digestion following agarose gel electrophoresis. All the ligations positively identified by PstI digestion were then confirmed by sequencing.

2.4 Cell culture

2.4.1 Cell lines

2.4.1.1 293T

293T cells are derived from the Human Embryonic Kidney 293 (HEK293) cell line and express the SV40 large T-antigen allowing the episomal replication of transfected plasmids containing the SV40 origin of replication. These adherent cells were expanded in 15 cm culture plates at 37°C under a humid atmosphere of 5% CO_2 in air using DMEM medium complemented with GlutaMAX, 10% fetal calf serum (FCS) and Penicillin/Streptromycin (Pen/Strep) at 1/100 (equivalent to a final concentration of 100 units/mL of Penicillin and 100 µg.mL^{-1} of Streptomycin). Cells were maintained at viable cell density between 8x10^3 and 8x10^4 cells/cm^2 by a twice-weekly split and were used before passage 10. For splitting, medium was removed and cells were washed with PBS to remove the remaining FCS. The cells were detached by incubation with trypsin/EDTA during 5 minutes at 37^{o}C and were resuspended in fresh medium containing FCS in order to inactivate the trypsin. The cell suspension was then pelleted by centrifugation at 300 rcf during 5 minutes and resuspended in fresh culture medium. The cells were then counted using a hematocytometer and plated in new culture plates at the desired density.

2.4.1.2 HeLa

HeLa and HeLa expressing Actin-GFP (HeLa ActGFP) were cultured at 37°C under a humid atmosphere of 5% CO_2 in air using DMEM medium complemented with GlutaMAX, 10% FCS and Pen/Strep. Cells were maintained at viable cell density between 8x10^3 and 8x10^4 cells/cm^2 by a twice-weekly split. Cells were used before passage 20.

2.4.1.3 HL-60

HL-60 cells were maintained in culture at a concentration between 0.1 and 1.5x10^6 cells/mL in RPMI supplemented with GlutaMAX, 10% FCS, Pen/Strep and 25 mM HEPES. To differentiate HL-60 into neutrophil-like cells (dHL-60), 1x10^6 cells were cultured for 5 days in medium supplemented with

1.3% of DMSO in a T25 flask. HL-60 cells were used before passage 20 as they become resistant to DMSO induced differentiation after too many passages.

2.4.1.4 HT1080

The Fibrosarcoma cell line HT-1080 was propagated at 37°C under an atmosphere of 5% CO_2 in air using DMEM medium complemented with GlutaMAX, 10% FCS and Pen/Strep. Cells were maintained at viable cell density between 10-80% confluence by a twice-weekly split and used before passage 20.

2.4.1.5 THP1

THP1 cells were cultured in suspension in RPMI supplemented with GlutaMAX, 10% FCS and Pen/Strep. Cells were maintained at 0.5-1x10^6 cells/mL and used before passage 25. For dendritic cell differentiation, THP1 cells were cultured in the presence of 10 ng.mL^{-1} rhIL-4 (recombinant human interleukin-4) and 10 ng.mL^{-1} rhGM-CSF (granulocyte-macrophage colony stimulating factor) for 6 days. Cells were split on days 2 and 5 with addition of fresh cytokines. Both adherent and suspension cells were harvested for use on day 6 or 7.

2.4.1.6 U937

Monocytic U937 cells were propagated at 37°C under an atmosphere of 5% CO_2 in air using RPMI 1640 medium complemented with GlutaMAX, 10% FCS and Pen/Strep. Cells were maintained at viable cell density between 2x10^5 and 10^6 cells/mL by a three time a week split and used before passage 25.

2.4.2 Primary cells

Patient and healthy donors' samples were obtained with informed consent from the parents of the patient in accordance with the Declaration of Helsinki and with approval from local ethics committees (04/Q0501/119 and 06/Q0508/16).

2.4.2.1 Human neutrophil isolation

Neutrophils were isolated from healthy donor or patient blood. To sediment erythrocytes, 2 mL of a 5% dextran-saline solution was added to 10 mL of blood and gently mixed by inversion before let to sediment for 30 minutes. The plasma layer containing the granulocytes was collected and overlaid on an equal volume of Ficoll-Paque and centrifuged at 500 rcf for 10 minutes. After centrifugation, the neutrophils were pelleted at the bottom of the tube whereas the remaining PBMCs (monocytes and lymphocytes), basophils and platelets remained at the interface between the plasma layer and the Ficoll-Paque. It should be noted that during the collection of the plasma layer, erythrocytes may have inadvertently been collected at the same time, contaminating the neutrophil fraction. To ensure the absence of erythrocytes, an extra step was added in the protocol to lyse the potential remaining red blood cells: the neutrophil pellet was re-suspended in distilled water for 20 seconds to lyse the remaining red blood cells before addition of 2x saline solution to restore isotonocity. The neutrophils were then centrifuged at 250 rcf for 7 minutes and re-suspended in warm complete RPMI. When needed, the PBMC layer was taken before collection of the neutrophil pellet for CD14-positive cell selection.

2.4.2.2 Primary fibroblast

Skin fibroblasts from healthy donors were collected and provided by Dr Farhatullah Syed. The cells were cultured in RPMI 1640 medium supplemented with 10% FBS and Pen/Strep. Cells were maintained at viable cell density between 10-80% confluence by a twice-weekly split and used before passage 10.

2.5 Lentiviral production, cell transduction and cell transfection

Second generation lentivirus were produced by co-transfection of 293T cells with 1) the packaging plasmid pCMV 8.74, which contained the gag-pol, tat and rev genes, 2) the envelope plasmid pMD.G2 containing the insert for the VSVg envelope, and 3) the plasmid containing the gene of interest.

2.5.1 Lentiviral production

293T cells were expanded in 15 cm culture plates. The day before transfection, 15 million cells were seeded in cell culture plates. On the day of transfection, a PEI solution was prepared by diluting the stock solution (10 mM) into Opti-MEM to reach a final concentration of 2 μM. A DNA solution was prepared to contain a mix of the packaging (pCMV 8.74 at 6 $\mu g.mL^{-1}$), envelope (pMDG-2 at 2 $\mu g.mL^{-1}$) and gene of interest (8 $\mu g.mL^{-1}$) plasmids. Both PEI and DNA solutions were filtered through 0.22 μm filter before being mixed in a 1:1 ratio and left at room temperature to let the PEI-DNA complexes to form. Cell culture medium was removed and cells were gently washed with PBS, prior addition of 10 mL of the PEI-DNA solution. Alternatively, the PEI-DNA solution was directly added to the plates without removing the culture medium with no observed changes on the final viral titer. Cells were incubated with the PEI-DNA solution for 4 hours at 37°C and 5% CO_2. Then the PEI-DNA solution was removed and fresh culture medium was added to the plates. Viral supernatant was collected 48 hours after transfection and replaced with fresh culture medium, which was harvested 24 hours later. Viral supernatant was filtered through a 0.22 μm filter to remove cell debris and then was concentrated by ultracentrifugation at 50,000 rcf for 2 hours at 4°C. Alternatively, viral particle concentration was performed by centrifugation at 4,000 rcf for 20 hours at 4°C. The viral pellet was resuspended in 100 μL of RPMI, incubated on ice for 30 minutes, and then centrifuged at 1,300 rcf for 10 minutes to remove cell debris before being aliquoted and stored at -80^{o}C.

2.5.2 Lentivirus titration

The titer of viral preparations was determined by measuring the transgene expression in 293T cells. 293T cells were seeded at $5x10^4$ cells per well in 900 μL of culture medium in a 24 well plate. The day after, viral aliquots were thawed and $1:10^3$, $1:10^4$ and $1:10^5$ serial dilutions were prepared in 1 mL of complete medium. Then, 100 μL of diluted viral preparation was added to the cells to reach a final $1:10^4$, $1:10^5$ and $1:10^6$ dilution factors. Cells were incubated at 37°C and 5% CO_2 for 72 hours before the medium was removed, washed with PBS, and then incubated with 100 μL trypsin-EDTA for 5 minutes at 37°C and 5% CO_2. Cells were fixed and the transgene expression (tagged with a fluorescent protein such as GFP or mCherry) was determined by flow cytometry (see below). The

viral titration was calculated using the sample displaying 3 to 10% fluorescent positive cells and using the following formula:

$$Titer = \frac{(\%\ \text{fluorescent positive cells})\ \text{x}\ (\text{number of cells seeded})}{\text{virus dilution}}$$

2.5.3 Cell transduction with lentiviruses

The amount of viral particles added to the cells was defined by multiplicity of infection (MOI). This number indicates the amount of viruses per cell added to the culture medium.

In order to transduce adherent cells, the cells were plated in a 12 wells plate at $1x10^5$ cells per well in 1 mL of culture medium and incubated at 37°C and 5% CO_2. The day after, the lentiviral aliquots were thawed and diluted into DMEM at a final volume of 200 µL before being added to the culture medium in the well. Cells were expanded before being used or enriched by fluorescence activated cell sorting (as specified in the text).

The first protocol used to transduce HL-60 cells was to plate $5x10^5$ cells in a 12 well plate and mix lentiviral particles with the cells at a MOI of 10 before placing the plate in an incubator at 37°C and 5% CO_2. This protocol led to low transduction efficiency with less than 15% of transduced cells. Spin-induction was then used for transduction to increase interaction between cells and viral particles. The original protocol, which consists in spinning cells together with lentiviral particles at 2,000 rcf for several hours at room temperature (van Til and Wagemaker, 2014), was modified to avoid damaging the HL60 cells. $5x10^5$ cells were plated in a well of a 12 well plate and supplemented with viral particles at a MOI of 10 before being centrifuged at 950 rcf for 20 minutes at room temperature. The cells were then placed into an incubator at 37°C and 5% CO_2. This protocol resulted in 75% positive HL-60 cells and was used for the transduction of the cells in suspension. Cells were expanded before being used or enriched by fluorescence activated cell sorting (as specified in the text).

2.5.4 HT1080 transfection using Lipofectamine 2000

The day before transfection, HT1080 cells were plated in a 24 well plate at $8x10^4$ cells per well in 0.5 mL of their growth medium without antibiotics. For each well, two solutions were prepared: the DNA

solution consisting of 0.8 µg of DNA diluted in 50 µL of OPTI-MEM I without serum and the Lipofectamine solution (1.5 µL of Lipofectamine 2000 in 50 µL of OPTI-MEM I without serum). Both solutions were left to incubate 5 minutes at room temperature before being combined and left to incubate for a further 20 minutes at room temperature to allow the DNA-Lipofectamine complexes to form. Then, 100 µL of DNA-Lipofectamine complexes were added to each well containing the cells. After 24 hours of incubation, the expression of the transgene-tagged with a fluorescent protein was checked by epifluorescence microscopy.

2.6 Gene expression analysis

2.6.1 Real time quantitative PCR

Total mRNA samples were prepared using the RNeasy Plus Mini Kit (Qiagen) accordingly to manufacturer instruction, using $1x10^6$ cells as starting material. Retro-transcription was performed using the cDNA Verso Kit (Thermo Scientific) accordingly to manufacturer's instructions.

Real time quantitative PCR was accomplished on an ABI PRIASM 7000 Sequence Detection System (Applied Biosystem). The reactions were performed using the following set of TaqMan probes and primers: Hs00159522_m1 (*MYH9*), Hs00252979_m1 (*MKL1*), Hs00364926_m1 (*MYLK*), Hs00697086_m1 (*MYL9*), Hs01060665_g1 (*ACTB*), Hs02758991_g1 (*GAPDH*) at a final concentration of 0.25 µM together with the Platinum Quantitative PCR SuperMix-UDG w/ROX (Life Technologies) and 30 ng of cDNA in a 25 µL reaction volume. Gene expression levels were normalised to the GAPDH gene and calculated using the ΔΔCt method.

2.6.2 qPCR Arrays

Retro transcription was performed accordingly to manufacturer instructions using the RT2 First Strand Kit (Qiagen, 330401) using 1 µg of total mRNA extracted from dHL-60 SCR or MKL1 cells. Then Real-time quantitative PCR was achieved on an ABI StepOnePlus Real Time PCR System (Applied Biosystem) using Human Cytoskeleton Regulators RT² Profile PCR Array and RT² SYBR Green ROX qPCR Mastermix (Qiagen, 330231 and 330520, respectively) accordingly to manufacturer's instructions. Gene expression levels were analysed using the Web-based PCR Array

Data Analysis Software (www.SABiosciences.com/pcrarraydataanalysis.php). Gene expression levels were analysed using the ΔΔCt method and the GAPDH gene as control gene. The ΔΔCt method allows the analysis of the expression of target genes relative to reference genes such as GAPDH, β-actin or other housekeeping genes. This method is based on the analysis of the measure of the amplification of the signal of each gene in the thermocycler. The Ct (cycle threshold) of a gene is the number of cycles needed for the signal of this gene to cross the threshold, *i.e*. to be discriminated from the background. The first step of the analysis is to calculate the relative gene expression (ΔCt) by subtracting the Ct of the reference gene from the Ct of the genes of interest. The relative gene expression was performed in the control sample (ΔCt_{ref}) and in the MKL1 knock-down sample (ΔCt_{MKL1}). Then the relative expression of the genes of interest between samples (ΔΔCt) was calculated by subtracting relative expression of the control sample (ΔCt_{ref}) from the relative expression of the MKL1 sample (ΔCt_{MKL1}). The fold change of the gene expression between samples was then calculated as follows: fold change = $2^{-\Delta\Delta Ct}$.

2.6.3 RNA sequencing analysis

RNA sequencing of the total mRNA isolated from control and MKL1 patient B lymphoblastoid cells was performed by S. Nejentsev's laboratory. The data were pre-processed, giving for each gene a basic *p*-value, an adjusted *p*-value and the z-score (enrichment score) of the differentially expressed genes from the MKL1 sample compared to the control. Functional annotation clustering analysis was performed using the DAVID Bioinformatics resources 6.7 software (Huang et al., 2009). The analysis was carried out using lists of the significantly differentially expressed genes ($p < 0.05$) for all control *vs*. MKL1 cells. Clustering was performed using a high classification stringency and only clusters with an enrichment score higher than 1.3 were considered and reported.

2.7 Protein expression analysis

2.7.1 Western Blotting

Cell lysates were obtained by incubating $1x10^6$ cells for 30 minutes at 4^oC in 50 µL of NP-40 based buffer containing protease/phosphatase inhibitor cocktail (Cell Signalling Technology) and PMSF

(Cell Signalling Technology). During lysis, samples were vortex every 10 minutes. Samples were then centrifuged at 13,000 rcf at 4°C for 10 minutes to remove cells debris. Supernatant was then collected and mixed in a 1:1 ratio with Laemmli sample buffer and boiled at 95°C for 5 minutes. Cell lysates were separated on 12-14% NuPAGE Bis-Tris gels loaded with 30 µL of sample per well. Fermentas PageRuler Prestained Protein Ladder was included as a size marker. Following transfer on a previously activated PVDF membrane, the membrane was then blocked with 5% milk/TBS-Tween 0.1% (TBS-T) solution before being incubated with the antibody at 1/1000 in 5% milk /TBS-T overnight. After incubation with the appropriate secondary antibody conjugated with HRP, the membrane was then developed with PIERCE ECL Western Blotting substrate and the images acquired using UVIchemi imaging system.

2.7.2 Western blot analysis by densitometry

The Western blot images acquired with the chemiluminescence imaging system were analysed using the Gel analysis function of ImageJ/Fiji. First, each lane was selected using the rectangular selection tool encompassing the signal of the proteins (bands) and background. Then the selections were plotted to generate the profile of intensity of each lane. On each profile, the proteic signal generated a peak (due to the change in intensity) that could be distinguished from the background. The absence of signal saturation was confirmed prior to quantification. Using the straight line selection tool, the baselines were drawn on the lane profiles in order to close the peaks of interest and separate them from the background. Finally, using the wand tool, the intensities of the peaks of interest were measured. This process was performed on Western blots incubated with an antibody raised against the protein of interest and on Western blots incubated with the antibody detecting the house keeping protein GAPDH (used as loading control). The relative expression of the protein to the level of expression of GAPDH was calculated by dividing the value of the peak intensity of the protein of interest by the measure of the intensity of the GAPDH peak.

Table 2-2: Antibodies and fluorescent dyes

Name	Description	Raised in	Conjugate	Manufacturer	Reference	Assay	Dilution
CD11b-PECy5	human CD11b	mouse	PE-Cy5	BD bioscience	555389	FC	10 µL/sample
CD18-PE	human CD18	mouse	PE	BD bioscience	555924	FC	10 µL/sample
CD29-PE	human CD29	mouse	PE	BD bioscience	555443	FC	10 µL/sample
CD49d-PE	human CD49d	mouse	PE	BD bioscience	555503	FC	10 µL/sample
PE-Cy5 Mouse IgG1	isotype	mouse	PE-Cy5	BD bioscience	555750	FC	10 µL/sample
PE Mouse IgG1	isotype	mouse	PE	BD bioscience	555749	FC	10 µL/sample
FPR1-APC	human FPR1	REA169	APC	Myltenyi Biotec	130-100-812	FC	10 µL/sample
REA-isotype	isotype	REA293	APC	Myltenyi Biotec	130-104-614	FC	10 µL/sample
pMLC	human phospho-MLC	rabbit	none	Cell Signaling Technologies	3671	WB/IF	1:1000 / 1:50
Vinculin	human vinculin	mouse	none	Sigma	V9131	IF	1:100
MKL1	human MKL1	rabbit	none	Sigma	HPA030782	WB	1:250
MKL1(sc)	human MKL1	goat	none	Santa Cruz	sc-21558	WB	1:500
anti-goat HRP	goat	donkey	HRP	Santa Cruz	sc-2033	WB	1:2000
anti-mouse HRP	mouse	goat	HRP	ThermoFisher	31430	WB	1:2000
anti-rabbit HRP	rabbit	goat	HRP	ThermoFisher	31460	WB	1:2000
GAPDH	human GAPDH	mouse	none	Sigma	G8795	WB	1:10,000
anti-mouse AF568	mouse	donkey	AF568	Invitrogen	A10037	IF	1:1000
anti-rabbit AF568	rabbit	donkey	AF568	Invitrogen	A10042	IF	1:1000
AF488-phalloidin	n.a.	n.a.	AF488	Molecular Probes	A12379	IF/FC	1:200
AF647-phalloidin	n.a.	n.a.	AF647	Molecular Probes	A22287	IF/FC	1:200
DAPI	n.a.	n.a.	n.a.	Sigma	D9542	IF	1:250

PE: Phycoerythrine; APC: Allophycocyanin; Cy5: Cyanines5; AF: Alexa-fluor; HRP: Horseradish peroxidase; IF: immunofluorescence; FC: Flow cytometry; WB: Western blotting; n.a.: not applicable.

2.7.3 F/G actin ratio

The F/G actin ratio was determined using the G-Actin/F-actin In Vivo Assay Biochem Kit (Cytoskeleton Inc., # BK037), following the manufacturer's instructions. Ten million cells were lysed in Lysis and F-actin stabilisation buffer supplemented with 1 mM ATP and protease inhibitors. The samples were homogenised by pipetting and the lysates were then incubated at 37^{o}C for 10 minutes. Then 100 µL of each sample was centrifuged at 350 rcf for 5 minutes at room temperature. The supernatants were transferred into new tubes and centrifuged at 100,000 rcf for 1 hour at 37^{o}C. The ultracentrifugation resulted in the pelleting of the F-actin while leaving the G-actin in the supernatant. The supernatants were gently collected without disturbing the pellets and transferred to new tubes. Each pellet was resuspended in 100 µL of F-actin depolymerisation buffer on ice for 1 hour. Then 25 µL of 5x SDS sample buffer was added to each supernatant and pellet samples and mix thoroughly. Finally 10 µL of each supernatant and pellet samples were run on a SDS-PAGE gel and analysed accordingly to the manufacturer's instructions using the anti-actin rabbit polyclonal antibody supplied in the kit.

2.7.4 Flow cytometry

For flow cytometry, cells were washed in PBS, fixed with 4% PFA for 15 minutes and permeabilised with 0.1% Triton X-100 solution for 5 minutes. Antibodies or phalloidin were added in PBS-BSA (1%) for 45 minutes, then washed and analysed. For mixed population samples, cells were harvested and stained for 20 minutes with CFSE (5 µM in PBS) accordingly to the manufacturer's instructions. Cells were then washed twice in serum free medium, mixed with the unlabeled population, fixed, permeabilised and stained as above. For each antibody used, the corresponding isotype control was selected. Isotype controls are negative control antibodies that are designed to measure the level of the non-specific primary antibody binding that is responsible for the background signal. To correctly assess the non-specific binding of the primary antibody, the isotype control must match the host species, the type of immunoglobulin and fluorochrome conjugation of the primary antibody used in the study.

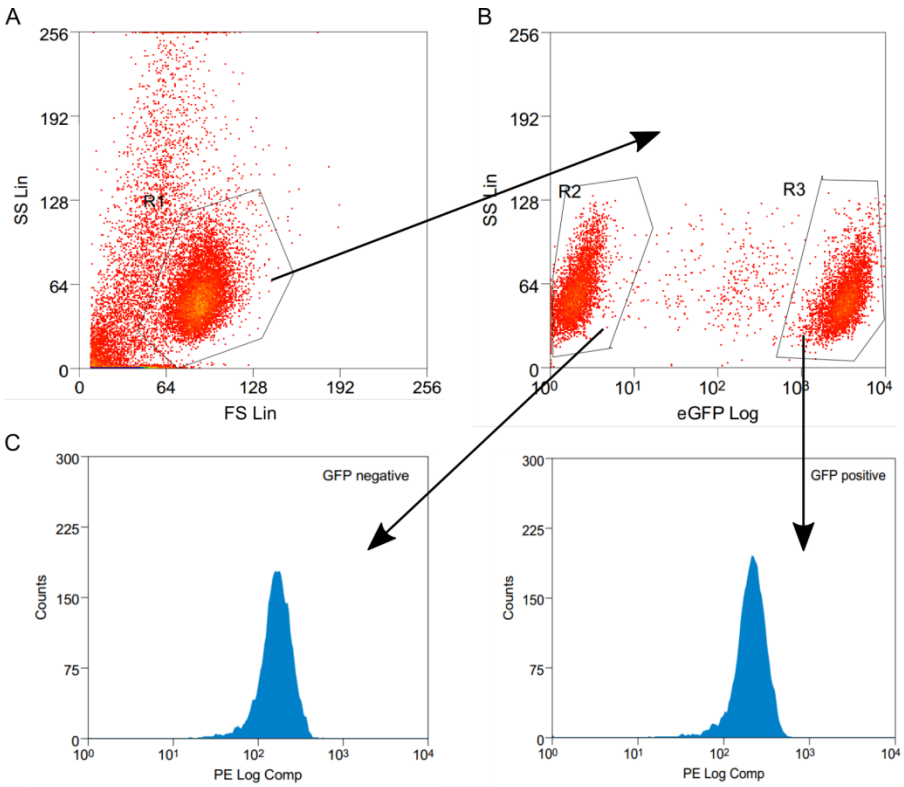

Figure 2-1: Flow cytometry gating strategy

A) Using the forward scatter (FS Lin) / side scatter (SS Lin) plot, a gate R1 was drawn to select the cell population of interest. B) The R1 gate was applied on the eGFP / SS Lin plot in order to visualise both negative and positive eGFP/CFSE populations which were selected by creating two new gates R2 and R3. C) The two gates R2 and R3 were then used to measure the signal of interest, here PE, of the unstained/eGFP negative and eGFP/CFSE positive cells.

All flow cytometry analysis was carried out on the Cyan ADP Analyser using the Summit 4.3 software (Beckman Coulter). For each experiment, unstained control, single stained samples and samples stained with isotype controls were prepared. The cells were gated using a forward scatter *vs.* side scatter plot (Figure 2-1 A). Before performing any analysis, the spectral overlap of the different dyes used in the experiments was corrected by using the compensation features of the Summit software. The compensation strategy was performed with all the dyes used in each experiment as follows (as an example, the compensation of GFP over PE is used): first an unstained control sample was run in order to establish the baseline signal. Then an unstained sample of cells expressing GFP was run. The PE signal of the GFP sample was then corrected to be similar to the unstained sample using the auto compensation feature of the software (the difference of the median of the PE signal between the unstained and GFP positive population must be < 1%). Once the compensation was setup, the analysis was performed as follows (as an example, the analysis of MKL1 *vs.* control undifferentiated HL-60 cells stained with an antibody conjugated with PE is used). The gate defined on the forward-scatter *vs.* side-scatter plot (Figure 2-1 A) was applied on the eGFP *vs.* side-scatter plot and the control (GFP negative) and the MKL1 KD (GFP positive) populations were gated (Figure 2-1 B). The two gates were applied on two PE histograms so the signal of the two populations could be measured (Figure 2-1 C).

2.8 Immunofluorescence

2.8.1 Confocal microscopy

For the staining of phosphorylated myosin light chain and actin cytoskeleton in neutrophil-like cells, dHL-60 cells were let to adhere on coverslips coated with fibronectin (100 $\mu g.ml^{-1}$) for 20 minutes. The coverslip was then gently washed to remove non-adherent cells. Cells were then uniformly stimulated with a solution of fMLP (final concentration 100 nM) for 2 minutes before fixation in 4% PFA for 20 minutes. The coverslips were washed with PBS, and the cells were then permeabilised with 0.1% Triton X-100 solution for 5 minutes. A 5% BSA solution was used to block the samples for 1 hour before incubation with the rabbit anti phosphorylated-MLC antibody (1/100) in 5% BSA for 1 hour. Coverslips were then washed three times with PBS

before incubation for 30 minutes with a solution containing the goat anti-rabbit secondary antibody conjugated with Alexa Fluor 647 (1/1000),Alexa 568-phalloidin (1/500) to stain F-actin and DAPI (4',6-diamidino-2-phenylindole) to stain the nucleus.

For analysis of podosomes, coverslips were coated with fibronectin (10 $\mu g.ml^{-1}$) for 1 hour at 37˚C or overnight at 4˚C. Coverslips were washed in PBS and primary DCs or THP1 cells were seeded for up to 2 hours at 37˚C. Once adhered, cells were fixed in 4% paraformaldehyde (PFA) for 30 minutes. Cell membranes were then permeabilised in 0.1% Triton X-100 for 5 minutes. Samples were blocked with 5% BSA in PBS for 20 minutes. Mouse anti-vinculin antibody was added at 1/100 dilution in PBS with 5% BSA for 1 hour at RT, followed by two 5 minutes washes. DAPI, Alexa Fluor 488-phalloidin and a secondary anti-mouse-Alexa Fluor 568 antibody (1/200) were added for 45 minutes. Washing was repeated and coverslips were mounted on glass slides using AquaPolymount. Images were acquired at room temperature on a Zeiss LSM 710 inverted confocal microscope using 40x (C-Apochromat NA 1.2, Water) or 63x (Plan-Apochromat NA 1.4, Oil) lens. Images were processed using FIJI (FIJI Is Just ImageJ) or Cell Profiler.

Controls:

When antibody staining were performed, secondary antibody staining alone were used as control to verify the specificity of the staining towards the protein of interest.

If drugs that perturbed the actin-myosin cytoskeleton such as CK-666 or blebbistatin were used, the control condition was the cells treated with the same concentration of the vehicle used to deliver the drug, *i.e.* if the cells were treated with a drug in DMSO diluted at 1/1000 in cell medium then the vehicle control was DMSO only diluted at 1/1000 in cell medium.

Image consistency:

Unless stated otherwise, for each experiment a minimum of three fields of view containing ≥ 10 cells each were acquired. Although image analysis was not performed in a blinded/double blinded condition, the images that were presented in figures for presentations or papers were chosen to be representative of the set of original images. To ensure objectivity, this was

confirmed by the visual inspection of the image presented and the original set of images by a colleague or supervisor.

2.8.2 Quantitative fluorescence microscopy

To quantify fluorescent signal from a confocal z-stack, a z-projection of the z-stack was created using the z-project (Addition) function and processed in Cell Profiler. For images containing a channel with nuclear staining such as DAPI, this channel was used to identify the nuclei as primary objects. The nuclei were then used as "seeds" to detect by propagation (either global or adaptive) the edges of the cells in the Actin channel (visualised by phalloidin staining). In the absence of nucleus channel, the Actin channel (phalloidin) was used to detect the cell edges using the Automatic threshold parameter. Regardless of the method used to detect the cell edges, all cells touching the boundaries of the image were automatically excluded from the analysis. Regions of interest for each cell were then created using the cells edges detected in the previous step. Then, the signal integrated intensity of the phalloidin or antibody staining was measured within the regions of interest. Background was not taken into account nor manipulated/subtracted during the analysis.

2.8.3 Phenotypes quantitation

Localisation of active myosin:

To differentiate the cells showing a low mCherry signal to the one highly expressing CA-WASp, the two populations were discriminated using the mCherry signal. All cells with a mCherry MFI higher than 3 times the value of the background were considered as high mCherry-CA-WASp expressing cells, while the cells with mCherry signal between 1 and 1.5 times the background signal were considered as having a low mCherry signal.

To study the activity of myosin in dHL-60 cells, the localisation of the signal of phosphorylated myosin (pMLC) staining was used. Using F-actin (phalloidin staining) confocal images, the lamellipodium and uropod of the cells were visually identified. The images of the F-actin and pMLC stainings, F-actin images were then used to visually score the pMLC cellular localisation as

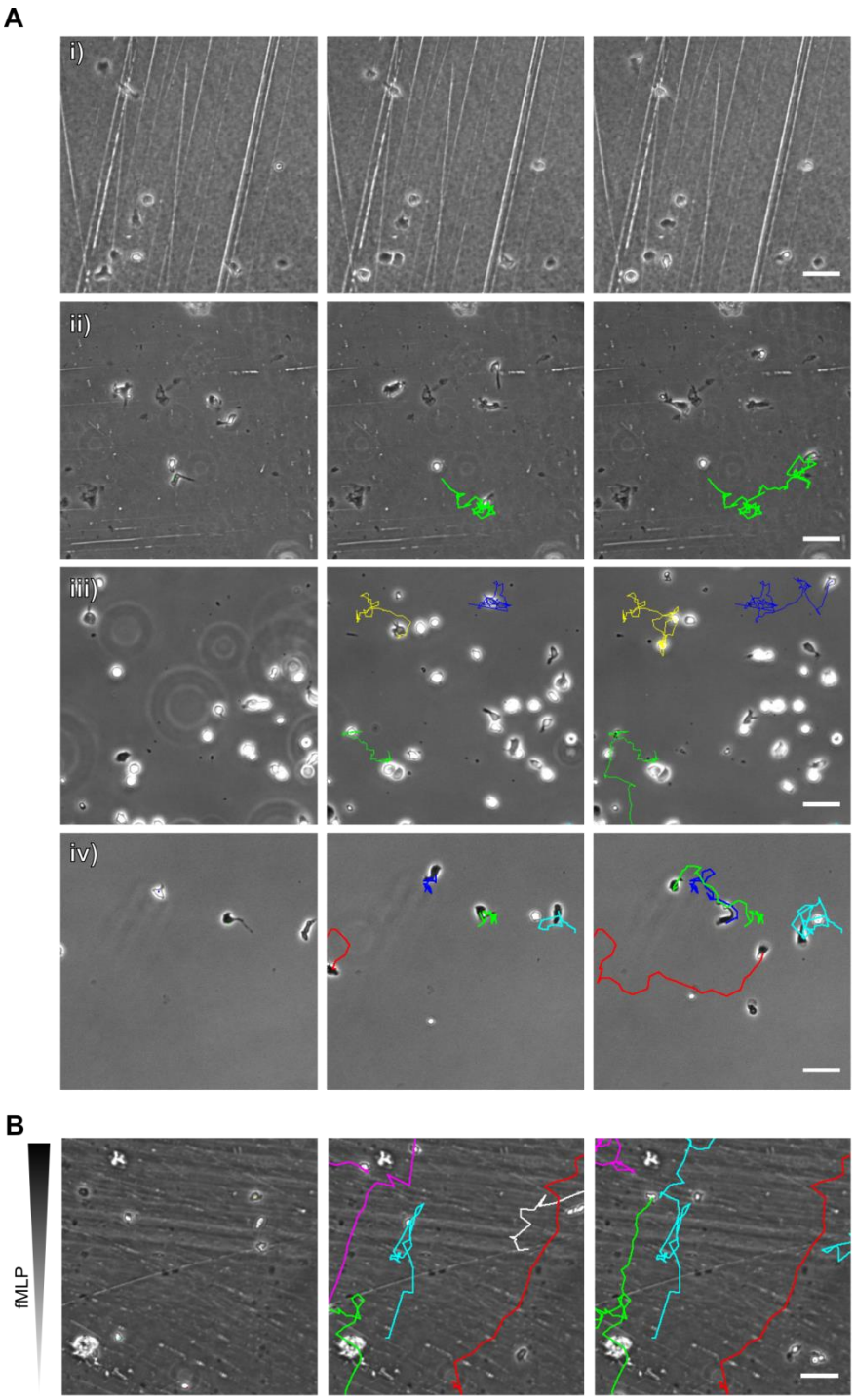

Figure 2-2: Development of the migration assay

A) Random migration of neutrophil-like cells (dHL-60 cells) on coverslips coated with solutions of i) fibrinogen at 1 mg.ml^{-1}, ii) fibrinogen at 100 µg.mL^{-1}, iii) 10% FCS and iv) 5% BSA. HL-60 cells were differentiated into dHL-60 cells by adding 1.3% DMSO in their culture medium for 5 days. Cells were then left to adhere 30 minutes before being stimulated with 200 nM of fMLP. B) Migration of dHL-60 cells in the agarose Dunn chamber. The coverslips were coated with a 100 µg.mL^{-1} fibronectin solution before being passivated with a 0.2% HAS solution. A and B: The experiments were used for optimisation of experimental conditions therefore three independent experiments were not performed. Data representative of two experiments. Scale bar = 50 µm.

predominantly in the lamellapodia, uropod, in both or neither structure. No ROI was used for this quantification. Each population was manually counted using the cell counter plug-in of imageJ/Fiji.

Uropod retraction and retraction fibres defects:

To quantify the extended uropods in dHL-60 cells and the retraction fibres in THP-1 macrophages, the F-actin confocal images of the cells were used. The dHL-60 cells with a thin uropod longer than the cell body were counted as “abnormally extended uropod”. In the THP-1 macrophages cells, the cells with more and longer retraction fibres (“hairy” phenotype) were counted as positive for a retraction defect. Cells were counted using the Cell Counter plug-in in ImageJ/Fiji in non-blinded conditions.

Cell mobility:

The number of motile cells was quantified using time-lapse images of cells migrating in the Dunn chamber. Cells that were migrating more than twice their diameter over the duration of the experiment were counted as motile. The determination of the motility was made visually and the cells counted using the Cell Counter plug-in of ImageJ/Fiji.

2.9 Cell Migration experiments:

2.9.1 Dunn chamber

Troubleshooting

To establish the Dunn chamber assay, the migration of primary neutrophils was first assessed using the protocol developed by Dr Bouma, a postdoc in the laboratory. The protocol described the coating of the coverslip using a solution of 10 $mg.mL^{-1}$ of fibrinogen and the different steps of the assembling of the Dunn chamber. HL-60 cells differentiated into neutrophil-like cells (dHL-60) were used as a model to study neutrophil migration. Using this protocol, the dHl-60 cells were not able to chemotax correctly:

- most of the cells were very active but unable to migrate, suggesting an adhesion too strong to allow the detachment of the cells.

- the few cells that were able to migrate did not migrate in the direction of the chemoattractant but showed a random migration pattern also known as chemokinesis indicating a possible failure in the establishment of the chemokine gradient.

To determine the conditions to allow the cells to adhere enough without impeding the migration, the dHL-60 cells were left to adhere on different adhesion molecules and then uniformly stimulated with fMLP at a final concentration of 200 nM. The cell chemokinesis was imaged at 37^{o}C for 1 hour at 1 image/minute using Axiovert 135 microscope, equipped with a Achroplan 10x/0.25 objective, an environmental chamber and a motorised stage. First lower concentration of fibrinogen of 1 mg.mL^{-1} (Figure 2-2 A i) and 100 µg.mL^{-1} (Figure 2-2 A ii) were used to coat the coverslip by immerging the coverslip in the fibrinogen solution for 1 hour at 37^{o}C before being washed three times with PBS. The cells were left to adhere 30 minutes and then imaged as described above. For both coating with 1 mg.mL^{-1} and 100 µg.mL^{-1} of fibrinogen, the cells adhered, spread but were unable to migrate suggesting an impaired detachment due to a strong adhesion. Then, the coverslips were coated with a solution of 10% FCS in RPMI medium using the same protocol as for fibrinogen (Figure 2-2 A iii). Numerous cells adhered but few cells spread and among them, less than 50% migrated. To reduce the cell adhesion strength, the coverslips were coated with a solution of 5% BSA in PBS (Figure 2-2 A iv). After 30 minutes of adhesion, a low number of cells adhered to the coverslip but most of them were able to migrate after stimulation with fMLP. A solution of 100 µg.mL^{-1} of fibronectin was then used to coat the coverslips before using a solution of 0.2% HSA to passivate the fibronectin coating (Figure 2-2 B). This method to coat the coverslip allowed a high number of cells to adhere with most of the cells migrating. The fibronectin coating passivated with 0.2% HSA gave satisfactory results and was then used to study dHL-60 cell migration.

The failure of the dHL-60 cells to migrate in the direction of the source of chemokine suggested a difficulty in the establishment of the chemokine gradient in the Dunn chamber. To assess the establishment of the gradient in the Dunn chamber, the outer well was either filled with a solution of 1 µg.mL^{-1} fluorescein or dextran-rhodamine in PBS or with an agarose gel

containing 1 µg.mL^{-1} of fluorescein whereas the inner well was filled with PBS only. The chamber was assembled and placed on an Axiovert 135 microscope, equipped with an Achroplan 10x/0.25 objective and a motorised stage. The imaging started 15 minutes after assembling the chamber due to the distance between the laboratory and the microscopy room, and one image of both the phase contrast channel and the FITC/TRITC channel were taken every 5 minutes during one hour or overnight. To analyse the gradient evolution over time, images recorded on the microscope were analysed using FIJI/ImageJ. Using the rectangular selection tool, a selection of 50 pixels wide and 350 pixels long was draw across the bridge (from the outer well towards the inner well) of the Dunn chamber on the phase contrast image. This selection was then duplicated on the FITC/TRITC image and the intensity of the fluorescence signal along the selection was plotted generating the profile of the fluorescein gradient over the bridge. The fluorescence profile across the bridge was plotted for different time points to determine the evolution of the gradient. As described in chapter 3, the use of FITC in the Dunn chamber showed the failure of the establishment of a gradient from the outer well to the inner well. To improve the establishment of the gradient, agarose was added to the outer well to act as reservoir and to allow the slow diffusion of the FITC over the bridge. Agarose was added to the outer well as follows: a 2x FITC solution (2 µg.mL-1) was mixed with a 2% agarose solution. After melting at a temperature > 90^{o}C, the agarose was left to cool to 37°C. This temperature was used to prevent the denaturation of the potential chemokines of interest for the experiments (here represented by FITC). Agarose was quickly mixed with FITC at 37°C and pipetted into the outer well of the chamber before gelation occurred at 36°C. To improve the process by allowing gelation at lower temperature, the molecular biology agarose was replaced with a low gelling temperature agarose that melted at temperatures > 65^{o}C and gelled between 26 and 30^{o}C. The low gelling temperature agarose was certified for cell culture to reduce the possible effect of impurities contained in the agarose on the cell migration. This low melting agarose together with the fibronectin coating of the coverslips allowed the development of the protocol described below.

Cell preparation:

dHL-60 cells were washed three times in a warm HBSS/2% HSA/100 mM HEPES solution. THP1 cells were washed three times in warm RPMI/1% FBS.

In some experiments, the two populations of interest (control and mutated) were mixed in a ratio 1:1 before being used in the Dunn chamber. This ensured that the cells were exposed to the same experimental conditions (extracellular matrix protein coating, chemoattractant gradient and chamber assembly). To distinguish the two populations, one of them was either expressing a GFP or mCherry tagged protein or stained with CFSE prior to the combination of the two populations as described in the flow cytometry section of this chapter. When CFSE was used, the staining was performed alternatively on the two populations: in one experiment, the control population was stained while in the other experiment, the population of interest was stained and the control left unstained.

Coverslips coating:

Depending on the cells used for the experiment, coverslips were coated with a solution of fibrinogen at 25 $mg.mL^{-1}$ (primary neutrophils), or with a solution of fibronectin at 100 $\mu g.mL^{-1}$ (dHL-60) or 10 $\mu g.mL^{-1}$ (THP1) for one hour at 37°C. The coverslips were washed twice with PBS before being used. Different extracellular matrix proteins for primary neutrophils and dHL-60 cells were used to obtain the appropriate adhesion of the cells on the coverslips. Protocols using fibrinogen to make primary neutrophils adhere on coverslips had previously been established (by Dr. Bouma and Dr. Burns from the laboratory), while following the evaluation of the suitability of various adhesion molecules described above, fibronectin was chosen to coat the coverslips in dHL60 migration experiments (Millius and Weiner, 2009). The need to use different extracellular matrix protein depending on the cells studied might be due to differences between primary neutrophils and neutrophil-like dHL-60 cells in their profile of integrin expression (Carrigan et al., 2005).

Cell adhesion:

$1x10^5$ neutrophils or dHL-60 cells were left to adhere on coated coverslip for 20 to 30 minutes. The coverslip was washed once with the medium used for the migration without chemokine to

remove non-adherent cells. $2x10^4$ THP1 cells were left to adhere for at least 2 hours in cell culture medium containing 1% of FBS, and the coverslip was washed with the same medium before use.

Chemokines:

A 100 nM fMLP solution was used for neutrophil/dHL-60 experiments. MIP-1α at 10 nM was used for THP1 migration.

Initial chamber assembly:

To setup the chamber, initially both wells were filled with control medium. Then the coverslip on which the cells had adhered was gently laid on the well ensuring that a narrow filling slit was left on the outer well. The coverslip was held on the chamber and excess medium was removed before sealing all coverslip edges with hot wax except for the filling slit. The outer well was then drained with a syringe and a needle before being refilled with the chemoattractant solution to create the chemoattractant gradient over the bridge. After removing the excess of solution on the glass slide, the filling slit was sealed with hot wax. The Dunn chamber was then placed on an environmentally-controlled microscope stage and was left idle for 15 minutes to allow gradient formation and temperature equilibration. Then cell migration was imaged over the bridge for one hour capturing one image per minute.

Chamber assembly in the agarose Dunn chamber set-up:

In order to stabilise the gradient in the Dunn chamber, 80 μL of a 1% agarose gel containing the chemokine was poured into the outer well of the chamber and let to polymerise for 2 minutes. The inner well was filled with 50 μL of the medium without chemokine, and the chamber was assembled by laying down the coverslip on which the cells were adhering. The chamber was then sealed with wax. Cells were the imaged at 37°C on an Axiovert 135 microscope, equipped with an Achroplan 10x/0.25 objective and a motorised stage, by capturing one image per minute during one hour for the neutrophil/dHL-60 or one image every 5 minutes for 4 hours for THP1 experiments, respectively.

Cell tracking:

To track the migrating dHL-60 cells on the movies created from the time-lapse imaging of the Dunn chamber, the Manual Tracking plug-in from ImageJ/Fiji was used. The following imaging parameters were entered in the plug-in: time interval: 1 minute, x/y calibration: 1.03093 µm, z calibration: 0.0 µm, search square size for centering: 5.0, dot size: 5.0, line width: 2.5, font size: 18. The cells were then tracked by clicking on each cell on each image of the movie following one cell at a time over the successive frames. The results were saved in an Excel file that was then processed as described below.

Analysis:

The cell tracking results were collected as a single text file containing all tracks one after each other with one measure per column: Track number, slice number, position X of the cell, position Y of the cell, distance, velocity, and pixel value. X and Y positions, distance and velocity are the four parameters required to do a minimal characterisation of the migration of each cell since they allow to calculate migration direction and speed. A Matlab routine was developed to automatically extract each track from the file and separately copy it into a database to allow easy and fast data processing (Figure 2-3-A). From the four initial parameters measured by the Manual tracking plug-in, several other parameters were calculated using the MatLab routine (Figure 2-3-B and C):

- A cell track is composed of n positions $(p_1, \dots, p_n)$, with each position p_i defined by its coordinates (x_i, y_i) where x is the coordinate along the horizontal axis (or x axis) of the image, y the coordinate along the vertical axis (or y axis) of the image and i the index of the position with $1 \leq i \leq n$.
- The instantaneous velocity: this parameter is calculated by the ImageJ/Fiji plug-in Manual tracking. The instantaneous velocity is defined as the distance between two successive positions divided by the time interval between the two successive positions, $v_i = d(p_i, p_{i+1})/\Delta t$.

- The mean velocity: the mean velocity of each cell was calculated by averaging the instantaneous velocities of the cell, $\bar{v} = (1/n)\sum_{i=1}^{n} v_i$.
- The total distance that each cell travelled was computed by adding all the distances between the successive positions during the migration: $d_{tot} = \sum_{i=1}^{n-1} d(p_i, p_{i+1})$
- The net distance, was defined as the direct distance between the starting and the ending point of the cell path, $d_{tot} = d(p_i, p_n)$.
- The Chemotactic Index: this parameter was determined from the net distance to total distance ratio: $CI = d_{net}/d_{tot}$. This parameter represents the directionality of the migration with a value of one indicating a migration in a straight line and a value close to zero indicating a random migration. Because it does not integrate any reference point, the chemotactic index does not indicate the ability of cells to specifically respond to the chemoattractant source.
- The instantaneous angle: for each time point the instantaneous angle between the gradient and the direction of the cell, $\alpha_i = \tan^{-1}(y_{i+1} - y_i/x_{i+1} - x_i)$ was calculated to ensure that the directionality of the cell migration is in the direction of the chemoattractant. By plotting the frequency distribution of instantaneous angles, a deviation of the cells from the chemoattractant could be determined.
- The angle variation: this parameter is defined as the difference between two angles, $\gamma_i = \alpha_{i+1} - \alpha_i$ and shows the angular variation between two successive migration positions. This allows to evaluate the persistence of cell migration: an angular variation of zero indicates that the cell does not change direction from the previous time point.
- The mean angle is the mean of the instantaneous angle values for each cell to simplify the graphical representation of the instantaneous angles and is calculated as follows, $\bar{\alpha} = \tan^{-1}(\sum_{i=1}^{n} \sin\alpha_i / \sum_{i=1}^{n} \cos\alpha_i)$. Indeed, when the frequency distribution of the instantaneous angles of a high number of cells is plotted, a high number of values in one direction can dominate over rare behaviours from other cells (Figure 2-3-C).

A

Track #1

	Track n°	Slice n°	X	Y	Distance	Velocity	Pixel Value
1	2	1	89	578	-1	-1	528
2	2	3	96	573	-8.868	-0.296	324
3	2	5	102	572	-6.271	-0.209	330
4	2	7	100	577	5.552	0.185	380
5	2	9	104	580	5.155	0.172	344
6	2	11	104	586	6.186	0.206	320
7	2	13	102	593	7.505	0.25	321
8	2	15	92	593	10.309	0.344	330

Track #n

3206	29	221	326	149	5.155	0.172	288
3207	29	223	326	155	6.186	0.206	280
3208	29	225	324	162	7.505	0.25	316
3209	29	227	323	166	4.251	0.142	313
3210	29	229	324	170	4.251	0.142	284
3211	29	231	326	175	5.552	0.185	316
3212	29	233	325	178	3.26	0.109	324
3213	29	235	326	185	7.29	0.243	283
3214	29	237	328	190	5.552	0.185	309
3215	29	239	327	194	4.251	0.142	300
3216	29	241	326	198	4.251	0.142	458

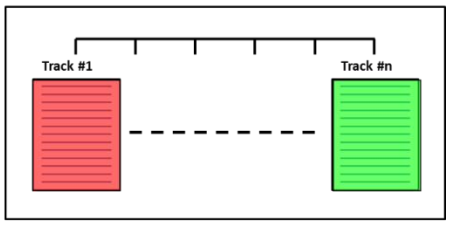

B

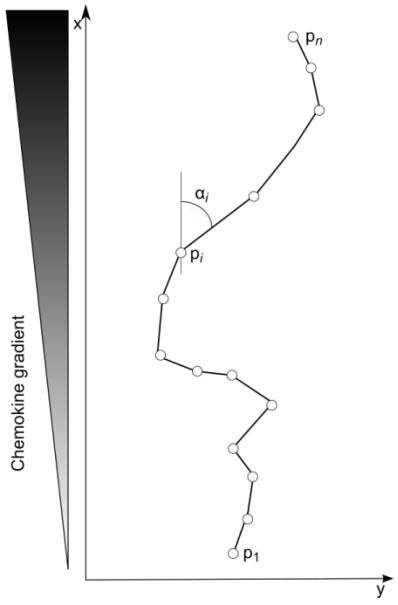

C

Parameter	Definition
Instantaneous speed	$v_{i=} \frac{d(p_i, p_{i+1})}{\Delta t}$
Mean speed	$\bar{v} = \frac{1}{n-1} \sum_{i=1}^{n} v_i$
Total distance	$d_{tot} = \sum_{i=1}^{n-1} d(p_i, p_{i+1})$
Net distance	$d_{net} = d(p_1, p_{n)}$
Chemotactic index	$CI = \frac{d_{net}}{d_{tot}}$
Instantaneous angle	$\alpha_i = arc\tan(\frac{y_{i+1} - y_i}{x_{i+1} - x_i})$
Angle variation	$\gamma_i = \alpha_{i+1} - \alpha_i$
Mean angle	$\bar{\alpha} = arc\tan(\frac{\sum_{i=1}^{n} \sin(\alpha_i)}{\sum_{i=1}^{n} \cos(\alpha_i)})$

Figure 2-3: Data processing and migration parameters

A) The manual tracking of the cells using the ImageJ plugin generates a unique result file containing the position of each cell at each time point. All these results are sequentially ordered within the file with no separation between the results from different cells. The MatLab routine then reads the result file from the tracking and organises the results in a set of tables with each table containing the data from only one cell. B and C). The MatLab routine then processes the data and for each track calculates the mean speed, the chemotactic index, the instantaneous angle, the angle variation, the total and the net distances and the mean angle.

2.9.2 Transwell migration:

To study dHL-60 migration in Transwell inserts, 24 well inserts with a pore size of 3 µm (BD Falcon #: 353096) were used. The inserts were first placed in the wells of the Companion plate (BD Falcon #: 353504) and were then coated with a fibronectin solution (100 $\mu g.mL^{-1}$) for 1 hour at 37°C before being washed three times with HBSS. Then, 1.2 mL of the chemoattractant solution (100 nM fMLP in HBSS/2% HSA/100 mM HEPES) was pipetted in the wells without removing the insert in order to avoid the formation of bubbles underneath the insert membrane. The dHL-60 cells were counted, washed twice with HBSS and resuspended in HBSS/2% HSA/100 mM HEPES at a concentration of $1x10^6$ cells/mL and then $4x10^5$ cells were seeded in the insert. The lids were placed on the plates and the plates were incubated at 37°C for the indicated time. Then, in order to detach the cells loosely adherent to the insert membrane or to the well plastic, 15 µL of a 0.5 M EDTA solution was added in each well and the plates were incubated at 4°C for 15 minutes. The inserts were then carefully removed and the cells in the well gently resuspended by pipetting and then counted using a haemocytometer. Each condition studied was run in triplicate on the plate.

2.9.3 Fibroblast migration

Fibroblast migration was monitored using the Oris cell migration assay (Platypus Technologies, CMA1.101). After sealing the Oris Cell Seeding Stoppers in each well, 40,000 cells were seeded in each well and left to adhere for 24 hours. The cell seeding stoppers were then gently removed, the cells were washed twice with PBS, and fresh medium was added. Cell migration was then monitored at 37°C for 18 hours with an Achroplan 10x/0.25 objective mounted on an Axiovert 135 time-lapse microscope equipped with a motorized stage. One image was captured every 15 minutes. Migration was quantified by measuring the area invaded by the cells using the ImageJ/Fiji software.

2.10 Fluorescence Time-Lapse Imaging of eGFP-CENPA HT1080 cells

2.10.1 Generation of HT1080 cells stably expressing eGFP-CENPA

The peGFP-N1 vector containing the eGFP-CENPA insert under CMV promoter and a neomycin/kanamycin resistance gene was provided by Dr Guillaume Charras. HT1080 cells were transfected using Lipofectamine 2000 as described in the 2.5.4 section of the chapter. Briefly, 0.8 µg of EGFP-CENPA vector were diluted together with 1.5 µL of Lipofectamine 2000 in OPTI-MEM I medium without serum. The solution containing the vector DNA complexed with the Lipofectamine was added on $8x10^4$ HT1080 cells for 24 hours before being replaced with fresh culture medium containing 1 $mg.mL^{-1}$ of G418/Geneticin. The cells were kept in culture with medium containing 1 $mg.mL^{-1}$ of G418 for two weeks before being sorted by FACS on a MoFlo XDP cell sorter (Beckman Coulter). Only the cells displaying a high eGFP signal were single cells sorted in 96 well plates containing conditioned medium (50% fresh culture medium and 50% medium from HT1080 cells cultivated for 3 days) supplemented with 1 $mg.mL^{-1}$ of G418/Geneticin. After the sort, the cells were kept in culture for 10 days before the 24 brightest clones were visually selected and transferred in a 48 well plate. The selected clones were left to grow in conditioned medium with G418 for 24 hours before the medium was changed for fresh culture medium containing G418. After a week, the 5 brightest clones were visually selected and transferred in a 6 well plate. After a week, each of the clones was transferred in several 10 cm petri dishes to expand the cells and freeze several aliquots. Cells from each clones were plated on coverslips, fixed and mounted using ProLong Gold mounting medium before being imaged by confocal microscopy using the 488 nm laser at the same intensity for all clones.

2.10.2 Imaging of kinetochore oscillations

To image kinetochore oscillations, HT1080 cells expressing eGFP-CENP-A were transduced using lentiviruses to express mCherry, mCherry-WASp wild type and mCherry-CA-WASp. The expression of the three different transgenes was driven by the CMV promoter. Five different conditions were imaged in this experiment: untransduced HT1080 and HT1080 expressing

mCherry alone as controls; HT1080 cells expressing mCherry WASp wild-type, or mCherry-CA-WASp treated or not with the ARP2/3 inhibitor CK666.

First, $2x10^5$ cells were seeded in glass-bottom dishes (FluoroDish, WPI) in 2 mL of DMEM supplemented with 10% FCS and Pen/Strep. Then, six hours after seeding, the attachment of the cells to the dishes was visually confirmed by microscopy and the medium was replaced with imaging medium (D-MEM medium without red phenol complemented with GlutaMAX, 10% FCS and 25 mM HEPES). Twenty-four hours after seeding, the cells were imaged using a 100×/1.4 NA oil objective lens on a Olympus IX81 microscope fitted with a 37°C environmental chamber and equipped with Andor iXon3 DU 897-BV camera and with an Andor Spinning Disk confocal microscopy system. Cells in metaphase with the chromosomes aligned on the equatorial plan were captured using a z-stack composed of 20 z sections (0.5 μm apart) every 7.5 s for 5 min.

2.10.3 Analysis of the oscillations of kinetochores (Kymograph)

The movements of the kinetochores were analysed using imageJ/Fiji. The z-stack produced by the imaging of the kinetochores was open in ImageJ/Fiji. Then, using the rectangular selection tool, a selection containing a pair of kinetochores was created. Using the Duplicate function, 3 z planes containing the selection were duplicated resulting in a new z-stack of 3 z planes restricted to the selection containing the pair of kinetochores of interest. A z-projection of the new z-stack was created using the z-project (Maximum Intensity) function. Using the Montage function, each image of the new z-stack was put one after each other as one column creating a kymograph (a *x*-*t* scan). The oscillation of the kinetochore pair was then visible on the kymograph and the amplitude, period and speed of the kinetochore oscillation could be analysed.

2.11 Statistical analysis

Unless otherwise stated, the statistical power of the experiments presented in this thesis was assessed by unpaired t-test with two-tailed *p*-value. The normality of the distribution of the values was tested using the D'agostino and Pearson normality test.

A one-way ANOVA was used to test the statistical power of three or more conditions with only one parameter measured. The ANOVA test was used together with a Tukey post-test in order to compare all the conditions to each other and determine the significance of the variation between each condition.

The F-test was used to analyse the variance of the distribution of the angles between the gradient of fMLP and the migrating cell path of the dHL-60 control and CA-WASp cells. The distribution of the angles between the chemoattractant and the migrating control cells seemed to be more dispersed than the distribution obtained for the CA-WASp cells. Therefore, the variance of the distributions between the two populations was compared using the F-test. The null hypothesis of the test is that the variances of the two populations are equal. As the test evaluates the ratio of the variances of the two populations, if the variances are equal, then the ratio = 1. The F-test was performed using the vartest2 function in Matlab.

All statistical analyses, with the exception of the F-test, were performed using GraphPad Prism 5.0. Presentation of significance in figures was as follows: * = p-value < 0.05, ** = p-value < 0.01, *** = p-value < 0.001. Unless stated otherwise, data are represented as the mean +/- standard deviation. The number of measurements and independent experiments are stated in the figure legends.

Chapter 3 Cell migration in the Dunn chamber

3.1 Introduction

Cell migration is fundamental process needed for the development of multi cellular organism and its maintenance. Cells migrate in a specific direction in response to a specific chemical or mechanical stimulus in order to complete a define task. Some well-studied examples of processes relying on migration include the movement of cells throughout the embryo during development, the migration of metastatic cells towards a growth factor source or the migration of neutrophils towards the infection site in order to clear it from pathogens. Dysfunction in the chain of events that regulates the process of migration can lead to several pathologies such as metastatic cancer or primary immunodeficiency. To study migration, several tools exist and the correct one will be chosen depending on the question asked. Two types of experimental setups exist: those which do not allow direct visualisation of the cell nor the chemoattractant gradient called indirect assays, and those which allow direct visualisation of the cells and the gradient using a microscope that are defined as direct assays.

The Boyden/Transwell chamber is maybe the most common indirect assay. It consists of two chambers separated by a porous membrane. One of the chambers contains the cells and the other one the solution of chemoattractant. The chemoattractant will diffuse through the pores of the membrane into the chamber containing the cells, establishing a gradient of molecules that cells will follow. After a specific and usually long time, between 1 to 4 hours, the number of cells that successfully migrated through the pores of the membrane will be counted and the chemotaxis in response to the chemoattractant will be calculated. This assay is very useful to study several conditions in the same time and so is well suited for screening chemoattractants or migration inhibitors. However, because it is an indirect assay, it only allows an estimation of the chemotaxis and does not allow direct observation of cell migration. As cells migrate through the membrane pores, they obstruct these pores modifying the local gradient of chemoattractant which can further be dependent on unknown flow conditions making difficult to know the nature and concentration of the gradient. The Boyden/Transwell assay is a convenient and

sensitive tool to study cell migration but to study the chemotactic response to a gradient of chemoattractant, the direct visualisation of the cells is required.

The first tool available for direct visualisation of cell chemotaxis was the Zigmond chamber (Figure 3-1-A) and was used to study neutrophil migration in a shallow gradient. The chamber consists of a plexiglass slide in which two wells separated by a bridge have been cut. A coverslip on which the cell adhered is maintained on the slide using springs and the wells are filled with a control solution and a chemoattractant solution. The small space between the surface of the bridge and the coverslip allows the chemoattractant to diffuse towards the well that contains the control solution. Cells sense this gradient and migrate in the direction of the well filled with chemoattractant. Migration is observed and recorded on a microscope allowing a direct visualisation of cell chemotaxis. This setup is very good to study cell chemotaxis but the variation of the gap over the bridge and the deformation of the chamber due to the use of springs that are thermosensitive are responsible for variations in the gradient.

The Dunn chamber was first described to study the migration of fibroblasts and neutrophils (Zicha et al., 1991). This system revealed that fibroblasts display a very low velocity of around 1 $\mu m.min^{-1}$ whereas the leukocytes have previously been shown to migrate at a speed of up to 30 $\mu m.min^{-1}$. The chamber consists of a standard glass slide of 1 mm thickness in which two concentric ring-shaped wells were drilled (Figure 3-1-A). The bridge between the inner and outer wells was polished so the surface of the bridge laid 20 µm below the surface of the slide (Figure 3-1-B). Therefore, when the wells are covered with the coverslip, on which the cells adhere, there is a gap of 20 µm between the coverslip and the bridge surface. The inner well is filled with control medium and the outer well with a solution containing the chemoattractant. The gap over the bridge allows the diffusion of chemoattractant from the outer well to the inner well so that a linear gradient is established and maintained during several hours (Figure 3-1-B). To get around the gradient variation in the chamber, the authors designed the chamber so no string or other metallic part are used and they used thick #3 (0.25 – 0.35 mm) coverslips to reduce its sensibility to change of temperature that would result in variations in the

gap over the bridge. The Dunn chamber was designed to establish very stable gradient that fibroblasts, due to their low speed, necessitate to establish a good chemotactic response. Zicha *et al*. showed that this allowed the formation of a gradient that was stable over a period of 96 hours (Zicha et al., 1991).

The Insall chamber is a new chamber derived from the Dunn chamber. It consists of a square inner well surrounded by the outer well. On two faces of the inner well, two coverslip supports stand to avoid any deformation of the coverslip that could crush the cells or modify the gradient. Two bridges of different widths close the inner well: one 0.5 mm and one 1 mm width bridges which provide different gradient steepnesses (Figure 3-1-A). The chamber also includes two loading wells to easily change the medium in the outer well. This new chamber has a promising design that is well suited to study cell chemotaxis (Muinonen-Martin et al., 2010) and has recently been used in several studies (Phillips and Gomer, 2012; Roberts et al., 2015; Sapey et al., 2014, 2011).

I chose to use the Dunn chamber to study neutrophil migration because it has been shown to allow the establishment of chemoattractant gradient and neutrophils have been shown to chemotax in this chamber. Furthermore, the Dunn chamber is a well-known setup to study cell migration and is re-usable since it is made of glass.

To investigate neutrophil migration, I used the human promyelocytic leukemia HL-60 cell line that can be differentiated into neutrophil-like cells, called dHL-60 (Figure 3-2-A and B). The differentiation was achieved by culturing the cells for 5-6 days in their culture medium complemented with 1.3% DMSO (Millius and Weiner, 2010). When compared to primary human neutrophils, the dHL-60 cells displayed a similar migrating response towards the chemotactic peptide fNLPNTL, an fMLP analogue, but a very poor response to IL-8 (Hauert et al., 2002), making the dHL-60 a good model to study neutrophil migration when formyl peptides such as fMLP are used as chemoattractant.

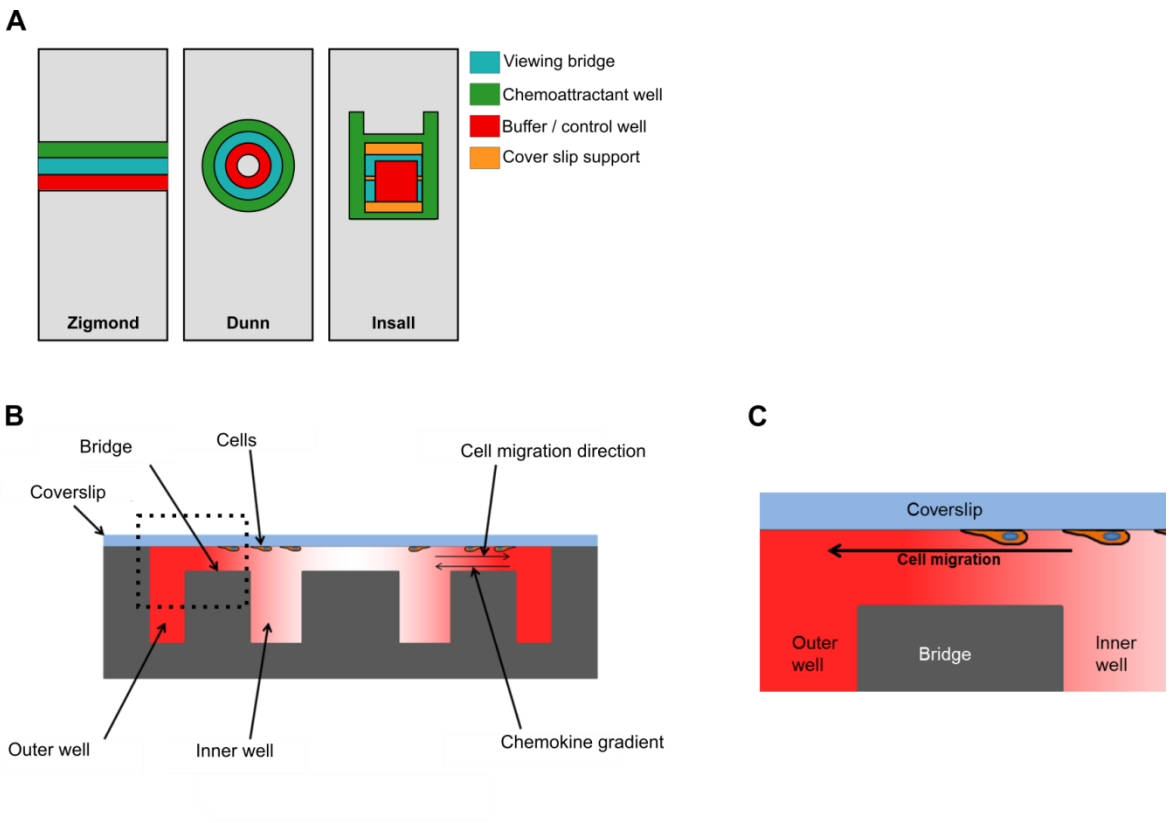

Figure 3-1: Chambers for direct visualisation of chemotaxis

A) Schematic representation of the Zigmond, Dunn and Insall chambers. The Zigmond chamber is composed of two wells separated by a bridge, one well is filled with medium while the other well is filled with medium containing the chemoattractant. The coverslip on which the cells adhere will be laid on top of the chamber, creating a small gap between the bridge and the coverslip that will allow the formation of a gradient of chemoattractant. The Dunn chamber was built by drilling two concentric rings separated by a bridge. The inner well is filled with medium and the outer well is filled with medium containing chemoattractant. The diffusion of the chemoattractant over the bridge from the outer well to the inner well creates a gradient of chemoattractant that will be followed by the cells. The Insall chamber is composed of an inner well surrounded by a bridge and an outer well. The bridge has two different widths to allow the creation of chemoattractant gradients with different steepnesses. B) Profile view of the Dunn chamber. C) Inset of the view over the bridge delimited by the dotted square in B).

3.2 Results

To investigate neutrophil migration, I decided to use the Dunn chamber as it allows a direct visualisation of the cells during migration and this assay is commonly used to study migration. I first defined the conditions adapted for the migration of primary neutrophils and dHL-60. Both cell types respond well to 100 nM of fMLP and only differ in the extra-cellular matrix protein used to coat the coverslip: I used fibrinogen for the primary neutrophils and fibronectin for the dHL-60 cells. In these conditions, I was able to observe that the cells randomly migrated in all directions but not towards the fMLP gradient suggesting a failure of chemotaxis (Figure 3-2-C). The presence of random migration indicated that the migration conditions allowed cells to move without adhesion problems but the absence of chemotaxis suggested a problem in sensing the gradient. To evaluate if the gradient was well established and maintained in our imaging conditions, I firstly identified the gradient characteristics using 70 kDa rhodamine-dextran This experiment showed a quick establishment of the gradient as described in the original Dunn chamber paper. Nevertheless, since fMLP is a small molecule (437 Da), I also tested the establishment of the gradient with a solution of FITC (360 Da). Surprisingly, there was no establishment of a FITC gradient with a steep slope over the bridge. Instead, a gradient was observed only in the first 20 µm adjacent to the outer well, followed by a uniform distribution over the rest of the bridge (Figure 3-2-D), explaining the absence of chemotaxis during dHL-60 migration. The difference in gradient formation between the rhodamine-dextran (70 kDa) and the FITC (360 Da) might be due to the important difference of size of the two molecules. Indeed, the diffusion coefficient is higher for molecules of small size resulting in a faster diffusion of FITC over the bridge and therefore a faster uniformisation of the concentration between the two wells and the absence of gradient.

To allow the establishment of a gradient of small-sized molecules such as fMLP and FITC in the Dunn chamber, I decided to slow down the quick molecule diffusion from the outer well over the bridge. To do so, I decided to pour an agarose-gel containing FITC into the outer well to slow down the diffusion in the outer well (Figure 3-3-A).

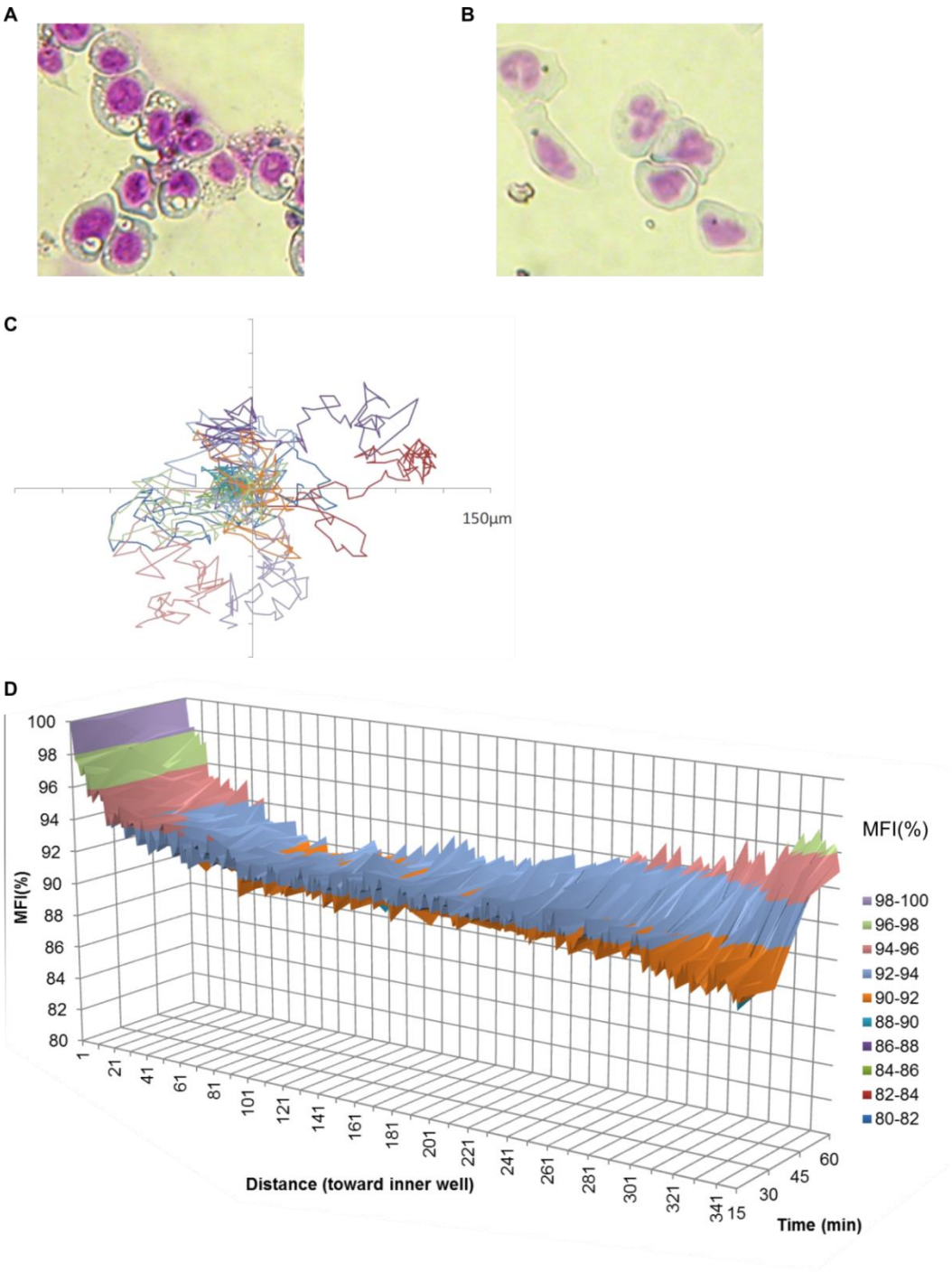

Figure 3-2: Cell migration in the Dunn chamber

A and B) Cytospin of HL-60 cells and dHL-60 cells respectively. HL-60 cells were differentiated by adding 1.3% DMSO in their culture medium for 5 days. Cells were stained using the Diff-Quick staining. C) Tracks of 12 dHL-60 cells migrating during 60 minutes in the Dunn chamber, imaged at 37^{o}C at 1 image/minute using an Axiovert 135 microscope, equipped with an Achroplan 10x/0.25 objective, an environmental chamber and a motorised stage. Cells were tracked using the ImageJ manual tracking plug-in and plotted in Excel. D) FITC gradient stability in the Dunn chamber over 60 minutes. FITC (1 µg.mL^{-1}) was loaded into the outer well of the Dunn chamber and the Dunn chamber was imaged at 37^{o}C at 1 image/minute using an Axiovert 135 microscope, equipped with an Achroplan 10x/0.25 objective and an environmental chamber. The FITC signal was quantified using ImagejJ using a rectangular selection of 50 pixels of width that stretched from the inner well to the outer well. A-D: The experiments were used for optimisation of experimental conditions therefore three independent experiments were not performed Data representative of two independent experiments, one replicate per experiment.

The use of the agarose gel in the outer well did not allow us to setup the Dunn chamber as it has been described before so I defined a new protocol to setup the chamber.

I first melted the 2% low gelling-temperature agarose gel at 75^{o}C for 45 min and then let it cool down at 37^{o}C. I mix, in a 1:1 ratio, the agarose gel with a solution of FITC previously warmed at 37^{o}C, resulting in a FITC-loaded 1% agarose gel solution. I immediately poured 80 µL of this agarose gel in the outer well of the Dunn chamber taking care of not spilling gel on the bridge or within the inner well. I let the gel to set for 2 minutes and then filled the inner well with 60 µL of control medium. I then closed the chamber with the coverslip, which allows control medium to flood the gap over the bridge, and I sealed the chamber by applying wax on the coverslip four edges (Figure 3-3-A). Then, I imaged the formation of the FITC gradient over the bridge using the same microscope setup and imaging conditions as previously described. Using this modified system, I could observe the formation of a gradient from the outer well to the inner well within 15 minutes: At this time point, the FITC concentration at the inner-well edge was between 30 to 50 % of the concentration at the outer-well edge (Figure 3-3-B). I could observe very little change in the gradient over one hour after the setup of the chamber. I tested the stability of the gradient over longer periods of time and I could observe that, within a 100 µm distance from the inner well, FITC concentration remained stable for 6 hours with 40-50 % of the maximum concentration and then increased to 50-60%. The middle region of the bridge displayed a low but noticeable increase in FITC concentration over time and the 100 µm-wide zone adjacent to the outer well showed virtually no change in concentration (Figure 3-3-C). The use of FITC-loaded agarose gel in the outer well of the Dunn chamber allowed the formation of a gradient between the outer well and the inner well and appeared suitable to reliably monitor neutrophil migration towards a gradient of fMLP.

Then, I tested if neutrophils migrating in the agarose Dunn chamber showed a chemotactic response. The outer well was filled with a solution of melted agarose at a concentration of 1% and fMLP at a final concentration of 100 nM.

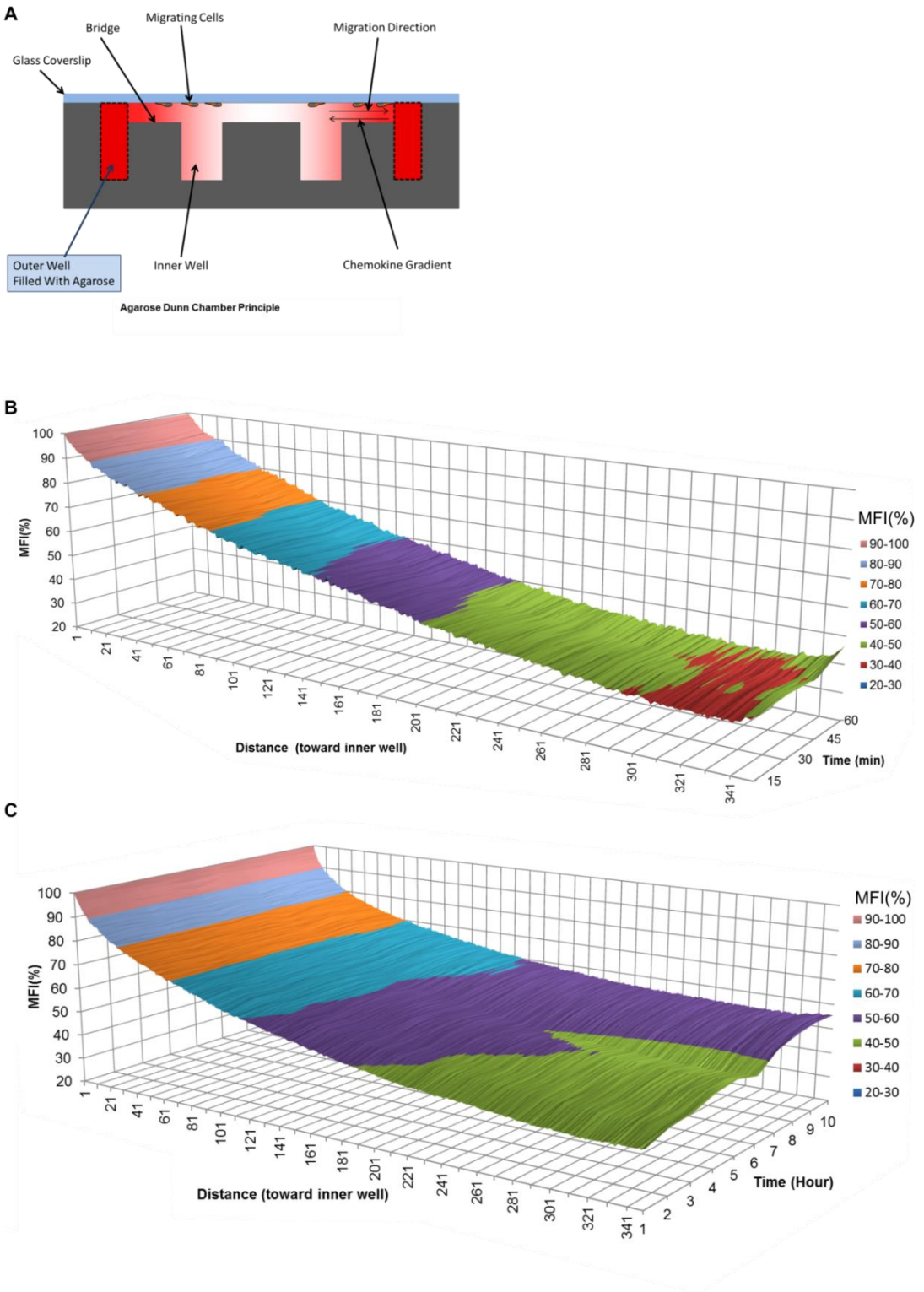

Figure 3-3: Agarose Dunn chamber and impact on chemoattractant gradient

A) Schematic of the Agarose Dunn chamber. B and C) Stability of a FITC gradient in the Agarose Dunn chamber over B) one hour and C) 10 hours. A FITC-loaded 1% agarose gel solution (1 µg FITC per mL) was loaded to the outer well of the Dunn chamber and the agarose Dunn chamber was imaged at 37°C at 1 image/minute using an Axiovert 135 microscope, equipped with an Achroplan 10x/0.25 objective, an environmental chamber. The FITC signal was quantified using ImageJ using a rectangular selection of 50 pixels of width that stretched from the inner well to the outer well. B-C: The experiments were used for optimisation of experimental conditions therefore three independent experiments were not performed. Data representative of two independent experiments, one replicate per experiment.

The Dunn chamber was assembled and setup on the microscope as described in the Materials and Method section. Cells were imaged for one hour and one image was captured every minute and migrating cells were manually tracked using the Manual Tracking plug-in in Fiji/ImageJ.

When I used neutrophils that I plated on fibrinogen, I could observe directed migration of most of the cells towards the outer well (Figure 3-4-A, upper line, Figure 3-4-C). Neutrophils displayed a good mobility in the agarose Dunn chamber with 74% of mobile cells. Within the mobile population, 73% of cells showed directed migration towards the outer well indicating the ability of the cells to do chemotaxis in this setup (Figure 3-4-B). I also tested the ability of HL-60 cells to do chemotaxis in the agarose Dunn chamber. Most of the dHL-60 cells migrated in the direction of the outer well (Figure 3-4-A, bottom line, Figure 3-4-E) and displayed a good chemotaxis with 95% of mobile cells and 88% of directed migration. This showed that the use of agarose gel to cage fMLP and slowly release it into the bridge gap not only resulted in the establishment of a gradient of chemoattractant but also allowed cells to do chemotaxis in response to the chemoattractant gradient. This setup appeared well-adapted to study neutrophil or dHL-60 migration.

Using the MatLab routine I developed, I analysed the migration of neutrophils and dHL-60 described above. Neutrophils displayed an average velocity of 8.6 $\mu m.min^{-1}$ (+/- 2.8 $\mu m.min^{-1}$), with some cells migrating up to a speed of 15 $\mu m.min^{-1}$ (Figure 3-5-A). dHL-60 cells overall migrated at a faster velocity with an average velocity of 14.9 $\mu m.min^{-1}$ (+/- 2.8 $\mu m.min^{-1}$) and a maximum speed of 21.5 $\mu m.min^{-1}$ (Figure 3-5-C). In this experiment, neutrophils showed a better directionality than dHL-60 cells with a chemotactic index of 0.69 and 0.55, respectively (Figure 3-5-B and D). The weak directionality of dHL-60 cells was confirmed by analysing instantaneous angle distributions where I could see a more spread distribution of the values in comparison to the neutrophil instantaneous angle distribution (Figure 3-5-E and H). The angle variation analysis of the dHL-60 population showed that these cells deviated much more than primary neutrophils with mainly a turning angle up to 60^{o} and even some values up to 180^{o} indicating a temporary migration in the opposite way of the gradient (Figure 3-5-F and I).

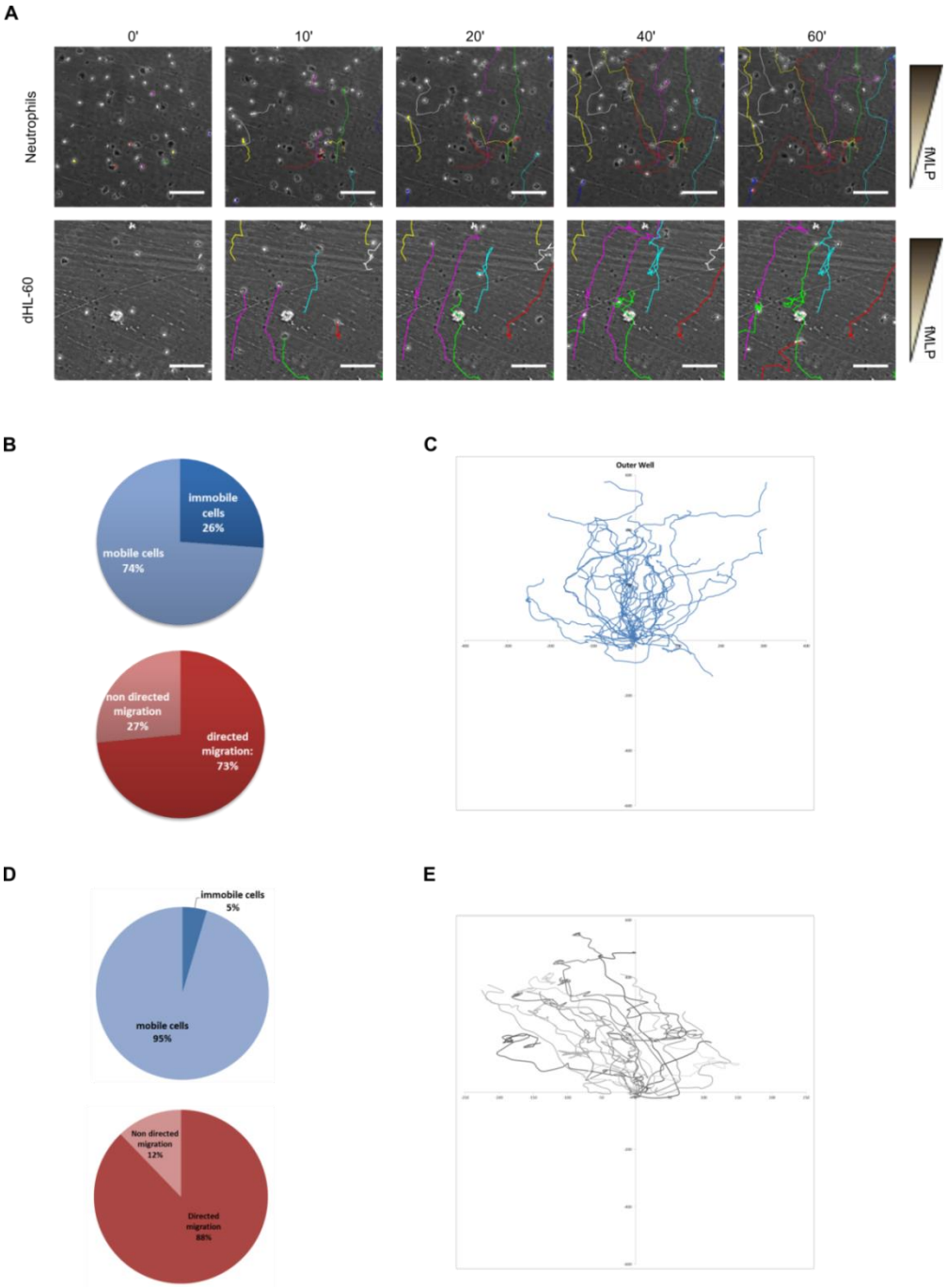

Figure 3-4: Migration of primary neutrophils and dHL-60 in the agarose Dunn chamber

A) Magnification of part of the bridge shows several neutrophil and dHL-60 cell migration in the direction of the chemoattractant, 100nM of fMLP, during 60 minutes. Scale bar: 100 µm. B and D) Mobile and directed migration fractions of the whole population of migrating primary neutrophils and dHL-60, respectively. C and E) Tracks of C) 33 neutrophils or E) 19 dHL-60 cells migrating from their initial position in the agarose Dunn chamber. The outer well, source of the chemoattractant, is located at the top of the graphs. The cells were imaged at 37^{o}C at 1 image/minute using an Axiovert 135 microscope, equipped with an Achroplan 10x/0.25 objective, an environmental chamber and a motorised stage. Cells were tracked using the ImageJ manual tracking plug-in and tracks were processed in Matlab using a custom-written routine. A-E: The experiments were used for optimisation of experimental conditions therefore three independent experiments were not performed. Data representative of two independent experiments, one replicate per experiment.

Nevertheless, mean angle analysis confirmed that most of the population of neutrophils and dHL-60 were migrating in the chemoattractant direction with few values deviating from the 30^{o} arc from the chemoattractant (Figure 3-5-H and J).

3.2.1 Assay reliability

In order to use the modified Dunn chamber as routine assay to detect neutrophil migration defect, I analysed the reliability of this method. To reduce the possible influence of the variation from different healthy donors, I used dHL-60 as a standard. The advantage of using this cell line as a model for neutrophil migration is that the cell characteristics should remain similar from one experiment to another, reducing variations in the results obtained. To analyse the inter-experiment variability of the dHL-60 chemotactic response, I used the control cells of 9 experiments where cells displayed a chemotactic response to fMLP which allowed me to determine the average speed, standard deviation and coefficient of variation of dHL-60 chemotaxis in the agarose Dunn chamber. Experiments in which neutrophils from healthy volunteers showed no directionality in their migration (possibly due to a failure to establish an fMLP gradient) where excluded from the analysis of chemotaxis. The coefficient of variation (CV) is a standardised measure of the dispersion of a probability distribution and is defined as the ratio of the standard deviation to the mean. Measure of the CV is often used as quality control for intra- or inter-assays in laboratory (Hanneman et al., 2011) and reflects the performance of the assay in the hand of the user. In my studies, neutrophil-like dHL-60 migrated on average at a speed of 14.5 μm.min^{-1} (+/- 2 μm.min^{-1}) and showed a variation of 14% from one experiment to another (Figure 3-6-A and C). Compared to dHL-60, primary neutrophils displayed a slower average speed of 12.6 μm.min^{-1} (+/- 2.6 μm.min^{-1}) and a CV of 20.7% (Figure 3-6-A and B). These data were obtained from 6 independent experiments, using different donors. The higher standard deviation and CV of primary neutrophils probably reflect the variation between patient genetic backgrounds which could represent up to 38% of the cause of variation (Kabbur et al., 1997) but also the additional steps of cell manipulation necessary to isolate primary cells.

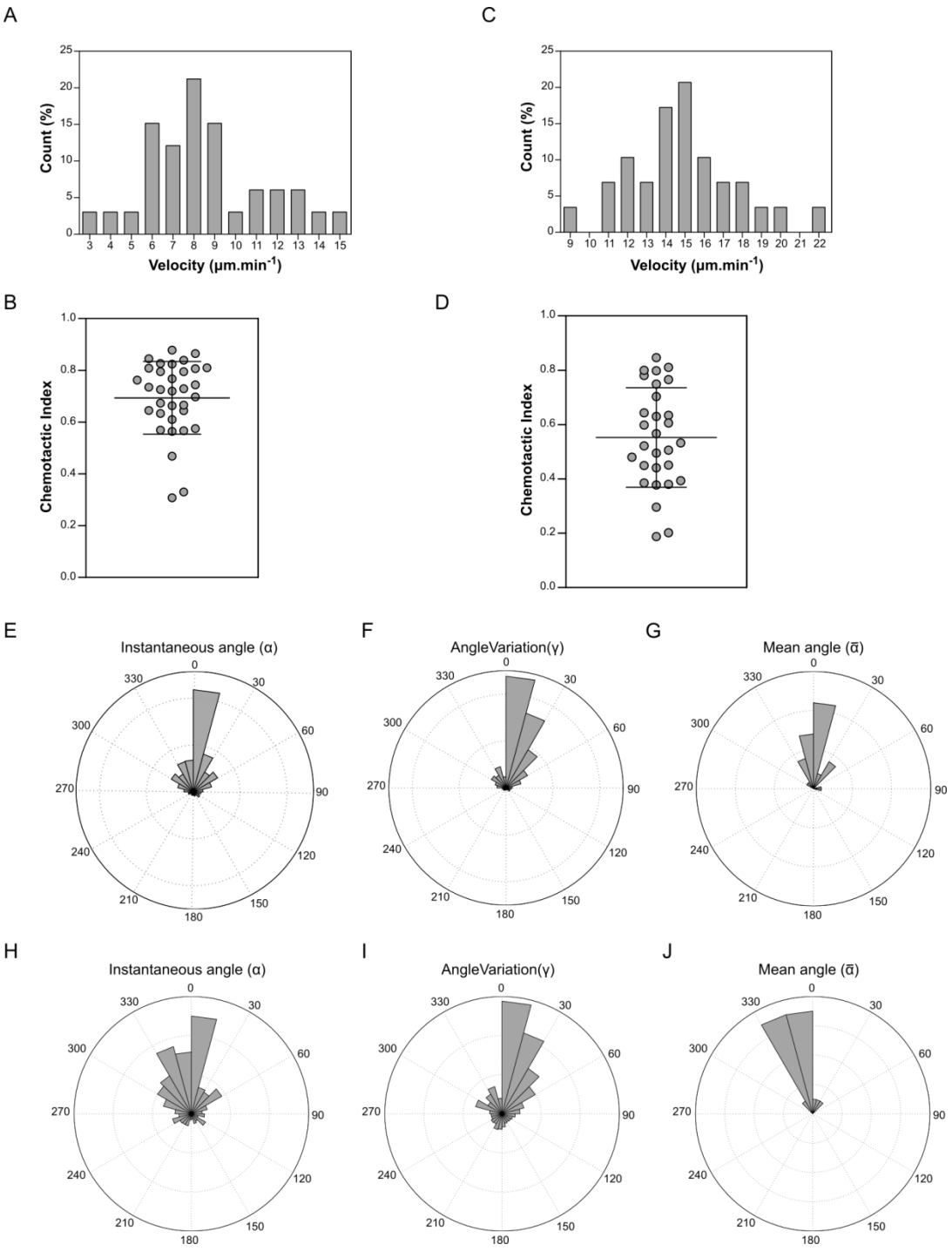

Figure 3-5: Migration parameters

A) Velocity frequency distribution of migrating primary neutrophils. B) Chemotactic index of primary neutrophils during migration. C) Velocity frequency distribution and D) chemotactic index of migrating dHL-60. E and H) Instantaneous angle (α), F and I) angle variation (γ) and, G and J) mean angle ($\bar{\alpha}$) of migrating primary neutrophils and dHL-60, respectively. Cells migration was followed during 60 minutes in the agarose Dunn chamber in response to 100nM of fMLP. The migration parameters were calculated using a custom-written Matlab routine from cell tracks obtained by manually tracking cells using the manual tracking plug-in of ImageJ. The graphs E to J were generated using the Matlab routine while the graphs A to D were done in GraphPad Prism. A-H: The experiments were used for optimisation of experimental conditions therefore three independent experiments were not performed. Data representative of two independent experiments, one replicate per experiment.

To estimate the reliability of the measures obtained from neutrophils migrating in the agarose Dunn chamber, I evaluated the number of tracked cells needed within each experiment to have the average velocity within the 95% confidence interval of all experiments combined. In both primary neutrophils and dHL-60 experiments, the tracking of 10 cells was enough to reach 60% of the average velocity of the different experiments within the 95% confidence interval.

Increasing the number of cells tracked to 15 or 20 did not seem to increase the number of values within the 95% confidence interval but allowed to identify the outliers neighbouring the 95% confidence interval.

3.3 Discussion

The Dunn chamber is a well-established direct visualisation chamber for cell migration and has been used numerous times to study immune cells migration. I chose to use this setup because it has been shown to allow the establishment of a stable gradient of chemoattractant and also it is reusable since made of glass. Accordingly to the literature, I determined the conditions for neutrophils and dHL-60 cells to adhere and migrate on fibrinogen and fibronectin coated coverslips, respectively. When I first tried to make cells migrate in the Dunn chamber, I was surprised to observe only random migration. Since I used the same cells, the same fMLP concentration, and the same coverslip coating with fibronectin as members of Dr. Charras' group who achieved successful dHL-60 chemotaxis towards fMLP delivered through micropipettes, I concluded that the random migration was not the consequence of a defect in cell differentiation or an issue with the concentration of chemoattractant or with the extra-cellular matrix protein used to coat the coverslip but more probably due to a failure in the formation of the chemoattractant gradient. To confirm that the gradient formation did not occur correctly, I filled the outer well with fluorescent dyes to visualise the gradient formation over the bridge and its maintenance over long durations. First I used 70 kDa dextran-rhodamine and could observe the establishment of a steep and stable gradient. Because diffusion is correlated to the molecule size, I decided to use a molecule which size is closer to the one of fMLP in order to have a better characterisation of the fMLP gradient formation. I used FITC to do so and I could only

A

	Number of samples	Average	SD	Inter-assay coefficient of variation (%)
Primary neutrophils	6	12.57933	2.598141	20.7
dHL-60	9	14.525	2.041262	14.1

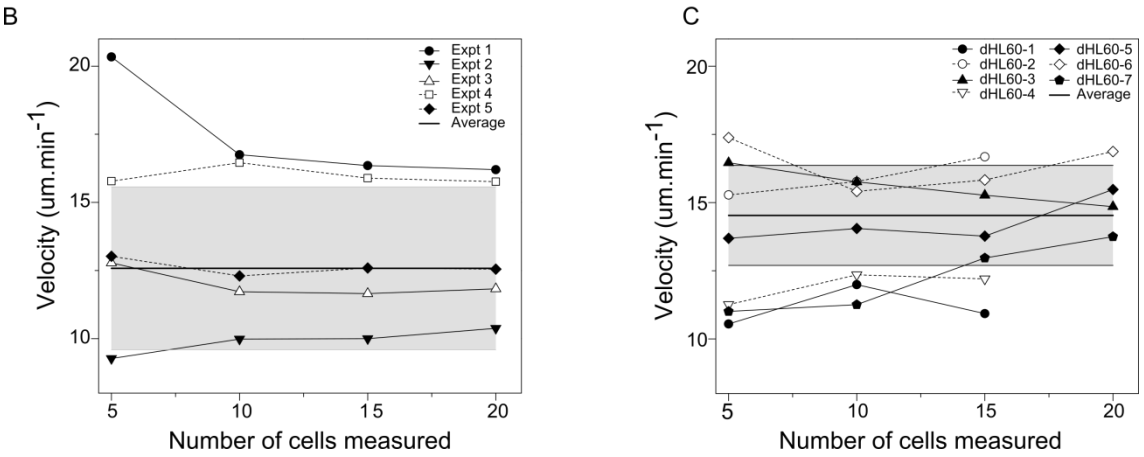

Figure 3-6: Evaluation of the Dunn chamber assay variability

Cells migration was followed during 60 minutes in the agarose Dunn chamber in response to 100nM of fMLP. The cells were imaged at 37°C at 1 image/minute using Axiovert 135 microscope, equipped with a Achroplan 10x/0.25 objective, an environmental chamber and a motorised stage. A) Variation between successive assays was evaluated using the coefficient of variation defined as CV = SD/average. B and C) Evolution of the average velocity in function of the number of cells tracked during the migration in the agarose Dunn chamber for B) primary neutrophils and C) dHL-60 respectively. B: Results were obtained from 5 independent experiments. C: results from 9 independent experiments.

observe a gradient close to the outer well but not on the rest of the bridge. Several hypotheses could explain this result. The first one is the distance between the cell culture room where the Dunn chambers were setup and the time-lapse microscope room where I carried-out the observations. When patient samples were processed, we isolated PBMCs from the blood samples and therefore, we needed to do the cell isolation under sterile conditions. Therefore, all the material for the Dunn chamber was set in the cell culture room. Assembling the Dunn chamber in the cell culture room also prevented the cells from being exposed to bacterial products. Indeed, the main lab was primarily used for molecular biology experiments with bacterial cultures processed on a weekly basis, generating aerosols that could have contaminated and stimulated the cells. Unfortunately, it was not possible to use a room closer to the microscope to assemble the chamber. The time-lapse microscope used was located in a different wing of the building and the route to reach it included stairs and a lift. In theory, once the Dunn chamber is setup, liquid inside is assumed to be incompressible and so should not be much influenced by movement of the slide due to the user. Nevertheless, it is always recommended to be gentle when carrying the chamber but when one has to go down stairs before taking a lift even being very careful, it can be challenging to avoid vibrations. These vibrations may be enough to perturb the gradient of small molecules over the bridge. It is important to notice that usually scientific articles describing direct visualisation chambers such as the Dunn chamber do not mention how the handling of the chamber can influence the gradient. It would have been interesting to image the FITC gradient before going out of the room where the chamber was assembled and after the travel to the room where the microscope was located to evaluate how much the travel between the two rooms may have perturbed the gradient. The second hypothesis is that the use of #1.5 coverslips modifies the gradient. The Dunn chamber was originally designed to be used with a thick #3 coverslip to prevent any deformation of the coverslip due to change of temperature that could induce a variation of the height of the gap between the bridge and the coverslip and thus perturb the gradient. It was originally decided to use both low magnification lenses to be able to record the behaviour of a whole population and high magnification lenses to image specific cell structures such as the lamellipodium during migration. Low magnification lenses are usually air lenses with a long working distance and

both thin (#1.5 coverslips) and thick (#3 coverslips) coverslips can be used. On the other hand, high magnification lenses are oil immersion objectives with short working distances and therefore one must use #1.5 coverslips. To be able to use the Dunn chamber with either air and oil microscope lens, I decided to use #1.5 coverslips. Because of its thinness, this coverslip model is highly sensible to change in temperature and can expand and contract easily. It is possible that during the period the Dunn chamber reaches the temperature of 37°C in the microscope environmental chamber, the coverslip expands resulting in a variation of height of the gap over the bridge altering correct gradient establishment. Unfortunately, due to technical issues with the microscope, I could not use the high magnification lenses and eventually did not record high-resolution migration of neutrophil or dHL-60 cells in the Dunn chamber. A third hypothesis is that because fMLP is a small molecule, it diffuses too fast from the outer well over the bridge to enable the formation of a stable gradient. It would have been interesting to use a chemoattractant of higher molecular weight such as IL-8 that would diffuse more slowly and maybe easily allow the formation of a gradient. Because of the very poor response of dHL-60 to IL-8, fMLP was chosen. These hypotheses combined with the difficulty to setup the chamber as described in the original paper may explain why I was not able to create a gradient of FITC and fMLP.

To be able to establish a gradient in the Dunn chamber, I modified the protocol and filled the outer well with an agarose gel containing FITC. I was able to observe the formation of a steep gradient as early as 15 minutes after assembling the chamber. The gradient revealed itself to be stable over 10 hours indicating the robustness of this new protocol. The agarose gel decreases the diffusion coefficient of FITC in the outer well, restoring the role of *reservoir* of the outer well. By pouring agarose gel only in the outer well and not over the bridge, only the release of FITC from the outer well to the bridge should be slowed whereas the conditions for the diffusion of FITC over the bridge should be comparable between the initial and new Dunn chamber setups allowing the formation of the gradient of FITC similar to that described by Zicha *et al.*. The use of agarose showed two advantages: firstly by acting as a reservoir, it may reduce the sensitivity of the Dunn chamber to vibration during transport from the cell culture

room to the microscope. Secondly, during the time required for the chamber to reach 37°C prior to image acquisition, the FITC-containing agarose may be less sensible to possible coverslip expansion reducing or buffering the perturbations produced during gradient establishment. Using agarose with fMLP in the outer well, I was able to observe directional migration towards the chemoattractant of primary neutrophils and dHL-60 which I was unable to do using the original setup. The use of agarose in the Dunn chamber raised the question of possible contamination of the agarose with lipopolysaccharides (LPS) secreted by bacteria which can alter neutrophil migration. It has been shown that LPS induces cell polarisation and actin rearrangement in neutrophils leading to an increase of cell stiffness together with neutrophil retention in lung capillaries or polycarbonate filters due to the impaired deformability of neutrophils activated with LPS (Erzurum et al., 1992). Activation of neutrophils by LPS also directly inhibits chemotaxis in response to IL-8 (Bignold et al., 1991) but it is still not clear if LPS directly alters chemotaxis in response to fMLP since contradictory results have been described in different studies (Bignold et al., 1991; Kharazmi et al., 1991). In order to limit the possible contamination of the agarose used in the Dunn chamber with LPS, I used an agarose that was certified for cell culture. Because LPS could alter the actin polymerisation and the migration of neutrophils or dHL-60 it would be important to test the possible contamination of the agarose used in the Dunn chamber with LPS using assays used by the industry to test LPS contamination such as the Limulus Amoebocyte Lysate (LAL) assay or the Factor C ELISA.

Analysing the reliability of this assay showed that there was an important inter-assay variation (up to 20%). These analyses demonstrated that, in most of the cases, tracking 20 cells per sample is necessary to have a reliable average velocity value. The situation of the outliers which even after the tracking of 20 cells were still outside of the 95% confidence interval showed the necessity to repeat the experiments in order to confirm the results and rule out the possible effect of the patient condition on the day the blood sample is taken (fatigue, physical activity, seasonal disease) that could affect neutrophil response. The study of the response of neutrophils from numerous healthy donors would allow the determination of a standard response facilitating the analysis of results from patient cells. A deep study of the parameters that could influence the

success of the assay should be performed in order to enhance its reliability. In the meantime, the use of intracellular dyes such as CFSE (carboxyfluorescein succinimidyl ester) is a simple way to improve the assay reliability. Indeed, staining one of the populations (e.g. control) with CFSE and mixing it with the unstained population (e.g. patient) guarantees that, when monitored in the same chamber, both patient and control cells are subjected to the same conditions. In order to use this dye, we would first need to assess that it does not influence cell migration. This could be tested by labelling control cells with CFSE and mixing labelled and unlabelled control cells to monitor their respective migration in the same Dunn chamber. If the CFSE does not display any interference with cell migration, it would help to quickly identify chemotaxis failure, adhesion impairment or migration defect of one of the samples.

The association of the agarose Dunn chamber with the semi-automatic tracking/processing routine I developed is a robust tool to study neutrophil migration. Using this new setup, I could study the consequences of the expression of CA-WASp on dHL-60 migration (Chapter 4) and the impact of MKL1 deficiency on primary neutrophils and dHL-60 cells (Chapter 5).

Chapter 4 The constitutively activate Wiskott-Aldrich protein alters neutrophil migration and the spindle assembly checkpoint.

4.1 Introduction

The actin cytoskeleton is attached to the cell membrane and is a key element in the regulation of cell shape. The components of actin are dynamically regulated and undergo a rapid turnover allowing the quick reorganisation of the cytoskeleton in response to stimuli. Cortical actin has recently attracted increasing attention and its regulation in cellular processes such as cytokinesis, cell migration, and embryogenesis has been thoroughly investigated. These changes in cell shape are fundamental for the immune cells to perform numerous tasks from cell division to migration and phagocytosis making the actin cytoskeleton one of the main structures to achieve correct protection of the organism.

One of the regulators of actin turnover is the Wiskott-Aldrich Syndrome protein and is expressed in the hematopoietic cell lineages driving actin rearrangement through spatial and temporal activation of the Arp2/3 complex, which triggers the nucleation of new branched actin filaments. Mutations in the CBD domain of WASp have been described and result in the loss of the auto-inhibited conformation of the protein producing a constitutively activated form of WASp (Ancliff et al., 2006; Devriendt et al., 2001). So far three mutations have been described in patients, L270P, S272P and I294T; they result in similar phenotypes and are considered as equivalent. The constitutively activated forms of WASp are responsible for an unregulated and mislocalised actin polymerisation which results in the alteration of actin structures involved in cell migration (Ancliff et al., 2006) and leads to an excess of F-actin throughout the cell (Moulding et al., 2007). In patients, these mutations are responsible for severe neutropenia and

monocytopenia causing recurrent bacterial infections. Patients with these mutations also present cellular division defects indicating chromosomal instability or myeloid malignancy (Ancliff et al., 2006; Beel et al., 2009; Moulding et al., 2007).

In most of the patients, bone marrow examination showed an arrest of the neutrophil development at the promyelocyte/myelocyte stage (Ancliff et al., 2006; Devriendt et al., 2001)). This myelopoeisis arrest went along with a dramatic increase of apoptosis during *in vitro* neutrophil production from CD34+ cells isolated from patient bone marrow (Ancliff et al., 2006). From these results it was hypothesised that a defect during cell division might be responsible for the neutrophil maturation arrest and increase of apoptosis. A study of the underlying mechanism of the impact of CA-WASp (I294T) by gene transfer on cell division and apoptosis, performed by Moulding *et al.*, showed that during mitosis, the excess of F-actin surrounded the spindle and chromosomes all the time from their alignment to their separation and was accumulated at the cleavage furrow around the middle of the spindle. Live cell imaging experiments revealed a delay in mitosis from metaphase to anaphase and an increase of cytokinesis failure. It was shown that the cytokinesis failure was responsible for the rise of multinucleated cells and that the expression of WASp I294T was responsible for a decreased proliferation and an increase of apoptosis. Because WASp has no known role in cell division, it was hypothesised that the excess of F-actin throughout the cell altered the mechanical properties of the cell leading to the impairment of mitosis. When I started this project, preliminary data from Dale Moulding *et al.* (since published as (Moulding et al., 2012) showed that the expression of the constitutively active WASp induced a two fold increase of the cytoplasmic viscosity and elasticity resulting in a diminution of chromosomal movement by around 20%. This was less than what it was expected given the two fold increase in viscosity, thus suggesting an upregulation of the motive forces applied on chromosomes. From these preliminary results, it was hypothesised that since chromosome motility was perturbed at anaphase, then chromosome movements during the spindle assembly checkpoint should also be altered. The spindle assembly checkpoint ensures the correct segregation towards each pole of the two sister

chromatids of the chromosomes and delays mitosis until correct attachment of the chromosomes to the spindle.

When entry to mitosis is imminent, the chromosomes are replicated and condensed to facilitate their movement through the cell. To be able to be pulled by the microtubules of the spindle, chromosomes build a structure called kinetochore that allows their attachment to microtubules. Kinetochores are divided in three regions: the inner kinetochore, which constitutes the interface between chromatin and other kinetochore regions; the outer kinetochore which contains the attachment sites to microtubules, also called kinetochore microtubules (kMT); and the central kinetochore between the inner and outer kinetochore regions (reviewed in (Cheeseman and Desai, 2008)). One particularly important protein of the inner kinetochore is CENP-A, a variant of the histone H3, which is the first protein assembled in the kinetochore and is essential to the incorporation of other CENP proteins involved in the kinetochore assembly. Once the kinetochore structure is complete, it acts as an interface where kMTs can be attached in order to pull each sister chromatid towards the opposite poles of the dividing cell. In order to ensure correct distribution of genomic material to each pole, the correct attachment, known as amphitelic attachment, of paired sister kinetochores to opposite poles is checked by successive cycles of pulling forces from the opposites poles (reviewed in Watanabe, 2012). The amphitelic attachment generates tensions that are generated by the pulling forces by the kMTs, from the opposite poles, attached to each sister kinetochore and this tension has an important role in stabilising the attachment. As a matter of fact, the mono-polar attachment due to this lack of tension is very unstable and allows a new cycle of capture of the kinetochores by the kMT until the correct attachment is achieved. This cycle of trial and error is mainly regulated by the protein kinase Aurora B which is located between the two sister kinetochores. The tension generated in the case of amphitelic attachment stretches the kinetochore increasing the distance between the kinetochore and Aurora B, whereas in the case of mono-polar attachment Aurora B is located close to the kinetochores. The Aurora B-kinetochore proximity allows Aurora B to destabilise the microtubule attachment sites by phosphorylating proteins of the kinetochores whereas the remoteness due to amphitelic attachment prevents kinetochore phosphorylation thus stabilising the microtubule attachment (Watanabe, 2012). Overall, incorrect kinetochore

attachment to kMTs blocks, through the spindle assembly checkpoint, the progression of the cell cycle. Once all the chromosomes are correctly attached to the spindle, the checkpoint allows chromosome segregation and cell division progress. Considering the importance of the tension generated during the spindle assembly checkpoint, alteration of cytoplasmic mechanical properties may perturb the checking of the correct attachment of the chromosomes to the kMTs and delay or prevent mitosis completion.

We hypothesised that the lack of circulating neutrophils and monocytes in the blood may be the result of combinatory defects in migration and mitosis caused by the modification of the cellular mechanical properties due to the dramatic alteration of the actin cytoskeleton regulation.

The group had been investigating the role of CA-WASp using the mutation in the CBD domain replacing the isoleucine by a threonine at the position 294 (I294T) as a model for CA-WASp and had generated published and preliminary data. Here, I used the same mutation to study how the constitutively activated WASp (CA-WASp) altered neutrophil migration and cellular division during the spindle assembly checkpoint.

4.2 Results

4.2.1 The loss of the auto-inhibited conformation of WASp alters neutrophil migration

To express CA-WASp in the cells of interest, I used two different backbones: one under the CMV promoter and the other one under the SFFV promoter. As the CMV promoter is strongly silenced in hematopoietic cell lineages, the SFFV promoter allows a more stable expression of the transgene. I removed the eGFP tag from the backbones and replaced it with mCherry (Figure 4-1-B).

To validate that the new vectors I made were resulting in the correct phenotype, I transduced the HT-1080 fibrosarcoma cell line with CMV-mCherry–WASp and CMV-mCherry-CA-WASp lentiviruses. As expected, mCherry-CA-WASp expression resulted in an excess of F-actin mislocalised through the cytoplasm (Figure 4-1-C, iii and iv) whereas WT-WASp expression (Figure 4-1-C, ii and v) resulted in a similar phenotype as control cells (Figure 4-1-C, i and iv). I

then determined by Western blot the expression pattern of CA-WASp in HL-60 cells transduced with sffv-mCherry-CA-WASp lentiviruses (Figure 4-1-D). In the transduced cells, we could clearly observe the endogenous WASp as well as the mCherry-WASp which had a higher molecular weight due to the mCherry tag. Expression levels of CA-WASp were in the same order of magnitude as the endogenous WASp, which was consistent with results obtained from previous studies in the group using CA-WASp lentiviruses on hematopoietic cell lines (Moulding et al., 2007). Such levels of expression had been shown to be sufficient to induce unregulated and mislocalised actin polymerisation (Moulding et al., 2007).

To evaluate the possible impact of CA-WASp on neutrophil migration, I transduced HL-60 cells with SFFV-mCherry- CA-WASp lentiviruses and the day after, I added 1.3% DMSO into the cell medium to induce the differentiation into neutrophil-like cells (dHL-60 CA-WASp). Untransduced cells were used as control (dHL-60). As shown in Chapter 2, the protocol used to monitor the migration in the agarose Dunn chamber displayed a high inter-assay variability. Therefore, to make sure that both control and transduced cells were subjected to the same experimental conditions, Dunn chamber experiments were performed by mixing both populations together in a 1:1 ratio and by monitoring control and transduced cells in the same Dunn chamber. Both control and CA-WASp dHL-60 were able to migrate towards the source of fMLP in the agarose Dunn chamber (Figure 4-2-A, VideoS4-1). The dHL-60 expressing the mutant WASp exhibited reduced average velocity with an average value of 11.3 $\mu m.min^{-1}$ (+/- 0.48 $\mu m.min^{-1}$), which is significantly different ($p < 0.001$) than the control cell average velocity of 14.2 $\mu m.min^{-1}$ (+/- 0.40 $\mu m.min^{-1}$) (Figure 4-2-B). Cell velocity alteration by CA-WASp was not accompanied by a modification of the cell directionality since no significant difference was detected between the chemotactic index of control and CA-WASp cells (Figure 4-2-C). The chemotaxis of both populations was confirmed by analysis of the average angle between the gradient of fMLP and the cell path during the migration (Figure 4-2-D and E). The distribution of the average angle of cells expressing the mutant WASp was more compact (-5.7 +/- 12.1 degrees) than the distribution in control cells (-2.5 +/- 19.8 degrees), indicating less variation between the gradient of fMLP and the cell path during migration. The significant difference in

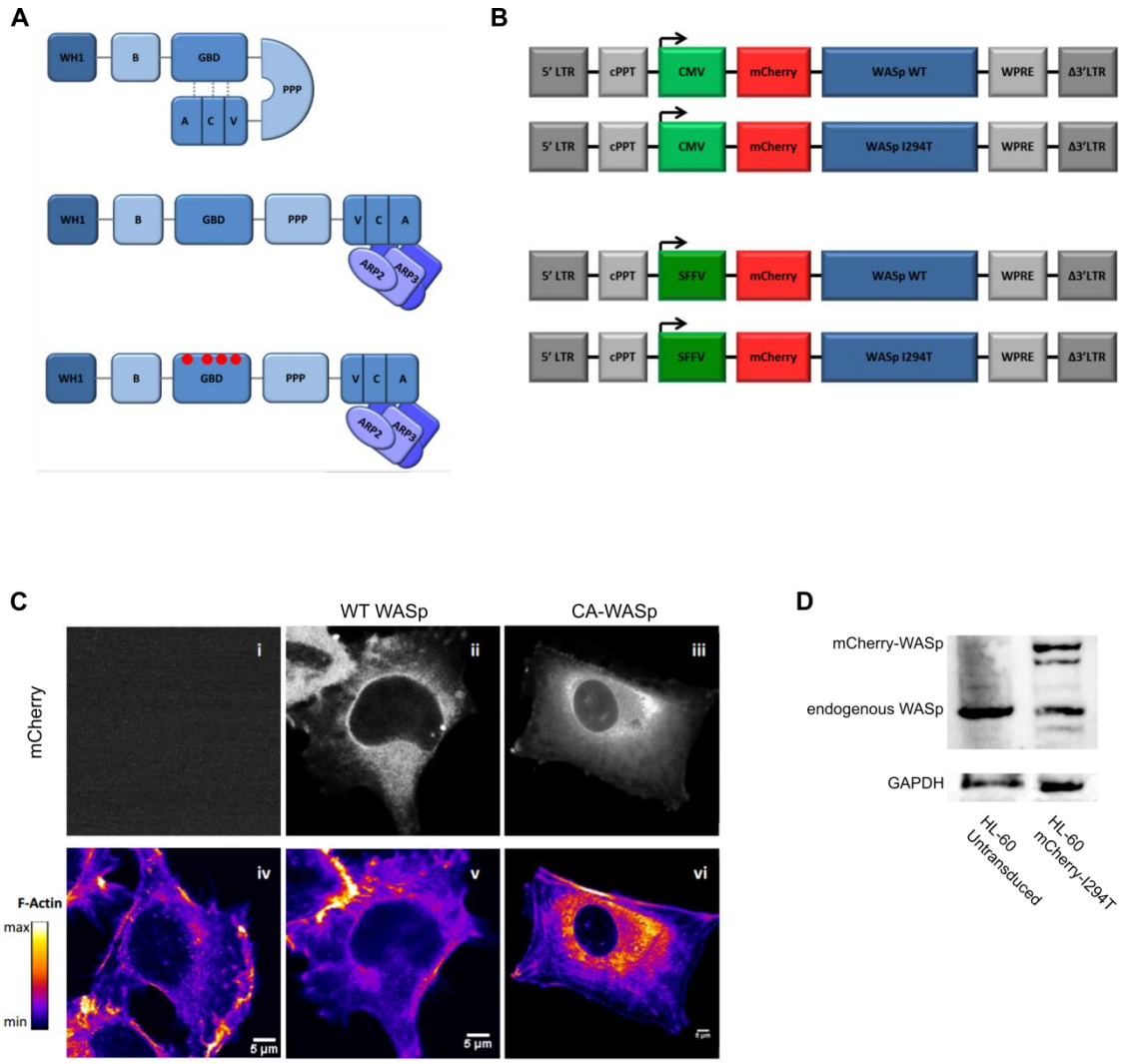

Figure 4-1: Mutations in the CBD domain resulted in a constitutively active WASp

A) Mutations in the CBD domain of WASp have been described (bottom), resulting in a loss of the auto-inhibited conformation of WASp (top) and opening the protein in its active form (middle). B) Replacement of the eGFP insert in the WASp and CA-WASp (I294T) vectors by the mCherry fluorescent protein. These vectors are under CMV and SFFV promoters. C) Expression of CA-WASp in the HT1080 fibrosarcoma cell line using the CMV-mCherry-WT-WASp and CMV-mCherry-CA-WASp vectors. Two days after transduction, the HT1080s were plated onto coverslips and left to adhere overnight at 37^{o}C with 5% CO_2 before being fixed. The cells were then permeabilised and stained with phalloidin conjugated with Alexa647. Expression of CA-WASp resulted in an excessive and mislocalised F-actin content compared to control and WT WASp expressing cells. The cells were imaged using a Zeiss LSM710 confocal microscope using a 40x/1.0 water objective. D) Expression of WASp and CA-WASp in HL-60 cells wild-type (untransduced) or transduced with lentivirus carrying WASp-I294T. HL-60 cells were transduced with SFFV-mCherry-CA-WASp before being lysed using RIPA buffer three days after transduction. 20µL of samples were loaded in each lane. C and D: The experiments were used for optimisation of experimental conditions therefore three independent experiments were not performed. Results representative of two independent experiments. One replicate per experiment.

the variance of the two populations, 6.88 and 2.54 for control and CA-WASp cells, respectively, was confirmed by a positive F-test result indicating less variation in the distribution angle between the gradient of fMLP and the migrating cell path. This could be interpreted as the cells expressing the mutant WASp were more directional than the control cells but this interpretation is in contradiction with the result of the chemotactic index.

To determine if the defect in migration of the dHL-60 expressing the mutant WASp observed in 2D, as in the Dunn chamber, would be similarly seen in 3D, I studied the migration of control and CA-WASp dHL-60 in Transwell inserts (Figure 4-3-A). The membrane of the insert is about 10 µm thick and the pores 3 µm in diameter forcing cells to change shape and migrate in confined space. Cells were seeded into the upper well whereas the lower well contained a solution of fMLP. Cells were left to migrate for 1 or 2 hours at 37^{o}C and 5% CO2 in an incubator. After 1 or 2 hours, cells in the lower well were counted: up to 25% of the cell input had migrated through the insert membrane and fell into the lower well. No significant difference was found between the two populations at the 1 hour and 2 hour time points (Figure 4-3-B). This result was surprising since it was hypothesised that excess of F-actin due to CA-WASp would alter the dynamics of the change in cell shape that is required for the cells to migrate through the insert. I verified by confocal fluorescence imaging if any alteration of cell shape was observable during migration through the membrane pores (Figure 4-3- C and D). I could clearly observe an increase of F-actin signal into cells expressing WASp mutant (Figure 4-3-D) but no abnormal cell shape in comparison to control cells (Figure 4-3-C). In both populations, I could observe cells on both sides of the membrane validating their correct migration.

Then, I investigated the hypothesis that the migratory defect observed in the agarose Dunn chamber may be due to an alteration of actin dynamics. Control and CA-WASp cells were mixed in a single tube before being stimulated with fMLP for different time points. Actin polymerisation was stopped by addition of a concentrated solution of PFA fixing cells instantaneously. Cells were then stained for F-actin using phalloidin-Alexa647 and analysed by flow cytometry. The experiments were performed at two different temperatures, 22^{o}C and 37^{o}C, because actin polymerisation is a temperature sensitive process. While performing the

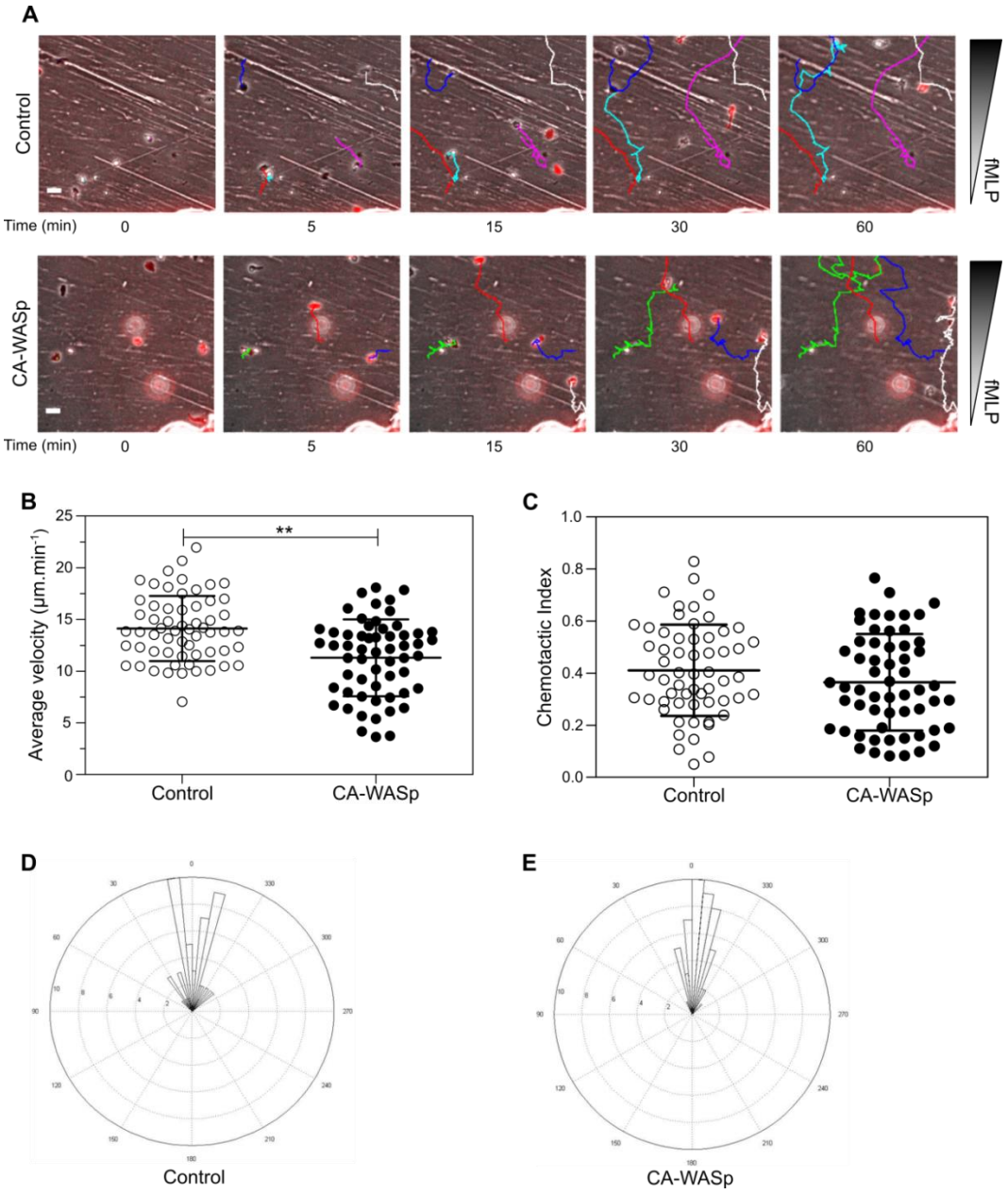

Figure 4-2: Expression of CA-WASp in dHL-60 cells altered migration towards fMLP

A) Snapshot of time-lapse video of control and CA-WASp expressing dHL-60 migrating in the agarose Dunn chamber towards the outer well which contained 100 nM of fMLP. To ensure that both populations were subjected to the same experimental conditions, control and CA-WASp cells were mixed before being plated on the coverslip. Control (top row) and CA-WASp (bottom row). The cells were imaged at 37^{o}C at 1 image/minute for 1 hour using an Axiovert 135 microscope, equipped with an Achroplan 10x/0.25 objective, an environmental chamber and a motorised stage. Scale bar = 20 μm. Cells were tracked using the ImageJ manual tracking plug-in and tracks were processed in Matlab using an in-house routine. B) Average velocity of control and CA-WASp cells. C) Cells expressing the mutant WASp did not display any significant change in the chemotactic index. D and E) Frequency distribution of the average angle between the chemoattractant gradient and the cell path during migration of D) control cells or E) cells expressing CA-WASP. A: Data representative of three independent experiments. B-E: Data pooled from three independent experiments. One replicate per experiment. Data analysed by t-test. In B: **: p <0.01.

experiment at 37°C is more representative of physiological conditions, using a lower temperature (22°C) was expected to decrease the actin polymerisation kinetics and, as a consequence, to facilitate the visualisation of possible defects in actin dynamics in CA-WASp cells. In all experiments, cells expressing CA-WASp had a stronger signal than the control cells at baseline level and during the stimulation with fMLP. This suggested a higher content of F-actin in the cells expressing the mutant WASp although no significant difference was found when compared to the control cells (Figure 4-4-A and B). Interestingly, the difference between the mutant and control cells was not altered significantly during the stimulation with fMLP, suggesting that the actin polymerisation dynamics was similar between the two populations. These results indicated there was no major defect of the actin polymerisation machinery in the cells expressing the mutant WASP. To confirm this, I studied the possible effect of CA-WASp on the Arp2/3 complex, which is activated by WASp to nucleate new branched actin filaments, by examining the expression and localisation in dHL-60 cells of Arp2/3 complex subunit p34. Two populations were determined using the mCherry signal: cells with a mCherry signal equal to 1 to 1.5 time the background signal were considered to have a low expression of mCherry-CA-WASp while the cells with a mCherry signal higher than three time the background were considered to have a high expression of CA-WASp. The impact of CA-WASp on the cells was then evaluated in these two populations. Confocal images revealed a trend in cells highly expressing CA-WASp showing a small increase of their p34 signal suggesting a possible upregulation of this protein (Figure 4-4-C and E). This was associated with a higher content in F-actin in CA-WASp cells (Figure 4-4-F). The trend showing an increased expression of p34 in the cells expressing the mutant WASp was not confirmed by Western blot since no difference in the p34 content was observed in CA-WASp cells in comparison with controls (Figure 4-4-D). I finally analysed if the mutant WASp had any impact on the cell area indicating difficulties or ease for the cells to spread. I could not observe from the confocal images any difference in the area of the two populations suggesting that CA-WASp had no impact on it (Figure 4-4-G). Taken together, these results indicated that CA-WASp did not affect actin polymerisation dynamics nor the expression and localisation of Arp2/3 complex.

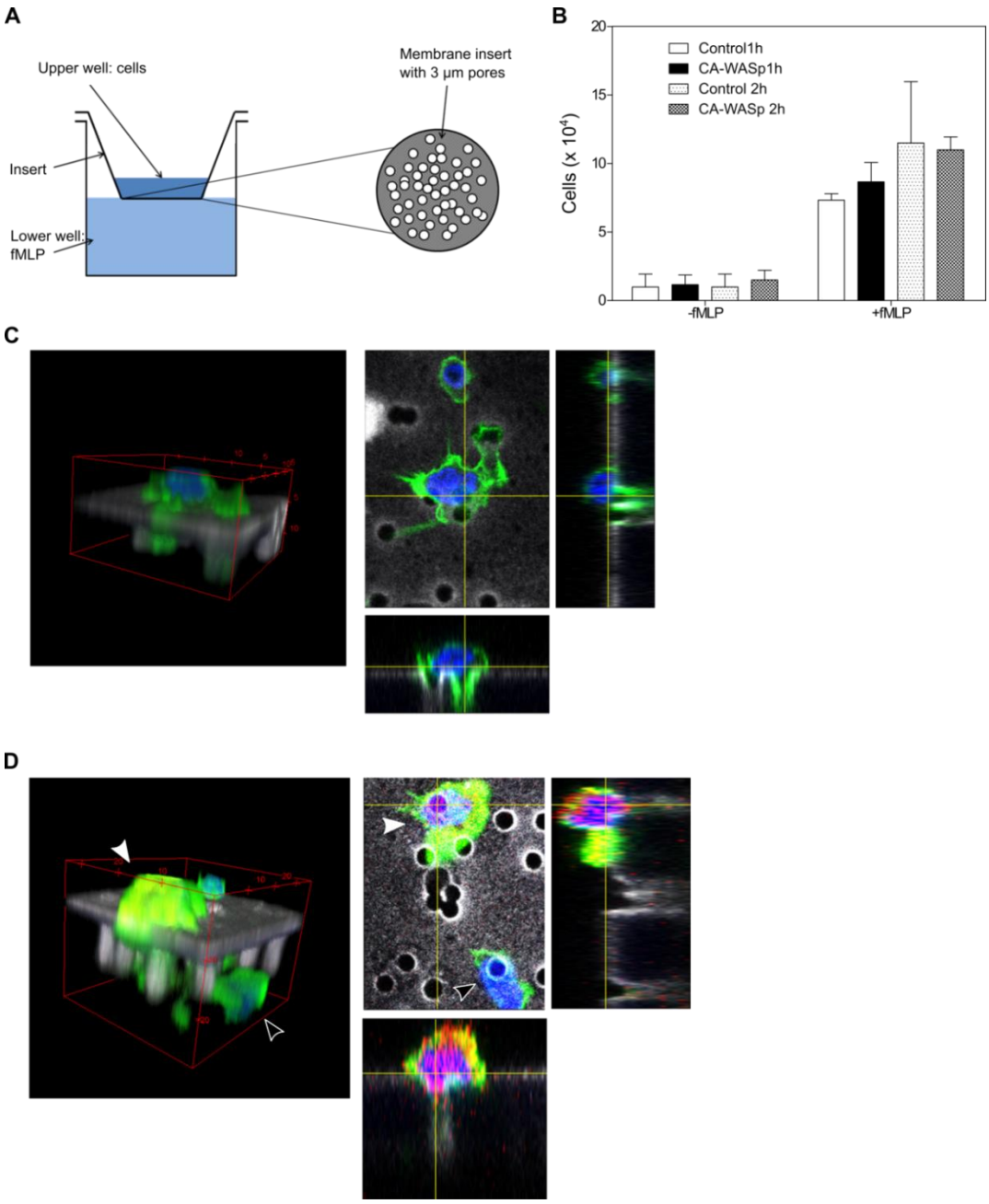

Figure 4-3: CA-WASp did not alter cell migration through 3D environment

A) Schematic representation of the Transwell insert system used to assess the migration of dHL-60 cells. B) Cells expressing CA-WASp did not show significant alteration of their migration in response to 100 nM of fMLP after migrating for 1 hour or 2 hours through the Transwell insert. After the cells were left to migrate for 1 or 2 hours, EDTA was added to each well and the plate placed at 4°C for 15 minutes in order to enhance the detachment of the cells that migrated through the membrane but were still attached to it. Then the medium in the well was resuspended before 20 µL was taken out and mixed in a 1:1 ratio with trypan blue and the cells were counted using a haemocytometer. C and D) 3D and orthogonal views of C) control and D) CA-WASp dHL-60 migrating through the pores of a Transwell membrane, 1 hour after the cells were seeded in the insert. The lower chamber contained 100nM of fMLP. The cells were imaged using a Zeiss LSM710 confocal microscope using an oil immersion 63x/1.4 N.A. objective. Green: F-actin, Red: mCherry-CA-WASp, Blue: Dapi and Grey: fibronectin. Close arrow head: cell of interest; open arrow head: cell that already migrated through the membrane. B: Exploratory experiments that were not investigated further, therefore three independent experiments were not performed. Data from two independent experiments. Three replicates per experiments. C and D: Data representative of two independent experiments.

It has been shown that the expression of CA-WASp induces, through the excess of mislocalised F-actin, an increase of the cytoplasm viscosity (Moulding, 2013). This change of the cell physical properties could alter the forces generated by myosin IIa to ensure the contractility needed to ensure cell migration. Therefore, I studied if myosin activity was altered by CA-WASp expression. Uniformly stimulated dHL-60 expressing or not the mutant WASp were fixed and stained for F-actin and phospho-MLC, which is the active form of the regulatory light chain of myosin (Figure 4-5-A). As previously described, two populations were determined using the mCherry-CA-WASp signal: low mCherry (signal equal to 1 to 1.5 time the background) and high mCherry (signal higher than three time the background). The impact of CA-WASp on the cells was then evaluated in these two populations. Preliminary results suggested that cells expressing CA-WASp may display a modification of pMLC signal with a possible increase of the number of cells that exhibited pMLC localised only at either the lamellipodium or the uropod (Figure 4-5-B), while the number of cells showing a pMLC signal at both lamellipodium and uropod appeared to decrease. These preliminary observations of the cells expressing the mutant WASp further suggested a small increase of the total signal of pMLC per cell (Figure 4-5-C) correlated with an increase of F-actin (Figure 4-5-D). The trend showing the possible increase of pMLC signal was similarly observed by Western blot in two independent experiments (Figure 4-5-E and F). Additional independent experiments would be required to confirm these data. Next, I investigated the possibility to rescue CA-WASp phenotype. As CA-WASp activates Arp2/3 complex to trigger the nucleation of new branched actin filament, I used Arp2/3 inhibitor CK-666 to try and clear the excess of F-actin due to the mutant WASp. I first decided to determine the concentration of CK-666 needed to clear the excess of filamentous actin in the cytoplasm without altering the cortical actin cytoskeleton. To do so, I measured F-actin content in CA-WASp dHL-60 cells, stimulated or not with fMLP and treated with increasing CK-666 concentrations, and compared it with the values obtained for untreated wild-type dHL-60 cells (Figure 4-6-A and B). Using CKK-666 concentrations up to 100 µM was determined as suitable, as it has previously been reported that even at such high concentration, CK-666 did not alter the morphology of Arp2/3 depleted fibroblasts (Wu et al., 2012). This suggested that, despite the low potency of the compound, CK-666 does not seem to

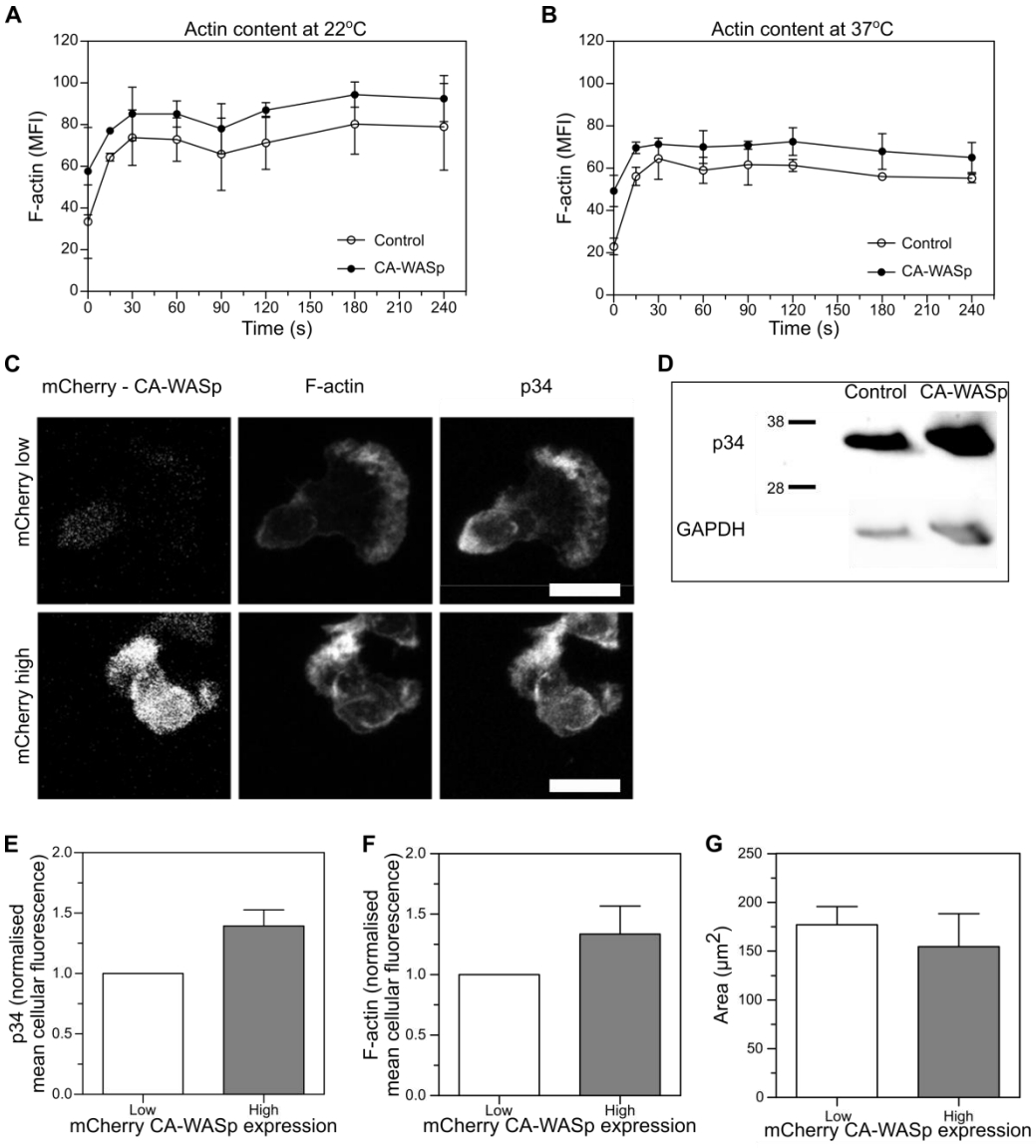

Figure 4-4: CA-WASp did not alter actin polymerisation kinetics and p34 expression

A and B) Actin polymerisation kinetics of control and CA-WASp cells measured at A) 22°C and B) 37°C. Both populations were mixed into the same tube before being stimulated for the indicated time with 100nM of fMLP, fixed using a solution of 4% paraformaldehyde, permeabilised using a 0.2% Triton-X solution and stained with phalloidin-Alexa647. F-actin content was then measured by flow cytometry. C) Confocal images of dHL60 control (top row) or highly expressing mCherry-CA-WASp (bottom row). The cells were stimulated with 100nM of fMLP before being fixed, permeabilised and stained. The cells were stained for F-actin (middle column) and the Arp2/3 subunit p34 (right column). The cells were imaged using a Zeiss LSM710 confocal microscope using an oil immersion 63x/1.4 objective. Scale bar = 10µm. Signals of interest were measured from z-stack projection using CellProfiler. The F-actin signal was used to detect the cell edges and to define ROI in which the p34 and F-actin signals were measured. The ROIs were also used to measure the area of the cells. D) Expression of p34 in control and CA-WASp cells was evaluated by Western blot. E) p34 intracellular signal, F) F-actin content and, G) cell area were measured from the image showed in C) using Cell profiler software (>= 30 cells measured). A-G: Exploratory experiments that were not investigated further, therefore three independent experiments were not performed. Results from two independent experiments, one replicate per experiment.

have off-target effects at concentrations up to 100 µM. Therefore, it was decided to test CK-666 at 10, 20, 40 and 80 µM. In unstimulated conditions, the CA-WASp cells displayed a two fold increase of their F-actin content in comparison to control cells. Treatment with 10 µM of CK-666 for 5 min resulted in a strong decrease of total filamentous actin in cells expressing the mutant WASp. The use of higher concentrations of CK-666 (20, 40 and 80 µM) showed a content of F- actin in CA-WASp cells similar as the one in wild-type cells (Figure 4-6-A). When cells were treated with CK-666 and stimulated with fMLP, only the 10 µM concentration of Arp2/3 inhibitor showed a reduction of the total F-actin but with still a signal still above the wild-type cell baseline. Higher CK-666 concentrations produced a signal below wild-type cell baseline suggesting a complete inhibition of actin polymerisation in response to fMLP stimulation (Figure 4-6-B). From the results of the two experiments described above, I decided to use a concentration of 10 µM of CK-666 since it was the only concentration allowing to clear some of the F-actin due to CA- WASp without preventing actin polymerisation in response to fMLP stimulation. When I tested the effects of CK-666 on cell migration, I could observe that CA-WASp cells treated with the inhibitor had an average velocity of 10.74 $\mu m.min^{-1}$ (+/- 0.65 $\mu m.min^{-1}$) that was lower than untreated CA-WASp (12.46 +/- 0.89 $\mu m.min^{-1}$) or control (14.35 +/- 0.99 $\mu m.min^{-1}$) cells (Figure 4-6-C). The fact that addition of CK-666 seemed to decrease the migration speed of dHL-60 cells expressing CA-WASp revealed that this Arp2/3 inhibitor might not be suitable to rescue the phenotype resulting from the mutant WASp.

4.2.2 CA-WASp impairs cell division through mechanical alteration of the spindle assembly checkpoint

In order to monitor kinetochore oscillations during the spindle assembly checkpoint, I stably expressed the CENP-A protein tagged with GFP in the HT1080 fibroblast cell line. Cells that have been selected to express eGFP-CENP-A, following Neomycin selection treatment for 14 days, were single sorted by Fluorescence-Activated Cell Sorting (FACS) and cultured under Neomycin pressure for 14 additional days. The eGFP-CENPA expression is restricted to the nuclei during interphase with a weak diffuse background and bright dots (Figure 4-7-A). From nuclear envelope breakdown until the end of mitosis, the eGFP-CENPA protein would be

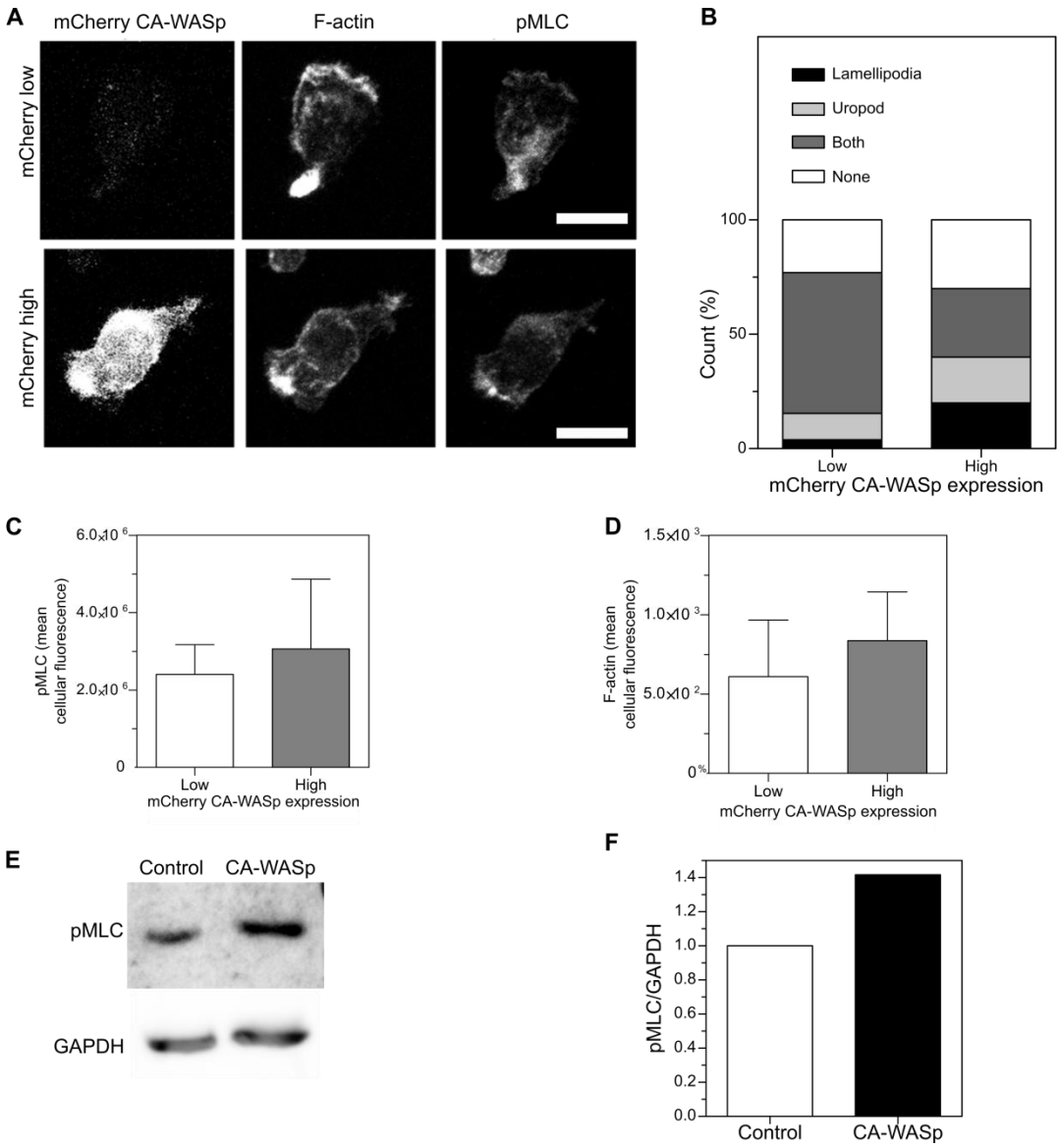

Figure 4-5: Expression of the mutant WASP altered the activity of myosin IIa

A) Confocal images of dHL-60 displaying low or high expression of CA-WASp (top and bottom row, respectively). The cells were stimulated with 100nM of fMLP before being fixed, permeabilised and stained. Cells were stained for F-actin and phospho-MLC, the active form of the myosin. Cells were imaged using a Zeiss LSM710 confocal microscope using an oil 63x/1.4 objective. Scale = 10 µm. B) Localisation of the pMLC signal in control cells and cells expressing the mutant WASp. Signals of interest were measured from z-stack projection using CellProfiler: using the F-actin signal, the cell edges were detected and used to define ROI in which the pMLC and F-actin signals were measured. C) Total intracellular pMLC signal measurement in cells showing a low and high expression of the mutant WASp. D) F-actin content in cells showing a low and high expression of CA-WASp. E) Activity of MLC was assessed by Western blot in control and CA-WASp cells. Band intensity of the Western blot shown in D) was evaluated using ImageJ F). A-F: Exploratory experiments that were not investigated further, therefore three independent experiments were not performed. A-D: data from a single experiment. E) and F) are representative of two independent experiments. One replicate per experiment.

localised to the kinetochores allowing me to track their movement during the spindle assembly checkpoint. The five brightest clones were visually selected (Figure 4-7-B) in order to be able to setup live imaging conditions in which the lowest laser possible would be used to avoid damaging the cells. I measured the five clones' respective signal/noise ratio in order to select the best clone for our experiments by measuring the lowest, corresponding to the background, and brightest, which would be similar to the signal observed when the kinetochores would be assembled, fluorescence signal in a defined region of interest through each slide of the stack (Figure 4-7-C). Of the five clones, three had a signal/noise ratio under 500 and were eliminated. Clones 2 and 3 had a signal/noise ratio of 946 and 810, respectively (Figure 4-7-D). Only clone 2 allowed me to reach the imaging conditions required: an exposure time of 30 ms, low laser power and no delay in mitosis. As a result, clone 2 was used for all following experiments. I monitored kinetochore oscillations in metaphase cells over 5 minutes with one time point every 7.5 seconds imaging a stack of 21 slices through a height of 10 µm to acquire most of the nucleus volume (Jaqaman et al., 2010).

During the spindle assembly checkpoint, I could observe the pairs of kinetochore oscillating (Figure 4-8-A, VideoS4-2 and4-3) confirming the correct localisation of the eGFP-CENP-A constructs during mitosis. A kymograph of a selected kinetochore pair was then prepared and used to measure the amplitude and period of the kinetochore's oscillations (Figure 4-8-B). In control cells, the average period was 96.5 seconds (+/-21.9 sec) (Figure 4-8-C). When wild-type WASp tagged with mCherry or the control vector is expressed carrying mCherry alone, the average period is 98.25 sec (+/- 21.9 sec) and 102.3 sec (+/- 16.3 sec), respectively, with no significant difference from the control. When CA-WASp was expressed, the mean period increased to 118.25 seconds (+/- 18.1 sec) and was significantly different form the control conditions ($p<0.001$). To rescue CA-WASp phenotype, I used the Arp2/3 inhibitor, CK666 at a concentration of 40 µM to clear unregulated polymerisation of actin in the cytoplasm due to CA-WASp. The use of this inhibitor significantly decreased the viscosity of cells expressing CA-WASp, reaching a value close to the one of control cells (Moulding, 2013). When cells expressing CA-WASp were treated with the Arp2/3 inhibitor CK666, the period decreased to

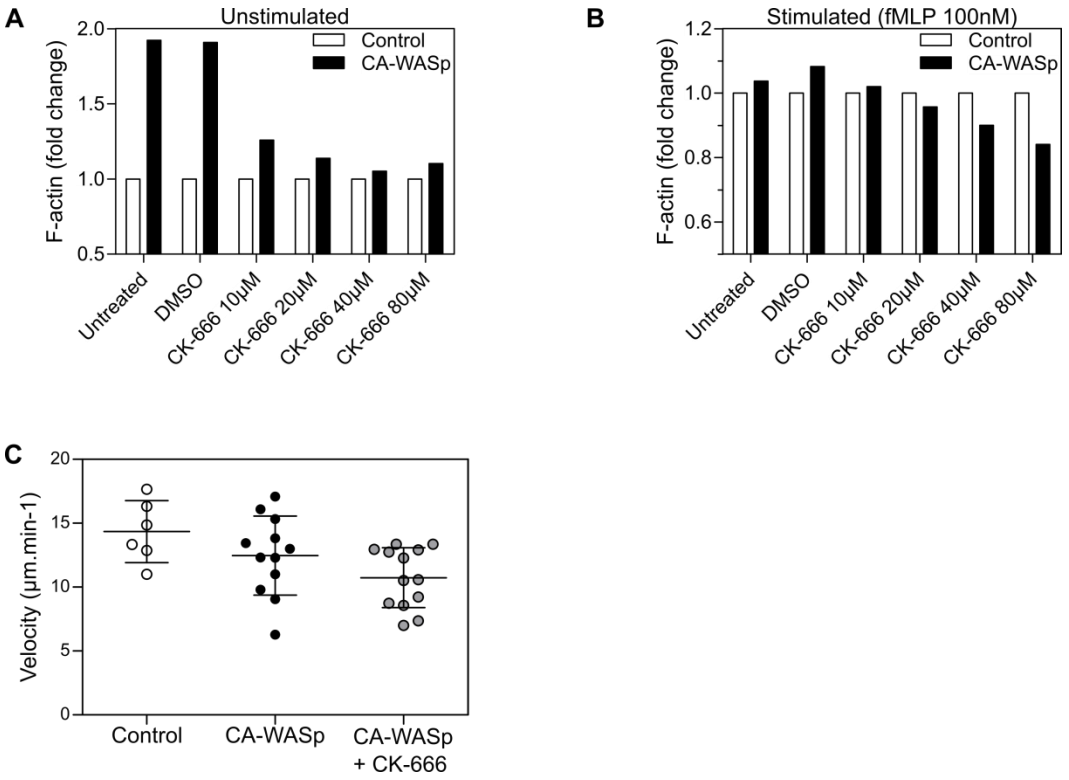

Figure 4-6: Inhibition of Arp2/3 did not rescue of the phenotype caused by CA-WASp

A and B) Assessment of the CK-666 concentration needed to clear the excess of F-actin due to CA-WASp in order to have a similar F-actin content as control cells in unstimulated and fMLP stimulated conditions, respectively. In both unstimulated and stimulated conditions, the cells were processed as follows: in all conditions, control cells were left untreated while the CA-WASp cells were independently treated with CK-666 or DMSO alone (DMSO at a final concentration of 0.2%. This is equivalent to the concentration of DMSO when CK-666 was used at 80µM). Then, control and CA-WASp cells were fixed separately before being mixed together at a 1:1 ratio resulting in a mixed population containing untreated control cells and CA-WASp cells, treated or not. In the stimulated condition B), both control and CA-WASp cells were stimulated with 100 nM of fMLP. The cells were then processed to be stained with phalloidin-Alexa647 in order to measure their F-actin content by flow cytometry. Results from each condition was normalised to the F-actin content of the control cells of that condition. C) Average velocity of control cells, CA-WASp cells and CA-WASp cells treated with CK-666 in the agarose Dunn chamber. A-B: Exploratory experiments that were not investigated further, therefore three independent experiments were not performed. Results from a single experiment, three replicates per condition. C: Results from a single experiment, one replicate per condition.

103.7 seconds (+/- 19.6 sec) with no significant differences from the control conditions but significantly different from the cell expressing CA-WASp ($p<0.05$).

The amplitude of oscillations was 3.12 µm (+/- 0.65 µm), 2.86 µm (+/- 0.45 µm) and 3.42 µm (+/- 0.59 µm) in control cells, cells expressing WT-WASp and cells expressing CA-WASp, respectively (Figure 4-8-D). No significant difference was found between the various conditions. To calculate the oscillation speed, the speed was defined as the following:

$$S = {}^{A}/_{P}$$

Where S is the speed (in $\mu m.s^{-1}$), A is the amplitude (in µm) and P is the period (in seconds) of the oscillations. The speed of control cells was 34.3 $nm.s^{-1}$ (+/- 8.2 $nm.s^{-1}$) whereas in WT-WASp or CA-WASp cells, the oscillation speed was 29 $nm.s^{-1}$ (+/- 5.2 $nm.s^{-1}$) and 27 $nm.s^{-1}$ (+/- 4.3 $nm.s^{-1}$) respectively. The speed difference between CA-WASp expressing cells and control cells was significant (Figure 4-8-E).

4.3 Discussion

4.3.1 The loss of the auto-inhibited conformation of WASp alters neutrophil migration

To investigate the consequences of constitutively activated WASp expression on neutrophil migration, I used HL-60 cell line differentiated into neutrophil-like cells and expressed in these cells the mutant protein by transduction with lentiviruses.

Expression of CA-WASp in HL-60 cells using lentiviruses resulted in expression levels of the mutant WASp in the same order of magnitude than the endogenous WASp. This result was expected as a previous study in the lab (Moulding et al., 2007) showed the difficulty to express CA-WASp at high levels. This might be due to the open conformation of CA-WASp that might enhance its degradation. Nevertheless, such expression pattern of CA-WASp as the one observed in HL-60 were previously shown to be sufficient to induce an excess of F-actin in the cytoplasm causing mitotic defects in other hematopoietic cells (Moulding et al., 2007). This suggested that such expression levels of CA-WASp in HL-60 cells would lead to unregulated

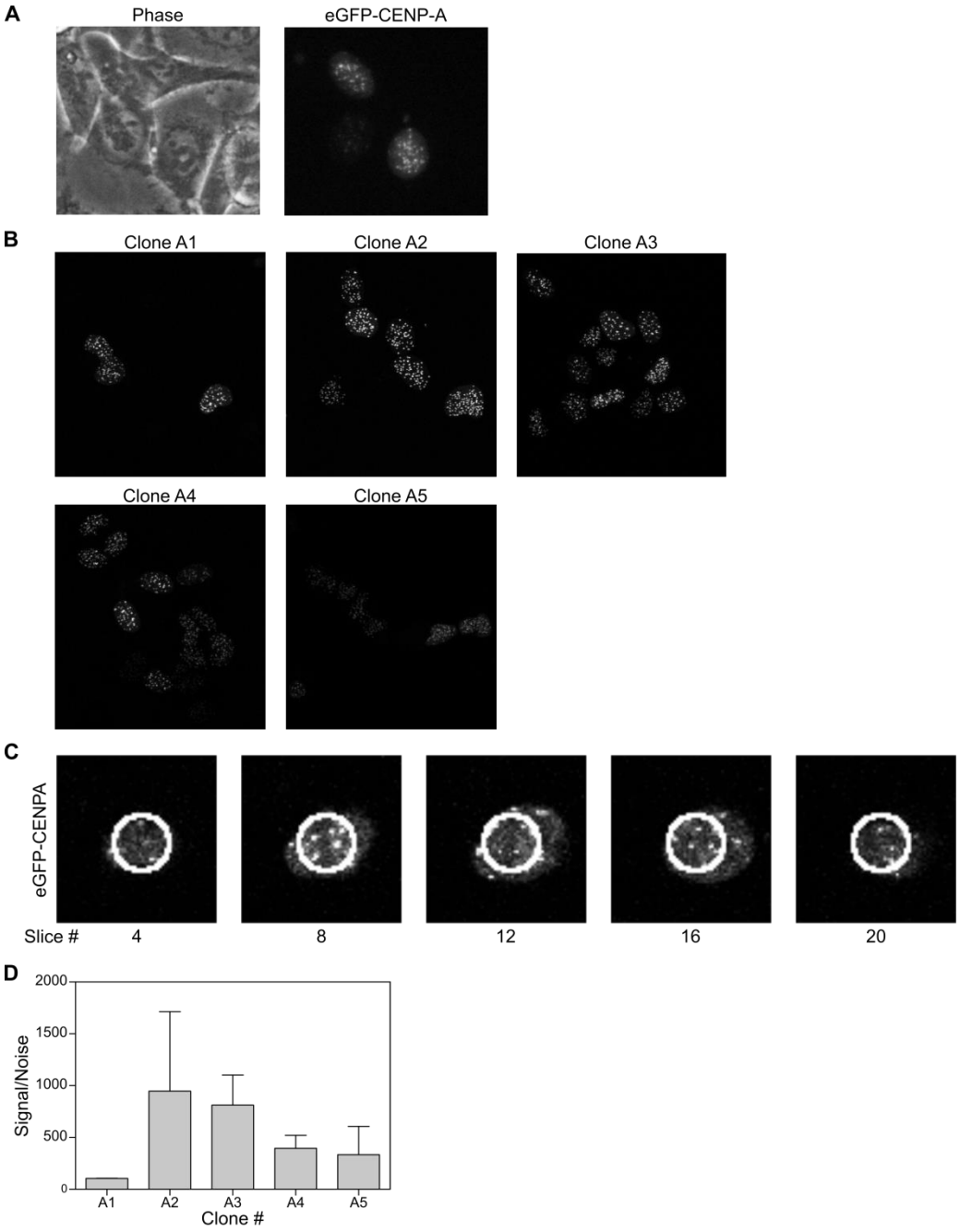

Figure 4-7: Expression of eGFP-CENP-A construct in HT-1080

A) Expression of eGFP-CENP-A in the HT-1080 fibroblast cell line observed using an epifluorescence microscope equipped with a 20x/0.2 air objective. Phase contrast image is shown on the left panel, while on the right the cells expressing the eGFP construct can be seen in the FITC channel. We can observe that eGFP-CENP-A expression is restricted to the cell nucleus. B) Z-projection of confocal images of the 5 brightest clones shows different levels of eGFP-CENP-A expression. The cells were left to adhere for 24 hours on coverslips before being fixed and mounted using prolong gold mounting medium. Then the cells were imaged using a LSM710 confocal microscope equipped with a 40x/1.0 water objective. C) Representative measurement of the signal/noise ratio. Using ImageJ/Fiji, a ROI was drawn in the nucleus of each cell (white circle). Within the ROI, the lowest (noise) and highest (eGFP-CENP-A structures) fluorescent signals were measured in each slice of the z-stack to calculate the signal/noise ratio. Here a cell from the clone A2 was used as example. For clarity, only the slices 4, 8, 12, 16 and 20 are shown here. D) Signal/noise ratio calculated using the method showed in C). A-D: The experiments were used for optimisation of experimental conditions therefore three independent experiments were not performed. Data from two independent experiments. One replicate per experiment.

and mislocalised actin polymerisation and might affect cell mechanical properties. Our subsequent results (Figure 4-4-A) confirmed an increase of actin content in CA-WASp cells of about 40-50% when compared to untransduced control cells, suggesting a similar phenotype as the one of U937 cells transduced with CA-WASp lentiviruses (Moulding et al., 2007).

The use of lentiviruses to transiently express the mutant WASp in cell lines was chosen over the constitutive expression of CA-WASp as it was known in the group that the latter resulted in cell death after 5-7 days of expression due to mitosis defects. Considering that HL-60 cells required a 5 day-treatment with DMSO in order for them to differentiate into dHL-60, we could argue that the expression of CA-WASp in these cells would result in a high number of dead cells due to apoptosis, and as such may introduce a bias in the results obtained. However, during HL-60 differentiation into neutrophil-like cells, the HL-60 stop dividing after 1-2 days in the presence of DMSO in the culture medium (Sun and Wang, 1995). In the current study, the cells were transduced only 24 hours before treatment with DMSO to differentiate them, and would as a consequence stop dividing quickly after the transduction, probably limiting the effect of the expression of CA-WASp on cell division and death. Nevertheless, it would be interesting to confirm this by studying apoptosis and necrosis of HL-60 expressing the mutant WASp during differentiation. The dHL-60 cells expressing CA-WASp showed an alteration of their ability to migrate characterised by a decrease of their velocity. Their directionality during migration was not altered and their chemotactic capacity was similar to that of control cells. The average angle distribution suggested that cells expressing the mutant protein were less likely to change direction from the fMLP gradient; but this tendency was not reflected in the chemotactic index, which was nearly identical between CA-WASp and control cells. Surprisingly, the migratory defect was not observed in confined environment through the pores of a Transwell insert when the cells were left to migrate for 2 hours (Figure 4-3). On the contrary, when the cells were allowed to migrate for only one hour the CA-WASp cells seemed to display a better, although not significant, migratory response compared to control. This was unexpected as this does not correlate with the Dunn chamber results and would then need to be confirmed. The possible small difference between control and CA-WASp cells could be investigated further by repeating

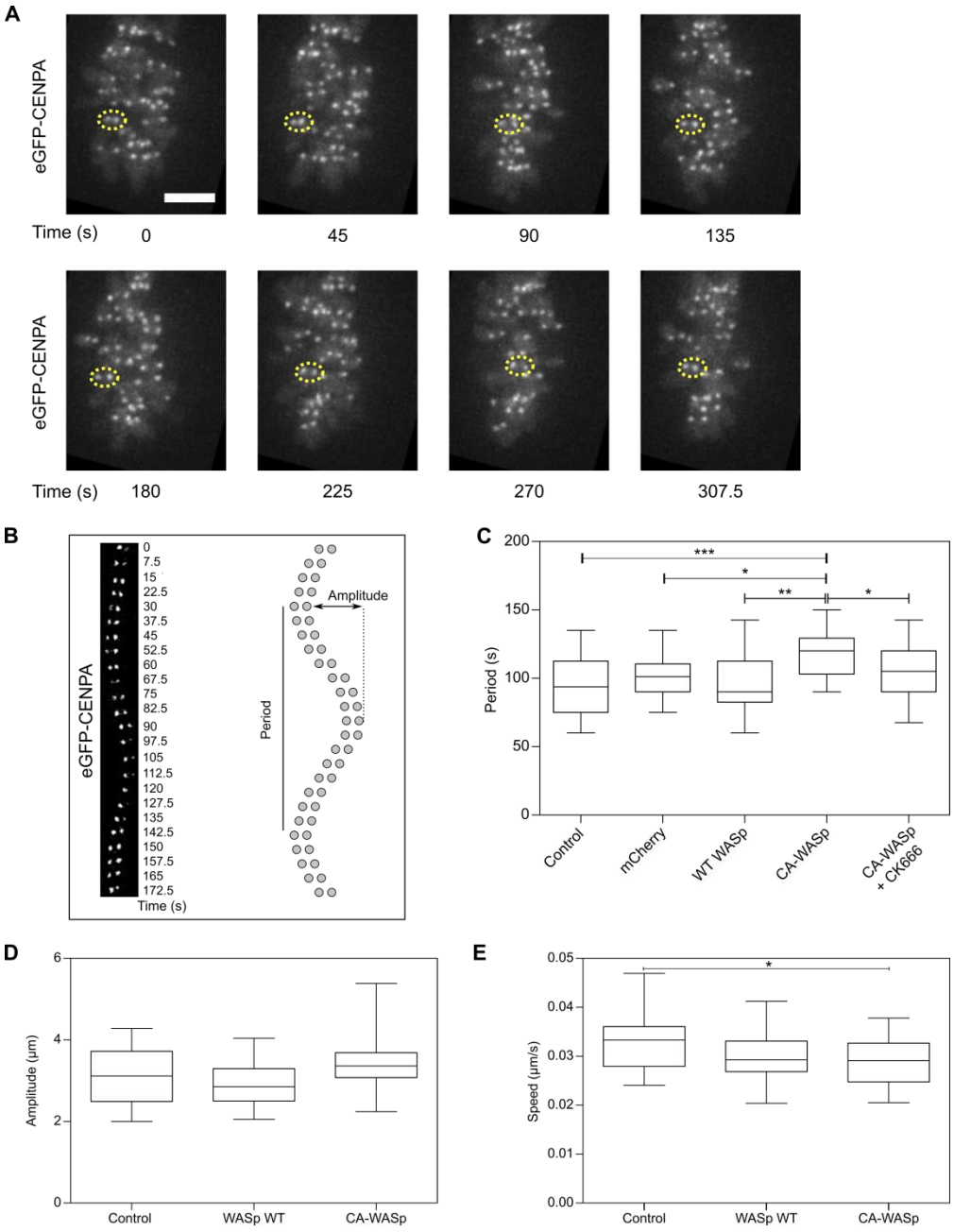

Figure 4-8: F-actin excess due to CA-WASp altered kinetochore dynamics

A) Time lapse of kinetochore pair oscillations during the spindle checkpoint image using a100×/1.4 NA oil objective lens on a Olympus IX81 microscope fitted with Andor Spinning Disk confocal system and a 37°C environmental chamber. A z-stack composed of 20 z sections (0.5 µm apart) was taken every 7.5 s for 5 minutes. One pair of kinetochore was highlighted (dashed circle). Z-projection of 5 successive slices of the whole stack was visualised here. Scale bar = 8 µm. B) Kymograph of a kinetochore pair oscillating over time and graphical representation of the oscillation. C) Period of the kinetochore oscillation in control cells (control and mCherry) and in cells expressing wild-type WASp, CA-WASp, and CA-WAp in presence of the Arp2/3 inhibitor CK-666. The mCherry, mCherry-WASp wild type and mCherry-CA-WASp transgenes were expressed in the cells using lentiviruses carrying the transgene under CMV promoter. D and E) Amplitude and speed of the kinetochore oscillation in control, WT WASp and CA-WASp cells. A: Images representative of three independent experiments. C-E: Data from three independent experiments. Data analysed by ANOVA; C and E: *: p <0.05. C: **: p <0.01, ***: p <0.001.

the experiment at a shorter time point, such as 30 minutes, as the CA-WASp cells might have an advantage at short time point but not at longer time points such as 2 hours. Nevertheless, it remains challenging to directly compare results from the Transwell system and the Dunn chamber. The cells do not migrate in the same environment, 2D in the Dunn chamber and the confined environment of the pore of the membrane of the Transwell insert, suggesting that different mechanisms could be involved. The defect observed in CA-WASp cells in the Dunn chamber could be explained by two different hypotheses: a) the constitutively activated WASp mutant altered actin polymerisation by sequestering components of the actin polymerisation machinery such as Arp2/3 complex or b) the excess of F-actin would change cell properties, impairing the physical abilities of cells to migrate. I investigated both hypotheses and tried to rescue the phenotype using the Arp2/3 inhibitor CK-666.

Firstly, the misclocalisation of the filamentous actin excess through the cytoplasm was hypothesised to alter the spatio-temporal regulation of the actin polymerisation in CA-WASp cells by hijacking the molecular components that are responsible for actin filament nucleation, such as Arp2/3. However, I could show that actin polymerisation did not seem to be defective in the cells expressing CA-WASp (Figure 4-4). Nevertheless, despite similar kinetics between control and CA-WASp cells during the stimulation with fMLP, the initial response of the two populations to the chemoattractant might be different. The slope of the initial response of control cells to fMLP seemed slightly steeper than the slope of the CA-WASp cells. This suggested that the mutant cells might have a lower initial polymerisation rate before reaching a plateau at 30 seconds of stimulation. It would be very interesting to confirm this result and investigate the possible mechanism. The absence of strong defect in actin polymerisation was supported by results showing that Arp 2/3 complex expression was not modified and was still strongly located in the lamellipodium. This could be the result of a too low expression of the mutant WASp to completely hijack the Arp2/3 machinery. Indeed, it has been shown that Arp2/3 concentration in neutrophils was about 10 µM, a concentration far above the limiting Arp2/3 concentration to nucleate actin filament (Higgs et al., 1999). Higgs *et al.* also showed that *in vitro*, in presence of a low concentration of G-actin (4 µM) and of Arp2/3 (50 nM), actin

nucleation reached a plateau in presence of 1 µM of WASp VCA domain. This suggested that, to prevent spatio-temporal regulation of Arp2/3 resulting in the alteration of actin structure in the cells, CA-WASp should have been expressed at very high level which was not possible in these cells.

The fact that the mutant WASp did not alter Arp2/3 localisation in the lamellipodium could explain why I could not observe any strong modification of the cell directionality. Indeed, it has been shown that Arp2/3 was required for lamellipodium establishment and for directional migration of fibroblasts (Suraneni et al., 2012). The high concentration of Arp2/3 in neutrophils preventing its depletion in the lamellipodium due to the actin polymerisation in the cytoplasm may have avoided directionality alteration of CA-WASp dHL-60 cells in the agarose Dunn chamber. I observed that the variation of the average angle distribution of cells expressing the mutant WASp was reduced indicating a more directional migration than that of control cells; but I could not identify the same effect from the chemotactic index calculation. These two results showed that both measures had their limits: the chemotactic index may not be sensitive enough to detect small changes, whereas the F-test used to determine the significance of the variance difference between the two conditions is highly sensible to bias introduced by the possible non-normal distribution of the results (Fisher et al., 1995). This shows that interpretation of directionality measurement need to be carefully performed.

The second hypothesis was that excess of F-actin due to CA-WASp would alter cell properties and lead to migratory defects. It has been shown that F-actin excess in the cytoplasm modified cell physical properties by increasing cytoplasm viscosity by two fold when compared to control cells (Moulding et al., 2012). Because contractility of the acto-myosin cortex is required for cell migration, it was hypothesised that the change in physical properties would influence myosin II activity. It has been shown that myosin II activity is necessary to break cell symmetry (Yam et al., 2007) to allow the formation of protrusions, is involved in actin retrograde flow regulation in the lamellipodium (Cai et al., 2006; Yang et al., 2012) and drives the retraction of the rear of the cells (Eddy et al., 2000, p. 200). We could think that the increase of cytoplasm viscosity may prevent the correct retraction of the rear and may necessitate an increase of myosin activity

in the uropod to generate enough forces to allow the correct retraction of the cell rear. Preliminary results are in line with this hypothesis: a possible increase of MLC activity in CA-WASp cells was observed by immunofluorescence and Western blot (Figure 4-5). This increase in pMLC signal seemed to be accompanied by a change in pMLC localisation pattern with a preferential accumulation of signal in the lamellipodium. If new evidences support these findings, we could hypothesise that MLC activity would compensate the change in cell physical properties, which may explain why no uropod retraction defect was observed in cells expressing CA-WASp. Also, as myosin is involved in the regulation of the actin retrograde flow in the lamellipodium, an increase of pMLC signal in the lamellipodium could be a consequence of the alteration of actin dynamics in the lamellipodium (Ponti et al., 2004; Vicente-Manzanares et al., 2007).

To demonstrate that the excess of cytoplasmic F-actin was responsible for the observed migratory defect and for the increased myosin light chain activity, I tried to rescue the phenotype by clearing cytoplasmic actin using the Arp2/3 inhibitor CK-666. Preliminary results showed that at a low concentration of 10 µM, CK-666 seemed to partially clear F-actin excess without altering actin polymerisation in response of fMLP stimulation. When I used the Arp2/3 inhibitor on migrating cells expressing the mutant WASp, preliminary results showed a decrease of cell velocity when compared to untreated CA-WASp expressing cells. The interpretation of this result was delicate as a control condition with the vehicle (here DMSO) would have been more suitable. Nevertheless, it seemed that the inhibitor might not only have been clearing the cytoplasmic actin in excess due to the mutant WASp but probably also altering normal actin migratory structures in the cells. This result together with published evidences that CK-666 lead to a switch from lamellipodium to bleb based migration (Bergert et al., 2012) prevented the use of CK-666 to rescue the phenotype resulting from the constitutively activated WASp.

It should be noted that the results presented here were obtained from cells transduced with lentiviruses driving the expression of CA-WASp under the SFFV promoter and these were compared to untransduced cells. It would have been of great importance to use cell transduced with lentiviruses driving the expression of the tag protein mCherry alone similarly to the control

used in the kinetochore experiments. However, for reasons that were not identified, the titre of the production of lentiviruses driving the expression of mCherry alone under the promoter SFFV was repetitively too low to be used hence preventing the use of these lentiviruses as control. Using such control would strengthen the results and allow to discard any possible alteration of the cells by the transduction process.

To conclude this first section, it was hypothesised that the unregulated actin polymerisation due to the mutant WASp would alter the actin structures or the mechanical properties of neutrophils and would lead to a migratory defect. Surprisingly, the mutant WASp did not seem to dramatically alter neutrophil actin migratory structures as it has been described in patient macrophages (Ancliff et al., 2006). This suggested that only the modification of the cytoplasmic viscosity might be responsible for the migratory defects observed in CA-WASp dHL-60. As migration is heavily based on rearrangement of the actin cytoskeleton and that it has been very challenging to discriminate the actin structures independent of the mutant, like the lamellipodium, from the excess of F-actin resulting from the WASp mutant, it has been difficult to study in-depth this mutant role in neutrophil migration and to understand the molecular mechanism responsible for the migratory defect.

However, it would have been interesting to study the effect of CA-WASp on other regulators of the actin cytoskeleton. It has been shown that the actin cytoskeleton depending of formins are competing for G-actin with the actin cytoskeleton depending of Arp2/3 (Burke et al., 2014). Since it has been shown that the formin mDia1 is required for polarisation and migration of neutrophils (Shi et al., 2009b), it would have been interesting to investigate the effects of CA-WASp on the localisation, expression and activity of mDia1. Another interesting candidate would have been the cofilin protein, which is involved in actin filament depolymerisation. It has been shown that cofilin is necessary for the chemotaxis of dHL-60 cells (Hirayama et al., 2007). It would also be interesting to investigate how expression of cofilin was affected by the expression of CA-WASp in order to maintain correct actin filament depolymerisation.

The expression of CA-WASp mildly altered neutrophil migration suggesting the neutropenia and recurrent bacterial infection affecting XLN patients may not be primarily caused by a

migratory defect. This would indicate that a cell division defect would be the main factor responsible of the neutropenia and the subsequent bacterial infections.

4.3.2 CA-WASp impairs cell division through mechanical alteration of the spindle assembly checkpoint

The expression of CA-WASp resulted in a mislocalised excess of F-actin through the whole cell and has been shown to result in a two fold increase of the cytoplasmic viscosity (Moulding et al., 2012). The mitosis defects with the reduction in chromosome speed during their segregation suggested they were due to the increase in cytoplasm viscosity. Therefore, I looked at the chromosome oscillation during the spindle assembly checkpoint, hypothesising that the excess of F-actin could alter the sensing of the correct attachment of the microtubules to the kinetochores.

I studied the oscillation of kinetochores by time-lapse imaging and could observe that the kinetochore oscillation period was increased in cells expressing CA-WASp and this phenotype could be rescued by inhibiting Arp2/3 actin polymerisation using the CK-666 inhibitor. The increase of the kinetochore oscillation period in CA-WASp cells could be due to either a decrease of speed or an increase of amplitude. The measurement of these parameters demonstrated that the speed but not the amplitude was affected by the excess of F-actin. As it has been shown that the excess of F-actin due to CA-WASp caused an increase of cytoplasmic viscosity (Moulding et al., 2012), we hypothesised that the increased cytoplasmic viscosity only affected the speed of the chromosome movement. This was supported by previous results from the group showing a decrease of chromosome speed during their segregation (Moulding et al., 2012) in cells expressing CA-WASp. Surprisingly, the decrease of speed was less than what was expected. Indeed, because cytoplasm can be defined as a viscous fluid (Darling et al., 2006), the relationship between velocity, viscosity and force applied on the kinetochores to generate the movement is defined by: $F \sim \mu V$ where F is the force applied, μ the viscosity and V the velocity. Thus, for a two fold increase of viscosity, we should have expected a decrease of 50% of the speed of the chromosome movement. Here, we observed a reduction of speed of 22%, far from what was envisioned suggesting a possible compensation mechanism. We

subsequently showed that an increase in quantity of kMT compensated the increased viscosity (Moulding et al., 2012).

Cell division is a process that mechanically segregates the genomic content of one cell into two identical daughter cells. This process relies on the physical properties of the cell in division and, if the alterations of these properties exceed the resistance of the cell, it leads to the impairment of the cell division completion. The results presented here and the one published by Moulding *et al.* (Moulding et al., 2012, 2007) showed that the mechanical alteration of cell properties due to the excess of filamentous actin as a result of constitutively active WASp is responsible for inducing cell division defects. This was consistent with our knowledge that WASp has no role, by itself, in cell division. Nevertheless, the tight regulation of actin cytoskeleton during cytokinesis is critical to ensure that the physical properties of the cleavage furrow do not prevent cell division completion. It would be of interest to investigate if the excess of F-actin due to CA-WASp could lead to a mislocalisation and/or to the alteration of expression of regulators of the acto-myosin cytoskeleton.

We could think for example of cofilin which regulates actin filament disassembly and when its activity was inhibited led to an increase in F-actin content in the cells resulting in delay in mitosis, and increased the number of cells with nuclear abnormalities (Gohla et al., 2005). Another candidate could be the actin interacting protein 1 that is involved in the regulation of actin filament disassembly by cofilin and, when AIP1 expression was knocked down, it resulted in F-actin excess in the contractile ring during cytokinesis, which further led to an increase of multinucleated cells (Kato et al., 2008).

Another important player of cell mechanics is the non-muscular myosin II. It has been shown that myosin II activity was important for the position of the cytokinetic furrow (Sedzinski et al., 2011) and for actin localisation and dynamics at the contractile ring (Murthy and Wadsworth, 2005). It has also been shown that inhibition of myosin II at the contractile ring prevented the achievement of the cytokinesis (Guha et al., 2005; Murthy and Wadsworth, 2005). We could speculate that concomitantly to the partial clearance of F-actin by cofilin, an increase of myosin II activity could be increased in order to compensate the alteration of the cell physical properties and allow cytokinesis completion.

As the expression of CA-WASp results in an excess of F-actin in the cytoplasm that is responsible for an increase of cytoplasmic viscosity (Moulding et al., 2012), it would be interesting to investigate if CA-WASp could be used as a model to study mechanical dependent mechansims.

For example, it is known that Aurora B plays an important role in sensing the amphitelic attachment tension and that during the oscillation of the spindle assembly checkpoint, the distance between the inner and outer kinetochores was modified depending if the kinetochore was pulled or pushed away from the cell pole (Dumont et al., 2012). Thus, we could use the expression of the mutant WASp to alter the cytoplasm properties and perturb the kinetochore stretching in order to study Aurora B activity on the different kinetochore structures. This would allow us to get a better understanding of the mechanisms of the spindle checkpoint.

In conclusion, we showed that CA-WASp expression resulting in excess of F-actin impaired both the spindle assembly checkpoint and neutrophil migration. The defect in the spindle assembly checkpoint could be responsible for the neutropenia observed in the patients, while the migratory alteration could prevent the few circulating neutrophils to reach the infection site. This highlights the importance of the mechanical properties of the cytoplasm in the correct achievement of processes that rely on cell shape changes. The mutant WASp perturbs processes in which it has no known role and could be used as a model to perturb cell mechanics in other cellular functions such as cell spreading, apoptosis and mechanosensing.

Chapter 5 Role of MKL1 in neutrophil migration

5.1 Introduction

MKL1 and its homolog MKL2 are members of the myocardin-related transcription factor (MRTF) protein family and shuttle between the cytoplasm and the nucleus to regulate the transcriptional activity of the Serum Response Factor (SRF) (reviewed in (Olson and Nordheim, 2010). MKL1 has the ability to bind G-actin through its RPEL domains. In the cytoplasm, G-actin binding to MKL1 prevents the import of MKL1 into the nucleus, inhibiting the transcription of MKL1/SRF-dependent genes. In the nucleus, the binding of G-actin to MKL1 promotes the export of MKL1 into the cytoplasm, inhibiting its transcriptional activity. It has been shown that, when globular actin is incorporated into actin filament due to the stimulation of the actin polymerisation machinery, the subsequent decrease of available G-actin in the cytoplasm releases MKL1 that can shuttle into the nucleus to activate the transcription of SRF dependent genes (Figure 5-1:). Therefore, MKL1 activity depends on the G-actin levels in the cytoplasm and nucleus and reflects the dynamics of actin filament polymerisation. The actin-MKL1-SRF circuit modulates the transcription of genes in correlation with the dynamics of polymerisation and depolymerisation of the actin cytoskeleton. SRF targets genes that encode proteins involved in the regulation of the actin cytoskeleton as well as the actin protein itself (Miralles et al., 2003; Vartiainen et al., 2007) creating a feedback regulation of all cellular activities dependent on the actin cytoskeleton. MKL1 and MKL2 are widely expressed and have been shown to regulate muscle tissue, contractile, actin cytoskeleton and cell motility genes (Gilles et al., 2009; Olson and Nordheim, 2010). Recently, MKL1 and MKL2 have been shown to be involved in megakaryocyte maturation (Cheng et al., 2009; Smith et al., 2013, 2012) and several studies

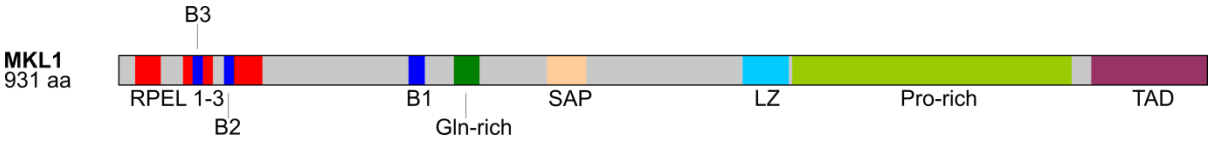

Figure 5-1: MKL1 domains

MKL1 binds to G-actin via its RPEL domains. When not bound to G-actin, the basic nuclear localisation sequences B2-3 in the RPEL domains is free to interact with importin α/β leading to the accumulation of MKL1 in the nucleus. Once in the nucleus, MKL1 binds to the Serum Factor Response (SRF) and drives the transcription of numerous genes, including actin cytoskeleton related genes, via its transactivation domain. RPEL:actin-binding domain; B1-3: basic nuclear localisation sequence; Gln-rich: glutamine rich sequence; SAP: DNA-binding domain; LZ: Leu Zipper coiled-coil region; Pro-rich: Proline-rich domain; TAD: Trans-Activating Domain; MKL1: Megakaryocytic Leukemia 1 protein

emphasise the importance of MKL1 in the maturation and migration of megakaryocytes (Cheng et al., 2009; Gilles et al., 2009). Despite these evidences, the role of MKL1 in immune cells has not been reported. The work presented here describes for the first time a patient with a deficiency of MKL1 resulting in a severe immunodeficiency syndrome. The absence of MKL1 is responsible for low levels of polymerised actin in neutrophil, myeloid and lymphoid cells and results in impaired migration of neutrophils.

Disclaimer: Part of this work has been done in collaboration. Figure 5-2 A and B have been done in Kimberley Gilmour's Lab. Figure 5-3A, B, C, and Figure 5-5 A has been done by Dessi Malinova. Figure 5-7D was done by Karolin Nowak. Primary fibroblasts from healthy donors were kindly provided by Dr Syed.

5.2 Results

A young patient was treated for Pseudomonas septic shock associated with meningitis, malignant otitis externa, and more than thirty cutaneous and subcutaneous abscesses. The patient responded slowly to the antibiotic therapy and after initial investigation, a neutrophil deficiency was suspected.

Neutrophil phagocytosis was tested and showed a dramatic decrease of patient neutrophils to phagocyte pre-opsonised *E. Coli* over time (Figure 5-2-A and B). To test the possibility that not only phagocytosis was deficient, indicating a possible cytoskeletal defect, the ability of patient neutrophils to migrate was tested using the agarose Dunn chamber setup. Patient cells displayed severe migratory defects with more than 90% of cells unable to migrate, compared to healthy donor cells where only 35% failed to migrate (Figure 5-2-C and E, Video S5-1 and5-2). The few patient neutrophils that were able to migrate did so with a reduced velocity of 6.3 $\mu m.min^{-1}$ (+/- 0.6 $\mu m.min^{-1}$) compared with 12.4 $\mu m.min^{-1}$ (+/-0.4 $\mu m.min^{-1}$) for control cells (Figure 5-2-E). Nevertheless, these rare migrating cells followed the direction of the fMLP gradient, suggesting a correct signal transduction in response to fMLP (Figure 5-2-F and G).

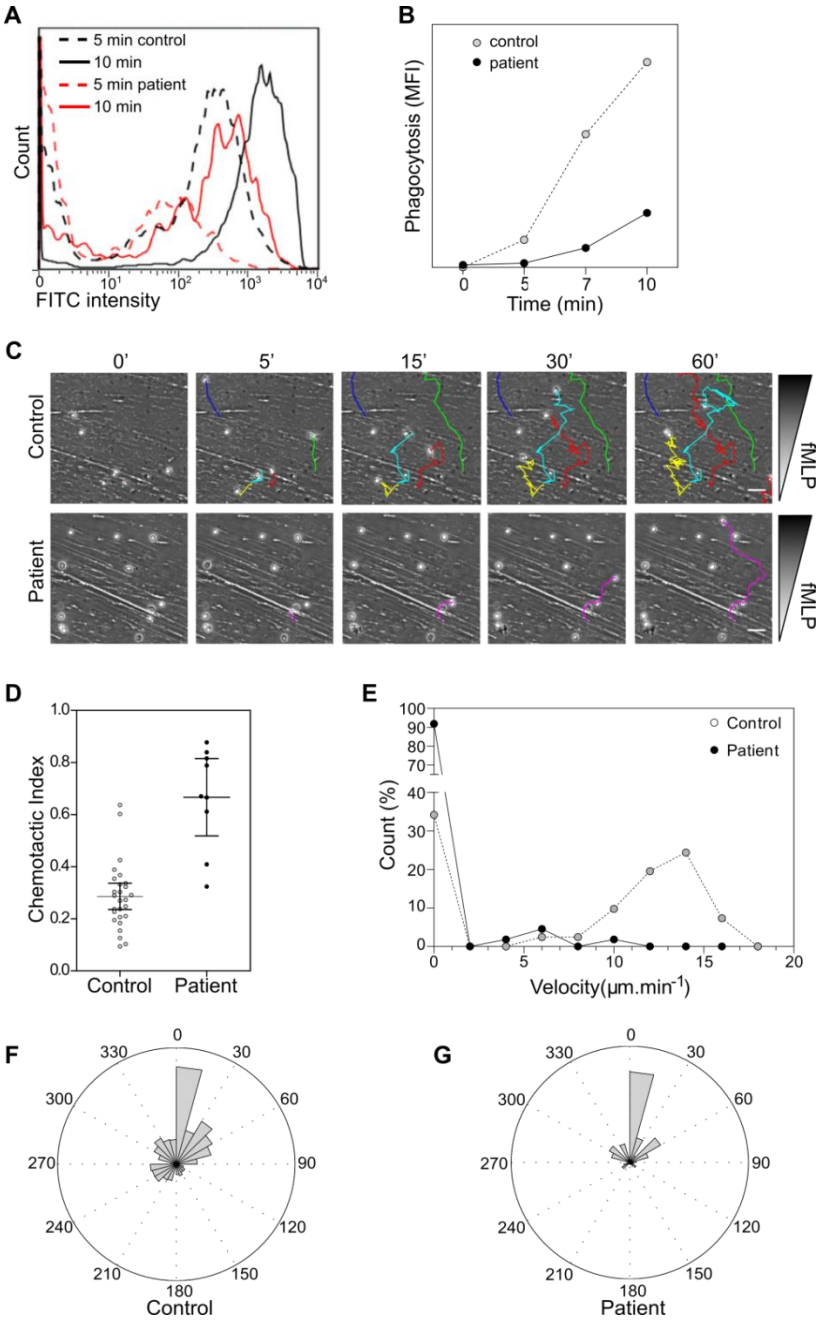

Figure 5-2: Patient neutrophils displayed phagocytosis and migration defects.
A) Bacteria uptake measured by flow cytometry at 5 and 10 minutes after mixing the blood sample with the opsonised FITC *E.coli* ($4x10^7$ bacteria per 100µl of whole blood). B) Quantification of the bacterial uptake as seen in A) at 5, 7 and 10 minutes. C) Snapshots from the video of migrating neutrophils from patient and control samples in the agarose Dunn chamber in the direction of 100nM of fMLP. The cells were imaged at 37°C at 1 image/minute for 1 hour using an Axiovert 135 microscope, equipped with an Achroplan 10x/0.25 objective, an environmental chamber and a motorised stage. Cells were tracked using the ImageJ manual tracking plug-in and tracks were processed in Matlab using an in-house routine. D) Chemotactic index calculated from the migration experiment. E) Frequency distribution of the average velocity of the individual cells during the migration of control and patient neutrophils in the agarose Dunn chamber. F and G) Frequency distribution of the average angle between the chemoattractant gradient and the cell migration path of F) control and G) patient neutrophils. A-G: The data were collected from a single experiment, one replicate.

Patient neutrophils also showed a higher mean chemotactic index compared to control (Figure 5-2-D). These results need to be considered carefully due to the low percentage of patient cells migrating (<10%). This set of results showed that both phagocytosis and migration were impaired suggesting an alteration of the actin cytoskeleton, myosin regulation or integrin function. Supporting the hypothesis of an actin cytoskeletal defect, low levels of polymerised actin were found in lymphoid (Figure 5-3-A and B) and myeloid (Figure 5-3-A and C) cells. The patient's clinical results suggested an unidentified disorder and since the patient was born to second cousin consanguineous parents, we hypothesised a recessive mutation was responsible for the defects observed. Using whole exome sequencing, a nonsense variant K723X in the *MKL1* gene was identified, predicting a truncated MKL1 protein. The presence of the mutation was confirmed by Sanger sequencing (Figure 5-3-D) and Western blot of patient peripheral blood mononuclear cells (PBMC) and EBV-transformed lymphoblastoid cell line (LCL) showed the absence of full length MKL1 protein (Figure 5-3-E and F respectively).

To confirm that the disruption of MKL1 in neutrophils was responsible for the observed phenotype, MKL1 expression in the HL-60 cell line was knocked-downed using lentiviral vectors carrying shRNA against MKL1 (HL-60 MKL1). Protein expression levels were analysed by Western blot and showed that HL-60 MKL1 and neutrophil-like differentiated HL-60 MKL1 (dHL-60 MKL1) expressed only 10-20% of the protein compared to the HL-60 SCR and dHL-60 SCR cells carrying the scrambled shRNA (Figure 5-4-A-C). The dHL-60 MKL1 cells displayed low levels of F-actin compared to dHL-60 SCR cells as in patient cells (Figure 5-4-D). Since MKL1 controls the expression of numerous genes involved in the actin cytoskeleton regulation, I tested the ability of the differentiated cells to polymerise actin in response to fMLP. dHL60 cells showed an almost 2 fold increase in polymerized F-actin when treated with fMLP, as did cells expressing the scrambled shRNA (Figure 5-4-E). MKL1 shRNA cells displayed a lower level of F-actin representing 70% of the F-actin level of dHL-60 WT (Figure 5-4-F). Stimulation of dHL-60 MKL1 with fMLP triggered actin polymerization resulting in an increase of the F-actin content representing 50 % of the F-actin content of stimulated dHL-60 WT (Figure 5-4-F). These results show that cells lacking normal

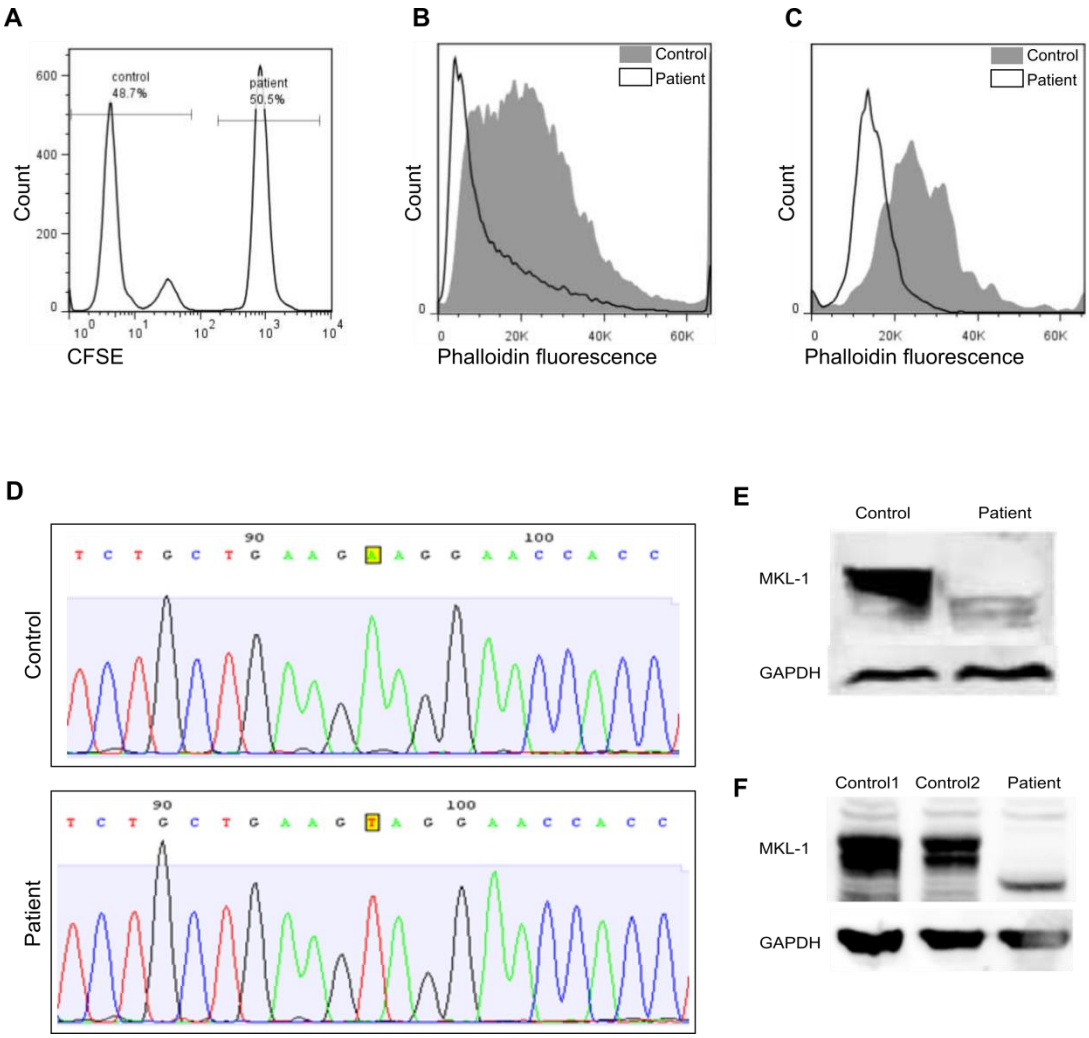

Figure 5-3: Patient cells displayed low level of F-actin correlated to the lack of normal MKL1 expression

A) In order to reduce the variation between samples and obtain an accurate measure of F-actin levels in both populations, patient cells were stained with CFSE. Then the two populations were mixed before fixation and staining with phalloidin-Alexa 647. B and C) Phalloidin signal was collected by flow cytometry in B) lymphoid and C) myeloid cells. D) Whole genome sequencing indicated a non-sense mutation of the MKL1 gene carried by the patient. This mutation was confirmed by Sanger sequencing. E and F) MKL1 expression detected in E) PBMC and F) B LCLs from healthy donors and the patient. A-E: data were collected from a single experiment, one replicate and F: data from two independent experiments, one replicate per experiment.

expression of MKL1 are still able to polymerise actin in response to a stimulus; however this response is weaker than in control cells.

Then, I tested if the severe reduction of MKL1 expression in dHL-60 mimicked the patient phenotype and altered cell migration. Migration of dHL-60 MKL1 cells was impaired with 21% of immobile cells whereas only 2% of control cells were immobile (Figure 5-4-G, Video S5-3 and 5-4). Cell velocity was also altered with an average velocity of 11.9 $\mu m.min^{-1}$ (+/- 0.4 $\mu m.min^{-1}$) and 15.1 $\mu m.min^{-1}$ (+/- 0.6 $\mu m.min^{-1}$) for the dHL-60 MKL1 and dHL-60 SCR, respectively (Figure 5-4-G). The dHL-60 MKL1 cells, as control cells, showed a good chemotactic response (Figure 5-4-I and J) but also displayed a better persistence during migration than the control cells as shown by a chemotactic index of 0.64 (+/- 0.02) and 0.51 (+/- 0.02), respectively (Figure 5-4-H). Taken together, these results show that the knock-down of MKL1 in the differentiated HL-60 cells mimics the patient phenotype. The striking reduction of F-actin content in dHL-60 MKL1 cells suggested that actin polymerization machinery could be impaired. When the F-actin and G-actin contents were determined by Western blot, dHL-60 MKL1 cells displayed a strongly reduced F- and G-actin contents but a similar F/G-actin ratio compared to dHL-60 SCR cells (Figure 5-5-A). To confirm this result, I expressed G-actin-mCherry in HL-60 MKL1 cells and differentiated these cells into neutrophil-like phenotype. I then measured the F-actin content and could observe that expression of the G-actin-mCherry construct reduced the difference of F-actin content between dHL-60 MKL1 cells and dHL-60 WT cells (Figure 5-5-B and C), although this difference remained statistically significant. I also evaluated if actin regulator expression was altered by the knock down of MKL1 in dHL-60 cells by using RT-qPCR arrays with primers for actin and microtubules genes. I could observe that, in the set of genes with differential expression, most of the actin regulators were upregulated in absence of MKL1 with only *ACTB, CDC42BPA*, *FNBP1L* and *CTTN* that were downregulated (Figure 5-5-D).

When uniformly stimulated with fMLP, 43% (+/- 5%) of MKL1-silenced dHL-60 cells displayed an elongated uropod, compared with 15% (+/- 1.5%) of control cells (Figure 5-6-A and B), suggesting an uropod retraction impairment.

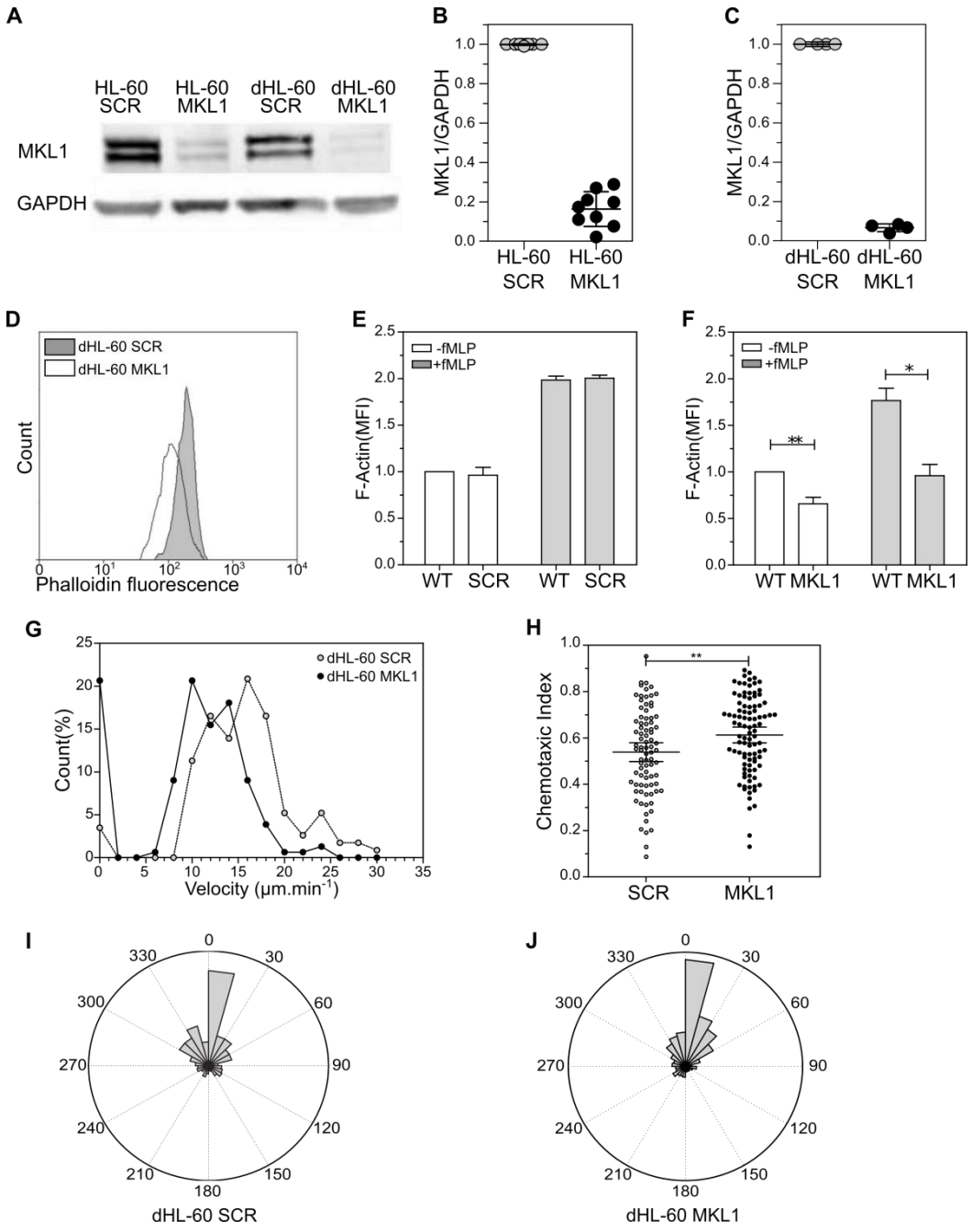

Figure 5-4: Silencing of MKL1 in differentiated HL-60 mimicked the patient phenotype

A) MKL1 expression in undifferentiated HL-60 cells and differentiated dHL-60 cells expressing shRNA against MKL1 or scrambled shRNA assessed by Western blot. B and C) Semi-quantitation by densitometry of MKL1 expression levels in B) HL-60 and C) dHL-60 cells. D-F) Quantification of F-actin by flow cytometry. Both dHL-60 WT and dHL-60 MKL1 or SCR were mixed together before being fixed, permeabilised and stained for F-actin using phalloidin-A647. D) Flow cytometry plot showing F-actin in dHL-60 MKL1 and SCR cells. E) F-actin levels in dHL-60 WT and SCR. F) F-actin levels in dHL-60 WT and MKL1. G-J) Migration of dHL-60 SCR and MKL1 in the agarose Dunn chamber in the direction of 100 nM fMLP was imaged at 37oC for 1 hour at 1 image/minute using Axiovert 135 microscope, equipped with a Achroplan 10x/0.25 objective, an environmental chamber and a motorised stage. Cells were tracked using the ImageJ manual tracking plug-in and tracks were processed in Matlab using an in-house routine. G) Frequency distribution of the average velocity of migrating dHL-60 SCR and MKL1. H) Chemotactic index of MKL1 and SCR cells. I and J) Frequency distribution of the average angle between the chemotactic gradient and the cell migration path of I) dHL-60 SCR and J) MKL1. D-F: Both dHL-60 WT and dHL-60 MKL1 or SCR were mixed together before being fixed, permeabilised and stained for F-actin using phalloidin-A647. A-C: Measures were from 9 (A and B) and 4 (C) experiments. and G-J: data were collected from three independent experiments, A-C and G-J) One replicate per experiment. D-F: data were collected from three independent experiments, three replicates per experiment. Data analysed by t-test. F: * $p < 0.05$, F and H: ** $p < 0.01$

To understand if this phenotype could be observed in other myeloid cells, I also used the monocytic cells THP-1 differentiated into macrophage-like cells to investigate the effect of MKL1 knock down on macrophage migration. In THP-1 macrophages, I observed an increase in the number of cells with elongated retraction fibres, suggesting an impairment of the detachment of the cell rear (Figure 5-6-C and D). As uropod retraction is regulated by the Myosin IIa complex and MKL1 has been shown to regulate expression of the light chain of this complex, I investigated if the elongated uropod was a result of a modification of the Myosin IIa complex due to the silencing of MKL1. The inhibition of the interaction of Myosin IIa with F-actin in dHL-60 WT cells, by treatment with blebbistatin, resulted in a similar phenotype with elongated uropod (Figure 5-7-A). Moreover, I found that mRNA and protein expression of the myosin regulatory light chain (*MYL9*) component of myosin IIa complex was severely reduced in MKL1 deficient HL-60 (Figure 5-7-B, D). There was also a moderate reduction in β-actin mRNA but no changes in myosin regulatory heavy chain (*MYH9*) expression were observed in HL-60 MKL1 cells (Figure 5-7-B). The same changes in *MYL9*, *ACTB* and *MYH9* expression have been observed in EBV-transformed lymphoblastoid cell line (LCL) of the patient compared to healthy donor LCL (Figure 5-7-C). Taken together with previously published work (Gilles et al., 2009), these findings show that myosin regulatory light chain expression is regulated by MKL1 and may be responsible for the impairment of the migration of MKL1 deficient neutrophils due to the uropod retraction defect.

The migration impairment observed in the dHL-60 MKL1 cells could also be due to a defect of the cell maturation in absence of MKL1. Therefore, I verified that the differentiation of HL-60 expressing MKL1 shRNA was similar to control cells. I could observe in both dHL-60 SCR and MKL1 cells the presence of multi-lobed nuclei, one of the main characteristic of mature neutrophils, suggesting a correct maturation of the cells (Figure 5-8-A). The maturation of HL-60 into neutrophil-like cells is characterised by the upregulation of CD11b expression and downregulation of CD49d at the cell surface. As expected, CD11b was upregulated in dHL-60 MKL1 cells but at a higher level than in control cells. Also, CD29/CD49d was downregulated in the MKL1 deficient cells at a similar level than the SCR cells (Figure 5-8-C).

A

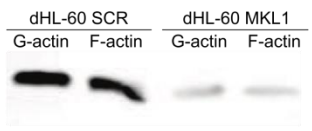

	SCR	MKL1
F/G-actin	0.61	0.66

B

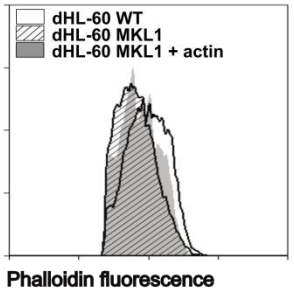

C

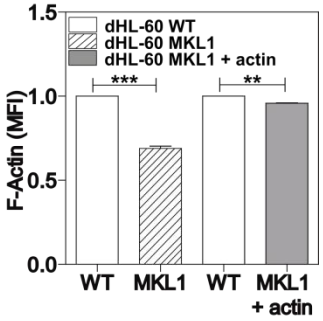

D

Upregulated genes

Gene symbol	Fold change	Gene symbol	Fold change
ARHGAP6	*1.8117*	*CYFIP2*	*1.6496*
ARHGEF11	*3.2422*	*FSCN2*	*2.6368*
ARPC1B	*1.7815*	*LIMK1*	*1.6485*
ARPC4	*1.6004*	*PFN2*	*1.6517*
CDC42EP2	*1.639*	*RAC1*	*1.8577*
CDC42EP3	*1.7405*	*WAS*	*1.8735*
CRK	*1.7697*	*WASL*	*1.5468*

Downregulated genes

CDC42BPA	*-2.9896*	*FNBP1L*	*-1.622*
CTTN	*-6.1696*	*ACTB*	*-1.5001*

Figure 5-5: MKL1 deficiency altered actin expression

A) Amounts of F-actin and G-actin in dHL-60 SCR and dHL-60 MKL1 cells were determined using the G-Actin/F-actin In Vivo Assay Biochem Kit. The F- and G- actin fraction were then run on a SDS-PAGE gel and analysed by Western blot. Quantification of the F/G actin ratio was performed using Gel analysis function of ImageJ/Fiji. B) and C) Measurement of the F-actin content by flow cytometry in dHL-60 WT (white bars) and MKL1 (striped bar) and in MKL1 expressing G-actin-mCherry (grey bar). Both WT and MKL1, +/- mCherry-actin, cells were mixed together before being fixed, permeabilised and stained for actin using phalloin-Alexa647. D) Fold change of actin regulators mRNA expression levels quantified by RT-qPCR arrays in dHL-60 MKL1 cells compared to dHL-60 SCR cells. Only significantly differentially expressed genes ($p < 0.05$) were reported. A-D: results from three independent experiments, one replicate per experiment. Data analysed by ANOVA with Tukey post-test. C: ** $p < 0.01$, *** $p < 0.001$

The expression of FPR1, the receptor for fMLP, was similar on both SCR and MKL1 dHL-60 cells indicating that the migration impairment was not due to a signalling defect at the cell surface (Figure 5-8-B). One of the clinical features of MKL1 deficiency was that the patient presented numerous scars due to subcutaneous abscesses. Therefore it was hypothesised that the absence of MKL1 could alter the healing process. Since fibroblast migration is an essential step in the process of wound healing, I knocked down MKL1 in fibroblasts and monitored their migration in a scratch-wound assay. I could observe that MKL1 fibroblasts were slower than SCR fibroblasts (Figure 5-9-A and B) and also that their morphology was altered. Strong differences could be observed between SCR and MKL1 fibroblasts: on the one hand, SCR fibroblasts spread well and displayed well defined cortical actin filaments together with numerous stress fibres; on the other hand, stress fibres could not be observed in MKL1 fibroblasts which did not spread and displayed a spindle like shape (Figure 5-9-C).

To understand which set of genes involved in actin cytoskeleton and cell migration were regulated by MKL1, I analysed data from a RNA-seq experiment performed on the patient B LCLs in Sergey Nejentsev's team. As expected, the regulation of the actin cytoskeleton is an important target of MKL1, as observed by the down regulation of 17 unique actin-related genes and 2 redundant genes in patient cells. Software analysis of functional clustering identified cytoskeletal organisation, migration and adhesion as the major groups (Figure 5-10-A). Among the downregulated genes involved in actin cytoskeleton and cell migration, 5 genes are known to be expressed in immune cells and directly involved in cell migration: *ACTN1*, *ITGB1*, *PLS1*, *UTRN* and *ZYX*. *ACTN1* encodes the actinin alpha 1 protein that is involved in bundling actin filaments and has been shown to regulate neutrophil and T lymphocyte migration (Yuruker and Niggli, 1992). *ITGB1* gene encodes the CD29 receptor that binds fibronectin and regulates cell adhesion (Elloumi-Hannachi et al., 2015). L-plastin 1 (*PLS1*) is, as *ACTN1*, involved in actin filament bundle regulation and has been shown to regulate neutrophil and T lymphocyte migration (Morley, 2012). Utrophin (*UTRN*) is expressed in B lymphocytes, B LCLs and

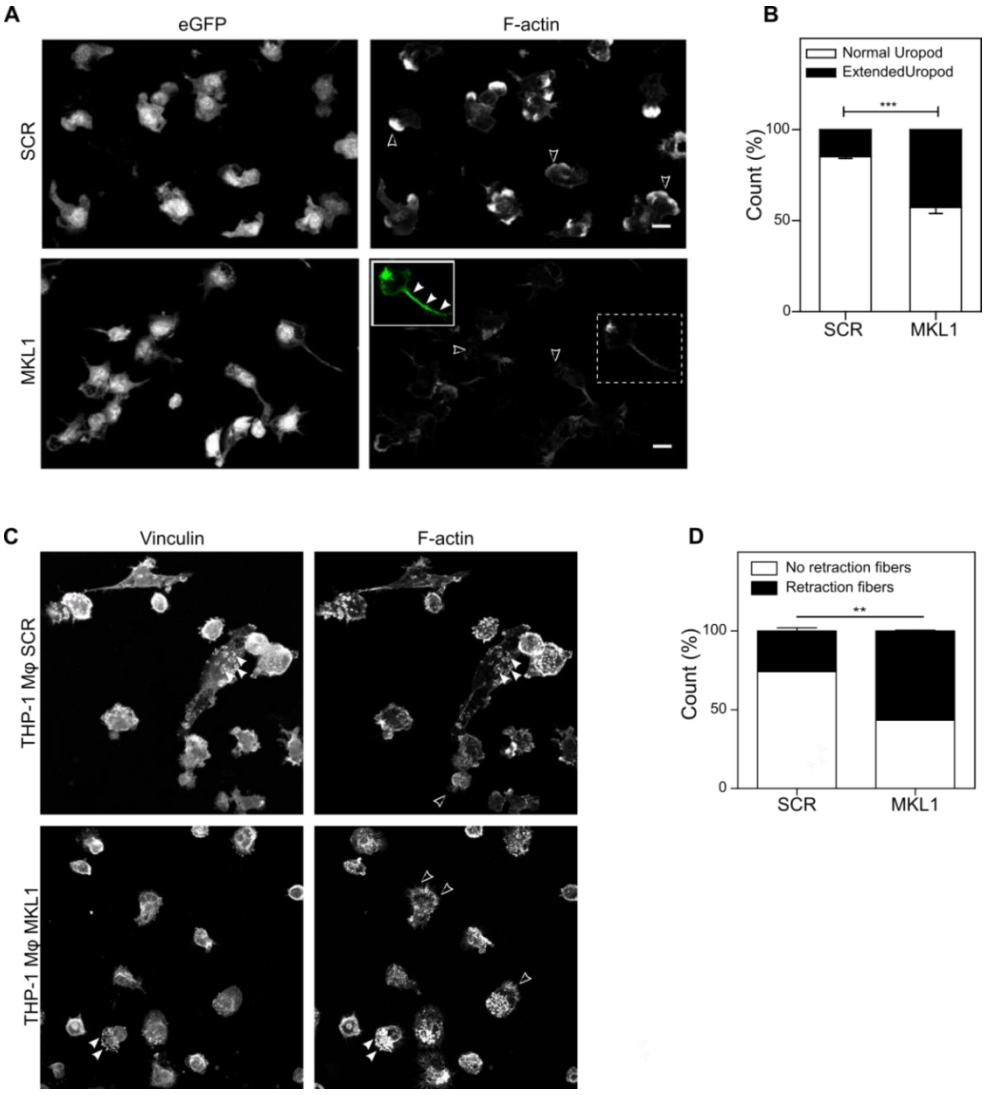

Figure 5-6: MKL1 deficient cells displayed retraction defect of the rear of the cell

A) dHL-60 SCR and MKL1 were plated on fibronectin-coated coverslips for 20 minutes before being uniformly stimulated with a solution of fMLP at a final concentration of $1x10^{-7}$ M. Control cells displayed well defined lamellipodia at the leading edge of the cell while MKL1 deficient cells did not (open arrow head). A high proportion of the cells lacking MKL1 presented abnormally extended uropod (closed arrow head). For easier visualisation, an inset has been added on the top left corner of the image showing a MKL1 dHL-60 cell with an extended uropod (originally in the dashed square). The image intensity of the inset has been increased 500% compared to the original image. B) Quantification of the extended uropod in the SCR and MKL1 deficient populations seen in A. C) THP-1 cells differentiated into macrophage-like cells were plated on fibronectin-coated coverslips and let to adhere for 4 hours. The cells were stained for actin and vinculin. Both populations displayed podosomes composed of an actin core surrounded by a vinculin ring (closed arrow head). MKL-1 cells also displayed a high number of retraction fibres (open arrow head). Image intensity of the MKL-1 population was increased by 500%. D) Quantification of the proportion of THP-1 macrophage like cells presenting retraction fibres. B and D) Quantification was performed using the Cell Counter plug-in in InageJ. A and C: cells were images using a Zeiss LSM710 confocal microscope using an oil immersion 63x/1.4 objective. A-D: data from three independent experiments, one replicate per experiment. Data analysed by t-test. B: *** $p < 0.001$, D: ** $p < 0.01$.

neutrophils where it regulates cell chemotaxis (Cerecedo et al., 2010). *ZYX* gene encodes the zyxin protein which interacts with α-actinin and is involved in signal transduction during cell adhesion (Reinhard et al., 1999). In addition to the cytoskeletal regulatory genes identified in the screen, the other major functional cluster identified was regulators of transcription. Surprisingly, *MYL9* was not among the genes downregulated in the patient B LCL. Although it has been detected as downregulated in the RNA-seq, its *p*-value was too high to be considered as significant *(*downregulated by 3.15 *p*-value = 0.065). The *ACTB* gene was also downregulated (by 2.46) but also failed to reach significance (for which the *p*-value was 0.3). The absence of normal MKL1 expression also resulted in the upregulation of numerous genes including 6 genes involved in cell migration (Figure 5-10-B). The myosin 1f belongs to this cluster of genes and has been shown to be involved in neutrophil adhesion, migration and maintenance of correct cortical actin cytoskeleton. This preliminary analysis of the RNA-seq experiment surprisingly showed that the genes expected to be downregulated were not in this set of genes and that these data, at this stage, do not support the results obtained by qRT-PCR. The RNA-seq and qRT-PCR taken together raise questions about the genes targeted by MKL1 and stress the need of a deeper analysis of these experiments.

5.3 Discussion

MKL1 is a ubiquitously expressed transcription co-factor that regulates the expression of numerous genes related to the β-actin cytoskeleton including the β-actin gene itself but it had no known role in the immune system. So far, few murine models have been developed to investigate the role of MKL1, MKL2 (which is the homologue of MKL1), and SRF. It has been shown that MKL1 knockout in mice displayed partial embryonic lethality due necrosis of myocardial cells. Yet $MKL1^{-/-}$ mice that develop to birth have normal life spans although they show abnormal mammary gland function and low platelet count in peripheral blood (Sun et al. 2006; Cheng et al. 2009). MKL1 is needed for the maturation and migration of megakaryocytes (Cheng et al. 2009; Gilles et al. 2009). However, in mice, MKL2 can partially compensate for MKL1 loss in megakaryocytes. Indeed, the KO of MKL1 together with the conditional KO of MKL2 resulted in a more severe phenotype than KO of MKL1 alone (Smith et al. 2012). MKL1

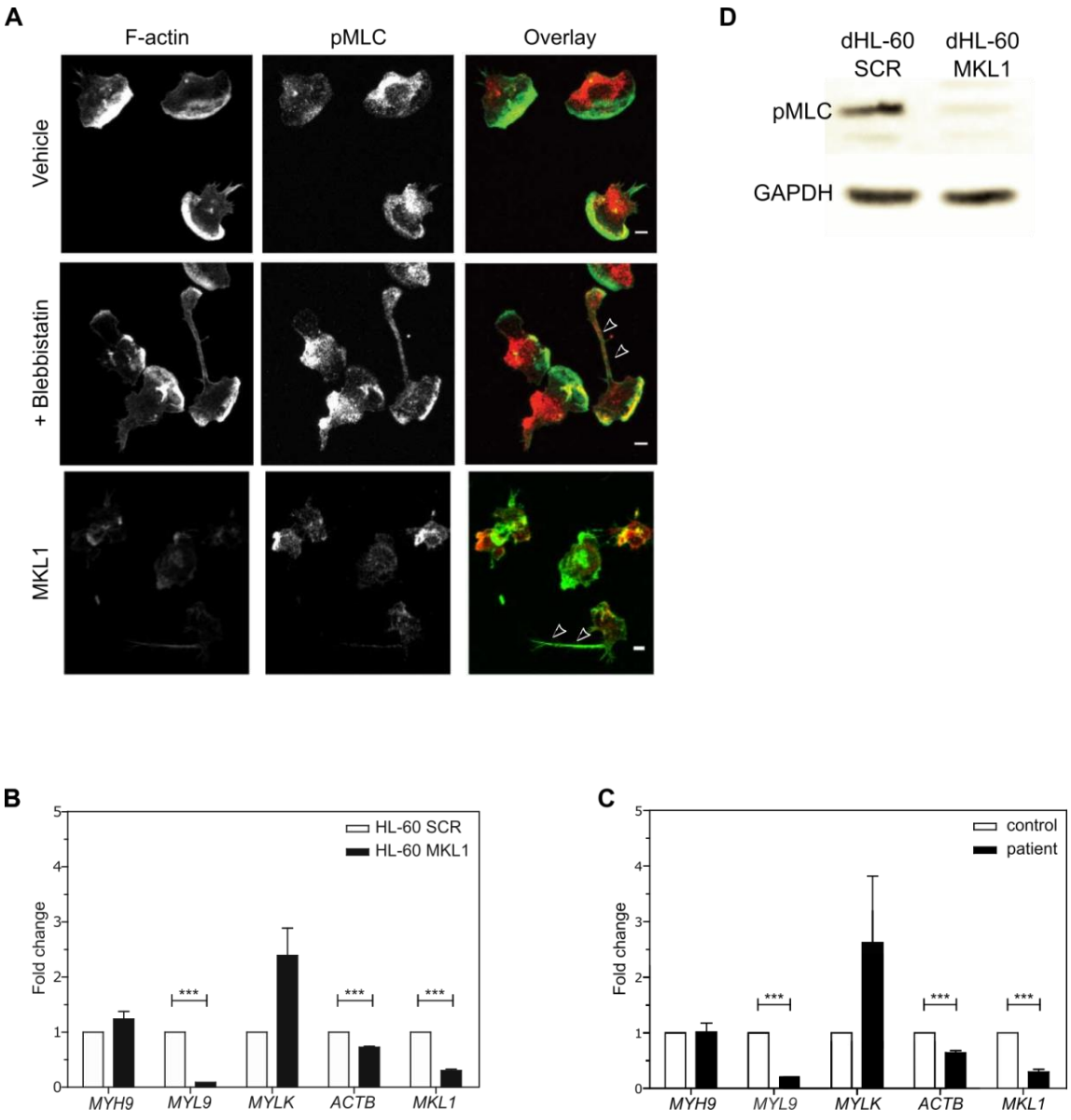

Figure 5-7: The uropod retraction defect of MKL-1 deficient cells was due to the MYL9 downregulation

A) Wild-type dHL-60 cells were pre-incubated or not with the myosin II activity inhibitor blebbistatin before being plated on fibronectin-coated coverslips for 20 minutes in medium containing blebbistatin (100 µM, cells were incubated for 30 minutes with the inhibitor) or not (vehicle: DMSO). Cells treated with blebbistatin (middle lane) displayed abnormally extended uropods (open arrow head) as it was possible to observe in dHL-60 MKL1 silenced cells (bottom lane). Cells were images using a Zeiss LSM710 confocal microscope using an oil immersion 63x/1.4 objective. Scale bar = 10 µm. B) The RNA expression in dHL-60 SCR and MKL1 cells was quantified by qRT-PCR. We could observe a downregulation of the expression of *ACTB* and *MKL1* genes but also a dramatic decrease of expression of the *MYL9* gene encoding the regulatory light chain of myosin IIa. C) Transcript expression of B LCLs from the patient and a healthy donor showed the same profile as the transcript expression in HL-60 cells showed in B. D) Western blot expression of pMLC in dHL-60 MKL1 cells. A: data from three independent experiments, one replicate per experiment. B and C: data from three independent experiments, three replicates per experiment. D: Due to time restriction, only two experiments could be performed. Data from two independent experiments, one replicate per experiment. Data analysed by ANOVA with Tukey post-test. B and C: *** $p < 0.001$.

KO partial embryonic lethality is in line with results from MKL2 knockout and SRF conditional knockout that displayed embryonic lethality due to a spectrum of cardiovascular defects (Oh, Richardson, and Olson 2005; Miano et al. 2004) while SRF null mice were shown to die at a very early stage of embryogenesis (Arsenian et al. 1998). These results suggested that MKL1 partial embryonic lethality was possibly due to a compensatory mechanism by MKL2 or myocardins that are expressed in the same tissues as MKL1. So far none of the murine models has revealed a critical role of MKL1 in regulating the immune actin cytoskeleton and immune function. In this chapter, we showed that the severe immunodeficiency syndrome of the patient was correlated with the absence of normal expression of the protein MKL1 due to a non-sense mutation in the protein. The patient carried a mutation in MKL1 replacing the Lysine in position 723 by a stop codon. This truncated protein would have all the RPEL domains binding the G-actin and also be able to dimerise through its Leu zipper domain. The SAP domain, which activates a specific subset of SRF-dependent genes in muscles, would also be present in the mutant protein. The activity of the SAP domain in MKL1 is controversial since the deletion of this domain has no effect on the ability of MKL1 to interact with SRF (Miralles et al., 2003). However, the K723X MKL1 mutant would lose its C-terminal region containing the potent transcriptional activity domain needed for the stimulation of the SRF activity. It has previously been shown that a MKL1 mutant called C723 with its C-terminal region deleted from the 723 position completely lost its activity and could be used as a weak dominant negative mutant (Cen et al., 2003). In our study, the truncated MKL1 has been predicted to have a molecular weight of 77 kDa and in theory should be detected by Western blot using antibodies raised against an amino acid sequence included in the 1-723 first amino acids. The antibody I used for the detection of MKL1 by Western blot was raised against the amino acid sequence 556-680 of MKL1 and as such was expected to be able to detect the mutated protein. As shown in Figure 5-3-E and F, I could detect a faint band of protein with a lower molecular weight (~80-85 kDa) than the original band (~110 kDa) corresponding to MKL1. This lower band could be the truncated protein, and the low intensity of the band would suggest that the mutant protein is poorly expressed or quickly degraded. Taken together, these results suggested that there is no

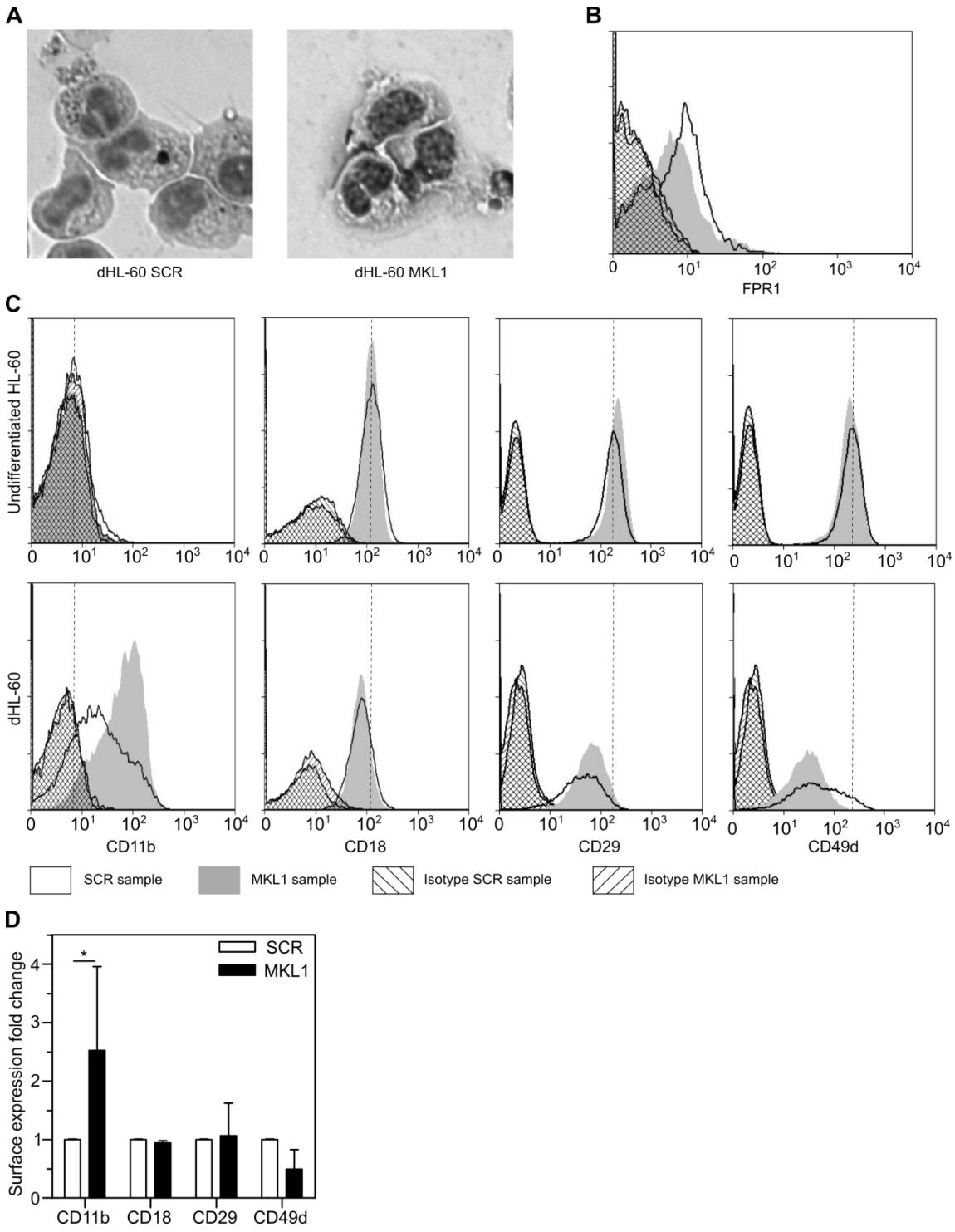

Figure 5-8: MKL1 deficiency did not alter HL-60 maturation into neutrophil-like cells

A) Using a cytospin centrifuge, dHL-60 SCR and MKL1 cells were concentrated and spread on microscope slides. The cells were then stained using the Diff-quick staining. B) Evaluation by flow cytometry of FPR1 expression at the cell surface of dHL-60 SCR and MKL1. C) Expression of CD11b, CD18, CD29 and CD49d at the surface of undifferentiated and differentiated HL-60 MKL1 and SCR cells was assessed by flow cytometry. D) Quantification of the flow cytometry histograms seen in C. A-D: data from three independent experiments, one replicate per experiment. Data analysed by t-test. D: * : $p < 0.05$.

activity of MKL1 in the cells of the patient. The patient neutrophils displayed phagocytosis and migration impairments. Both processes are dependent on the fast rearrangement of the cell cytoskeleton suggesting an actin cytoskeleton defect which is consistent with the lack of correct MKL1 expression.

The actin cytoskeleton defect was confirmed by the dramatic reduction of the F-actin level in myeloid and lymphoid cells from the patient. Despite the low level of F-actin in lymphoid cells, the patient did not display abnormalities in lymphoid phenotype nor function with the exception of a defective T-cell proliferation in response to anti-CD3 antibody and patient's B LCL impaired migration toward MIP3α. This suggested a possible impairment of signal transduction in the T cell receptor pathway and defective migration of the cells from the lymphoid lineage.

Phagocytosis is the process by which immune cells engulf and destroy pathogens they encounter. This process is actin dependent (reviewed in (Rougerie et al., 2013)) and is divided in four steps: 1) the initiation of the phagocytic cup which recruits the molecular element for the polymerization of actin, 2) the extension of the initial pseudopod along the pathogen, 3) the elongation of the pseudopod and 4) the closure of the phagocytic cup into the nascent phagosome. The three first steps are highly dependent on actin polymerization and the lack of F-actin in patient cells could explain the phagocytosis defect observed in the patient neutrophils. The three last steps of the phagocytosis are also dependent on the cellular contractile activity in the pseudopod. These contractions are due to myosin II activity during the primary extension of the pseudopod (Araki et al., 2003; Olazabal et al., 2002) and to the activity of other non-conventional myosin during the elongation of the pseudopod and the closure of the phagocytic cup. Our results show that myosin IIa expression was dramatically reduced and correlate previous results showing that myosin IIa expression was regulated by MKL1 (Gilles et al., 2009; Medjkane et al., 2009) suggesting that in addition to the lack of correct actin polymerisation, an alteration of the myosin II activity could decrease the ability of MKL1 deficient neutrophils to phagocyte pathogens.

Using the neutrophil-like differentiated HL-60 cells, I further showed that the silencing of MKL1 was responsible for the migration impairment and also for the reduced levels of F-actin.

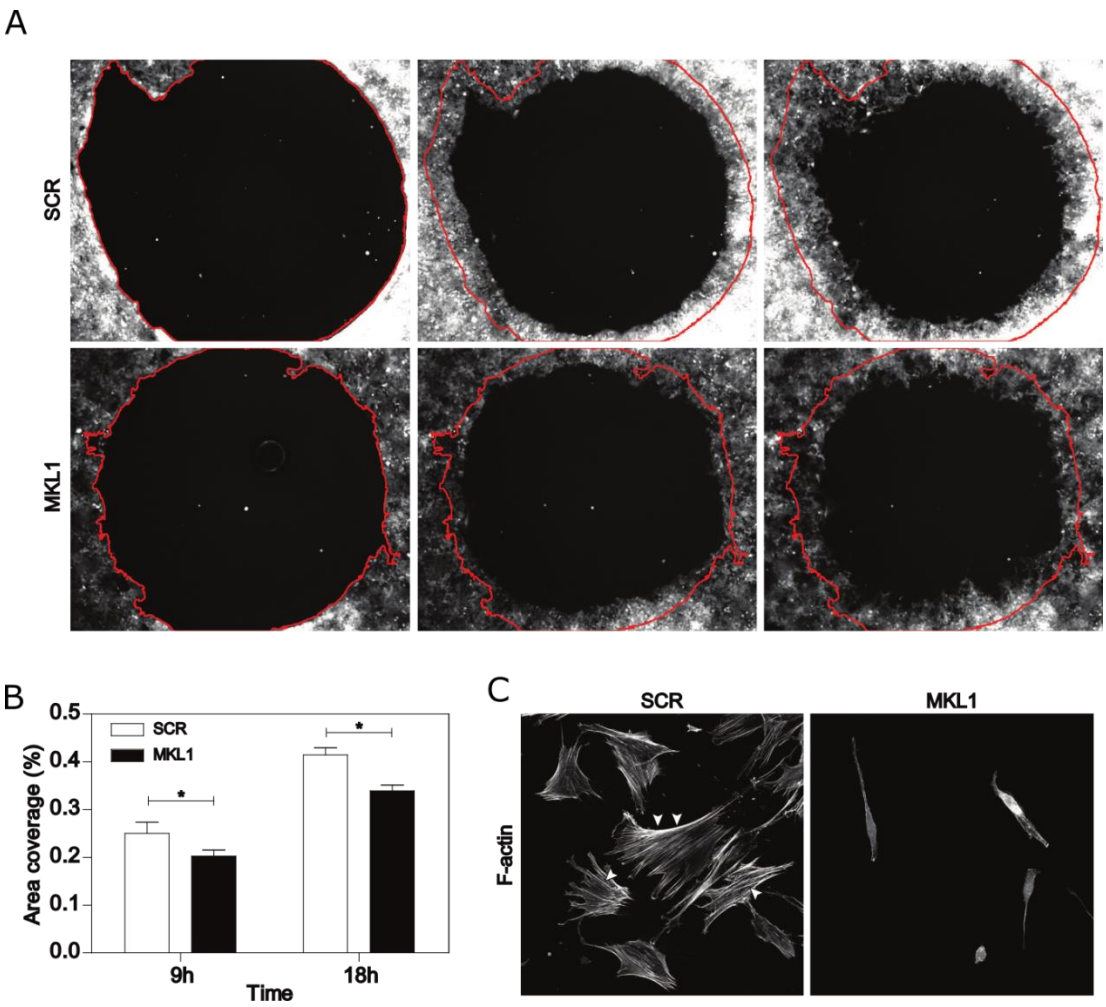

Figure 5-9: MKL1 deficiency altered fibroblast shape and migration

A) Migration of fibroblasts expressing SCR or MKL1 shRNA over 18 hours in a wound scratch assay using the Oris cell migration assay. Cell migration was imaged at 37°C by taking one image every 15 minutes for 18 hours with an Achroplan 10x/0.25 objective mounted on an Axiovert 135 time-lapse microscope equipped with a motorized stage. B) Measure of the areas of migration observed in A). Analysis was performed in ImageJ/Fiji by detecting and measuring the cell free area using the threshold and measure particles functions. C) Fibroblasts expressing SCR and MKL1 shRNA were fixed and stained for actin using phalloidin Alexa647. Cells were images using a Zeiss LSM710 confocal microscope using an oil immersion 40x/1.0 objective. Arrow heads indicate stress fibres that are present in SCR fibroblasts but absent in MKL1 KD fibroblasts. MKL1 KD fibroblasts image intensity was increased 5 times. A-C: data from three independent experiments, one replicate. Data analysed by ANOVA with Tukey post-test. B: * $p < 0.05$.

We hypothesised that the migration defect observed in MKL-1 deficient primary neutrophils and dHL-60 neutrophil-like cells could be explained by three different but probably complementary causes: 1) the lack of G-actin available in the cells, 2) the nearly complete absence of myosin light chain activity and 3) the possible overexpression of integrines or alteration of their cycling.

1) dHL-60 MKL1 deficient cells responded to fMLP stimulation by increasing their F-actin content but to a much lower level than the non-silenced cells, suggesting that the low levels of F-actin were mainly due to the low level of G-actin available. We confirmed by Western blot that F- and G-actin levels were low in MKL1 deficient cells. The decrease of F-actin in the dHL-60 MKL1 cells is consistent with results from $SRF^{-/-}$ neutrophils studied by Taylor *et al.*. By knocking-out SRF in the hematopoietic cell lineages, they could analyse the G- and F-actin content in $SRF^{-/-}$ neutrophils by labelling the cells with DNaseI and phalloidin, respectively. While phalloidin binds with high affinity to F-actin, DNaseI binds with high affinity to G-actin (Mannherz et al., 1980). When DNaseI is labelled with a fluorophore, it can be used to determine G-actin content in fixed cells using flow cytometry or microscopy (Cramer et al., 2002). In Taylor et al., the phalloidin staining showed the $SRF^{-/-}$ cells had a strong decrease in F-actin content while the DNAseI staining did not show any alteration of the G-actin content (Taylor et al., 2014). This result was surprising as SRF drives the expression of β-actin (Miano et al., 2007). A decrease of actin levels would have been expected, with consequences on both F- and G-actin contents in the $SRF^{-/-}$ neutrophils. It would be interesting to confirm their result using a different method than the DNaseI staining. In our study, when we expressed a β-actin construct tagged with mCherry in MKL1 deficient dHL-60 cells, we observed the restoration of F-actin to levels close to wild-type cells, although they remain significantly lower. This result suggested that the actin polymerisation machinery was not severely impaired in MKL1 deficient cells and that the migratory defect could indeed be due to the reduced levels of actin alone. The knock down of β-actin has been shown to be responsible for a defective migration of fibroblasts and T-lymphocytes (Bunnell et al., 2011; Joseph et al., 2014). These studies were strengthened by Salvany's work which showed that the overexpression of β-actin in MKL1 deficient cells

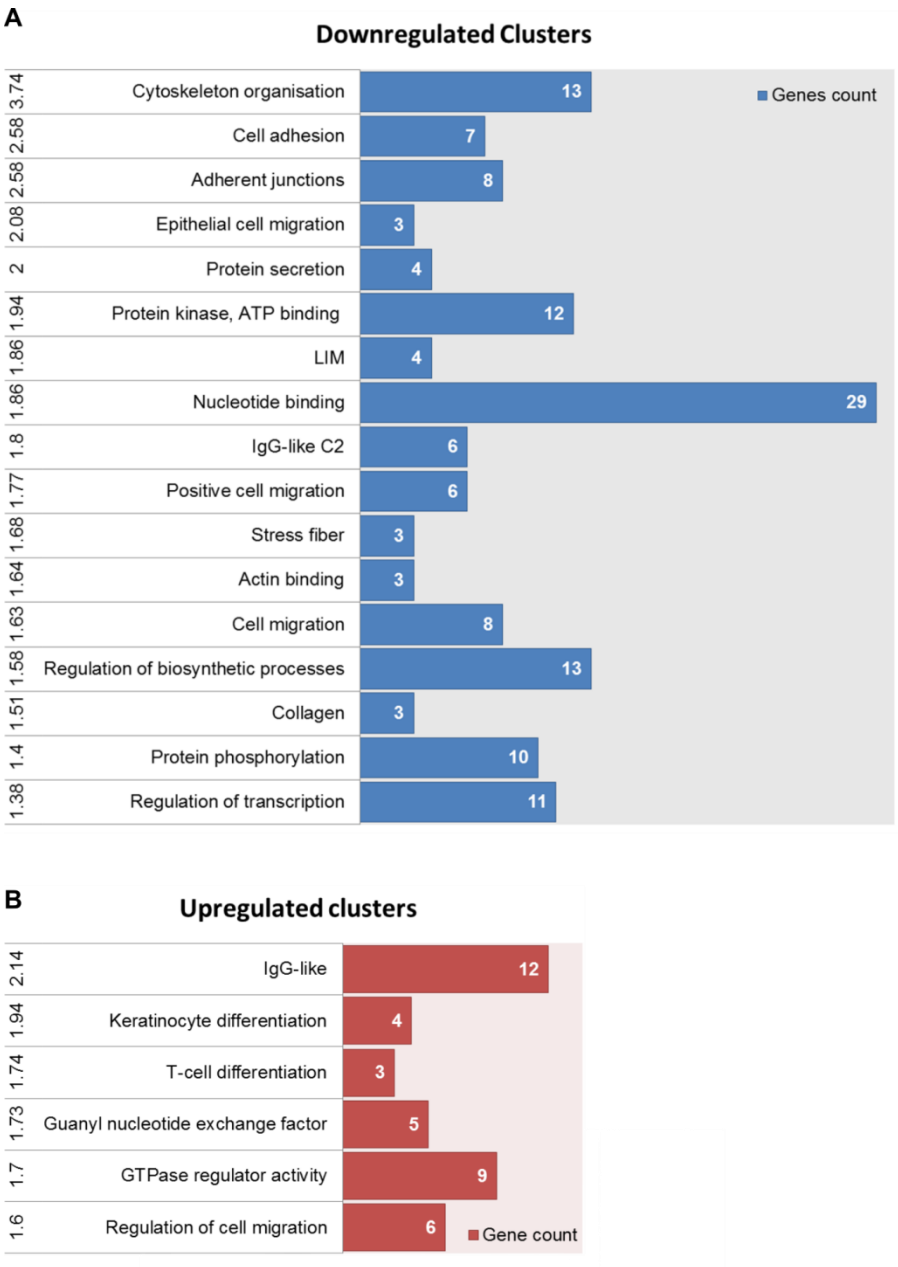

Figure 5-10: Functional annotation clustering of the differentially expressed genes of MKL1 deficient LCLs

Functional annotation clustering analysis of RNA-seq results from healthy donor and MKL1 patient B lymphoblastoid cells performed using the DAVID software. Using the lists of the significantly differentially expressed genes ($p < 0.05$) for all healthy donor vs. MKL1 cells, clustering was performed with a high classification stringency and only clusters with an enrichment score higher than 1.3 were considered and reported. A and B) Set of cluster of genes A) downregulated and B) upregulated by the absence of MKL1 when compared to healthy donor. A and B: Exploratory experiment aiming at identifying possible target gene for future studies. Therefore only one experiment performed. Results from a single experiment. One replicate.

was enough to rescue the migratory defect of human breast cancer cells and border cells in drosophila (Salvany et al., 2014). These works are in line with our results and confirm the influence of β-actin expression on cell migration. It would be similarly interesting to investigate if the restoration of actin levels in MKL1 deficient dHL-60 cells using a plasmid encoding for the gene of β-actin would also restore other dHL-60 functions such as phagocytosis and migration.

2) When uniformly stimulated with fMLP, the dHL-60 cells displayed an elongated uropod. This phenotype was similar to the one described by Eddy et al. where they show that the inhibition of myosin II induced the formation of extended uropods in neutrophils. The abnormal uropod extension in MKL1 deficient dHL-60 was correlated with an increase of elongated retraction fibres found in macrophage-like differentiated THP-1 cells suggesting an impairment of the retraction of the uropod, for which myosin II activity is required (Worthylake et al., 2001). It has been shown that the activation of the non-muscle myosin IIa is important for the determination of the polarity of migrating cells (Yam et al., 2007) and is localised at the rear of the cell in leukocytes (Eddy et al., 2000) where it is essential for the formation of a defined rear compartment in the cell. Using blebbistatin, an inhibitor of myosin II light chain (Kovács et al., 2004), I confirmed that inhibition of myosin II light chain interaction with the actin cytoskeleton led to uropod retraction defects in dHL-60 cells. Knowing that MYL9, the gene that encodes the myosin IIa light chain, is also a gene regulated by MKL1 (Medjkane et al., 2009) I then demonstrated that MKL1 deficient cells displayed an important decrease in the expression of the myosin IIa light chain transcript. This was associated with a reduced level of the phosphorylated form of myosin IIa light chain which is the active form of the protein. These results showed that the MKL1 deficient cell migration impairment was, at least partially, due to the downregulation of the myosin IIa light chain expression.

3) As the integrin CD11b is a marker of neutrophil maturation, I used it to monitor HL-60 maturation into dHL-60 cells. I could observe that HL-60 MKL1 cells displayed significantly higher expression of CD11b at the cell surface compared to the HL-60 SCR cells. This result is consistent with the higher cell surface expression of CD11b shown in $SRF^{-/-}$ neutrophils when

compared to wild-type cells (Taylor et al., 2014). This high expression of CD11b in MKL1 deficient cells could be the consequence of reduced myosin light chain activity since it has been shown that inhibition of myosin activity is also responsible for the accumulation of integrins at the tail of migrating cells (Worthylake et al., 2001). The accumulation of integrins at the cell surface could also be the consequence of the impairment of integrin trafficking similarly to what has been observed in SRF deficient neutrophils (Taylor et al., 2014). Since the MKL1 deficient dHL-60 showed an increased expression of CD11b at the cell surface, we could hypothesise that the excessive expression of CD11b was involved in the uropod retraction defect observed in the migrating cells. Further investigations would be required to understand by which mechanism integrins are overexpressed at the cell surface and what is the impact on cell migration.

It has been shown that myosin II is not involved in the formation of the lamellipodium and the lamellae at the leading edge of the cell (Cai et al., 2006; Vicente-Manzanares et al., 2007) but has an important role in the regulation of the retrograde actin flow in the lamellopodium and lamellae (Ponti et al., 2004). Thus the absence of clear protrusion at the leading edge of patient neutrophils during the migration in the Dunn chamber and the absence of well-defined actin structure at the front of uniformly stimulated MKL1 deficient dHL-60 cells (Figure 5-7-A) may be attributed to the nearly complete absence of myosin IIa transcript resulting in an alteration of the retrograde flow in the lamellipodium and lamellae. This phenotype could also be due to the global lack of F-actin in the MKL1 silenced cells preventing a correct accumulation of F-actin at the leading edge resulting in actin-poor and probably less stable lamellipodium. To determine the consequences of the silencing of MKL1 at the leading edge of neutrophils, it would be necessary to study actin structures and its components' dynamics using super-resolution microscopy, Fluorescence Recovery After Photobleaching (Lai et al., 2008) and Speckle microscopy techniques (Danuser and Waterman-Storer, 2006).

Altogether, our results suggest that the migration defect observed in MKL1 deficient neutrophils is the result of several components of the migration process: the G-actin pool, the reduced myosin IIa light chain activity and the altered expression of integrins. Nevertheless, the results presented by Salvany *et al.* that the sole overexpression of β-actin was able to rescue migratory

defects of MKL1 deficient cells may imply that despite the fact that MKL1 drives the expression of numerous genes involved in the regulation of the actin cytoskeleton dynamics and cell migration, the effect of MKL1 deficiency on all other genes but β-actin may be negligible on the migration defect.

To get a better understanding of the role of MKL1, I analysed an RNA-seq experiment performed on patient B LCL. This study showed, as expected, that actin cytoskeleton genes were down regulated in the absence of MKL1 but unfortunately I could not correlate these preliminary results with our qRT-PCR experiments on the B LCLs. This highlights the difficulties to correlate gene expression levels between two experiments made using different methods and the necessity to confirm transcript expression results by protein expression analysis. Nevertheless, the results from the qRT-PCR on the HL-60 and B LCLs were consistent with previously published articles in which the expression of *MYL9* and *ACTB* have been shown to be strongly downregulated when MKL1 was silenced (Gilles et al., 2009; Medjkane et al., 2009).

Little is known regarding MKL1 and MKL2 expression in human hematopoietic cell lineages, but their expression can be estimated from databases, such as Immgen.org, which gather microarray results from published studies. Using Immgen results from hematopoieitic cells (group: Human hematopoietic (D-MAP), query MKL1 and MKL2), I could see that MKL2 is more expressed than MKL1 in megakaryocytes from umbilical cord blood. This would explain why the patient displayed mild thrombocytopenia when compared to the mouse model that showed more severe thrombocytopenia. In human neutrophils (group: Human Immune Cells, query MKL1 and MKL2), there is a near absence of MKL2 expression suggesting that there is not compensation of MKL1 loss in neutrophils while in lymphocytes, MKL1 and MKL2 are expressed to similar levels suggesting a possible compensation of MKL1 loss of function by MKL2. These data fit the patient phenotype as only neutrophils displayed impaired function and most of lymphocyte functions did not seemed to be altered. Nevertheless, we could observe that the patient's PBMCs F-actin content was much lower than in the control suggesting that MKL1 loss was not completely compensated by MKL2. Protein levels of MKL1 and MKL2 in immune

cells need to be investigated to confirm microarray results and understand the role of these two proteins in the immune system. The hypothesis that MKL2 could compensate MKL1 deficiency in most immune cells is strengthened by the role of MKLs in the nervous system. Indeed, MKL1 and MKL2 are both expressed in the nervous system and they have been shown to redundantly regulate, with SRF, the maturation, migration, apoptosis and neural structure growth (Cao et al., 2011; Mokalled et al., 2010a). This would also suggest that a double deficiency in MKL1 and MKL2 proteins would have much more dramatic effects on the immune response than the MKL1 deficiency already has (and may even be embryonic lethal). Keeping in mind that the deletion of SRF has been shown to induce similar defects than the silencing of MKL1, this highlights the importance of the MKL1/2-SRF pathway in the immune response and the need for further studies to understand the exact role of each player of this pathway.

Here, I showed that MKL1 deficiency had an important impact on immune cells and was responsible for phagocytosis and migration defects in MKL1 deficient cells. By driving the expression of genes involved in the regulation actin cytoskeletal dynamics, MKL1 potentially regulates numerous immune functions in addition to phagocytosis and migration. The alteration of β-actin expression in MKL1 deficient cells might also strongly affect other immune processes like the formation of the immune synapse or the antigen processing in B cells for example. The wide variety of genes regulated by MKL1 may also be directly involved in immune function.

It has also been shown that MKL1 was involved in neuron and adipocyte differentiation (Nobusue et al., 2014) and a similar role could be possible within the immune system. Indeed, analysis of the transcripts of MKL1 deficient LCLs showed that clusters of genes involved in T cell differentiation and in keratinocyte differentiation were upregulated. A possible role of MKL1 in immune cell differentiation may explain how it affects the gene expression in neutrophils. Transcription in mature neutrophils is often considered to be very low even if hundreds of genes are still transcribed. Most of the genes transcribed in differentiated neutrophils are related to the inflammasome but also numerous transcription factors are still expressed in mature neutrophils. Due to the early need of the actin cytoskeleton in the extremely

fast neutrophil response to an infection, it would be interesting to evaluate if MKL1 is more involved in the transcription activity of differentiating cells rather than in fully mature cells that change their transcript expression profile in response to a stimulus. Thorough studies of MKL1 targets in the immune system are needed to better understand the temporal activity of MKL1 and the immune functions dependent on its activity.

Finally, some pathogens also hijack the actin cytoskeleton to infect host cells and escape the immune system (reviewed in (Bhavsar et al., 2007)). The modification of actin dynamics might be sensed by MKL1 resulting in a modification of the expression profile of infected cells. The beneficiary of this possible modification of the actin related gene expression would be difficult to predict since both the pathogen and the host could use this new environment to either fight the invader or to evade defense mechanisms.

The ability of MKL1 to sense the drop of G-actin level in the cytoplasm due to the activation of the actin polymerization machinery in response to extracellular chemicals or mechanical stimuli and to shuttle to the nucleus to induce transcription of numerous genes related to the actin cytoskeleton make MKL1 a unique regulator of actin dynamics in the immune system. Its role in the highly motile immune cells still need to be understood and might reveal the role of genes regulated by its transcriptional activity in the defense of the host.

Chapter 6 Screening of immunodeficient patients for neutrophil defect using the modified Dunn chamber

6.1 Introduction

Patients with recurrent bacterial infections are considered as possibly immunodeficient. In the case of recurrent fungal infections (*Candida* and *Aspergillus* species) as well as *S. aureus, P. aeruginosa, Nocardia asteroides, S. typhi* infections, neutrophils and monocytes are the first cell types suspected to be defective (Notarangelo, 2010). Several primary neutrophil dysfunctions are diagnosable through well-established screen tests:

Syndrome	Molecular mechanism	Screen tests
Chronic Granulomatous Disease	Reactive oxygen species deficiency	NBT reduction, detection of superoxide by flow cytometry
Leucocyte adhesion deficiency	Integrins and focal adhesion	Detection of integrin CD11a, CD11b and CD18 integrins expression by flow cytometry, chemotaxis and bacterial killing
Specific granule deficiency	*C/EBPε expression during granulocyte maturation*	Chemotaxis and staining of lactoferrin in neutrophils
Actin deficiency	Defective actin binding by regulators	Detection of F-actin content by flow cytometry, chemotaxis, bacterial killing and detection of phagocytosis by flow cytometry

Table 6-1: Primary neutrophil dysfunctions

Neutrophil chemotaxis defects are rarely diagnosed as the only cause of infections and are often associated with phagocytosis and/or superoxide production defects (Keszei and Westerberg, 2014). The Shwachman-Diamond syndrome which is caused by a mutation in the SBDS gene, encoding for a protein predicted to be involved into RNA-processing is maybe the only known disease causing neutropenia and neutrophil chemotaxis defect towards fMLP (Keszei, 2014). The assessment of neutrophil migratory ability of patients with recurrent bacterial infections would help to understand the molecular mechanisms of the defect and, for example, when associated with a phagocytosis defect could lead the investigators to look more closely to any mutation in actin cytoskeleton regulators.

Following the successful use of the modified Dunn chamber to monitor neutrophil migration and in the detection of neutrophil migration defect of the MKL1 patient, it was decided to use it to assess the migration of neutrophils from other patients. As the patients had already undergone standard immunological testing that excluded common causes of immune defect, it was expected that performing this assay would help in the identification of a possible neutrophil defect.

Here, I describe the test of neutrophil migration from four different patients using the modified Dunn chamber. The three first cases presented in this chapter are patients with unknown cause of immunodeficiency. Therefore, the test was used to evaluate neutrophil migration as a possible cause of immunodeficiency. The fourth case that is presented is a patient with a known mutation; the patient clinical features matched description from the scientific literature which helped the identification of the mutated gene. While each of these tests could be considered as successful, meaning they were completed and control cells behaved as expected, they also underlined the limitations of the use of the Dunn chamber as a routine assay to detect neutrophil migration defects and highlighted the need of a standardised and well-characterised assay.

6.2 Results

6.2.1 Case 1: Patient1

Once left to adhere on fibrinogen-coated coverslips, patient neutrophils displayed a strikingly different phenotype than control cells. Patient cells were indeed much more spread than control cells with a dark shape (open arrow head) compared to the bright cells (closed arrow head) from the control sample (Figure 6-1). The dark and spread state could be seen in control cells (open arrow head) as a transitory state during migration when neutrophils expand their lamellipodia and spread before uropod retraction and the cells returning to a more spherical shape. Surprisingly, the patient 1 cells did not alternate between these two states: over the course of the experiment, most of the cells kept their dark and spread shape and did not move. Only a few patient cells were able to change shape and these cells were able to migrate in the direction of the fMLP gradient (Figure 6-1-A and D, VideoS6-1 and 6-2) with an average velocity of 9 $\mu m.min^{-1}$ lower than the control neutrophil velocity of 16 $\mu m.min^{-1}$ (Figure 6-1-B). Patient 1 neutrophils also displayed a reduced persistence compared to control cells with a chemotactic index of 0.34 and 0.5, respectively (Figure 6-1-C). Overall 62% of control neutrophils were able to migrate whereas only 8% of patient cells migrated (Figure 6-1-E).

6.2.2 Case 2: Patient 2 & 3

In this assay, two patient samples (P2 and P3 patients) were tested and one healthy donor was used as control. All three samples correctly migrated in the direction of the outer well containing the fMLP, as shown in the time-lapse snapshots (Figure 6-2, VideoS6-3, -4 and-5), and displayed a good directionality (Figure 6-3-C). While P2 patient neutrophils migrated with an average velocity of 8.6 $\mu m.min^{-1}$, a not significant lower value than control cells, which migrated with an average velocity of 10.4 $\mu m.min^{-1}$. With an average velocity of 13.5 $\mu m.min^{-1}$, P3 patient neutrophils were faster than P2 patient and control neutrophils (Figure 6-3-A). Analysis of the frequency distribution of the average speed in these three populations showed that both control and P2 patient cell velocity had a Gaussian distribution around the average. P3

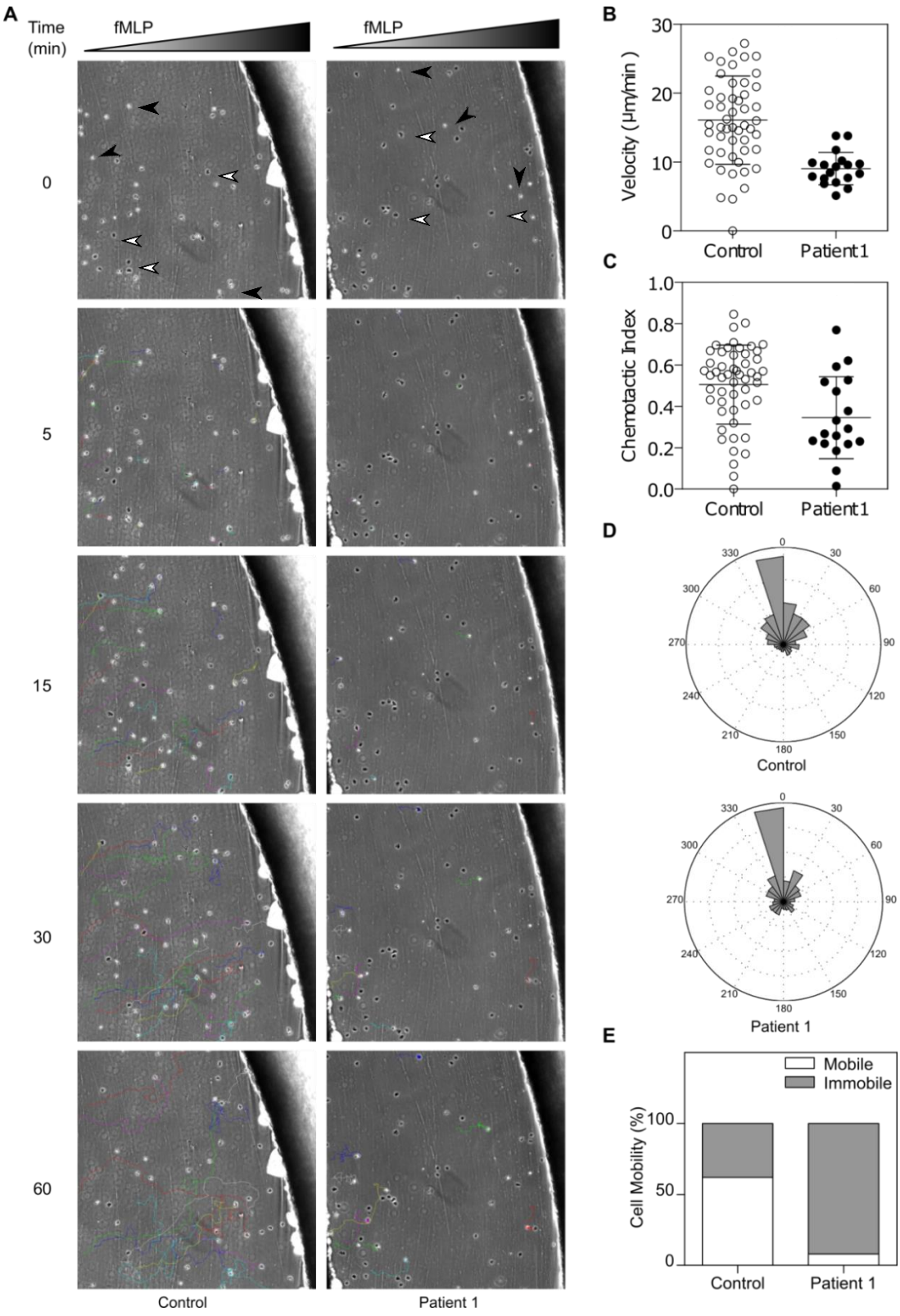

Figure 6-1: Migration of patient 1 neutrophils

A) Control and patient 1 neutrophil migration towards fMLP (100nM) in the agarose Dunn chamber. The cells were imaged at 37^{o}C at 1 image/minute for 1 hour using an Axiovert 135 microscope, equipped with an Achroplan 10x/0.25 objective, an environmental chamber and a motorised stage. Cells were tracked using the ImageJ manual tracking plug-in and tracks were processed in Matlab using an in-house routine. B) Average velocity and C) the chemotactic index were calculated from the cell tracks. Control and patient 1 cells displayed D) good chemotaxis, but showed E) different motility. A-D: data from a single experiment, one replicate.

patient cell velocity distribution revealed three distinct populations, one slow with an average of 8 μm.min^{-1}, one faster with an average of 16.5 μm.min^{-1} and a very fast one with an average speed of 20 μm.min^{-1}. Control, P2 patient and P3 patient neutrophils showed similar persistence during migration with a chemotactic index of 0.44, 0.38 and 0.48, respectively (Figure 6-3-B).

6.2.3 Case 3: Patient 4 with a mutation in the WDR1 gene.

It is the description of a previously established mouse model with reduced WDR1 function due hypomorphic allele that helped identifying the mutated gene responsible for the patient disease. The severe loss of WDR1 function was lethal at the embryonic stage whereas mice carrying the hypomorphic allele developed macrothrombocytopenia and autoinflammatory disease. In mice, macrothromcytopenia was characterised by a failure of megakaryocyte maturation and autoinflammation was described as a massive neutrophil infiltration into inflammation lesions (Kile et al., 2007). Similarities between the patient and the mouse model facilitated the identification of a mutation in the patient WDR1 gene. WD repeat 1 protein (WDR1), also known as Actin interacting protein 1 (AIP1), is a highly-conserved protein in eukaryotes that interacts with cofilin and is involved in the regulation of actin cytoskeleton turn-over. Cofilin is an essential regulator of the actin cytoskeleton and is involved in actin cytoskeleton rearrangement during numerous processes such as cell polarity (Dawe et al., 2003), motility (Dawe et al., 2003; Hirayama et al., 2007), endocytosis (Okreglak and Drubin, 2007), morphogenesis (Zhang et al., 2011), and cytokinesis (Chen and Pollard, 2011). WDR1 interacts with the cofilin/actin complex increasing cofilin severing activity and might also cap the barbed-end of actin filament hastening its depolymerisation (Tsuji et al., 2009). It has been shown that WDR1 has a critical role in the regulation of the actin cytoskeleton during mitosis, migration and inflammation (Fujibuchi et al., 2005; Kato et al., 2008; Li et al., 2007; Tsuji et al., 2009). The role of WDR1 in migration suggested that a migratory defect might be the cause of the patient's immunodeficiency hence I used the modified Dunn chamber to monitor the patient neutrophil migration.

In order to limit intra-assay variations between the Dunn chambers, it was decided to monitor patient and control neutrophils in the same Dunn chamber; this would ensure the two

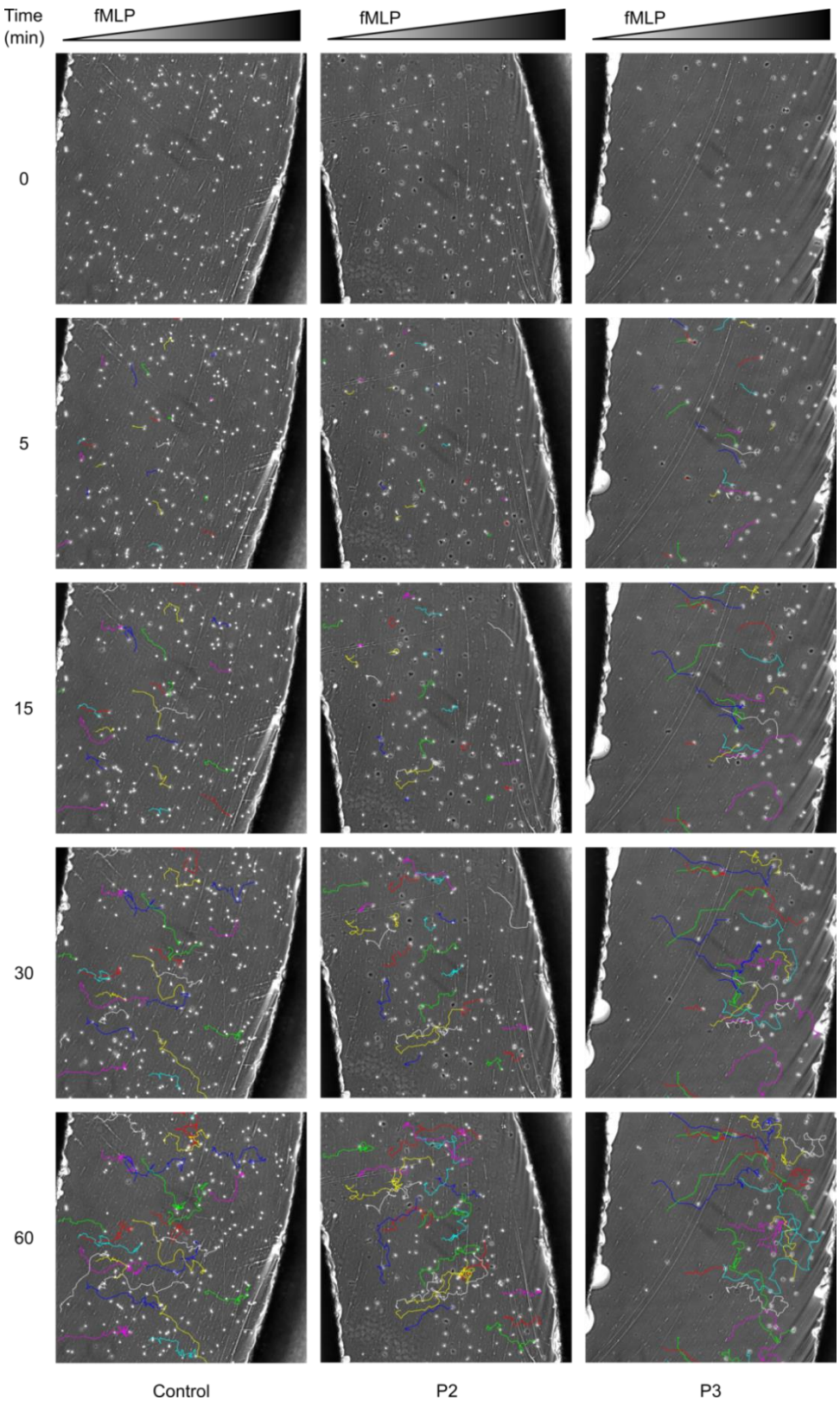

Figure 6-2: Patient 2 and 3 neutrophil migration

Migration tracks of control, patients P2 and P3 neutrophils towards fMLP (100nM) in agarose Dunn chambers was monitored over one hour. The cells were imaged at 37^{o}C at 1 image/minute using an Axiovert 135 microscope, equipped with an Achroplan 10x/0.25 objective, an environmental chamber and a motorised stage. Data from a single experiment, one replicate.

populations would be subjected to the same protein coating, the same chemoattractant gradient and the same conditions of temperature and light exposure. In order to differentiate the two populations, either patient or control neutrophils were stained with the cell permeant dye CFSE (carboxyfluorescein succinimidyl ester) and mixed with unstained control or patient cells in a 1:1 ratio. As CFSE is a dye that covalently binds to amine residues and might alter dynamic cellular processes, the CFSE staining was swapped between the control and patient samples to ensure that the results obtained would not be an artefact due to CFSE treatment. Two independent experiments were performed from patient samples: in the first experiment patient neutrophils were stained with CFSE and mixed with unstained control neutrophils (Figure 6-4-A, VideoS-6-6) whereas in the second experiment control neutrophils were stained with CFSE and mixed with unstained patient neutrophils. The cells were left to adhere on fibrinogen coated coverslips before being assembled in the Dunn chamber. Both control and patient neutrophils displayed a good directionality towards the fMLP gradient (Figure 6-4-D) during migration. Control cells showed a good persistence with a chemotactic index of 0.37, whereas patient cells seemed to display a less persistent migration with a lower, but not significantly different, chemotactic index of 0.3 (Figure 6-4-C). Similarly, control cells displayed a higher, but not statistically different, velocity compared to patient cells of 11 $\mu m.min^{-1}$ and 9.5 $\mu m.min^{-1}$ respectively (Figure 6-4-B). It is to be noted that CFSE might partly affect cell migration as CFSE+ control cells migrated slightly slower than CFSE- control neutrophils. To reduce a possible bias by the staining, the data from the two experiments were pooled together.

Staining of F-actin using phalloidin conjugated with Alexa 647 dye revealed that patient cell F-actin content was two fold higher than that in control cells (Figure 6-5-B, Figure 6-6-B and Figure 6-7) which is consistent with the possible loss of actin disassembly activity due to the mutation in WDR1 in patient cells. Interestingly, analysis of the total staining intensity (sum of the z-stack) from confocal images of patient cells also showed an increase in cofilin (Figure 6-5-

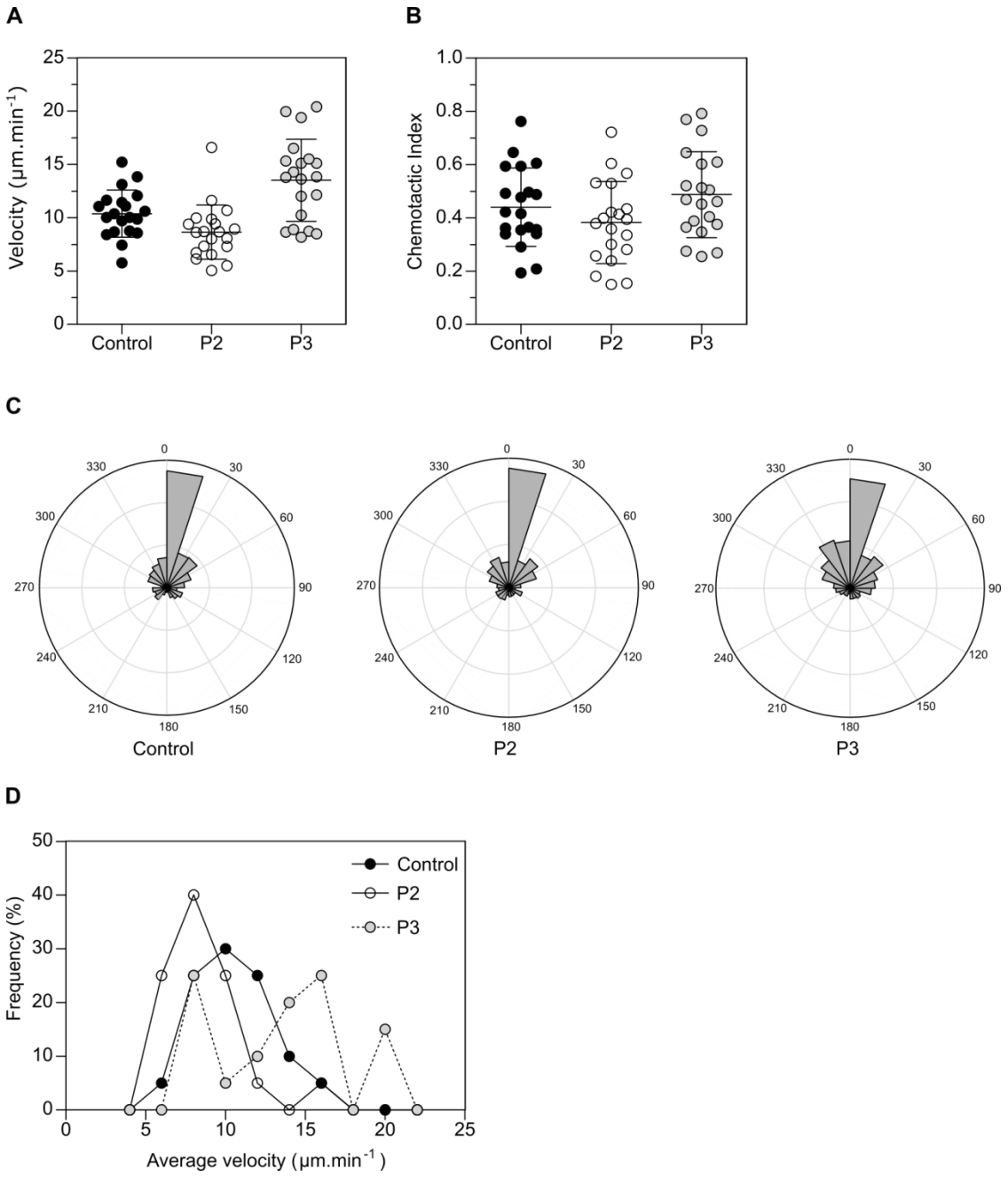

Figure 6-3: Characterisation of patient 2 and patient 3 neutrophil migration

A-D) Analysis of the cell migration shown in Figure 6-2. Cells were tracked using the ImageJ manual tracking plug-in and tracks were processed in Matlab using an in-house routine. A and B) The average velocity and chemotactic index of control, patient P2 and P3 neutrophils were calculated from the data showed in Figure 6-2. The three samples displayed C) good chemotaxis but D) very different distribution of the cell velocity. A-D: results from a single experiment, one replicate.

A and C) and in WDR1 (Figure 6-6-A and C) content of 138% and 38%, respectively, when compared to controls. Increase of WDR1 expression was confirmed by Western blot analysis of lysates from patient and control B LCLs (Figure 6-6 D). The Western blot showed two bands: one of similar molecular weight as WDR1wt and another one of lower molecular weight which could indicate that the mutation was a splice site mutation. The content of the upper band together with the lower band indicates an overexpression of WDR1 when compared to controls.

6.3 Discussion

Despite the fact that the most well-established primary neutrophil defects are at least partially due to chemotaxis impairment, the diagnosis of these neutrophil defects is mainly done by detecting cell surface expression or intracellular protein expression by flow cytometry. Detecting impaired migration could help to diagnose neutrophil immunodeficiencies by quickly narrowing down potential mutated candidates but it could also benefit the detection of new deficiencies as demonstrated, in this thesis, for the patient with the mutated MKL1 protein. This highlights the need for a well-established and robust migration assay that could be implemented in clinical laboratories. We hypothesised that the modified Dunn chamber could fit this need and therefore we investigated its potential to screen patients with a possible neutrophil defect. I tested several patient samples of which four of them were described above. Through these successive assays, I was able to determine that the standardisation of the assay was needed in order to establish a robust assay easily usable by other users.

The P1 patient displayed a dramatic adhesion alteration with more than 90% of the cell population showing an important spreading and the inability to migrate. The few cells that were able to migrate showed a reduced speed and persistence in their migration towards the fMLP gradient. Despite this striking phenotype, the possibility exists that the enhanced adhesion resulted from an activation of the cells during their isolation and did not represent a potential cause for the patient recurrent bacterial infection. Discussion with clinical scientists involved in

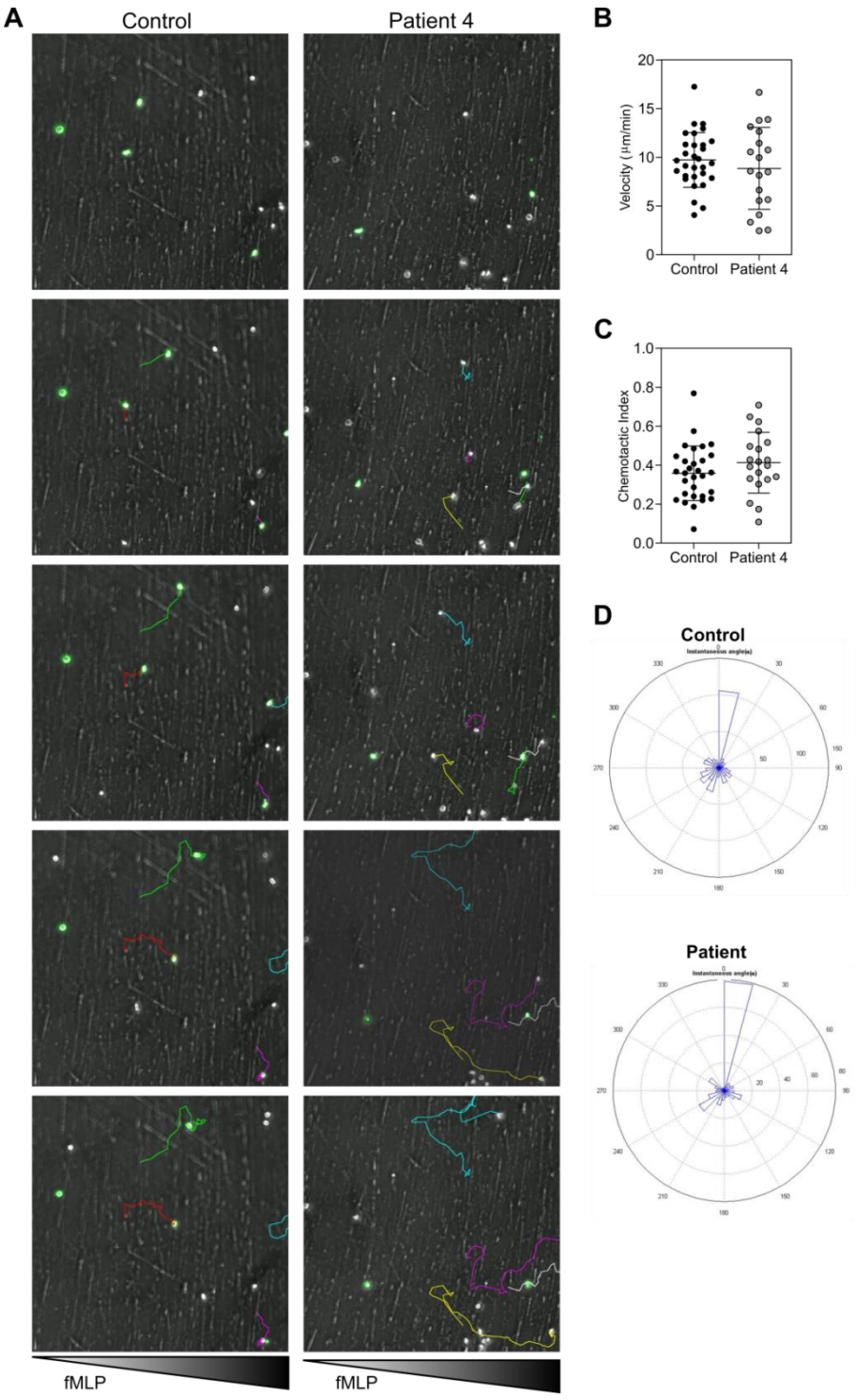

Figure 6-4: Migration of patient 4 neutrophils

A) Migration of control (CFSE+) and patient neutrophils (CFSE-) towards fMLP (100 nM) in agarose Dunn chamber. The cells were imaged at 37°C at 1 image/minute for 1 hour using an Axiovert 135 microscope, equipped with an Achroplan 10x/0.25 objective, an environmental chamber and a motorised stage. Cells were tracked using the ImageJ manual tracking plug-in and tracks were processed in Matlab using an in-house routine. B) Average velocity, C) chemotactic index and D) and chemotaxis of both populations. A-D: Results from two independent experiments one replicate per experiment. CFSE staining was swapped between the two experiments: in the first experiment control were CFSE positive and patient cells were unstained while in the second experiment it was the opposite.

the treatment of this patient allowed the comparison of this result with the absence of phagocytosis defect and enabled me to rule out the alteration of the actin cytoskeleton as possible cause of the phenotype. However, as it was not possible to get more samples to repeat the experiment, I was unable to confirm the phenotype observed in the Dunn chamber.

In the second case, the two patient samples migrated well with a similar directionality and persistence as the control. P2 patient neutrophils exhibited a slightly slower, but not significantly different, velocity than control cells whereas P3 patient cells showed a significantly higher velocity than control neutrophils. The average velocity of P3 patient neutrophils was 13.5 $\mu m.min^{-1}$ which is in the range of what I observed with control neutrophils over the successive assays I performed (10 to 16 $\mu m.min^{-1}$) indicating that, despite the significant difference with the control, P3 patient neutrophils seemed to have a normal migration. Interestingly, the P3 patient neutrophil population was divided in 3 sub-populations with different average speed. This is the only time that I observed an average speed frequency distribution that is not one Gaussian distribution but that could be described as three successive normal distributions. The causes of this phenotype are yet unknown and several hypotheses such as variations in the activation state, the integrin expression and activation status or variations in the fibrinogen coating could explain it and should be further investigated. It is important to mention that the use of only one control in this experiment would have mislead a scientist who was not used to the assay and the response you could expect from normal primary neutrophils to consider the difference between the control and P3 patient neutrophils velocity as a positive result. This stressed the need to define a standard protocol and to evaluate the range of the standard response of the cell for this assay so it could be easily used as a screen test for neutrophil migration.

Regarding the patient with the WDR1 mutation, monitoring neutrophil migration in the modified Dunn chamber was expected to underline a possible migration alteration due to the excess of F-actin. It was previously shown that, despite accumulation of F-actin and modification of actin turnover, WDR1 deficient neutrophils massively infiltrated inflammatory lesions indicating that migration was not defective. I confirmed this result by showing that

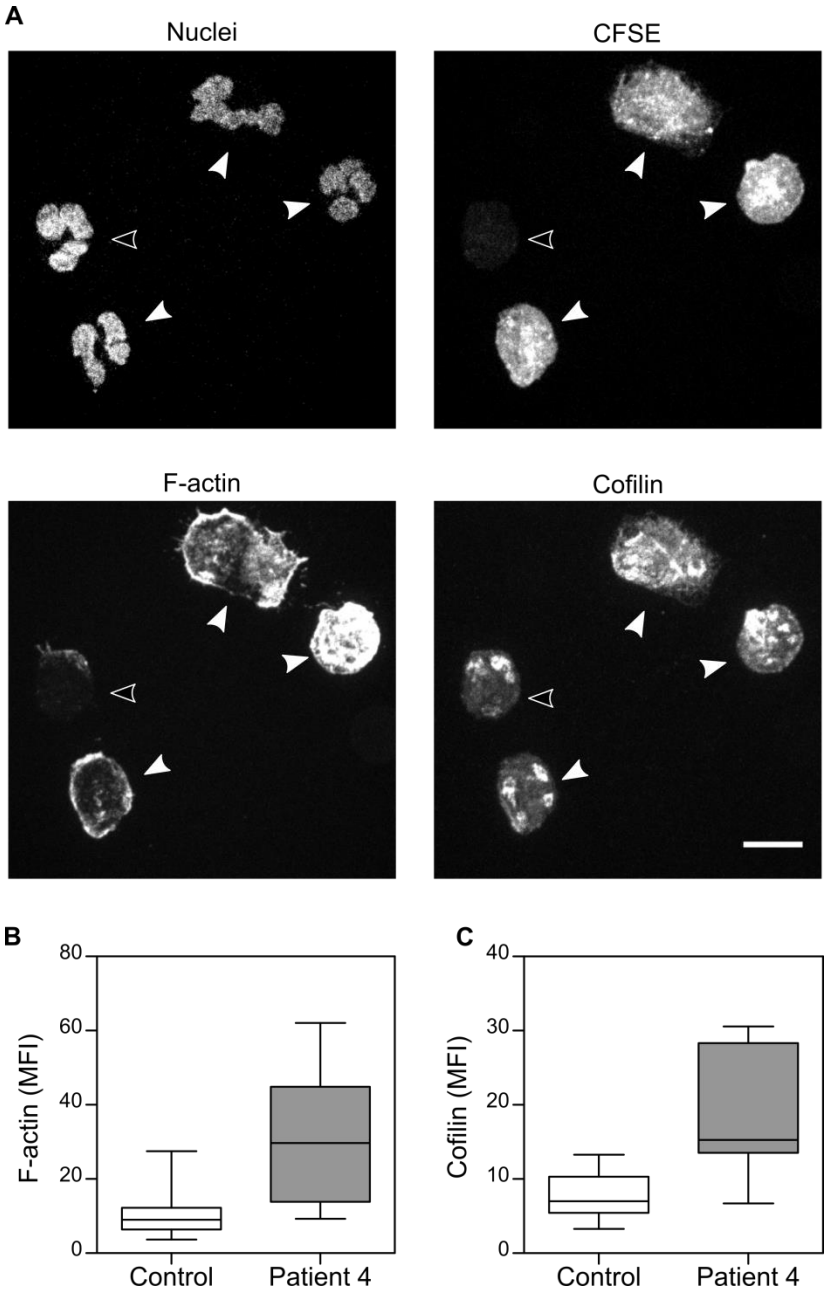

Figure 6-5: F-actin and cofilin in WDR1 patient

A) Confocal images of control (CFSE negative, open arrow head) and patient neutrophils (CFSE positive, closed arrow head). Cells were left to adhere on coverslips coated with fibrinogen for 30 minutes at 37^{o}C before being fixed, permeabilised and stained with DAPI (nuclei), phalloidin-Alexa 568 (F-actin) and anti-cofilin antibody. Cells were imaged using a Zeiss LSM710 confocal microscope using an oil immersion 63x/1.4 objective. B and C) Quantification of F-actin and cofilin contents in both control and patient neutrophils observed in A). Image analysis was performed using CellProfiler: using the DAPI and F-actin signals, the cell edges were detected and used to define ROIs in which the F-actin and cofilin signals were measured. A-C: Results from a single experiment with a single replicate.

patient's neutrophils normally migrated in the Dunn chamber. To reduce the possible impact of CFSE on the result of the experiments, the labelling with the dye was swapped between the two experiments (*i.e.* control cells were CFSE+ in the first experiment and CFSE- in the second experiment). However it was difficult to assess the possible impact of CFSE on these results as they were collected from two independent experiments. It was then difficult to identify the parameter(s) responsible for the small variations observed between the experiments as the cell isolation, CFSE labelling and Dunn chamber preparation could influence the outcome of the experiment. To be sure that the CFSE did not interfere with cell migration, it would have been of interest to label control cells with CFSE and mix them with unlabelled control cell before monitoring their migration in the Dunn chamber. Nevertheless, patient cells seemed to stop migrating before control cells which could be consistent with the accumulation of F-actin during migration to a level that prevents correct extension of the lamellipodia and/or a reduced contractility. WDR1 analysis by confocal microscopy showed that patient cells had a higher content of WDR1. This was at first surprising since it was thought that the mutation was a nonsense mutation. The increase of WDR1 expression was confirmed by Western blot analysis and showed the presence of two bands: a first one similar to WDR1wt and a second band of lower molecular weight, suggesting that the mutation was a splice site mutation. However, the mutant protein might not be functional since we could observe an increase in F-actin by two fold in the patient cells correlated with a strong increase of cofilin expression suggesting a possible compensation mechanism due to the reduction of WDR1 related cofilin severing activity. The patient had bone marrow transplantation in the weeks after the first experiment.

The improvement of the Dunn chamber using agarose to stabilise the gradient of fMLP allowed me to successfully use it to reveal the migration defect of MKL1 deficient primary neutrophils and of dHL-60 expressing CA-WASp. Based on these results, I have used the Dunn chamber to monitor neutrophil migration of other patients with unknown immunological defect. While being preliminary, this study allowed me to highlight the potency as well as the limitations of this assay to be used in routine clinical setting. The Dunn chamber provides a direct functional

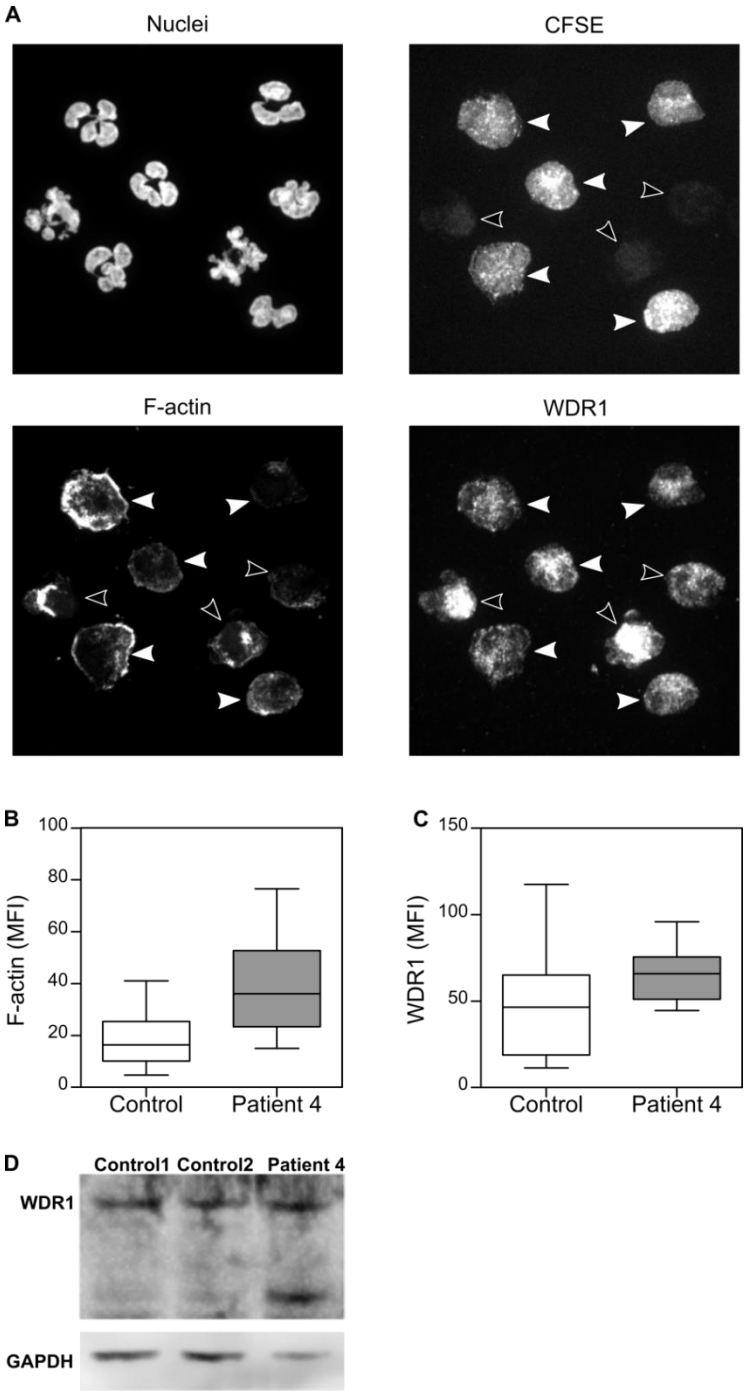

Figure 6-6: WDR1 expression and localisation in patient cells

A) Confocal images of control (CFSE negative, open arrow head) and patient neutrophils (CFSE positive, closed arrow head). Cells were left to adhere on coverslips coated with fibrinogen for 30 minutes at 37^{o}C before being fixed, permeabilised and stained with DAPI (nuclei), phalloidin-Alexa 568 (F-actin) and anti-WDR1 antibody. Cells were imaged using a Zeiss LSM710 confocal microscope using an oil immersion 63x/1.4 objective. B and C) Quantification of F-actin and WDR1 contents in both control and patient neutrophils observed in A). Image analysis was performed using CellProfiler: using the DAPI and F-actin signals, the cell edges were detected and used to define ROIs in which the F-actin and WDR1 signals were measured. D) WDR1 expression levels were also evaluated by Western blot using B LCL lysates. A-D: Results from a single experiment with a single replicate.

assessment of the patient cells while in the same time give information about the cell shape changes. It also allows differentiating several subpopulations which would not be possible in a bulk assay such as the Transwell migration assay. This assay, used in combination with standard immunological clinical assays, would allow narrowing down the possible cause of the defect as shown in MKL1 patient. Nevertheless, to be applied in routine screening, the Dunn chamber would need to be standardised (*e.g.* determining the range of response of healthy donors' neutrophils). Also, due to limited access to patient samples, it is important to improve the robustness of the assay by including internal controls or standards.

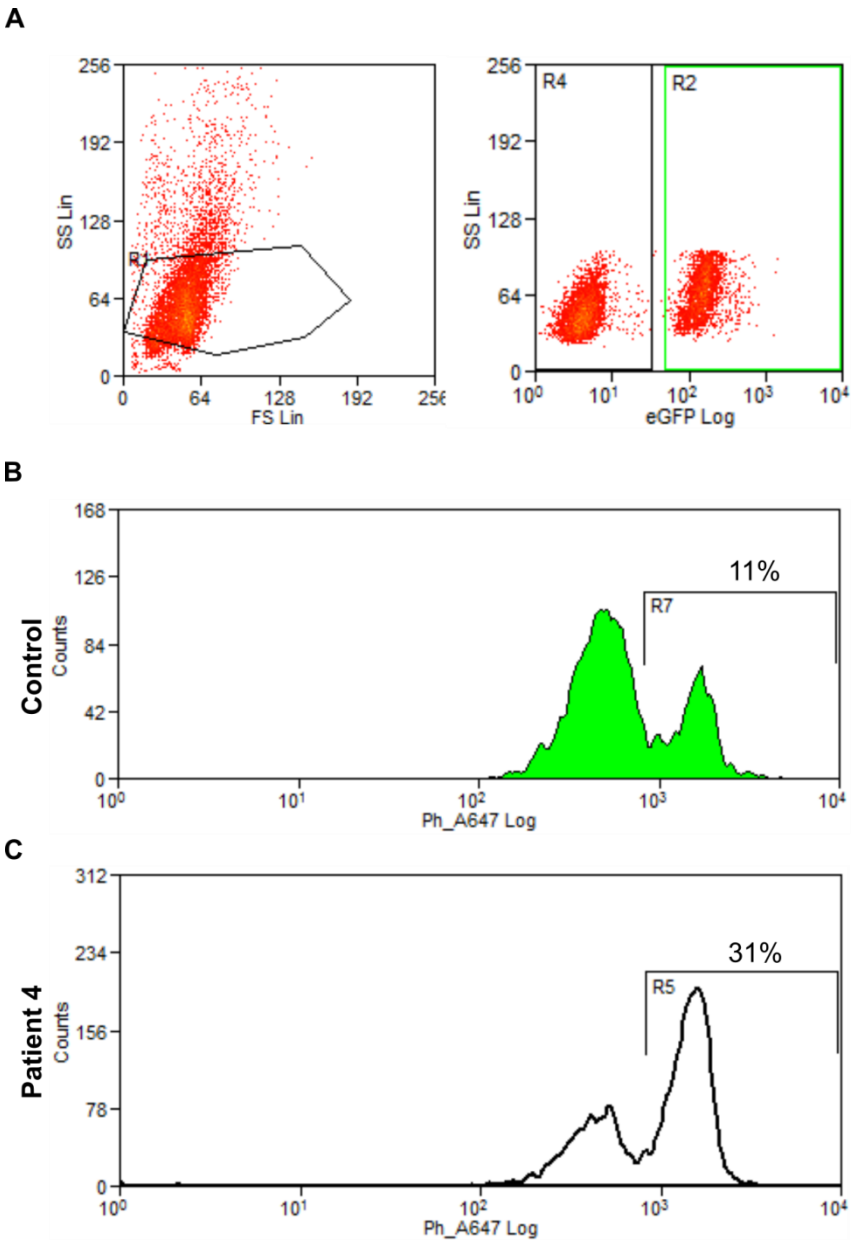

Figure 6-7: F-actin content in WDR1 neutrophils

A-C) Measurement of F-actin content in parient 4 and control primary neutrophils by low cytometry. Patient 4 neutrophils stained with CFSE and unstained control neutrophils were mixed in the same tube before being fixed, permeabilised and stained for F-actin using phalloidin-alexa 647. A) Using flow cytometry, both populations were distinguished from each other using the CFSE staining and B and C) F-actin content was measured. A-C: Data collected from a single experiment and a single replicate.

Chapter 7 General Discussion

Cell migration is an essential process of the immune system. Alteration of this process prevents the clearance of infectious agents by immune cells and can be life threatening. Therefore, evaluating immune cell ability to migrate in the context of immunodeficiency is important as it can both help uncovering the causes of the disease and can provide a better understanding of the influence of specific genes/mutations in the mechanism of action of immune cell migration. This requires accessibility to reliable and relevant tools that allow both a direct visualisation of migrating immune cells and a quantitative assessment of migration.

I started my PhD research project by working on the establishment of a robust migration protocol based on the Dunn chamber (chapter 3), as the direct observation and quantification of immune cell migration in the context of immunodeficiency was key to the completion of my PhD work. Indeed, I was interested in assessing neutrophil migration with the aim to not only decipher the mechanisms of cell migration in immune pathological contexts (chapter 4: the constitutively activated WASp, and chapter 5: MKL1) but also to uncover previously unknown functional migration defects associated with newly-identified patient immunodeficiencies (as shown in chapter 5: MKL1), and to evaluate its potential/limitations for being used for the screening of patients with unknown causes of immune defects in the long term (chapter 6: screening of patients).

To study neutrophil migration in 2D routinely, I decided to use the well-established Dunn chamber, as a system to study directional migration, which was essential for my projects to determine if parameters such as directionality and persistence have been altered in the experimental conditions used. The bacterial peptide fMLP was used as chemoattractant since my main cell model, the neutrophil like dHL-60 cells, was known to respond well to fMLP but poorly to IL-8. However, using the original Dunn chamber setup, in my hands, experimental conditions and laboratory setup, the gradient of fMLP was not stable enough, preventing directional cell migration. Therefore, I decided to modify the Dunn chamber and I managed to stabilise the gradient by pouring an agarose gel containing fMLP in the outer well; the agarose

gel working as a reservoir and slowly delivering the chemokine over time. Using fMLP in the agarose Dunn chamber, I could observe the directional migration of neutrophil-like dHL-60 cells as well as primary neutrophils and I developed a semi-automatic MatLab routine using cell tracks to calculate all the migration parameters needed for my future studies such as velocity, chemotactic index, instantaneous angle, angle variation and average angle.

As I was interested in determining the reliability of this assay, I evaluated the variation between experiments in the agarose Dunn chamber setup and I could establish that there was a 20% inter-assay variation. This result was encouraging although it demonstrated the need for further development, especially if it was to be used in routine. To first reduce the impact of this 20% inter-assay variation on the direct comparison between control and patient/mutated cells, I decided to further modify the protocol performed and mix the two populations to monitor them together in the same agarose Dunn chamber, a fluorescent marker allowing me to discriminate them from each other. Although constituting an improvement, this protocol still requires the planning of additional experiments to include the additional controls that ensure that any possible bias introduced by the addition of dyes or genetic manipulation are taken into consideration, and will necessitate further optimisations (choice of the dye, optimisation of the staining conditions, development of adapted transduced fluorescently-tagged controls) to be used in routine.

In a second part of my project, I focused on studying the impact of the expression of the constitutively activated WASp on neutrophil function. It was hypothesised that the neutropenia observed in patients expressing the mutant WASp might be due to either a migration defect that would prevent neutrophils to reach the infection site or a cell division defect that would prevent neutrophils from proliferating.

The hypothesis of a possible impairment of cell division by CA-WASp was based on previous data from Dr Dale Moulding's experiments that showed that the expression of CA-WASp resulted in an excess of F-actin surrounding chromosomes during cell division, causing a reduction of chromosome movement around the metaphase plate. From these observations, it was hypothesised that the excess of F-actin might also alter the kinetochore dynamics during the

spindle checkpoint, a critical step during cell division which evaluates the correct attachment of microtubules to the chromosomes' kinetochores. Using a cell line expressing a kinetochore protein tagged with GFP, I could track the movement of kinetochores and demonstrate that CA-WASp expression resulted in an increased period of oscillation due to the decrease of the kinetochore movement speed. These results together with the data gathered by Dr Dale Moulding and collaborators allowed us to show that CA-WASp altered cell mechanical properties leading to cytokinesis failure.

In parallel to this defect in cell division, I was interested in investigating the possible alteration of neutrophil migration by CA-WASp. I used the agarose Dunn chamber with dHL-60 cells as a cell model for neutrophils and lentivirus to express CA-WASp in these cells. I observed a decrease in CA-WASp cell velocity concomitantly with a reduction of direction variation during migration when compared to control cells. Preliminary results showed that dHL-60 expressing CA-WASp did not seem to display any alteration in actin cytoskeleton regulator localisation nor expression levels but suggested a possible increase of myosin II activity. This possible higher myosin activity might be a cellular response to changes in cytoplasmic viscosity due to the excess of cytoplasmic F-actin polymerised by CA-WASp. Unfortunately, as the CA-WASp project was going on, it became more and more evident that the technical difficulties encountered would prevent the in-depth study of the mechanism by which the mutant WASp altered neutrophil migration. Indeed, since CK-666 seemed to increase myosin activity and to impair cell migration, it became extremely challenging to establish a causal link between the excess of F-actin caused by CA-WASp and the phenotype observed.

Around the same time it was decided to take advantage of the previous establishment of the agarose Dunn chamber assay to assess neutrophil migration of a patient with recurrent bacterial infections and carrying a mutation in an actin cytoskeleton regulator. The patient's mutation was in MKL1, a regulator of the expression of numerous genes, of which several actin cytoskeleton components and regulators. Since the patient neutrophils displayed a phagocytosis defect, it was hypothesised that the neutrophils actin cytoskeleton might be affected and lead to a migration impairment. As the first results showed a defective migration of the patient's

neutrophils together with a dramatic decrease of the immune cells F-actin content, the focus shifted from the CA-WASp project to the MKL1 project.

Because of the difficulties in obtaining patient samples on a regular basis, I then used, as a neutrophil model, dHL-60 cells in which I silenced MKL1 to further study the mechanism of MKL1 deficiency. I could show that silencing MKL1 in dHL-60 mimicked the patient cell migration phenotype and that the phenotype was likely the result of a strong decrease in β-actin and myosin light chain 9 (encoding myosin IIa light chain) expressions together with an increase in CD11b expression at the cell surface. I also showed that re-expression of β-actin in the cells could nearly completely restore the F-actin content and that actin nucleator expression, such as the ARP2/3 complex, the formin Diaph1 or WASp, was not altered by the lack of MKL1 suggesting that actin polymerisation mechanisms were probably almost unaffected.

These data, together with the one gathered by colleagues, allowed to show that MKL1 was involved in the regulation of the actin cytoskeleton of immune cells and thus driving neutrophils functions. The role of MKL1 in the immune system was previously unknown and it was unexpected that a patient carrying a nonsense mutation in MKL1 displayed an immunodeficiency syndrome. Since MKL1 is a co-transcription factor for ~30 genes related to the actin cytoskeleton, it is very challenging to have a clear and complete overview of the genes that are affected by the loss of MKL1 and of the impact that their altered expression would have on immune functions. In this work, I focused on neutrophils but data from co-workers showed that PBMCs and dendritic cells actin cytoskeleton was affected by MKL1 loss of expression. Thus to have a better understanding of the role of MKL1 in the immune system, it will also be necessary to evaluate the effects of MKL1 deficiency on actin regulator expression levels in all immune myeloid and lymphoid cells. As microarray databases such as Immgen showed that MKL2 expression varies a lot between the different immune cells lineages, it would of interest to investigate the respective role of MKL1 and MKL2 in the regulation of actin cytoskeleton in different immune cells and therefore of their function. It also has been shown that MKL1 has known roles in other tissues such as in neuronal migration (Mokalled et al., 2010b) and adipocyte differentiation (Nobusue et al., 2014). Therefore, it would interesting to investigate if

MKL1 deficiency has any effect on other tissues in the patient especially in neurons since neuronal defects might not have appeared yet due to the young age of the patient.

It is interesting to mention that the phenotypes caused by both CA-WASp and MKL1 mutations shared common features. Indeed, despite the fact that CA-WASp lead to an increase of approximately 50% of F-actin in the cells while MKL1 mutation had the opposite effect with a ~30% decrease of filamentous actin, both mutations resulted in a decrease of neutrophil velocity during migration in the agarose Dunn chamber. In both cases, no dramatic alteration of the actin polymerisation was observed suggesting that the differences observed in F-actin content were only the result of the low expression level of actin in MKL1 cells and the high basal level of F-actin in the CA-WASp cells, respectively. This result also indicated that the defects in migration for both these mutations did not seem to be due to an inability of the cells to create new F-actin structures in response to the chemoattractant stimulus.

We could hypothesised that the impaired migration was only the result of the modification of actin content due to the alteration of the transcription level of actin in MKL1 deficient cells or of the unregulated spatio-temporal activation of WASp in the cells expressing CA-WASp. This would be supported by: 1) our result showing that the re-expression of actin in MKL1 deficient cells allowed to restore F-actin level to a level comparable as the one of wild-type cells; 2) a study showing that the restoration of the expression actin in MKL1 deficient cancerous cells restored their ability to migrate (Salvany et al., 2014).

However, it is more likely that the acto-myosin cytoskeleton needs to be investigated as a whole rather than considering the influence of these mutations on the actin content alone. Indeed, CA-WASp cells seemed to show a possible increase of myosin activity, which was likely a response to the alteration of the cell mechanical properties. In parallel, MKL1 deficient cells showed a strong reduction of myosin IIa light chain expression both at mRNA and protein levels suggesting that the migration defect could be at least partially due to a defective myosin activity.

This highlights that to study actin cytoskeleton defects, it is essential to investigate beyond the polymerisation/depolymerisation of actin and aim to understand the consequences of the defect

on the whole acto-myosin cytoskeleton. The results obtained in both CA-WASp and MKL1 projects were interesting and underlined that, by regulating cell shape, the actin cytoskeleton also affects cell mechanical properties which could lead to diseases. The study of the immune cell mechanics is an on-going field of research whose importance will likely rise in the future with the realisation that immune cells need to migrate through different tissues with different mechanical properties in order to perform their function and need to adapt quickly to these changes of environment.

While it is likely that the mutations described here would alter cell mechanical properties, which may explain the results obtained, it is also not to be excluded that there may be a direct link between CA-WASp and MKL1. Indeed, as MKL1 senses the level of monomers of G-actin in the cytoplasm, it would be very interesting to study MKL1 expression and activity in the context of CA-WASp. We could hypothesise that when CA-WASp is expressed, the excess of F-actin in the cytoplasm decreases the G-actin available to interact with MKL1 resulting in an accumulation of MKL1 in the nucleus. This would allow the increase of the expression the beta actin gene and of several actin cytoskeleton regulators. Another gene regulated by MKL1 is *MYL9* encoding the regulatory light chain of myosin IIa. An increase of MKL1 activity due to CA-WASp could result in an increased expression of myosin which would be in line with the preliminary results showing a possible increase myosin activity in CA-WASp cells.

The MKL1 project also showed that the agarose Dunn chamber was useful to uncover impaired migration of neutrophils isolated from patient samples. Therefore, it was decided to further evaluate the potential of this set-up to screen PID patients for neutrophil migratory defects. In chapter 6, I assessed possible migratory defects in neutrophils from four PID patients. For three of these patients, the cause of the PID was unknown, while the fourth patient suffered from a mutation in *WDR1*, which encodes a protein involved in the severing of actin filaments.

The first patient I tested showed a decreased neutrophil velocity and a reduced chemotactic index indicating a possible neutrophil migratory defect. The presence of spread and immobile

neutrophils in the Dunn chamber in both the control and patient samples indicated a possible over activation of neutrophils during the collection of the samples.

The second and third patients were siblings and their neutrophils displayed a good migration. The third patient neutrophils showed a significantly faster migration than control neutrophils. Deeper analysis of the speed revealed three distinct cell populations, each with a specific average speed. This is so far the only time that I could observe a non-Gaussian distribution of the neutrophil velocity in a patient sample. The causes of this phenotype are still unknown and could have been the result of differences in the activation state of the neutrophils, the integrin expression and activation status or variations in the fibrinogen coating. This result needs further investigations to elucidate if these observations are resulting from a potential issue with the setup or if a patient mutation is responsible for the phenotype.

The neutrophils from the fourth patient with the mutation in WDR1 did not display any significant differences in their migration behaviour but I could show that the patient neutrophils displayed an increased F-actin content together with a higher expression of cofilin and WDR1. Analysis of the WDR1 expression by Western blot showed that both the full length and a truncated mutated version of the protein were expressed. The patient then underwent a bone marrow transplant preventing us from further studying this mutation.

The screening of patients showed that the agarose Dunn chamber had limitations in detecting differences between samples. To clearly establish a difference between samples, several repeat experiments are absolutely necessary and this is unfortunately not always possible due to the difficulties to acquire samples from patients.

The incorporation of agarose in the outer well of the Dunn chamber to stabilise chemokine gradients improved the setup and allowed a more reliable study of neutrophil directional migration. Nevertheless the assay remained too variable to be used routinely in a clinical lab and still needs to be optimised.

The first step would be to monitor the migration of tens of healthy controls to evaluate accurately the limits of the agarose Dunn chamber setup and define the pitfalls from the cell

isolation, the cell adhesion, the pouring of the gel and the chamber assembly. From these results three directions are anticipated: first the variability is considered adapted for a routine assay and the critical steps are reproducibly performed when the setup is used by an experienced user.

The second option would be to find easy ways to improve the setup reliability. For instance, as discussed above, the use of dyes to label one population (control or patient) and monitoring the mixed - stained and unstained - population in the same chamber is a good method to reduce intra-assay variability since both populations will adhere on the same substrate, will be handled identically and be subjected to the same chemokine gradients, and could be optimised to eliminate biases.

Another issue that can be easily avoided is the use of only one control in each experiment. Using only one healthy control is risky since no one is absolutely sure that the donor is totally healthy. For example, the donor could have a mild neutrophil defect not detected, which will not show a significant difference with the patient sample. The establishment of correct statistics, by testing tens of healthy donors, would allow us to know the confidence intervals of healthy neutrophil velocity, chemotactic index, instantaneous angle and distance and would allow the user to quickly determine if the control used is in the good range of values.

The third possibility may be that the setup could not be improved to fit the requirements to be used as a routine assay. As an alternative, it would be interesting to consider a setup with static gradient and a ready-assembled chamber. The static gradient is usually easier to setup than a dynamic gradient using, for example, a microfluidic device. The fact that the chamber would already be assembled would decrease possible operator errors during the chamber assembly. The current agarose Dunn chamber allows only the study of neutrophil migration in 2D. In the body, neutrophils migrate in 2D on the surface of the blood vessels but the rest of their migration in tissues is in 3D environments. The development of a standardized 3D assay for clinical diagnostics would also be beneficial as 2D and 3D migration rely on different biological and physical processes. Therefore, one assay may reveal a defect that would remain undetected using the other method. A good example are neutrophils from patients suffering from leukocyte adhesion deficiency 1 which lack expression of CD18 integrins and cannot adhere and migrate on 2D but display random and directed migration when compressed between a slide and a

coverslip (Malawista et al., 2000). This highlights the need for the creation of a standardized assay to assess neutrophil migration as its current lack slows down neutrophil migratory defect investigations.

The work presented here showed that the actin cytoskeleton is a prime actor in the function of the immune system. Therefore, the understanding of the actin cytoskeleton regulation in immune functions is important and using PID as models is useful as they can provide a better understanding of the role of actin regulators in the immune system homeostasis and function.

References

Accetta, D., Syverson, G., Bonacci, B., Reddy, S., Bengtson, C., Surfus, J., Harbeck, R., Huttenlocher, A., Grossman, W., Routes, J., Verbsky, J., 2011. Human phagocyte defect caused by a Rac2 mutation detected by means of neonatal screening for T-cell lymphopenia. J. Allergy Clin. Immunol. 127, 535-538.e1–2. https://doi.org/10.1016/j.jaci.2010.10.013

Alblas, J., Ulfman, L., Hordijk, P., Koenderman, L., 2001. Activation of RhoA and ROCK Are Essential for Detachment of Migrating Leukocytes. Mol. Biol. Cell 12, 2137–2145. https://doi.org/10.1091/mbc.12.7.2137

Alonso-Lebrero, J.L., Serrador, J.M., Domínguez-Jiménez, C., Barreiro, O., Luque, A., Pozo, M.A. del, Snapp, K., Kansas, G., Schwartz-Albiez, R., Furthmayr, H., Lozano, F., Sánchez-Madrid, F., 2000. Polarization and interaction of adhesion molecules P-selectin glycoprotein ligand 1 and intercellular adhesion molecule 3 with moesin and ezrin in myeloid cells. Blood 95, 2413–2419.

Amann, K.J., Pollard, T.D., 2001. Direct real-time observation of actin filament branching mediated by Arp2/3 complex using total internal reflection fluorescence microscopy. Proc. Natl. Acad. Sci. U. S. A. 98, 15009–15013. https://doi.org/10.1073/pnas.211556398

Ambruso, D.R., Knall, C., Abell, A.N., Panepinto, J., Kurkchubasche, A., Thurman, G., Gonzalez-Aller, C., Hiester, A., deBoer, M., Harbeck, R.J., Oyer, R., Johnson, G.L., Roos, D., 2000. Human neutrophil immunodeficiency syndrome is associated with an inhibitory Rac2 mutation. Proc. Natl. Acad. Sci. 97, 4654–4659. https://doi.org/10.1073/pnas.080074897

Ancliff, P.J., Blundell, M.P., Cory, G.O., Calle, Y., Worth, A., Kempski, H., Burns, S., Jones, G.E., Sinclair, J., Kinnon, C., Hann, I.M., Gale, R.E., Linch, D.C., Thrasher, A.J., 2006. Two novel activating mutations in the Wiskott-Aldrich syndrome protein result in congenital neutropenia. Blood 108, 2182–2189. https://doi.org/10.1182/blood-2006-01-010249

Andrianantoandro, E., Pollard, T.D., 2006. Mechanism of Actin Filament Turnover by Severing and Nucleation at Different Concentrations of ADF/Cofilin. Mol. Cell 24, 13–23. https://doi.org/10.1016/j.molcel.2006.08.006

Appleton, B.A., Wu, P., Wiesmann, C., 2006. The Crystal Structure of Murine Coronin-1: A Regulator of Actin Cytoskeletal Dynamics in Lymphocytes. Structure 14, 87–96. https://doi.org/10.1016/j.str.2005.09.013

Araki, N., Hatae, T., Furukawa, A., Swanson, J.A., 2003. Phosphoinositide-3-kinase-independent contractile activities associated with Fcgamma-receptor-mediated phagocytosis and macropinocytosis in macrophages. J. Cell Sci. 116, 247–257.

Arana, E., Vehlow, A., Harwood, N.E., Vigorito, E., Henderson, R., Turner, M., Tybulewicz, V.L.J., Batista, F.D., 2008. Activation of the small GTPase Rac2 via the B cell receptor regulates B cell adhesion and immunological-synapse formation. Immunity 28, 88–99. https://doi.org/10.1016/j.immuni.2007.12.003

Bachelerie, F., Ben-Baruch, A., Burkhardt, A.M., Combadiere, C., Farber, J.M., Graham, G.J., Horuk, R., Sparre-Ulrich, A.H., Locati, M., Luster, A.D., Mantovani, A., Matsushima, K., Murphy, P.M., Nibbs, R., Nomiyama, H., Power, C.A., Proudfoot, A.E.I., Rosenkilde, M.M., Rot, A., Sozzani, S., Thelen, M., Yoshie, O., Zlotnik, A., 2014. International Union of Basic and Clinical Pharmacology. LXXXIX. Update on the Extended Family of Chemokine Receptors and Introducing a New Nomenclature for Atypical Chemokine Receptors. Pharmacol. Rev. 66, 1–79. https://doi.org/10.1124/pr.113.007724

Badolato, R., Sozzani, S., Malacarne, F., Bresciani, S., Fiorini, M., Borsatti, A., Albertini, A., Mantovani, A., Ugazio, A.G., Notarangelo, L.D., 1998. Monocytes from Wiskott-Aldrich patients display reduced chemotaxis and lack of cell polarization in response to monocyte chemoattractant protein-1 and formyl-methionyl-leucyl-phenylalanine. J. Immunol. Baltim. Md 1950 161, 1026–1033.

Badour, K., Zhang, J., Shi, F., McGavin, M.K.H., Rampersad, V., Hardy, L.A., Field, D., Siminovitch, K.A., 2003. The Wiskott-Aldrich Syndrome Protein Acts Downstream of

CD2 and the CD2AP and PSTPIP1 Adaptors to Promote Formation of the Immunological Synapse. Immunity 18, 141–154. https://doi.org/10.1016/S1074-7613(02)00516-2

Bargatze, R.F., Kurk, S., Butcher, E.C., Jutila, M.A., 1994. Neutrophils roll on adherent neutrophils bound to cytokine-induced endothelial cells via L-selectin on the rolling cells. J. Exp. Med. 180, 1785–1792.

Beel, K., Cotter, M.M., Blatny, J., Bond, J., Lucas, G., Green, F., Vanduppen, V., Leung, D.W., Rooney, S., Smith, O.P., Rosen, M.K., Vandenberghe, P., 2009. A large kindred with X-linked neutropenia with an I294T mutation of the Wiskott-Aldrich syndrome gene. Br. J. Haematol. 144, 120–126. https://doi.org/10.1111/j.1365-2141.2008.07416.x

Beltzner, C.C., Pollard, T.D., 2004. Identification of Functionally Important Residues of Arp2/3 Complex by Analysis of Homology Models from Diverse Species. J. Mol. Biol. 336, 551–565. https://doi.org/10.1016/j.jmb.2003.12.017

Bergert, M., Chandradoss, S.D., Desai, R.A., Paluch, E., 2012. Cell mechanics control rapid transitions between blebs and lamellipodia during migration. Proc. Natl. Acad. Sci. https://doi.org/10.1073/pnas.1207968109

Bhavsar, A.P., Guttman, J.A., Finlay, B.B., 2007. Manipulation of host-cell pathways by bacterial pathogens. Nature 449, 827–834. https://doi.org/10.1038/nature06247

Bianchi, M., Hakkim, A., Brinkmann, V., Siler, U., Seger, R.A., Zychlinsky, A., Reichenbach, J., 2009. Restoration of NET formation by gene therapy in CGD controls aspergillosis. Blood 114, 2619–2622. https://doi.org/10.1182/blood-2009-05-221606

Bignold, L.P., Rogers, S.D., Siaw, T.M., Bahnisch, J., 1991. Inhibition of chemotaxis of neutrophil leukocytes to interleukin-8 by endotoxins of various bacteria. Infect. Immun. 59, 4255–4258.

Blomgran, R., Ernst, J.D., 2011. Lung Neutrophils Facilitate Activation of Naive Antigen-Specific CD4+ T Cells during Mycobacterium tuberculosis Infection. J. Immunol. 186, 7110–7119. https://doi.org/10.4049/jimmunol.1100001

Blundell, M.P., Bouma, G., Metelo, J., Worth, A., Calle, Y., Cowell, L.A., Westerberg, L.S., Moulding, D.A., Mirando, S., Kinnon, C., Cory, G.O., Jones, G.E., Snapper, S.B., Burns, S.O., Thrasher, A.J., 2009. Phosphorylation of WASp is a key regulator of activity and stability in vivo. Proc. Natl. Acad. Sci. U. S. A. 106, 15738–15743. https://doi.org/10.1073/pnas.0904346106

Bobkov, A.A., Muhlrad, A., Pavlov, D.A., Kokabi, K., Yilmaz, A., Reisler, E., 2006. Cooperative Effects of Cofilin (ADF) on Actin Structure Suggest Allosteric Mechanism of Cofilin Function. J. Mol. Biol. 356, 325–334. https://doi.org/10.1016/j.jmb.2005.11.072

Borregaard, N., 2010. Neutrophils, from Marrow to Microbes. Immunity 33, 657–670. https://doi.org/10.1016/j.immuni.2010.11.011

Bouma, G., Burns, S., Thrasher, A.J., 2007. Impaired T-cell priming in vivo resulting from dysfunction of WASp-deficient dendritic cells. Blood 110, 4278–4284. https://doi.org/10.1182/blood-2007-06-096875

Buckley, C.D., Ross, E.A., McGettrick, H.M., Osborne, C.E., Haworth, O., Schmutz, C., Stone, P.C.W., Salmon, M., Matharu, N.M., Vohra, R.K., Nash, G.B., Rainger, G.E., 2006. Identification of a phenotypically and functionally distinct population of long-lived neutrophils in a model of reverse endothelial migration. J. Leukoc. Biol. 79, 303–311. https://doi.org/10.1189/jlb.0905496

Bunnell, T.M., Burbach, B.J., Shimizu, Y., Ervasti, J.M., 2011. B-Actin Specifically Controls Cell Growth, Migration, and the G-Actin Pool. Mol. Biol. Cell 22, 4047–4058. https://doi.org/10.1091/mbc.E11-06-0582

Burke, T.A., Christensen, J.R., Barone, E., Suarez, C., Sirotkin, V., Kovar, D.R., 2014. Homeostatic Actin Cytoskeleton Networks Are Regulated by Assembly Factor Competition for Monomers. Curr. Biol. 24, 579–585. https://doi.org/10.1016/j.cub.2014.01.072

Burns, A.R., Bowden, R.A., MacDonell, S.D., Walker, D.C., Odebunmi, T.O., Donnachie, E.M., Simon, S.I., Entman, M.L., Smith, C.W., 2000. Analysis of tight junctions during neutrophil transendothelial migration. J. Cell Sci. 113, 45–57.

Burns, S., Hardy, S.J., Buddle, J., Yong, K.L., Jones, G.E., Thrasher, A.J., 2004. Maturation of DC is associated with changes in motile characteristics and adherence. Cell Motil. Cytoskeleton 57, 118–132. https://doi.org/10.1002/cm.10163

Burns, S., Thrasher, A.J., Blundell, M.P., Machesky, L., Jones, G.E., 2001. Configuration of human dendritic cell cytoskeleton by Rho GTPases, the WAS protein, and differentiation. Blood 98, 1142–1149.

Burns, S.O., Killock, D.J., Moulding, D.A., Metelo, J., Nunes, J., Taylor, R.R., Forge, A., Thrasher, A.J., Ivetic, A., 2010. A congenital activating mutant of WASp causes altered plasma membrane topography and adhesion under flow in lymphocytes. Blood 115, 5355–5365. https://doi.org/10.1182/blood-2009-08-236174

Cai, L., Makhov, A.M., Bear, J.E., 2007. F-actin binding is essential for coronin 1B function in vivo. J. Cell Sci. 120, 1779–1790. https://doi.org/10.1242/jcs.007641

Cai, L., Makhov, A.M., Schafer, D.A., Bear, J.E., 2008. Coronin 1B antagonizes Cortactin and remodels Arp2/3-containing actin branches in lamellipodia. Cell 134, 828–842. https://doi.org/10.1016/j.cell.2008.06.054

Cai, Y., Biais, N., Giannone, G., Tanase, M., Jiang, G., Hofman, J.M., Wiggins, C.H., Silberzan, P., Buguin, A., Ladoux, B., Sheetz, M.P., 2006. Nonmuscle Myosin IIA-Dependent Force Inhibits Cell Spreading and Drives F-Actin Flow. Biophys. J. 91, 3907–3920. https://doi.org/10.1529/biophysj.106.084806

Campellone, K.G., Webb, N.J., Znameroski, E.A., Welch, M.D., 2008. WHAMM is an Arp2/3 complex activator that binds microtubules and functions in ER to Golgi transport. Cell 134, 148–161. https://doi.org/10.1016/j.cell.2008.05.032

Campellone, K.G., Welch, M.D., 2010. A nucleator arms race: cellular control of actin assembly. Nat Rev Mol Cell Biol 11, 237–251. https://doi.org/10.1038/nrm2867

Cao, X., Hu, X.-M., Hu, J.-Q., Zheng, W.-X., 2011. Myocardin-related transcription factor-A promoting neuronal survival against apoptosis induced by hypoxia/ischemia. Brain Res. 1385, 263–274. https://doi.org/10.1016/j.brainres.2011.02.016

Carrigan, S.O., Weppler, A.L., Issekutz, A.C., Stadnyk, A.W., 2005. Neutrophil differentiated HL-60 cells model Mac-1 (CD11b/CD18)-independent neutrophil transepithelial migration. Immunology 115, 108–117.

Cavnar, P.J., Berthier, E., Beebe, D.J., Huttenlocher, A., 2011. Hax1 regulates neutrophil adhesion and motility through RhoA. J. Cell Biol. 193, 465–473. https://doi.org/10.1083/jcb.201010143

Cen, B., Selvaraj, A., Burgess, R.C., Hitzler, J.K., Ma, Z., Morris, S.W., Prywes, R., 2003. Megakaryoblastic Leukemia 1, a Potent Transcriptional Coactivator for Serum Response Factor (SRF), Is Required for Serum Induction of SRF Target Genes. Mol. Cell. Biol. 23, 6597–6608. https://doi.org/10.1128/MCB.23.18.6597-6608.2003

Cera, M.R., Fabbri, M., Molendini, C., Corada, M., Orsenigo, F., Rehberg, M., Reichel, C.A., Krombach, F., Pardi, R., Dejana, E., 2009. JAM-A promotes neutrophil chemotaxis by controlling integrin internalization and recycling. J. Cell Sci. 122, 268–277. https://doi.org/10.1242/jcs.037127

Cerecedo, D., Cisneros, B., Gómez, P., Galván, I.J., 2010. Distribution of dystrophin- and utrophin-associated protein complexes during activation of human neutrophils. Exp. Hematol. 38, 618–628.e3. https://doi.org/10.1016/j.exphem.2010.04.010

Chan, K.T., Creed, S.J., Bear, J.E., 2011. Unraveling the enigma: progress towards understanding the coronin family of actin regulators. Trends Cell Biol. 21, 481–488. https://doi.org/10.1016/j.tcb.2011.04.004

Cheeseman, I.M., Desai, A., 2008. Molecular architecture of the kinetochore-microtubule interface. Nat Rev Mol Cell Biol 9, 33–46. https://doi.org/10.1038/nrm2310

Chen, Q., Pollard, T.D., 2011. Actin filament severing by cofilin is more important for assembly than constriction of the cytokinetic contractile ring. J. Cell Biol. 195, 485–498. https://doi.org/10.1083/jcb.201103067

Cheng, E.-C., Luo, Q., Bruscia, E.M., Renda, M.J., Troy, J.A., Massaro, S.A., Tuck, D., Schulz, V., Mane, S.M., Berliner, N., Sun, Y., Morris, S.W., Qiu, C., Krause, D.S., 2009. Role for MKL1 in megakaryocytic maturation. Blood 113, 2826–2834. https://doi.org/10.1182/blood-2008-09-180596

Chou, H.-C., Antón, I.M., Holt, M.R., Curcio, C., Lanzardo, S., Worth, A., Burns, S., Thrasher, A.J., Jones, G.E., Calle, Y., 2006. WIP regulates the stability and localization of WASP to podosomes in migrating dendritic cells. Curr. Biol. CB 16, 2337–2344. https://doi.org/10.1016/j.cub.2006.10.037

Coates, T.D., Torkildson, J.C., Torres, M., Church, J.A., Howard, T.H., 1991. An inherited defect of neutrophil motility and microfilamentous cytoskeleton associated with abnormalities in 47-Kd and 89-Kd proteins. Blood 78, 1338–1346.

Condliffe, A.M., Kitchen, E., Chilvers, E.R., 1998. Neutrophil Priming: Pathophysiological Consequences and Underlying Mechanisms. Clin. Sci. 94, 461–471. https://doi.org/10.1042/cs0940461

Copeland, J.W., Copeland, S.J., Treisman, R., 2004. Homo-oligomerization Is Essential for F-actin Assembly by the Formin Family FH2 Domain. J. Biol. Chem. 279, 50250–50256. https://doi.org/10.1074/jbc.M404429200

Costa, C., Germena, G., Martin-Conte, E.L., Molineris, I., Bosco, E., Marengo, S., Azzolino, O., Altruda, F., Ranieri, V.M., Hirsch, E., 2011. The RacGAP ArhGAP15 is a master negative regulator of neutrophil functions. Blood 118, 1099–1108. https://doi.org/10.1182/blood-2010-12-324756

Cotta-de-Almeida, V., Westerberg, L., Maillard, M.H., Onaldi, D., Wachtel, H., Meelu, P., Chung, U., Xavier, R., Alt, F.W., Snapper, S.B., 2007. Wiskott–Aldrich syndrome protein (WASP) and N-WASP are critical for T cell development. Proc. Natl. Acad. Sci. 104, 15424–15429. https://doi.org/10.1073/pnas.0706881104

Coutts, A.S., Weston, L., Thangue, N.B.L., 2009. A transcription co-factor integrates cell adhesion and motility with the p53 response. Proc. Natl. Acad. Sci. 106, 19872–19877. https://doi.org/10.1073/pnas.0906785106

Cramer, L.P., Briggs, L.J., Dawe, H.R., 2002. Use of fluorescently labelled deoxyribonuclease I to spatially measure G-actin levels in migrating and non-migrating cells. Cell Motil. Cytoskeleton 51, 27–38.

Crequer, A., Troeger, A., Patin, E., Ma, C.S., Picard, C., Pedergnana, V., Fieschi, C., Lim, A., Abhyankar, A., Gineau, L., Mueller-Fleckenstein, I., Schmidt, M., Taieb, A., Krueger, J., Abel, L., Tangye, S.G., Orth, G., Williams, D.A., Casanova, J.-L., Jouanguy, E., 2012. Human RHOH deficiency causes T cell defects and susceptibility to EV-HPV infections. J. Clin. Invest. 122, 3239–3247. https://doi.org/10.1172/JCI62949

Cvejic, A., Hall, C., Bak-Maier, M., Flores, M.V., Crosier, P., Redd, M.J., Martin, P., 2008. Analysis of WASp function during the wound inflammatory response – live-imaging studies in zebrafish larvae. J. Cell Sci. 121, 3196–3206. https://doi.org/10.1242/jcs.032235

Danuser, G., Waterman-Storer, C.M., 2006. Quantitative Fluorescent Speckle Microscopy of Cytoskeleton Dynamics. Annu. Rev. Biophys. Biomol. Struct. 35, 361–387. https://doi.org/10.1146/annurev.biophys.35.040405.102114

Darling, E.M., Zauscher, S., Guilak, F., 2006. Viscoelastic properties of zonal articular chondrocytes measured by atomic force microscopy. Osteoarthritis Cartilage 14, 571–579. https://doi.org/10.1016/j.joca.2005.12.003

Dawe, H.R., Minamide, L.S., Bamburg, J.R., Cramer, L.P., 2003. ADF/Cofilin Controls Cell Polarity during Fibroblast Migration. Curr. Biol. 13, 252–257. https://doi.org/10.1016/S0960-9822(03)00040-X

de la Fuente, M.A., Sasahara, Y., Calamito, M., Antón, I.M., Elkhal, A., Gallego, M.D., Suresh, K., Siminovitch, K., Ochs, H.D., Anderson, K.C., Rosen, F.S., Geha, R.S., Ramesh, N., 2007. WIP is a chaperone for Wiskott-Aldrich syndrome protein (WASP). Proc. Natl. Acad. Sci. U. S. A. 104, 926–931. https://doi.org/10.1073/pnas.0610275104

de Noronha, S., Hardy, S., Sinclair, J., Blundell, M.P., Strid, J., Schulz, O., Zwirner, J., Jones, G.E., Katz, D.R., Kinnon, C., Thrasher, A.J., 2005. Impaired dendritic-cell homing in vivo in the absence of Wiskott-Aldrich syndrome protein. Blood 105, 1590–1597. https://doi.org/10.1182/blood-2004-06-2332

Derivery, E., Sousa, C., Gautier, J.J., Lombard, B., Loew, D., Gautreau, A., 2009. The Arp2/3 Activator WASH Controls the Fission of Endosomes through a Large Multiprotein Complex. Dev. Cell 17, 712–723. https://doi.org/10.1016/j.devcel.2009.09.010

Devriendt, K., Kim, A.S., Mathijs, G., Frints, S.G., Schwartz, M., Van Den Oord, J.J., Verhoef, G.E., Boogaerts, M.A., Fryns, J.P., You, D., Rosen, M.K., Vandenberghe, P., 2001. Constitutively activating mutation in WASP causes X-linked severe congenital neutropenia. Nat. Genet. 27, 313–317. https://doi.org/10.1038/85886

Ding, L., Morrison, S.J., 2013. Haematopoietic stem cells and early lymphoid progenitors occupy distinct bone marrow niches. Nature 495, 231–235. https://doi.org/10.1038/nature11885

Ding, L., Saunders, T.L., Enikolopov, G., Morrison, S.J., 2012. Endothelial and perivascular cells maintain haematopoietic stem cells. Nature 481, 457–462. https://doi.org/10.1038/nature10783

Duffy, D., Perrin, H., Abadie, V., Benhabiles, N., Boissonnas, A., Liard, C., Descours, B., Reboulleau, D., Bonduelle, O., Verrier, B., Van Rooijen, N., Combadière, C., Combadière, B., 2012. Neutrophils Transport Antigen from the Dermis to the Bone Marrow, Initiating a Source of Memory CD8+ T Cells. Immunity 37, 917–929. https://doi.org/10.1016/j.immuni.2012.07.015

Duleh, S.N., Welch, M.D., 2010. WASH and the Arp2/3 complex regulate endosome shape and trafficking. Cytoskeleton 67, 193–206. https://doi.org/10.1002/cm.20437

Dumont, S., Salmon, E.D., Mitchison, T.J., 2012. Deformations Within Moving Kinetochores Reveal Different Sites of Active and Passive Force Generation. Science 337, 355–358. https://doi.org/10.1126/science.1221886

Dupré, L., Aiuti, A., Trifari, S., Martino, S., Saracco, P., Bordignon, C., Roncarolo, M.-G., 2002. Wiskott-Aldrich Syndrome Protein Regulates Lipid Raft Dynamics during Immunological Synapse Formation. Immunity 17, 157–166. https://doi.org/10.1016/S1074-7613(02)00360-6

Dustin, M.L., Depoil, D., 2011. New insights into the T cell synapse from single molecule techniques. Nat. Rev. Immunol. 11, 672–684. https://doi.org/10.1038/nri3066

Eddy, R.J., Pierini, L.M., Matsumura, F., Maxfield, F.R., 2000. Ca2+-dependent myosin II activation is required for uropod retraction during neutrophil migration. J. Cell Sci. 113, 1287–1298.

Elks, P.M., Eeden, F.J. van, Dixon, G., Wang, X., Reyes-Aldasoro, C.C., Ingham, P.W., Whyte, M.K.B., Walmsley, S.R., Renshaw, S.A., 2011. Activation of hypoxia-inducible factor-1α (Hif-1α) delays inflammation resolution by reducing neutrophil apoptosis and reverse migration in a zebrafish inflammation model. Blood 118, 712–722. https://doi.org/10.1182/blood-2010-12-324186

Ellett, F., Elks, P.M., Robertson, A.L., Ogryzko, N.V., Renshaw, S.A., 2015. Defining the phenotype of neutrophils following reverse migration in zebrafish. J. Leukoc. Biol. jlb.3MA0315-105R. https://doi.org/10.1189/jlb.3MA0315-105R

Elloumi-Hannachi, I., García, J.R., Shekeran, A., García, A.J., 2015. Contributions of the integrin β1 tail to cell adhesive forces. Exp. Cell Res. 332, 212–222. https://doi.org/10.1016/j.yexcr.2014.11.008

Engelhardt, K.R., McGhee, S., Winkler, S., Sassi, A., Woellner, C., Lopez-Herrera, G., Chen, A., Kim, H.S., Lloret, M.G., Schulze, I., Ehl, S., Thiel, J., Pfeifer, D., Veelken, H., Niehues, T., Siepermann, K., Weinspach, S., Reisli, I., Keles, S., Genel, F., Kutukculer, N., Kutuculer, N., Camcioğlu, Y., Somer, A., Karakoc-Aydiner, E., Barlan, I., Gennery, A., Metin, A., Degerliyurt, A., Pietrogrande, M.C., Yeganeh, M., Baz, Z., Al-Tamemi, S., Klein, C., Puck, J.M., Holland, S.M., McCabe, E.R.B., Grimbacher, B., Chatila, T.A., 2009. Large deletions and point mutations involving the dedicator of cytokinesis 8 (DOCK8) in the autosomal-recessive form of hyper-IgE syndrome. J. Allergy Clin. Immunol. 124, 1289–1302.e4. https://doi.org/10.1016/j.jaci.2009.10.038

Erzurum, S.C., Downey, G.P., Doherty, D.E., Schwab, B., Elson, E.L., Worthen, G.S., 1992. Mechanisms of lipopolysaccharide-induced neutrophil retention. Relative contributions of adhesive and cellular mechanical properties. J. Immunol. 149, 154–162.

Esnault, C., Stewart, A., Gualdrini, F., East, P., Horswell, S., Matthews, N., Treisman, R., 2014. Rho-actin signaling to the MRTF coactivators dominates the immediate transcriptional response to serum in fibroblasts. Genes Dev. https://doi.org/10.1101/gad.239327.114

Fisher, T.C., Drost, E.M., Baerlocher, G.M., Meiselman, H.J., 1995. Regulation of F-actin content to neutrophil deformability. Biorheology 32, 127–128. https://doi.org/10.1016/0006-355X(95)91979-D

Föger, N., Rangell, L., Danilenko, D.M., Chan, A.C., 2006. Requirement for Coronin 1 in T Lymphocyte Trafficking and Cellular Homeostasis. Science 313, 839–842. https://doi.org/10.1126/science.1130563

Fritz-Laylin, L.K., Riel-Mehan, M., Chen, B.-C., Lord, S.J., Goddard, T.D., Ferrin, T.E., Nicholson-Dykstra, S.M., Higgs, H., Johnson, G.T., Betzig, E., 2017. Actin-based protrusions of migrating neutrophils are intrinsically lamellar and facilitate direction changes. eLife 6.

Fujibuchi, T., Abe, Y., Takeuchi, T., Imai, Y., Kamei, Y., Murase, R., Ueda, N., Shigemoto, K., Yamamoto, H., Kito, K., 2005. AIP1/WDR1 supports mitotic cell rounding. Biochem. Biophys. Res. Commun. 327, 268–275. https://doi.org/10.1016/j.bbrc.2004.11.156

Fulkerson, P.C., Zhu, H., Williams, D.A., Zimmermann, N., Rothenberg, M.E., 2005. CXCL9 inhibits eosinophil responses by a CCR3- and Rac2-dependent mechanism. Blood 106, 436–443. https://doi.org/10.1182/blood-2005-02-0489

Furze, R.C., Rankin, S.M., 2008. Neutrophil mobilization and clearance in the bone marrow. Immunology 125, 281–288. https://doi.org/10.1111/j.1365-2567.2008.02950.x

Gakidis, M.A.M., Cullere, X., Olson, T., Wilsbacher, J.L., Zhang, B., Moores, S.L., Ley, K., Swat, W., Mayadas, T., Brugge, J.S., 2004. Vav GEFs are required for β2 integrin-dependent functions of neutrophils. J. Cell Biol. 166, 273–282. https://doi.org/10.1083/jcb.200404166

Gambardella, L., Anderson, K.E., Jakus, Z., Kovács, M., Voigt, S., Hawkins, P.T., Stephens, L., Mócsai, A., Vermeren, S., 2013. Phosphoinositide 3-OH Kinase Regulates Integrin-Dependent Processes in Neutrophils by Signaling through Its Effector ARAP3. J. Immunol. 190, 381–391. https://doi.org/10.4049/jimmunol.1201330

Gambardella, L., Anderson, K.E., Nussbaum, C., Segonds-Pichon, A., Margarido, T., Norton, L., Ludwig, T., Sperandio, M., Hawkins, P.T., Stephens, L., Vermeren, S., 2011. The GTPase-activating protein ARAP3 regulates chemotaxis and adhesion-dependent processes in neutrophils. Blood 118, 1087–1098. https://doi.org/10.1182/blood-2010-10-312959

Gardiner, E.M., Pestonjamasp, K.N., Bohl, B.P., Chamberlain, C., Hahn, K.M., Bokoch, G.M., 2002. Spatial and Temporal Analysis of Rac Activation during Live Neutrophil Chemotaxis. Curr. Biol. 12, 2029–2034. https://doi.org/10.1016/S0960-9822(02)01334-9

Gilles, L., Bluteau, D., Boukour, S., Chang, Y., Zhang, Y., Robert, T., Dessen, P., Debili, N., Bernard, O.A., Vainchenker, W., Raslova, H., 2009. MAL/SRF complex is involved in platelet formation and megakaryocyte migration by regulating MYL9 (MLC2) and MMP9. Blood 114, 4221–4232. https://doi.org/10.1182/blood-2009-03-209932

Glogauer, M., Marchal, C.C., Zhu, F., Worku, A., Clausen, B.E., Foerster, I., Marks, P., Downey, G.P., Dinauer, M., Kwiatkowski, D.J., 2003. Rac1 Deletion in Mouse Neutrophils Has Selective Effects on Neutrophil Functions. J. Immunol. 170, 5652–5657. https://doi.org/10.4049/jimmunol.170.11.5652

Gohla, A., Birkenfeld, J., Bokoch, G.M., 2005. Chronophin, a novel HAD-type serine protein phosphatase, regulates cofilin-dependent actin dynamics. Nat. Cell Biol. 7, 21–29. https://doi.org/10.1038/ncb1201

Gomez, T.S., Billadeau, D.D., 2009. A FAM21-Containing WASH Complex Regulates Retromer-Dependent Sorting. Dev. Cell 17, 699–711. https://doi.org/10.1016/j.devcel.2009.09.009

Gu, Y., Filippi, M.-D., Cancelas, J.A., Siefring, J.E., Williams, E.P., Jasti, A.C., Harris, C.E., Lee, A.W., Prabhakar, R., Atkinson, S.J., Kwiatkowski, D.J., Williams, D.A., 2003. Hematopoietic cell regulation by Rac1 and Rac2 guanosine triphosphatases. Science 302, 445–449. https://doi.org/10.1126/science.1088485

Gu, Y., Jia, B., Yang, F.-C., D'Souza, M., Harris, C.E., Derrow, C.W., Zheng, Y., Williams, D.A., 2001. Biochemical and Biological Characterization of a Human Rac2 GTPase Mutant Associated with Phagocytic Immunodeficiency. J. Biol. Chem. 276, 15929–15938. https://doi.org/10.1074/jbc.M010445200

Guha, M., Zhou, M., Wang, Y., 2005. Cortical Actin Turnover during Cytokinesis Requires Myosin II. Curr. Biol. 15, 732–736. https://doi.org/10.1016/j.cub.2005.03.042

GUTHRIE, 1984. Priming of neutrophils for enhanced release of oxygen metabolites by bacterial lipopolysaccharide. Evidence for increased activity of the superoxide-producing enzyme. J. Exp. Med. 160, 1656–1671.

Haddad, E., Cramer, E., Rivière, C., Rameau, P., Louache, F., Guichard, J., Nelson, D.L., Fischer, A., Vainchenker, W., Debili, N., 1999. The Thrombocytopenia of Wiskott Aldrich Syndrome Is Not Related to a Defect in Proplatelet Formation. Blood 94, 509–518.

Hanneman, S.K., Cox, C.D., Green, K.E., Kang, D.-H., 2011. Estimating Intra- and Inter-Assay Variability in Salivary Cortisol. Biol. Res. Nurs. 13, 243–250. https://doi.org/10.1177/1099800411404061

Hannigan, M., Zhan, L., Li, Z., Ai, Y., Wu, D., Huang, C.-K., 2002. Neutrophils lacking phosphoinositide 3-kinase γ show loss of directionality during N-formyl-Met-Leu-Phe-induced chemotaxis. Proc. Natl. Acad. Sci. 99, 3603–3608. https://doi.org/10.1073/pnas.052010699

Harris, E.S., Rouiller, I., Hanein, D., Higgs, H.N., 2006. Mechanistic Differences in Actin Bundling Activity of Two Mammalian Formins, FRL1 and mDia2. J. Biol. Chem. 281, 14383–14392. https://doi.org/10.1074/jbc.M510923200

Hauert, A.B., Martinelli, S., Marone, C., Niggli, V., 2002. Differentiated HL-60 cells are a valid model system for the analysis of human neutrophil migration and chemotaxis. Int. J. Biochem. Cell Biol. 34, 838–854.

Heit, B., Robbins, S.M., Downey, C.M., Guan, Z., Colarusso, P., Miller, B.J., Jirik, F.R., Kubes, P., 2008. PTEN functions to "prioritize" chemotactic cues and prevent "distraction" in migrating neutrophils. Nat. Immunol. 9, 743–752. https://doi.org/10.1038/ni.1623

Hepper, I., Schymeinsky, J., Weckbach, L.T., Jakob, S.M., Frommhold, D., Sixt, M., Laschinger, M., Sperandio, M., Walzog, B., 2012. The Mammalian Actin-Binding Protein 1 Is Critical for Spreading and Intraluminal Crawling of Neutrophils Under Flow Conditions. J. Immunol. https://doi.org/10.4049/jimmunol.1100878

Hickey, M.J., Forster, M., Mitchell, D., Kaur, J., Caigny, C.D., Kubes, P., 2000. L-Selectin Facilitates Emigration and Extravascular Locomotion of Leukocytes During Acute Inflammatory Responses In Vivo. J. Immunol. 165, 7164–7170. https://doi.org/10.4049/jimmunol.165.12.7164

Higgs, H.N., 2005. Formin proteins: a domain-based approach. Trends Biochem. Sci., SPECIAL ISSUE: CELEBRATING 50 YEARS OF THE IUBMB 30, 342–353. https://doi.org/10.1016/j.tibs.2005.04.014

Higgs, H.N., Blanchoin, L., Pollard, T.D., 1999. Influence of the C Terminus of Wiskott-Aldrich Syndrome Protein (WASp) and the Arp2/3 Complex on Actin Polymerization†. Biochemistry (Mosc.) 38, 15212–15222. https://doi.org/10.1021/bi991843+

Hirayama, A., Adachi, R., Otani, S., Kasahara, T., Suzuki, K., 2007. Cofilin plays a critical role in IL-8-dependent chemotaxis of neutrophilic HL-60 cells through changes in phosphorylation. J. Leukoc. Biol. 81, 720–728. https://doi.org/10.1189/jlb.0506314

Hirsch, E., Katanaev, V.L., Garlanda, C., Azzolino, O., Pirola, L., Silengo, L., Sozzani, S., Mantovani, A., Altruda, F., Wymann, M.P., 2000. Central Role for G Protein-Coupled Phosphoinositide 3-Kinase γ in Inflammation. Science 287, 1049–1053. https://doi.org/10.1126/science.287.5455.1049

Howard, T., Li, Y., Torres, M., Guerrero, A., Coates, T., 1994. The 47-kD protein increased in neutrophil actin dysfunction with 47- and 89-kD protein abnormalities is lymphocyte-specific protein. Blood 83, 231–241.

Huang, D.W., Sherman, B.T., Lempicki, R.A., 2009. Systematic and integrative analysis of large gene lists using DAVID bioinformatics resources. Nat. Protoc. 4, 44–57. https://doi.org/10.1038/nprot.2008.211

Imai, K., Morio, T., Zhu, Y., Jin, Y., Itoh, S., Kajiwara, M., Yata, J.-I., Mizutani, S., Ochs, H.D., Nonoyama, S., 2004. Clinical course of patients with WASP gene mutations. Blood 103, 456–464. https://doi.org/10.1182/blood-2003-05-1480

Innocenti, M., Zucconi, A., Disanza, A., Frittoli, E., Areces, L.B., Steffen, A., Stradal, T.E.B., Fiore, P.P.D., Carlier, M.-F., Scita, G., 2004. Abi1 is essential for the formation and

activation of a WAVE2 signalling complex. Nat. Cell Biol. 6, 319–327. https://doi.org/10.1038/ncb1105

Ishihara, D., Dovas, A., Park, H., Isaac, B.M., Cox, D., 2012. The Chemotactic Defect in Wiskott-Aldrich Syndrome Macrophages Is Due to the Reduced Persistence of Directional Protrusions. PLoS ONE 7, e30033. https://doi.org/10.1371/journal.pone.0030033

Jaeger, B.N., Donadieu, J., Cognet, C., Bernat, C., Ordoñez-Rueda, D., Barlogis, V., Mahlaoui, N., Fenis, A., Narni-Mancinelli, E., Beaupain, B., Bellanné-Chantelot, C., Bajénoff, M., Malissen, B., Malissen, M., Vivier, E., Ugolini, S., 2012. Neutrophil depletion impairs natural killer cell maturation, function, and homeostasis. J. Exp. Med. 209, 565–580. https://doi.org/10.1084/jem.20111908

Jaqaman, K., King, E.M., Amaro, A.C., Winter, J.R., Dorn, J.F., Elliott, H.L., Mchedlishvili, N., McClelland, S.E., Porter, I.M., Posch, M., Toso, A., Danuser, G., McAinsh, A.D., Meraldi, P., Swedlow, J.R., 2010. Kinetochore alignment within the metaphase plate is regulated by centromere stiffness and microtubule depolymerases. J. Cell Biol. 188, 665–679. https://doi.org/10.1083/jcb.200909005

Jin, Y., Mazza, C., Christie, J.R., Giliani, S., Fiorini, M., Mella, P., Gandellini, F., Stewart, D.M., Zhu, Q., Nelson, D.L., Notarangelo, L.D., Ochs, H.D., 2004. Mutations of the Wiskott-Aldrich Syndrome Protein (WASP): Hotspots, Effect on Transcription, and Translation and Phenotype/Genotype Correlation. Blood 104, 4010–4019. https://doi.org/10.1182/blood-2003-05-1592

Jongstra-Bilen, J., Janmey, P.A., Hartwig, J.H., Galea, S., Jongstra, J., 1992. The lymphocyte-specific protein LSP1 binds to F-actin and to the cytoskeleton through its COOH-terminal basic domain. J. Cell Biol. 118, 1443–1453. https://doi.org/10.1083/jcb.118.6.1443

Jongstra-Bilen, J., Misener, V.L., Wang, C., Ginzberg, H., Auerbach, A., Joyner, A.L., Downey, G.P., Jongstra, J., 2000. LSP1 modulates leukocyte populations in resting and inflamed peritoneum. Blood 96, 1827–1835.

Joseph, R., Srivastava, O.P., Pfister, R.R., 2014. Downregulation of ?-actin and its regulatory gene HuR affect cell migration of human corneal fibroblasts. Mol. Vis. 20, 593–605.

Kabbur, M.B., Allen, L.J., Gardner, I.A., Cullor, J.S., 1997. Heterogeneity in phagocytic and oxidative burst activities of neutrophils and neonatal calves. Comp. Haematol. Int. 7, 30–36. https://doi.org/10.1007/BF01320996

Kato, A., Kurita, S., Hayashi, A., Kaji, N., Ohashi, K., Mizuno, K., 2008. Critical roles of actin-interacting protein 1 in cytokinesis and chemotactic migration of mammalian cells. Biochem. J. 414, 261. https://doi.org/10.1042/BJ20071655

Keller, H.U., Wilkinson, P.C., Abercrombie, M., Becker, E.L., Hirsch, J.G., Miller, M.E., Scottramsey, W., Zigmond, S.H., 1977. A proposal for the definition of terms related to locomotion of leucocytes and other cells. Clin. Exp. Immunol. 27, 377–380.

Keszei, M., Westerberg, L.S., 2014. Congenital Defects in Neutrophil Dynamics. J. Immunol. Res. 2014, e303782. https://doi.org/10.1155/2014/303782

Kharazmi, A., Fomsgaard, A., Conrad, R.S., Galanos, C., Høiby, N., 1991. Relationship between chemical composition and biological function of Pseudomonas aeruginosa lipopolysaccharide: effect on human neutrophil chemotaxis and oxidative burst. J. Leukoc. Biol. 49, 15–20.

Kile, B.T., Panopoulos, A.D., Stirzaker, R.A., Hacking, D.F., Tahtamouni, L.H., Willson, T.A., Mielke, L.A., Henley, K.J., Zhang, J.-G., Wicks, I.P., Stevenson, W.S., Nurden, P., Watowich, S.S., Justice, M.J., 2007. Mutations in the cofilin partner Aip1/Wdr1 cause autoinflammatory disease and macrothrombocytopenia. Blood 110, 2371–2380. https://doi.org/10.1182/blood-2006-10-055087

Kitzing, T.M., Sahadevan, A.S., Brandt, D.T., Knieling, H., Hannemann, S., Fackler, O.T., Großhans, J., Grosse, R., 2007. Positive feedback between Dia1, LARG, and RhoA regulates cell morphology and invasion. Genes Dev. 21, 1478–1483. https://doi.org/10.1101/gad.424807

Kolaczkowska, E., Kubes, P., 2013. Neutrophil recruitment and function in health and inflammation. Nat. Rev. Immunol. 13, 159–175. https://doi.org/10.1038/nri3399

Konno, A., Kirby, M., Anderson, S.A., Schwartzberg, P.L., Candotti, F., 2007. The expression of Wiskott–Aldrich syndrome protein (WASP) is dependent on WASP-interacting protein (WIP). Int. Immunol. 19, 185–192. https://doi.org/10.1093/intimm/dxl135

Kovács, M., Tóth, J., Hetényi, C., Málnási-Csizmadia, A., Sellers, J.R., 2004. Mechanism of Blebbistatin Inhibition of Myosin II. J. Biol. Chem. 279, 35557–35563. https://doi.org/10.1074/jbc.M405319200

Krendel, M., Mooseker, M.S., 2005. Myosins: Tails (and Heads) of Functional Diversity. Physiology 20, 239–251. https://doi.org/10.1152/physiol.00014.2005

Kumar, S., Xu, J., Perkins, C., Guo, F., Snapper, S., Finkelman, F.D., Zheng, Y., Filippi, M.-D., 2012. Cdc42 regulates neutrophil migration via crosstalk between WASp, CD11b, and microtubules. Blood 120, 3563–3574. https://doi.org/10.1182/blood-2012-04-426981

Kunisaki, Y., Nishikimi, A., Tanaka, Y., Takii, R., Noda, M., Inayoshi, A., Watanabe, K., Sanematsu, F., Sasazuki, T., Sasaki, T., Fukui, Y., 2006. DOCK2 is a Rac activator that regulates motility and polarity during neutrophil chemotaxis. J. Cell Biol. 174, 647–652. https://doi.org/10.1083/jcb.200602142

Lai, F.P., Szczodrak, M., Block, J., Faix, J., Breitsprecher, D., Mannherz, H.G., Stradal, T.E., Dunn, G.A., Small, J.V., Rottner, K., 2008. Arp2/3 complex interactions and actin network turnover in lamellipodia. EMBO J 27, 982–992. https://doi.org/10.1038/emboj.2008.34

Lämmermann, T., Afonso, P.V., Angermann, B.R., Wang, J.M., Kastenmüller, W., Parent, C.A., Germain, R.N., 2013. Neutrophil swarms require LTB4 and integrins at sites of cell death in vivo. Nature 498, 371–375. https://doi.org/10.1038/nature12175

Lammermann, T., Bader, B.L., Monkley, S.J., Worbs, T., Wedlich-Soldner, R., Hirsch, K., Keller, M., Forster, R., Critchley, D.R., Fassler, R., Sixt, M., 2008. Rapid leukocyte migration by integrin-independent flowing and squeezing. Nature 453, 51–55. https://doi.org/10.1038/nature06887

Lanzi, G., Moratto, D., Vairo, D., Masneri, S., Delmonte, O., Paganini, T., Parolini, S., Tabellini, G., Mazza, C., Savoldi, G., Montin, D., Martino, S., Tovo, P., Pessach, I.M., Massaad, M.J., Ramesh, N., Porta, F., Plebani, A., Notarangelo, L.D., Geha, R.S., Giliani, S., 2012. A novel primary human immunodeficiency due to deficiency in the WASP-interacting protein WIP. J. Exp. Med. 209, 29–34. https://doi.org/10.1084/jem.20110896

Lawson, C.D., Donald, S., Anderson, K.E., Patton, D.T., Welch, H.C.E., 2011. P-Rex1 and Vav1 Cooperate in the Regulation of Formyl-Methionyl-Leucyl-Phenylalanine–Dependent Neutrophil Responses. J. Immunol. 186, 1467–1476. https://doi.org/10.4049/jimmunol.1002738

Le, Y., Murphy, P.M., Wang, J.M., 2002. Formyl-peptide receptors revisited. Trends Immunol. 23, 541–548. https://doi.org/10.1016/S1471-4906(02)02316-5

LeClaire, L.L., Baumgartner, M., Iwasa, J.H., Mullins, R.D., Barber, D.L., 2008. Phosphorylation of the Arp2/3 complex is necessary to nucleate actin filaments. J. Cell Biol. 182, 647–654. https://doi.org/10.1083/jcb.200802145

Leverrier, Y., Lorenzi, R., Blundell, M.P., Brickell, P., Kinnon, C., Ridley, A.J., Thrasher, A.J., 2001. Cutting edge: the Wiskott-Aldrich syndrome protein is required for efficient phagocytosis of apoptotic cells. J. Immunol. Baltim. Md 1950 166, 4831–4834.

Ley, K., Laudanna, C., Cybulsky, M.I., Nourshargh, S., 2007. Getting to the site of inflammation: the leukocyte adhesion cascade updated. Nat. Rev. Immunol. 7, 678–689. https://doi.org/10.1038/nri2156

Li, B., Yu, H., Zheng, W., Voll, R., Na, S., Roberts, A.W., Williams, D.A., Davis, R.J., Ghosh, S., Flavell, R.A., 2000. Role of the guanosine triphosphatase Rac2 in T helper 1 cell differentiation. Science 288, 2219–2222.

Li, F., Higgs, H.N., 2005. Dissecting Requirements for Auto-inhibition of Actin Nucleation by the Formin, mDia1. J. Biol. Chem. 280, 6986–6992. https://doi.org/10.1074/jbc.M411605200

Li, J., Brieher, W.M., Scimone, M.L., Kang, S.J., Zhu, H., Yin, H., von Andrian, U.H., Mitchison, T., Yuan, J., 2007. Caspase-11 regulates cell migration by promoting Aip1–Cofilin-mediated actin depolymerization. Nat. Cell Biol. 9, 276–286. https://doi.org/10.1038/ncb1541

Li, Y., Zhang, Q., Aaron, R., Hilliard, L., Howard, T.H., 2000. LSP1 modulates the locomotion of monocyte-differentiated U937 cells. Blood 96, 1100–1105.

Li, Z., Dong, X., Wang, Z., Liu, W., Deng, N., Ding, Y., Tang, L., Hla, T., Zeng, R., Li, L., Wu, D., 2005. Regulation of PTEN by Rho small GTPases. Nat. Cell Biol. 7, 399–404. https://doi.org/10.1038/ncb1236

Li, Z., Hannigan, M., Mo, Z., Liu, B., Lu, W., Wu, Y., Smrcka, A.V., Wu, G., Li, L., Liu, M., Huang, C.-K., Wu, D., 2003. Directional Sensing Requires Gβγ-Mediated PAK1 and PIXα-Dependent Activation of Cdc42. Cell 114, 215–227. https://doi.org/10.1016/S0092-8674(03)00559-2

Linder, S., Nelson, D., Weiss, M., Aepfelbacher, M., 1999. Wiskott-Aldrich syndrome protein regulates podosomes in primary human macrophages. Proc. Natl. Acad. Sci. U. S. A. 96, 9648–9653.

Looney, M.R., Thornton, E.E., Sen, D., Lamm, W.J., Glenny, R.W., Krummel, M.F., 2011. Stabilized Imaging of Immune Surveillance in the Mouse Lung. Nat. Methods 8, 91–96. https://doi.org/10.1038/nmeth.1543

Lorenzi, R., Brickell, P.M., Katz, D.R., Kinnon, C., Thrasher, A.J., 2000. Wiskott-Aldrich syndrome protein is necessary for efficient IgG-mediated phagocytosis. Blood 95, 2943–2946.

Machesky, L.M., Atkinson, S.J., Ampe, C., Vandekerckhove, J., Pollard, T.D., 1994. Purification of a cortical complex containing two unconventional actins from Acanthamoeba by affinity chromatography on profilin-agarose. J. Cell Biol. 127, 107–115.

Machesky, L.M., Insall, R.H., 1998. Scar1 and the related Wiskott–Aldrich syndrome protein, WASP, regulate the actin cytoskeleton through the Arp2/3 complex. Curr. Biol. 8, 1347–1356. https://doi.org/10.1016/S0960-9822(98)00015-3

Mahlaoui, N., Pellier, I., Mignot, C., Jais, J.-P., Bilhou-Nabéra, C., Moshous, D., Neven, B., Picard, C., Saint-Basile, G. de, Cavazzana-Calvo, M., Blanche, S., Fischer, A., 2013. Characteristics and outcome of early-onset, severe forms of Wiskott-Aldrich syndrome. Blood 121, 1510–1516. https://doi.org/10.1182/blood-2012-08-448118

Majstoravich, S., Zhang, J., Nicholson-Dykstra, S., Linder, S., Friedrich, W., Siminovitch, K.A., Higgs, H.N., 2004. Lymphocyte microvilli are dynamic, actin-dependent structures that do not require Wiskott-Aldrich syndrome protein (WASp) for their morphology. Blood 104, 1396–1403. https://doi.org/10.1182/blood-2004-02-0437

Malek, A.M., Izumo, S., 1996. Mechanism of endothelial cell shape change and cytoskeletal remodeling in response to fluid shear stress. J. Cell Sci. 109, 713–726.

MANNHERZ, H.G., GOODY, R.S., KONRAD, M., NOWAK, E., 1980. The interaction of bovine pancreatic deoxyribonuclease I and skeletal muscle actin. Eur. J. Biochem. 104, 367–379.

Marathe, B.M., Prislovsky, A., Astrakhan, A., Rawlings, D.J., Wan, J.Y., Strom, T.S., 2009. Antiplatelet antibodies in WASP(−) mice correlate with evidence of increased in vivo platelet consumption. Exp. Hematol. 37, 1353–1363. https://doi.org/10.1016/j.exphem.2009.08.007

Massaad, M.J., Ramesh, N., Geha, R.S., 2013. Wiskott-Aldrich syndrome: a comprehensive review. Ann. N. Y. Acad. Sci. 1285, 26–43. https://doi.org/10.1111/nyas.12049

Massena, S., Christoffersson, G., Hjertström, E., Zcharia, E., Vlodavsky, I., Ausmees, N., Rolny, C., Li, J.-P., Phillipson, M., 2010. A chemotactic gradient sequestered on endothelial heparan sulfate induces directional intraluminal crawling of neutrophils. Blood 116, 1924–1931. https://doi.org/10.1182/blood-2010-01-266072

Mathias, J.R., Perrin, B.J., Liu, T.-X., Kanki, J., Look, A.T., Huttenlocher, A., 2006. Resolution of inflammation by retrograde chemotaxis of neutrophils in transgenic zebrafish. J. Leukoc. Biol. 80, 1281–1288. https://doi.org/10.1189/jlb.0506346

McDonald, B., Jenne, C.N., Zhuo, L., Kimata, K., Kubes, P., 2013. Kupffer cells and activation of endothelial TLR4 coordinate neutrophil adhesion within liver sinusoids during endotoxemia. Am. J. Physiol. - Gastrointest. Liver Physiol. 305, G797–G806. https://doi.org/10.1152/ajpgi.00058.2013

McDonald, B., Pittman, K., Menezes, G.B., Hirota, S.A., Slaba, I., Waterhouse, C.C.M., Beck, P.L., Muruve, D.A., Kubes, P., 2010. Intravascular Danger Signals Guide Neutrophils

to Sites of Sterile Inflammation. Science 330, 362–366. https://doi.org/10.1126/science.1195491
Medjkane, S., Perez-Sanchez, C., Gaggioli, C., Sahai, E., Treisman, R., 2009. Myocardin-related transcription factors and SRF are required for cytoskeletal dynamics and experimental metastasis. Nat. Cell Biol. 11, 257–268. https://doi.org/10.1038/ncb1833
Meyer-Bahlburg, A., Becker-Herman, S., Humblet-Baron, S., Khim, S., Weber, M., Bouma, G., Thrasher, A.J., Batista, F.D., Rawlings, D.J., 2008. Wiskott-Aldrich syndrome protein deficiency in B cells results in impaired peripheral homeostasis. Blood 112, 4158–4169. https://doi.org/10.1182/blood-2008-02-140814
Miano, J.M., Long, X., Fujiwara, K., 2007. Serum response factor: master regulator of the actin cytoskeleton and contractile apparatus. Am. J. Physiol. - Cell Physiol. 292, C70–C81. https://doi.org/10.1152/ajpcell.00386.2006
Millius, A., Weiner, O.D., 2010. Manipulation of neutrophil-like HL-60 cells for the study of directed cell migration. Methods Mol. Biol. Clifton NJ 591, 147.
Millius, A., Weiner, O.D., 2009. Chemotaxis in Neutrophil-Like HL-60 Cells. Methods Mol. Biol. Clifton NJ 571, 167–177. https://doi.org/10.1007/978-1-60761-198-1_11
Miralles, F., Posern, G., Zaromytidou, A.-I., Treisman, R., 2003. Actin Dynamics Control SRF Activity by Regulation of Its Coactivator MAL. Cell 113, 329–342. https://doi.org/10.1016/S0092-8674(03)00278-2
Miyamoto, Y., Yamauchi, J., 2010. Cellular signaling of Dock family proteins in neural function. Cell. Signal. 22, 175–182. https://doi.org/10.1016/j.cellsig.2009.09.036
Mokalled, M.H., Johnson, A., Kim, Y., Oh, J., Olson, E.N., 2010a. Myocardin-related transcription factors regulate the Cdk5/Pctaire1 kinase cascade to control neurite outgrowth, neuronal migration and brain. Development 137, 2365–2374. https://doi.org/10.1242/dev.047605
Mokalled, M.H., Johnson, A., Kim, Y., Oh, J., Olson, E.N., 2010b. Myocardin-related transcription factors regulate the Cdk5/Pctaire1 kinase cascade to control neurite outgrowth, neuronal migration and brain development. Dev. Camb. Engl. 137, 2365–2374. https://doi.org/10.1242/dev.047605
Mondal, S., Subramanian, K.K., Sakai, J., Bajrami, B., Luo, H.R., 2012. Phosphoinositide lipid phosphatase SHIP1 and PTEN coordinate to regulate cell migration and adhesion. Mol. Biol. Cell 23, 1219–1230. https://doi.org/10.1091/mbc.E11-10-0889
Morley, S.C., 2012. The Actin-Bundling Protein L-Plastin: A Critical Regulator of Immune Cell Function. Int. J. Cell Biol. 2012. https://doi.org/10.1155/2012/935173
Moseley, J.B., Sagot, I., Manning, A.L., Xu, Y., Eck, M.J., Pellman, D., Goode, B.L., 2004. A Conserved Mechanism for Bni1- and mDia1-induced Actin Assembly and Dual Regulation of Bni1 by Bud6 and Profilin. Mol. Biol. Cell 15, 896–907. https://doi.org/10.1091/mbc.E03-08-0621
Moshous, D., Martin, E., Carpentier, W., Lim, A., Callebaut, I., Canioni, D., Hauck, F., Majewski, J., Schwartzentruber, J., Nitschke, P., Sirvent, N., Frange, P., Picard, C., Blanche, S., Revy, P., Fischer, A., Latour, S., Jabado, N., de Villartay, J.-P., n.d. Whole-exome sequencing identifies Coronin-1A deficiency in 3 siblings with immunodeficiency and EBV-associated B-cell lymphoproliferation. J. Allergy Clin. Immunol. https://doi.org/10.1016/j.jaci.2013.01.042
Moulding, D.A., Blundell, M.P., Spiller, D.G., White, M.R.H., Cory, G.O., Calle, Y., Kempski, H., Sinclair, J., Ancliff, P.J., Kinnon, C., Jones, G.E., Thrasher, A.J., 2007. Unregulated actin polymerization by WASp causes defects of mitosis and cytokinesis in X-linked neutropenia. J. Exp. Med. 204, 2213–2224. https://doi.org/10.1084/jem.20062324
Moulding, D.A., Moeendarbary, E., Valon, L., Record, J., Charras, G.T., Thrasher, A.J., 2012. Excess F-actin mechanically impedes mitosis leading to cytokinesis failure in X-linked neutropenia by exceeding Aurora B kinase error correction capacity. Blood 120, 3803–3811. https://doi.org/10.1182/blood-2012-03-419663
Mueller, P., Massner, J., Jayachandran, R., Combaluzier, B., Albrecht, I., Gatfield, J., Blum, C., Ceredig, R., Rodewald, H.-R., Rolink, A.G., Pieters, J., 2008. Regulation of T cell survival through coronin-1-mediated generation of inositol-1,4,5-trisphosphate and calcium mobilization after T cell receptor triggering. Nat. Immunol. 9, 424–431. https://doi.org/10.1038/ni1570

Muinonen-Martin, A.J., Veltman, D.M., Kalna, G., Insall, R.H., 2010. An Improved Chamber for Direct Visualisation of Chemotaxis. PLoS ONE 5, e15309. https://doi.org/10.1371/journal.pone.0015309

Mullins, R.D., Heuser, J.A., Pollard, T.D., 1998. The interaction of Arp2/3 complex with actin: Nucleation, high affinity pointed end capping, and formation of branching networks of filaments. Proc. Natl. Acad. Sci. 95, 6181–6186.

Mulloy, J.C., Cancelas, J.A., Filippi, M.-D., Kalfa, T.A., Guo, F., Zheng, Y., 2010. Rho GTPases in hematopoiesis and hemopathies. Blood 115, 936–947. https://doi.org/10.1182/blood-2009-09-198127

Murthy, K., Wadsworth, P., 2005. Myosin-II-dependent localization and dynamics of F-actin during cytokinesis. Curr. Biol. CB 15, 724–731. https://doi.org/10.1016/j.cub.2005.02.055

Németh, T., Futosi, K., Hably, C., Brouns, M.R., Jakob, S.M., Kovács, M., Kertész, Z., Walzog, B., Settleman, J., Mócsai, A., 2010. Neutrophil Functions and Autoimmune Arthritis in the Absence of p190RhoGAP: Generation and Analysis of a Novel Null Mutation in Mice. J. Immunol. 185, 3064–3075. https://doi.org/10.4049/jimmunol.0904163

Nishio, M., Watanabe, K., Sasaki, J., Taya, C., Takasuga, S., Iizuka, R., Balla, T., Yamazaki, M., Watanabe, H., Itoh, R., Kuroda, S., Horie, Y., Förster, I., Mak, T.W., Yonekawa, H., Penninger, J.M., Kanaho, Y., Suzuki, A., Sasaki, T., 2007. Control of cell polarity and motility by the PtdIns(3,4,5)P3 phosphatase SHIP1. Nat. Cell Biol. 9, 36–44. https://doi.org/10.1038/ncb1515

Nobusue, H., Onishi, N., Shimizu, T., Sugihara, E., Oki, Y., Sumikawa, Y., Chiyoda, T., Akashi, K., Saya, H., Kano, K., 2014. Regulation of MKL1 via actin cytoskeleton dynamics drives adipocyte differentiation. Nat. Commun. 5, 3368. https://doi.org/10.1038/ncomms4368

Notarangelo, L.D., 2010. Primary immunodeficiencies. J. Allergy Clin. Immunol., 2010 Primer on Allergic and Immunologic Diseases 125, S182–S194. https://doi.org/10.1016/j.jaci.2009.07.053

Nunoi, H., Yamazaki, T., Tsuchiya, H., Kato, S., Malech, H.L., Matsuda, I., Kanegasaki, S., 1999. A heterozygous mutation of β-actin associated with neutrophil dysfunction and recurrent infection. Proc. Natl. Acad. Sci. 96, 8693–8698. https://doi.org/10.1073/pnas.96.15.8693

Ochs, Slichter, 1980. The Wiskott-Aldrich syndrome: studies of lymphocytes, granulocytes, and platelets. Blood.

Okreglak, V., Drubin, D.G., 2007. Cofilin recruitment and function during actin-mediated endocytosis dictated by actin nucleotide state. J. Cell Biol. 178, 1251–1264. https://doi.org/10.1083/jcb.200703092

Olazabal, I.M., Caron, E., May, R.C., Schilling, K., Knecht, D.A., Machesky, L.M., 2002. Rho-kinase and myosin-II control phagocytic cup formation during CR, but not FcgammaR, phagocytosis. Curr. Biol. CB 12, 1413–1418.

Olson, E.N., Nordheim, A., 2010. Linking actin dynamics and gene transcription to drive cellular motile functions. Nat. Rev. Mol. Cell Biol. 11, 353–365. https://doi.org/10.1038/nrm2890

Ono, S., Minami, N., Abe, H., Obinata, T., 1994. Characterization of a novel cofilin isoform that is predominantly expressed in mammalian skeletal muscle. J. Biol. Chem. 269, 15280–15286.

Orange, J.S., Ramesh, N., Remold-O'Donnell, E., Sasahara, Y., Koopman, L., Byrne, M., Bonilla, F.A., Rosen, F.S., Geha, R.S., Strominger, J.L., 2002. Wiskott–Aldrich syndrome protein is required for NK cell cytotoxicity and colocalizes with actin to NK cell-activating immunologic synapses. Proc. Natl. Acad. Sci. 99, 11351–11356. https://doi.org/10.1073/pnas.162376099

Otomo, T., Tomchick, D.R., Otomo, C., Panchal, S.C., Machius, M., Rosen, M.K., 2005. Structural basis of actin filament nucleation and processive capping by a formin homology 2 domain. Nature 433, 488–494. https://doi.org/10.1038/nature03251

Papayannopoulos, V., Zychlinsky, A., 2009. NETs: a new strategy for using old weapons. Trends Immunol. 30, 513–521. https://doi.org/10.1016/j.it.2009.07.011

Paul, A., Pollard, T., 2008. The Role of the FH1 Domain and Profilin in Formin-Mediated Actin-Filament Elongation and Nucleation. Curr. Biol. 18, 9–19. https://doi.org/10.1016/j.cub.2007.11.062

Pestonjamasp, K.N., Forster, C., Sun, C., Gardiner, E.M., Bohl, B., Weiner, O., Bokoch, G.M., Glogauer, M., 2006. Rac1 links leading edge and uropod events through Rho and myosin activation during chemotaxis. Blood 108, 2814–2820. https://doi.org/10.1182/blood-2006-01-010363

Petri, B., Kaur, J., Long, E.M., Li, H., Parsons, S.A., Butz, S., Phillipson, M., Vestweber, D., Patel, K.D., Robbins, S.M., Kubes, P., 2011. Endothelial LSP1 is involved in endothelial dome formation, minimizing vascular permeability changes during neutrophil transmigration in vivo. Blood 117, 942–952. https://doi.org/10.1182/blood-2010-02-270561

Petri, B., Phillipson, M., Kubes, P., 2008. The Physiology of Leukocyte Recruitment: An In Vivo Perspective. J. Immunol. 180, 6439–6446.

Phillips, J.E., Gomer, R.H., 2012. A secreted protein is an endogenous chemorepellant in Dictyostelium discoideum. Proc. Natl. Acad. Sci. 109, 10990–10995. https://doi.org/10.1073/pnas.1206350109

Phillipson, M., Heit, B., Colarusso, P., Liu, L., Ballantyne, C.M., Kubes, P., 2006. Intraluminal crawling of neutrophils to emigration sites: a molecularly distinct process from adhesion in the recruitment cascade. J. Exp. Med. 203, 2569–2575. https://doi.org/10.1084/jem.20060925

Phillipson, M., Heit, B., Parsons, S.A., Petri, B., Mullaly, S.C., Colarusso, P., Gower, R.M., Neely, G., Simon, S.I., Kubes, P., 2009. Vav1 Is Essential for Mechanotactic Crawling and Migration of Neutrophils out of the Inflamed Microvasculature. J. Immunol. 182, 6870–6878. https://doi.org/10.4049/jimmunol.0803414

Phillipson, M., Kaur, J., Colarusso, P., Ballantyne, C.M., Kubes, P., 2008. Endothelial Domes Encapsulate Adherent Neutrophils and Minimize Increases in Vascular Permeability in Paracellular and Transcellular Emigration. PLoS ONE 3. https://doi.org/10.1371/journal.pone.0001649

Phillipson, M., Kubes, P., 2011. The neutrophil in vascular inflammation. Nat. Med. 17, 1381–1390. https://doi.org/10.1038/nm.2514

Pollard, T.D., Borisy, G.G., 2003. Cellular Motility Driven by Assembly and Disassembly of Actin Filaments. Cell 112, 453–465. https://doi.org/10.1016/S0092-8674(03)00120-X

Ponti, A., Machacek, M., Gupton, S.L., Waterman-Storer, C.M., Danuser, G., 2004. Two Distinct Actin Networks Drive the Protrusion of Migrating Cells. Science 305, 1782–1786. https://doi.org/10.1126/science.1100533

Prislovsky, A., Marathe, B., Hosni, A., Bolen, A.L., Nimmerjahn, F., Jackson, C.W., Weiman, D., Strom, T.S., 2008. Rapid platelet turnover in WASP(−) mice correlates with increased ex vivo phagocytosis of opsonized WASP(−) platelets. Exp. Hematol. 36, 609–623. https://doi.org/10.1016/j.exphem.2007.12.019

Prislovsky, A., Zeng, X., Sokolic, R.A., Garabedian, E.N., Anur, P., Candotti, F., Strom, T.S., 2013. Platelets from WAS patients show an increased susceptibility to ex vivo phagocytosis. Platelets 24, 288–296. https://doi.org/10.3109/09537104.2012.693991

Proebstl, D., Voisin, M.-B., Woodfin, A., Whiteford, J., D'Acquisto, F., Jones, G.E., Rowe, D., Nourshargh, S., 2012. Pericytes support neutrophil subendothelial cell crawling and breaching of venular walls in vivo. J. Exp. Med. 209, 1219–1234. https://doi.org/10.1084/jem.20111622

Puri, K.D., Doggett, T.A., Douangpanya, J., Hou, Y., Tino, W.T., Wilson, T., Graf, T., Clayton, E., Turner, M., Hayflick, J.S., Diacovo, T.G., 2004. Mechanisms and implications of phosphoinositide 3-kinase δ in promoting neutrophil trafficking into inflamed tissue. Blood 103, 3448–3456. https://doi.org/10.1182/blood-2003-05-1667

Ramachandran, V., Williams, M., Yago, T., Schmidtke, D.W., McEver, R.P., 2004. Dynamic alterations of membrane tethers stabilize leukocyte rolling on P-selectin. Proc. Natl. Acad. Sci. U. S. A. 101, 13519–13524. https://doi.org/10.1073/pnas.0403608101

Ramesh, N., Antón, I.M., Hartwig, J.H., Geha, R.S., 1997. WIP, a protein associated with wiskott-aldrich syndrome protein, induces actin polymerization and redistribution in lymphoid cells. Proc. Natl. Acad. Sci. U. S. A. 94, 14671–14676.

Randall, K.L., Lambe, T., Johnson, A.L., Johnson, A., Treanor, B., Kucharska, E., Domaschenz, H., Whittle, B., Tze, L.E., Enders, A., Crockford, T.L., Bouriez-Jones, T., Alston, D., Cyster, J.G., Lenardo, M.J., Mackay, F., Deenick, E.K., Tangye, S.G., Chan, T.D., Camidge, T., Brink, R., Vinuesa, C.G., Batista, F.D., Cornall, R.J., Goodnow, C.C., 2009. Dock8 mutations cripple B cell immunological synapses, germinal centers and long-lived antibody production. Nat. Immunol. 10, 1283–1291. https://doi.org/10.1038/ni.1820

Reicher, B., Joseph, N., David, A., Pauker, M.H., Perl, O., Barda-Saad, M., 2012. Ubiquitylation-dependent negative regulation of WASp is essential for actin-cytoskeleton dynamics. Mol. Cell. Biol. https://doi.org/10.1128/MCB.00161-12

Reinhard, M., Zumbrunn, J., Jaquemar, D., Kuhn, M., Walter, U., Trueb, B., 1999. An α-Actinin Binding Site of Zyxin Is Essential for Subcellular Zyxin Localization and α-Actinin Recruitment. J. Biol. Chem. 274, 13410–13418. https://doi.org/10.1074/jbc.274.19.13410

Roberts, A.W., Kim, C., Zhen, L., Lowe, J.B., Kapur, R., Petryniak, B., Spaetti, A., Pollock, J.D., Borneo, J.B., Bradford, G.B., Atkinson, S.J., Dinauer, M.C., Williams, D.A., 1999. Deficiency of the Hematopoietic Cell-Specific Rho Family GTPase Rac2 Is Characterized by Abnormalities in Neutrophil Function and Host Defense. Immunity 10, 183–196. https://doi.org/10.1016/S1074-7613(00)80019-9

Roberts, H.M., Ling, M.R., Insall, R., Kalna, G., Spengler, J., Grant, M.M., Chapple, I.L., 2015. Impaired neutrophil directional chemotactic accuracy in chronic periodontitis patients. J. Clin. Periodontol. 42, 1–11. https://doi.org/10.1111/jcpe.12326

Rogers, S.L., Wiedemann, U., Stuurman, N., Vale, R.D., 2003. Molecular requirements for actin-based lamella formation in Drosophila S2 cells. J. Cell Biol. 162, 1079–1088. https://doi.org/10.1083/jcb.200303023

Rougerie, P., Miskolci, V., Cox, D., 2013. Generation of membrane structures during phagocytosis and chemotaxis of macrophages: role and regulation of the actin cytoskeleton. Immunol. Rev. 256, 222–239. https://doi.org/10.1111/imr.12118

Rouiller, I., Xu, X.-P., Amann, K.J., Egile, C., Nickell, S., Nicastro, D., Li, R., Pollard, T.D., Volkmann, N., Hanein, D., 2008. The structural basis of actin filament branching by the Arp2/3 complex. J. Cell Biol. 180, 887–895. https://doi.org/10.1083/jcb.200709092

Ruusala, A., Aspenström, P., 2004. Isolation and characterisation of DOCK8, a member of the DOCK180-related regulators of cell morphology. FEBS Lett. 572, 159–166. https://doi.org/10.1016/j.febslet.2004.06.095

Rzeniewicz, K., Newe, A., Gallardo, A.R., Davies, J., Holt, M.R., Patel, A., Charras, G.T., Stramer, B., Molenaar, C., Tedder, T.F., Parsons, M., Ivetic, A., 2015. L-selectin shedding is activated specifically within transmigrating pseudopods of monocytes to regulate cell polarity in vitro. Proc. Natl. Acad. Sci. 112, E1461–E1470. https://doi.org/10.1073/pnas.1417100112

Sabri, S., Foudi, A., Boukour, S., Franc, B., Charrier, S., Jandrot-Perrus, M., Farndale, R.W., Jalil, A., Blundell, M.P., Cramer, E.M., Louache, F., Debili, N., Thrasher, A.J., Vainchenker, W., 2006. Deficiency in the Wiskott-Aldrich protein induces premature proplatelet formation and platelet production in the bone marrow compartment. Blood 108, 134–140. https://doi.org/10.1182/blood-2005-03-1219

Sadhu, C., Masinovsky, B., Dick, K., Sowell, C.G., Staunton, D.E., 2003. Essential Role of Phosphoinositide 3-Kinase δ in Neutrophil Directional Movement. J. Immunol. 170, 2647–2654. https://doi.org/10.4049/jimmunol.170.5.2647

Sadik, C.D., Kim, N.D., Luster, A.D., 2011. Neutrophils cascading their way to inflammation. Trends Immunol. 32, 452–460. https://doi.org/10.1016/j.it.2011.06.008

Safaei, S., Fazlollahi, M.R., Houshmand, M., Hamidieh, A.A., Bemanian, M.H., Alavi, S., Mousavi, F., Pourpak, Z., Moin, M., 2012. Detection of six novel mutations in WASP gene in fifteen Iranian Wiskott-Aldrich patients. Iran. J. Allergy Asthma Immunol. 11, 345–348. https://doi.org/011.04/ijaai.345348

Salvany, L., Muller, J., Guccione, E., Rørth, P., 2014. The core and conserved role of MAL is homeostatic regulation of actin levels. Genes Dev. 28, 1048–1053. https://doi.org/10.1101/gad.237743.114

Sánchez-Madrid, F., Serrador, J.M., 2009. Bringing up the rear: defining the roles of the uropod. Nat. Rev. Mol. Cell Biol. 10, 353–359.

Sapey, E., Greenwood, H., Walton, G., Mann, E., Love, A., Aaronson, N., Insall, R.H., Stockley, R.A., Lord, J.M., 2014. Phosphoinositide 3-kinase inhibition restores neutrophil accuracy in the elderly: toward targeted treatments for immunosenescence. Blood 123, 239–248. https://doi.org/10.1182/blood-2013-08-519520

Sapey, E., Stockley, J.A., Greenwood, H., Ahmad, A., Bayley, D., Lord, J.M., Insall, R.H., Stockley, R.A., 2011. Behavioral and Structural Differences in Migrating Peripheral Neutrophils from Patients with Chronic Obstructive Pulmonary Disease. Am. J. Respir. Crit. Care Med. 183, 1176–1186. https://doi.org/10.1164/rccm.201008-1285OC

Sarraj, B., Massberg, S., Li, Y., Kasorn, A., Subramanian, K., Loison, F., Silberstein, L.E., Andrian, U. von, Luo, H.R., 2009. Myeloid-Specific Deletion of Tumor Suppressor PTEN Augments Neutrophil Transendothelial Migration during Inflammation. J. Immunol. 182, 7190–7200. https://doi.org/10.4049/jimmunol.0802562

Sasaki, T., Irie-Sasaki, J., Jones, R.G., Oliveira-dos-Santos, A.J., Stanford, W.L., Bolon, B., Wakeham, A., Itie, A., Bouchard, D., Kozieradzki, I., Joza, N., Mak, T.W., Ohashi, P.S., Suzuki, A., Penninger, J.M., 2000. Function of PI3Kγ in Thymocyte Development, T Cell Activation, and Neutrophil Migration. Science 287, 1040–1046. https://doi.org/10.1126/science.287.5455.1040

Sato, R., Iiizumi, S., Kim, E.-S., Honda, F., Lee, S.-K., Adachi, N., Koyama, H., Mizutani, S., Morio, T., 2012. Impaired cell adhesion, apoptosis, and signaling in WASP gene-disrupted Nalm-6 pre-B cells and recovery of cell adhesion using a transducible form of WASp. Int. J. Hematol. 95, 299–310. https://doi.org/10.1007/s12185-012-1013-1

Savina, A., Peres, A., Cebrian, I., Carmo, N., Moita, C., Hacohen, N., Moita, L.F., Amigorena, S., 2009. The small GTPase Rac2 controls phagosomal alkalinization and antigen crosspresentation selectively in CD8(+) dendritic cells. Immunity 30, 544–555. https://doi.org/10.1016/j.immuni.2009.01.013

Schwarz, K., Nonoyama, S., Peitsch, M.C., de Saint Basile, G., Espanol, T., Fasth, A., Fischer, A., Freitag, K., Friedrich, W., Fugmann, S., Hossle, H.-P., Jones, A., Kinnon, C., Meindl, A., Notarangelo, L.D., Wechsler, A., Weiss, M., Ochs, H.D., 1996. WASPbase: a database of WAS- and XLT-causing mutations. Immunol. Today 17, 496–502. https://doi.org/10.1016/S0167-5699(96)80901-7

Sedzinski, J., Biro, M., Oswald, A., Tinevez, J.-Y., Salbreux, G., Paluch, E., 2011. Polar actomyosin contractility destabilizes the position of the cytokinetic furrow. Nature 476, 462–466. https://doi.org/10.1038/nature10286

Shcherbina, Rosen, Remold-O'Donnell, 1999. WASP Levels in Platelets and Lymphocytes of Wiskott-Aldrich Syndrome Patients Correlate with Cell Dysfunction. J. Immunol.

Shi, C., Pamer, E.G., 2011. Monocyte recruitment during infection and inflammation. Nat. Rev. Immunol. 11, 762–774. https://doi.org/10.1038/nri3070

Shi, Y., Dong, B., Miliotis, H., Liu, J., Alberts, A.S., Zhang, J., Siminovitch, K.A., 2009a. Src kinase Hck association with the WASp and mDia1 cytoskeletal regulators promotes chemoattractant-induced Hck membrane targeting and activation in neutrophils. Biochem. Cell Biol. 87, 207–216.

Shi, Y., Zhang, J., Mullin, M., Dong, B., Alberts, A.S., Siminovitch, K.A., 2009b. The mDial Formin Is Required for Neutrophil Polarization, Migration, and Activation of the LARG/RhoA/ROCK Signaling Axis during Chemotaxis. J. Immunol. 182, 3837–3845. https://doi.org/10.4049/jimmunol.0803838

Shiow, L.R., Paris, K., Akana, M.C., Cyster, J.G., Sorensen, R.U., Puck, J.M., 2009. Severe combined immunodeficiency (SCID) and attention deficit hyperactivity disorder (ADHD) associated with a coronin-1A mutation and a chromosome 16p11.2 deletion. Clin. Immunol. 131, 24–30. https://doi.org/10.1016/j.clim.2008.11.002

Shiow, L.R., Roadcap, D.W., Paris, K., Watson, S.R., Grigorova, I.L., Lebet, T., An, J., Xu, Y., Jenne, C.N., Föger, N., Sorensen, R.U., Goodnow, C.C., Bear, J.E., Puck, J.M., Cyster, J.G., 2008. The actin regulator coronin 1A is mutant in a thymic egress–deficient mouse strain and in a patient with severe combined immunodeficiency. Nat. Immunol. 9, 1307–1315. https://doi.org/10.1038/ni.1662

Sims, T.N., Soos, T.J., Xenias, H.S., Dubin-Thaler, B., Hofman, J.M., Waite, J.C., Cameron, T.O., Thomas, V.K., Varma, R., Wiggins, C.H., Sheetz, M.P., Littman, D.R., Dustin, M.L., 2007. Opposing Effects of PKCθ and WASp on Symmetry Breaking and Relocation of the Immunological Synapse. Cell 129, 773–785. https://doi.org/10.1016/j.cell.2007.03.037

Smith, E.C., Teixeira, A.M., Chen, R.C., Wang, L., Gao, Y., Hahn, K.L., Krause, D.S., 2013. Induction of megakaryocyte differentiation drives nuclear accumulation and transcriptional function of MKL1 via actin polymerization and RhoA activation. Blood 121, 1094–1101. https://doi.org/10.1182/blood-2012-05-429993

Smith, E.C., Thon, J.N., Devine, M.T., Lin, S., Schulz, V.P., Guo, Y., Massaro, S.A., Halene, S., Gallagher, P., Italiano, J.E., Krause, D.S., 2012. MKL1 and MKL2 play redundant and crucial roles in megakaryocyte maturation and platelet formation. Blood 120, 2317–2329. https://doi.org/10.1182/blood-2012-04-420828

Smith, L.A., Aranda-Espinoza, H., Haun, J.B., Dembo, M., Hammer, D.A., 2007. Neutrophil Traction Stresses are Concentrated in the Uropod during Migration. Biophys. J. 92, L58–L60. https://doi.org/10.1529/biophysj.106.102822

Snapper, S.B., Meelu, P., Nguyen, D., Stockton, B.M., Bozza, P., Alt, F.W., Rosen, F.S., von Andrian, U.H., Klein, C., 2005. WASP deficiency leads to global defects of directed leukocyte migration in vitro and in vivo. J. Leukoc. Biol. 77, 993–998. https://doi.org/10.1189/jlb.0804444

Srinivasan, S., Wang, F., Glavas, S., Ott, A., Hofmann, F., Aktories, K., Kalman, D., Bourne, H.R., 2003. Rac and Cdc42 play distinct roles in regulating PI(3,4,5)P3 and polarity during neutrophil chemotaxis. J. Cell Biol. 160, 375–385. https://doi.org/10.1083/jcb.200208179

Steffen, A., Faix, J., Resch, G.P., Linkner, J., Wehland, J., Small, J.V., Rottner, K., Stradal, T.E.B., 2006. Filopodia Formation in the Absence of Functional WAVE- and Arp2/3-Complexes. Mol. Biol. Cell 17, 2581–2591. https://doi.org/10.1091/mbc.E05-11-1088

Stewart, D.M., Tian, L., Nelson, D.L., 1999. Mutations That Cause the Wiskott-Aldrich Syndrome Impair the Interaction of Wiskott-Aldrich Syndrome Protein (WASP) with WASP Interacting Protein. J. Immunol. 162, 5019–5024.

Strassheim, D., Kim, J.-Y., Park, J.-S., Mitra, S., Abraham, E., 2005. Involvement of SHIP in TLR2-Induced Neutrophil Activation and Acute Lung Injury. J. Immunol. 174, 8064–8071. https://doi.org/10.4049/jimmunol.174.12.8064

Subramanian, K.K., Jia, Y., Zhu, D., Simms, B.T., Jo, H., Hattori, H., You, J., Mizgerd, J.P., Luo, H.R., 2007. Tumor suppressor PTEN is a physiologic suppressor of chemoattractant-mediated neutrophil functions. Blood 109, 4028–4037. https://doi.org/10.1182/blood-2006-10-055319

Sullivan, K.E., Mullen, C.A., Blaese, R.M., Winkelstein, J.A., 1994. A multiinstitutional survey of the Wiskott-Aldrich syndrome. J. Pediatr. 125, 876–885.

Sun, C.X., Downey, G.P., Zhu, F., Koh, A.L.Y., Thang, H., Glogauer, M., 2004. Rac1 is the small GTPase responsible for regulating the neutrophil chemotaxis compass. Blood 104, 3758–3765. https://doi.org/10.1182/blood-2004-03-0781

Sun, C.X., Magalhães, M.A.O., Glogauer, M., 2007. Rac1 and Rac2 differentially regulate actin free barbed end formation downstream of the fMLP receptor. J. Cell Biol. 179, 239–245. https://doi.org/10.1083/jcb.200705122

Sun, H., Wang, Y., 1995. Apoptosis of human leukemic HL-60 cells induced to differentiate by treatment with RA or DMSO*. Cell Res. 5, 181–186. https://doi.org/10.1038/cr.1995.17

Sundd, P., Gutierrez, E., Koltsova, E.K., Kuwano, Y., Fukuda, S., Pospieszalska, M.K., Groisman, A., Ley, K., 2012. `Slings' enable neutrophil rolling at high shear. Nature 488, 399–403. https://doi.org/10.1038/nature11248

Sundd, P., Pospieszalska, M.K., Cheung, L.S.-L., Konstantopoulos, K., Ley, K., 2011. Biomechanics of leukocyte rolling. Biorheology 48, 1–35. https://doi.org/10.3233/BIR-2011-0579

Suraneni, P., Rubinstein, B., Unruh, J.R., Durnin, M., Hanein, D., Li, R., 2012. The Arp2/3 Complex Is Required for Lamellipodia Extension and Directional Fibroblast Cell Migration. J. Cell Biol. 197, 239–251. https://doi.org/10.1083/jcb.201112113

Szczur, K., Zheng, Y., Filippi, M.-D., 2009. The small Rho GTPase Cdc42 regulates neutrophil polarity via CD11b integrin signaling. Blood 114, 4527–4537. https://doi.org/10.1182/blood-2008-12-195164

Taylor, A., Tang, W., Bruscia, E.M., Zhang, P.-X., Lin, A., Gaines, P., Wu, D., Halene, S., 2014. SRF is required for neutrophil migration in response to inflammation. Blood 123, 3027–3036. https://doi.org/10.1182/blood-2013-06-507582

Thrasher, A.J., Burns, S.O., 2010. WASP: a key immunological multitasker. Nat. Rev. Immunol. 10, 182–192. https://doi.org/10.1038/nri2724

Trifari, S., Sitia, G., Aiuti, A., Scaramuzza, S., Marangoni, F., Guidotti, L.G., Martino, S., Saracco, P., Notarangelo, L.D., Roncarolo, M.-G., Dupré, L., 2006. Defective Th1 Cytokine Gene Transcription in CD4+ and CD8+ T Cells from Wiskott-Aldrich Syndrome Patients. J. Immunol. 177, 7451–7461. https://doi.org/10.4049/jimmunol.177.10.7451

Tsuboi, S., 2007. Requirement for a Complex of Wiskott-Aldrich Syndrome Protein (WASP) with WASP Interacting Protein in Podosome Formation in Macrophages. J. Immunol. 178, 2987–2995.

Tsuboi, S., Meerloo, J., 2007. Wiskott-Aldrich syndrome protein is a key regulator of the phagocytic cup formation in macrophages. J. Biol. Chem. 282, 34194–34203. https://doi.org/10.1074/jbc.M705999200

Tsuji, T., Miyoshi, T., Higashida, C., Narumiya, S., Watanabe, N., 2009. An Order of Magnitude Faster AIP1-Associated Actin Disruption than Nucleation by the Arp2/3 Complex in Lamellipodia. PLoS ONE 4, e4921. https://doi.org/10.1371/journal.pone.0004921

van Til, N.P., Wagemaker, G., 2014. Lentiviral gene transduction of mouse and human hematopoietic stem cells. Methods Mol. Biol. Clifton NJ 1185, 311–319. https://doi.org/10.1007/978-1-4939-1133-2_21

Van Troys, M., Huyck, L., Leyman, S., Dhaese, S., Vandekerkhove, J., Ampe, C., 2008. Ins and outs of ADF/cofilin activity and regulation. Eur. J. Cell Biol. 87, 649–667. https://doi.org/10.1016/j.ejcb.2008.04.001

Vartiainen, M.K., Guettler, S., Larijani, B., Treisman, R., 2007. Nuclear Actin Regulates Dynamic Subcellular Localization and Activity of the SRF Cofactor MAL. Science 316, 1749–1752. https://doi.org/10.1126/science.1141084

Vicente-Manzanares, M., Zareno, J., Whitmore, L., Choi, C.K., Horwitz, A.F., 2007. Regulation of protrusion, adhesion dynamics, and polarity by myosins IIA and IIB in migrating cells. J. Cell Biol. 176, 573–580. https://doi.org/10.1083/jcb.200612043

Walmsley, M.J., Ooi, S.K.T., Reynolds, L.F., Smith, S.H., Ruf, S., Mathiot, A., Vanes, L., Williams, D.A., Cancro, M.P., Tybulewicz, V.L.J., 2003. Critical Roles for Rac1 and Rac2 GTPases in B Cell Development and Signaling. Science 302, 459–462. https://doi.org/10.1126/science.1089709

Wang, C., Hayashi, H., Harrison, R., Chiu, B., Chan, J.R., Ostergaard, H.L., Inman, R.D., Jongstra, J., Cybulsky, M.I., Jongstra-Bilen, J., 2002. Modulation of Mac-1 (CD11b/CD18)-Mediated Adhesion by the Leukocyte-Specific Protein 1 Is Key to Its Role in Neutrophil Polarization and Chemotaxis. J. Immunol. 169, 415–423.

Wang, S., Voisin, M.-B., Larbi, K.Y., Dangerfield, J., Scheiermann, C., Tran, M., Maxwell, P.H., Sorokin, L., Nourshargh, S., 2006. Venular basement membranes contain specific matrix protein low expression regions that act as exit points for emigrating neutrophils. J. Exp. Med. 203, 1519–1532. https://doi.org/10.1084/jem.20051210

Watanabe, Y., 2012. Geometry and force behind kinetochore orientation: lessons from meiosis. Nat Rev Mol Cell Biol. https://doi.org/10.1038/nrm3349

Weaver, A.M., Karginov, A.V., Kinley, A.W., Weed, S.A., Li, Y., Parsons, J.T., Cooper, J.A., 2001. Cortactin promotes and stabilizes Arp2/3-induced actin filament network formation. Curr. Biol. 11, 370–374. https://doi.org/10.1016/S0960-9822(01)00098-7

Weiner, O.D., Neilsen, P.O., Prestwich, G.D., Kirschner, M.W., Cantley, L.C., Bourne, H.R., 2002. A PtdInsP3- and Rho GTPase-mediated positive feedback loop regulates neutrophil polarity. Nat. Cell Biol. 4, 509–513. https://doi.org/10.1038/ncb811

Weiner, O.D., Rentel, M.C., Ott, A., Brown, G.E., Jedrychowski, M., Yaffe, M.B., Gygi, S.P., Cantley, L.C., Bourne, H.R., Kirschner, M.W., 2006. Hem-1 Complexes Are Essential

for Rac Activation, Actin Polymerization, and Myosin Regulation during Neutrophil Chemotaxis. PLoS Biol 4, e38. https://doi.org/10.1371/journal.pbio.0040038

Welch, H.C.E., Condliffe, A.M., Milne, L.J., Ferguson, G.J., Hill, K., Webb, L.M.C., Okkenhaug, K., Coadwell, W.J., Andrews, S.R., Thelen, M., Jones, G.E., Hawkins, P.T., Stephens, L.R., 2005. P-Rex1 Regulates Neutrophil Function. Curr. Biol. 15, 1867–1873. https://doi.org/10.1016/j.cub.2005.09.050

Westerberg, L., Greicius, G., Snapper, S.B., Aspenström, P., Severinson, E., 2001. Cdc42, Rac1, and the Wiskott-Aldrich syndrome protein are involved in the cytoskeletal regulation of B lymphocytes. Blood 98, 1086–1094. https://doi.org/10.1182/blood.V98.4.1086

Westerberg, L., Larsson, M., Hardy, S.J., Fernández, C., Thrasher, A.J., Severinson, E., 2005. Wiskott-Aldrich syndrome protein deficiency leads to reduced B-cell adhesion, migration, and homing, and a delayed humoral immune response. Blood 105, 1144–1152. https://doi.org/10.1182/blood-2004-03-1003

Westerberg, L.S., Dahlberg, C., Baptista, M., Moran, C.J., Detre, C., Keszei, M., Eston, M.A., Alt, F.W., Terhorst, C., Notarangelo, L.D., Snapper, S.B., 2012. Wiskott-Aldrich syndrome protein (WASP) and N-WASP are critical for peripheral B cell development and function. Blood blood-2010-09-308197. https://doi.org/10.1182/blood-2010-09-308197

Westerberg, L.S., Meelu, P., Baptista, M., Eston, M.A., Adamovich, D.A., Cotta-de-Almeida, V., Seed, B., Rosen, M.K., Vandenberghe, P., Thrasher, A.J., Klein, C., Alt, F.W., Snapper, S.B., 2010. Activating WASP mutations associated with X-linked neutropenia result in enhanced actin polymerization, altered cytoskeletal responses, and genomic instability in lymphocytes. J Exp Med 207, 1145–1152. https://doi.org/10.1084/jem.20091245

Williams, D.A., Tao, W., Yang, F., Kim, C., Gu, Y., Mansfield, P., Levine, J.E., Petryniak, B., Derrow, C.W., Harris, C., Jia, B., Zheng, Y., Ambruso, D.R., Lowe, J.B., Atkinson, S.J., Dinauer, M.C., Boxer, L., 2000. Dominant negative mutation of the hematopoietic-specific Rho GTPase, Rac2, is associated with a human phagocyte immunodeficiency. Blood 96, 1646–1654.

Wong, J., Johnston, B., Lee, S.S., Bullard, D.C., Smith, C.W., Beaudet, A.L., Kubes, P., 1997. A minimal role for selectins in the recruitment of leukocytes into the inflamed liver microvasculature. J. Clin. Invest. 99, 2782–2790.

Wong, K., Pertz, O., Hahn, K., Bourne, H., 2006. Neutrophil polarization: Spatiotemporal dynamics of RhoA activity support a self-organizing mechanism. Proc. Natl. Acad. Sci. U. S. A. 103, 3639–3644. https://doi.org/10.1073/pnas.0600092103

Woodfin, A., Voisin, M.-B., Beyrau, M., Colom, B., Caille, D., Diapouli, F.-M., Nash, G.B., Chavakis, T., Albelda, S.M., Rainger, G.E., Meda, P., Imhof, B.A., Nourshargh, S., 2011. The junctional adhesion molecule JAM-C regulates polarized transendothelial migration of neutrophils in vivo. Nat. Immunol. 12, 761–769. https://doi.org/10.1038/ni.2062

Worthylake, R.A., Lemoine, S., Watson, J.M., Burridge, K., 2001. RhoA is required for monocyte tail retraction during transendothelial migration. J. Cell Biol. 154, 147–160. https://doi.org/10.1083/jcb.200103048

Wu, C., Asokan, S.B., Berginski, M.E., Haynes, E.M., Sharpless, N.E., Griffith, J.D., Gomez, S.M., Bear, J.E., 2012. Arp2/3 is critical for lamellipodia and response to extracellular matrix cues but is dispensable for chemotaxis. Cell 148, 973–987.

Xu, J., Wang, F., Van Keymeulen, A., Herzmark, P., Straight, A., Kelly, K., Takuwa, Y., Sugimoto, N., Mitchison, T., Bourne, H.R., 2003. Divergent Signals and Cytoskeletal Assemblies Regulate Self-Organizing Polarity in Neutrophils. Cell 114, 201–214. https://doi.org/10.1016/S0092-8674(03)00555-5

Xu, Y., Moseley, J.B., Sagot, I., Poy, F., Pellman, D., Goode, B.L., Eck, M.J., 2004. Crystal structures of a Formin Homology-2 domain reveal a tethered dimer architecture. Cell 116, 711–723.

Yam, P.T., Wilson, C.A., Ji, L., Hebert, B., Barnhart, E.L., Dye, N.A., Wiseman, P.W., Danuser, G., Theriot, J.A., 2007. Actin–myosin network reorganization breaks

symmetry at the cell rear to spontaneously initiate polarized cell motility. J. Cell Biol. 178, 1207–1221. https://doi.org/10.1083/jcb.200706012

Yamauchi, A., Kim, C., Li, S., Marchal, C.C., Towe, J., Atkinson, S.J., Dinauer, M.C., 2004. Rac2-Deficient Murine Macrophages Have Selective Defects in Superoxide Production and Phagocytosis of Opsonized Particles. J. Immunol. 173, 5971–5979. https://doi.org/10.4049/jimmunol.173.10.5971

Yamazaki, D., Suetsugu, S., Miki, H., Kataoka, Y., Nishikawa, S.-I., Fujiwara, T., Yoshida, N., Takenawa, T., 2003. WAVE2 is required for directed cell migration and cardiovascular development. Nature 424, 452–456. https://doi.org/10.1038/nature01770

Yang, C.-W., Strong, B.S.I., Miller, M.J., Unanue, E.R., 2010. Neutrophils Influence the Level of Antigen Presentation during the Immune Response to Protein Antigens in Adjuvants. J. Immunol. 185, 2927–2934. https://doi.org/10.4049/jimmunol.1001289

Yang, F.C., Atkinson, S.J., Gu, Y., Borneo, J.B., Roberts, A.W., Zheng, Y., Pennington, J., Williams, D.A., 2001. Rac and Cdc42 GTPases control hematopoietic stem cell shape, adhesion, migration, and mobilization. Proc. Natl. Acad. Sci. U. S. A. 98, 5614–5618. https://doi.org/10.1073/pnas.101546898

Yang, H.W., Collins, S., Meyer, T., 2016. Locally excitable Cdc42 signals steer cells during chemotaxis. Nat. Cell Biol. 18, 191–201. https://doi.org/10.1038/ncb3292

Yang, Q., Zhang, X.-F., Pollard, T.D., Forscher, P., 2012. Arp2/3 complex–dependent actin networks constrain myosin II function in driving retrograde actin flow. J. Cell Biol. https://doi.org/10.1083/jcb.201111052

Yoo, S.K., Deng, Q., Cavnar, P.J., Wu, Y.I., Hahn, K.M., Huttenlocher, A., 2010. Differential Regulation of Protrusion and Polarity by PI(3)K during Neutrophil Motility in Live Zebrafish. Dev. Cell 18, 226–236. https://doi.org/10.1016/j.devcel.2009.11.015

Yu, H., Leitenberg, D., Li, B., Flavell, R.A., 2001. Deficiency of Small Gtpase Rac2 Affects T Cell Activation. J. Exp. Med. 194, 915–926. https://doi.org/10.1084/jem.194.7.915

Yuruker, B., Niggli, V., 1992. Alpha-actinin and vinculin in human neutrophils: reorganization during adhesion and relation to the actin network. J. Cell Sci. 101, 403–414.

Zarbock, A., Ley, K., 2008. Mechanisms and Consequences of Neutrophil Interaction with the Endothelium. Am. J. Pathol. 172, 1–7. https://doi.org/10.2353/ajpath.2008.070502

Zarbock, A., Ley, K., McEver, R.P., Hidalgo, A., 2011. Leukocyte ligands for endothelial selectins: specialized glycoconjugates that mediate rolling and signaling under flow. Blood 118, 6743–6751. https://doi.org/10.1182/blood-2011-07-343566

Zhang, H., Schaff, U.Y., Green, C.E., Chen, H., Sarantos, M.R., Hu, Y., Wara, D., Simon, S.I., Lowell, C.A., 2006. Impaired integrin-dependent function in Wiskott-Aldrich syndrome protein-deficient murine and human neutrophils. Immunity 25, 285–295. https://doi.org/10.1016/j.immuni.2006.06.014

Zhang, H., Sun, C., Glogauer, M., Bokoch, G.M., 2009. Human Neutrophils Coordinate Chemotaxis by Differential Activation of Rac1 and Rac2. J. Immunol. 183, 2718–2728. https://doi.org/10.4049/jimmunol.0900849

Zhang, J., Shehabeldin, A., Cruz, L.A.G. da, Butler, J., Somani, A.-K., McGavin, M., Kozieradzki, I., Santos, A.O. dos, Nagy, A., Grinstein, S., Penninger, J.M., Siminovitch, K.A., 1999. Antigen Receptor–Induced Activation and Cytoskeletal Rearrangement Are Impaired in Wiskott-Aldrich Syndrome Protein–Deficient Lymphocytes. J. Exp. Med. 190, 1329–1342. https://doi.org/10.1084/jem.190.9.1329

Zhang, L., Luo, J., Wan, P., Wu, J., Laski, F., Chen, J., 2011. Regulation of cofilin phosphorylation and asymmetry in collective cell migration during morphogenesis. Dev. Camb. Engl. 138, 455–464. https://doi.org/10.1242/dev.046870

Zhang, Q., Davis, J.C., Lamborn, I.T., Freeman, A.F., Jing, H., Favreau, A.J., Matthews, H.F., Davis, J., Turner, M.L., Uzel, G., Holland, S.M., Su, H.C., 2009. Combined immunodeficiency associated with DOCK8 mutations. N. Engl. J. Med. 361, 2046–2055. https://doi.org/10.1056/NEJMoa0905506

Zhang, Q., Li, Y., Howard, T.H., 2000. Human Lymphocyte-Specific Protein 1, the Protein Overexpressed in Neutrophil Actin Dysfunction with 47-kDa and 89-kDa Protein Abnormalities (NAD 47/89), Has Multiple F-Actin Binding Domains. J. Immunol. 165, 2052–2058.

Zicha, D., Allen, W.E., Brickell, P.M., Kinnon, C., Dunn, G.A., Jones, G.E., Thrasher, A.J., 1998. Chemotaxis of macrophages is abolished in the Wiskott-Aldrich syndrome. Br. J. Haematol. 101, 659–665.

Zicha, D., Dunn, G.A., Brown, A.F., 1991. A new direct-viewing chemotaxis chamber. J. Cell Sci. 99 (Pt 4), 769–775.

Zuchero, J.B., Coutts, A.S., Quinlan, M.E., Thangue, N.B.L., Mullins, R.D., 2009. p53-cofactor JMY is a multifunctional actin nucleation factor. Nat Cell Biol 11, 451–459. https://doi.org/10.1038/ncb1852

Supplemental video legends

Video S4-1: Migration of a mixed population of dHL-60 control and I294T (red) toward fMLP (100nM) loaded in the outer well of the Dunn Chamber. Cells were imaged for one hour with a bright field microscope, one brightfield image taken every minute and one red fluorescence image taken every 6 minutes . Scale bar = 100μm.

Video S4-2: Kinetochore oscillations (CENP-A tagged GFP) in HT1080 control cells. A stack of 21 slices was took every 7.5 seconds during 5 minutes.

Video S4-2: Kinetochore oscillations (CENP-A tagged GFP) in HT1080 expressing CA-WASp. A stack of 21 slices was took every 7.5 seconds during 5 minutes.

Video S5-1: Migration of control neutrophils toward fMLP (100nM) loaded in the outer well of the Dunn Chamber. Cells were imaged for one hour with a bright field microscope, one image taken every minute. Scale bar = 100μm.

Video S5-2: Patient neutrophils migration toward fMLP (100nM) loaded in the outer well of the Dunn Chamber. Cells were imaged for one hour with a bright field microscope, one image taken every minute. Scale bar = 100μm.

Video S5-3: Neutrophil-like dHL-60 SCR migration toward fMLP (100nM) loaded in the outer well of the Dunn Chamber. Cells were imaged for one hour with a bright field microscope, one image taken every minute. Scale bar = 100μm.

Video S5-4: Neutrophil-like dHL-60 MKL1 migration toward fMLP (100nM) loaded in the outer well of the Dunn Chamber. Cells were imaged for one hour with a bright field microscope, one image taken every minute. Scale bar = 100μm.

Video S6-1: Migration of control neutrophils toward fMLP (100nM) loaded in the outer well of the Dunn Chamber. Cells were imaged for one hour with a bright field microscope, one image taken every minute. Scale bar = 100μm.

Video S6-2: Patient 1 neutrophils migration toward fMLP (100nM) loaded in the outer well of the Dunn Chamber. Cells were imaged for one hour with a bright field microscope, one image taken every minute. Scale bar = 100μm.

Video S5-3: Migration of control neutrophils toward fMLP (100nM) loaded in the outer well of the Dunn Chamber. Cells were imaged for one hour with a bright field microscope, one image taken every minute. Scale bar = 100μm.

Video S6-4: Patient 2 neutrophils migration toward fMLP (100nM) loaded in the outer well of the Dunn Chamber. Cells were imaged for one hour with a bright field microscope, one image taken every minute. Scale bar = 100μm.

Video S6-5: Patient 3 neutrophils migration toward fMLP (100nM) loaded in the outer well of the Dunn Chamber. Cells were imaged for one hour with a bright field microscope, one image taken every minute. Scale bar = 100μm.

Video S6-5: Control and patient 4 neutrophils ($CFSE^{+}$) migration toward fMLP (100nM) loaded in the outer well of the Dunn Chamber. Cells were imaged for one hour with a bright field microscope, one image taken every minute and one green fluorescence image taken every 6 minutes. Scale bar = 100μm.

Appendix A: MatLab routine source code

```
function [migFile, ProcessedTracks] = migration_analysis (Calibration,oV)
% Calibration is the pixel size in um/pixel.
[filename,path] = uigetfile; % opens up a similar dialog to uiimport to select a file
migFile = uiimport(fullfile(path,filename)); % directly imports the selected file
[pathstr, name, ext] = fileparts(fullfile(path,filename));
iMax = numel(migFile.x)-1;
TrackNumber = 0;
maxTrackNumber = max(migFile.TrackN0xB0);
for i=1:iMax
   if (migFile.Distance(i) == -1) && (migFile.Velocity(i) == -1)
      % index to browse one track only in the original file
      j = i+1;
      %index to browse the new created struct. For one track only.
      RSNumber = 1;
      % Convert the file form a struct with n parameters (one parameter
      % by column) to s struct wit x tracks defined by n parameters (one
      % column by parameter.
      while  j<=iMax && (migFile.Distance(j) ~= -1) && (migFile.Velocity(j) ~= -1)

         TrackNumber = migFile.TrackN0xB0(j);
         % Transfert all the value from one tracks to the new struct
         % dedicated to this track
         ProcessedTracks(TrackNumber).SliceNumber(RSNumber) = migFile.SliceN0xB0(j);
         ProcessedTracks(TrackNumber).RelSliceNumber(RSNumber) = RSNumber;
         ProcessedTracks(TrackNumber).X(RSNumber) = migFile.X(j);
```

```
        ProcessedTracks(TrackNumber).Y(RSNumber) = migFile.Y(j);

        ProcessedTracks(TrackNumber).Distance(RSNumber) = migFile.Distance(j);

        ProcessedTracks(TrackNumber).AbsDistance(RSNumber) = abs(migFile.Distance(j));

        ProcessedTracks(TrackNumber).Velocity(RSNumber) = migFile.Velocity(j);

        ProcessedTracks(TrackNumber).AbsVelocity(RSNumber)= bs(migFile.Velocity(j))*60;

          %Velocity is originally expressed in um/sec in this file, converting in um/min. Need to do a
          variable for that

        ProcessedTracks(TrackNumber).PixelValue(RSNumber) = migFile.PixelValue(j);

        j = j+1;

        RSNumber =RSNumber + 1;

    end

    %calculation of the Total distance: the distance between the start

    %and end point of the track and along the path taken by the cell

    %during the track.

    ProcessedTracks(TrackNumber).TotalDistance=
sum(ProcessedTracks(TrackNumber).AbsDistance);

    %Calculation of the Net Distance: the direct distance between the

    %start and end poibnt of the track.

    trackStart = 1;

    trackEnd = numel(ProcessedTracks(TrackNumber).SliceNumber);

    ProcessedTracks(TrackNumber).NetDistance=  sqrt((ProcessedTracks(TrackNumber).X(trackEnd)-
ProcessedTracks(TrackNumber).X(trackStart))^2+  (ProcessedTracks(TrackNumber).Y(trackEnd)-
ProcessedTracks(TrackNumber).Y(trackStart))^2)*Calibration;

     %Confinement Ratio (or chemotactic index): defined by NetDistance/TotalDistance. Measure

    %the straightness or confinement of the cell track.

    ProcessedTracks(TrackNumber).ConfRatio=
ProcessedTracks(TrackNumber).NetDistance/ProcessedTracks(TrackNumber).TotalDistance;

    %Average Distance between to successive points
```

```
ProcessedTracks(TrackNumber).AvDistance= mean(ProcessedTracks(TrackNumber).AbsDistance);

%Average Instant Velocity between to successive points

ProcessedTracks(TrackNumber).AvVelocity= mean(ProcessedTracks(TrackNumber).AbsVelocity);



[ProcessedTracks(TrackNumber).angleDist,ProcessedTracks(TrackNumber).angleVar]=
Instant_angles(ProcessedTracks(TrackNumber).X,ProcessedTracks(TrackNumber).Y,oV);

%test average angles

ProcessedTracks(TrackNumber).avAngle=
average_angle(ProcessedTracks(TrackNumber).angleDist);

ProcessedTracks(maxTrackNumber+1).TotDist(TrackNumber)=
ProcessedTracks(TrackNumber).TotalDistance;

ProcessedTracks(maxTrackNumber+2).NetDist(TrackNumber)=
ProcessedTracks(TrackNumber).NetDistance;

ProcessedTracks(maxTrackNumber+3).CF(TrackNumber)=
ProcessedTracks(TrackNumber).ConfRatio;

ProcessedTracks(maxTrackNumber+4).avDist(TrackNumber)=
ProcessedTracks(TrackNumber).AvDistance;

ProcessedTracks(maxTrackNumber+5).avVel(TrackNumber)=
ProcessedTracks(TrackNumber).AvVelocity;

%ProcessedTracks(maxTrackNumber+7).avAngles(TrackNumber)=
ProcessedTracks(TrackNumber).AvVelocity;
```

```
str = fprintf('Track number: %d Processed!!.\n',TrackNumber);
```

```
    end


end


ProcessedTracks(maxTrackNumber+6).allAngles = [];

ProcessedTracks(maxTrackNumber+6).allAnglesVar = [];

for mT=1:(maxTrackNumber - 1)

    ProcessedTracks(maxTrackNumber+6).allAngles=
cat(2,ProcessedTracks(maxTrackNumber+6).allAngles,ProcessedTracks(mT).angleDist);

end


ProcessedTracks(maxTrackNumber+7).allAvAngles = [];

for mT=1:(maxTrackNumber - 1)

    ProcessedTracks(maxTrackNumber+7).allAvAngles=
cat(2,ProcessedTracks(maxTrackNumber+7).allAvAngles,ProcessedTracks(mT).avAngle);

end


figure;

aDistAllAngles = rose(ProcessedTracks(numel(ProcessedTracks)-1).allAngles,24);

title('\bf Instantaneous angle(\alpha)');

set(gca,'View',[-90 90],'YDir','reverse');

set(aDistAllAngles,'Color','blue','LineWidth',1);


for mT=1:(maxTrackNumber - 1)

    ProcessedTracks(maxTrackNumber+6).allAnglesVar=
cat(2,ProcessedTracks(maxTrackNumber+6).allAnglesVar,ProcessedTracks(mT).angleVar);

end

figure;
```

```
aDistAllAnglesVar = rose(ProcessedTracks(numel(ProcessedTracks)-1).allAnglesVar,24);

title('\bf Angle Variation(\gamma)');

set(gca,'View',[-90 90],'YDir','reverse');

set(aDistAllAnglesVar,'Color','blue','LineWidth',1);


figure;

aAllAvAngles = rose(ProcessedTracks(numel(ProcessedTracks)).allAvAngles,24);

title('\bf avAngle(\gamma)');

set(gca,'View',[-90 90],'YDir','reverse');

set(aAllAvAngles,'Color','blue','LineWidth',1);


end




function [AnglesDist, AnglesVar] = Instant_angles (X,Y,oV)

if isequal(numel(X),numel(Y)) == 0

    disp('Error1')

end

iMax = numel(X)-1;

AnglesDist = [];

AnglesVar = [];


for i=1:iMax

    if (X(i)-X(i+1))~= 0 && (Y(i)-Y(i+1))~= 0

       AnglesDist(i)=mod(atan2((X(i+1)-X(i))*(oV(2,2)-oV(1,2))-(Y(i+1)-Y(i))*(oV(2,1)-
oV(1,1)),((X(i+1)-X(i))*(oV(2,1)-oV(1,1))+(Y(i+1)-Y(i))*(oV(2,2)-oV(1,2)))),2*pi);
```

```
    end
end
iMaxVar = numel(AnglesDist) - 1;
for j=1:iMaxVar
    AnglesVar(j) = abs(AnglesDist(j+1) - AnglesDist(j));
end
```